UNIVERSIDADE DO PORTO

Non-local Modelling of Ductile Damage:
Formulation and Numerical Issues

Filipe Xavier Costa Andrade

Faculdade de Engenharia
Departmento de Engenharia Mecânica

December 2011

"The absence of evidence is not the evidence of absence."

Carl Sagan (1934-1996)

A B S T R A C T

Most damage models induce material softening, which, within a standard local framework, consequently leads to a pathological dependency of results on the spatial discretisation. In the specialised literature, the *non-local approach*, where a given constitutive quantity is replaced by a weighted integral over a finite volume, has been proposed to overcome the aforementioned issue. However, despite the numerous advances in this field over the last years, many questions still remain open. The main objective of the present work is to answer some of these questions, both from a theoretical and numerical point of view. To this end, this thesis begins with a general overview on this topic as well as a brief review of some important, well-established concepts on computational mechanics. In the following, a thermodynamic consistent non-local ductile damage model at finite strains is proposed in Chapter 3. It is shown that the non-local model retrieves many of the advantages of the associated local model by assuming that the non-local averaging operator is independent of the history of deformation. The numerical implementation of the proposed model, which requires a global approach for its solution, is presented in detail, for which numerical examples clearly demonstrate mesh-independent solutions. In Chapter 4, the theoretical principles and numerical developments addressed in Chapter 3 are used to present a non-local Gurson-based damage model containing a shear mechanism. Again, the associated numerical results have lead to mesh-insensitive results. In order to guarantee the quadratic rates inherent to the Newton-Raphson Method, a general procedure for the establishment of the algorithmic consistent non-local tangent operator is presented in detail in Chapter 5. Numerical examples show that the approach is generic and able to deliver quadratic rates of asymptotic convergence. In Chapter 6, different non-local variables are selected to enhance the models presented in Chapters 3 and 4, for which it is shown that the damage variable is a optimal candidate for non-local variable in the case of implicit damage models. In Chapter 7, an approximate approach of the non-local method is proposed for explicit finite element implementations, which is particularly suitable for commercial finite element codes. This thesis ends with some final remarks and suggestions for future work.

R E S U M O

A maioria dos modelos de dano acaba por induzir um regime de amaciamento a nível constitutivo, cujos efeitos refletem-se na dependência patológica dos resultados em relação à discretização espacial. A abordagem não-local, na qual se substitui uma determinada variável local por uma média ponderada definida através de uma integral de volume, foi então proposta visando eliminar este problema. Entretanto, apesar de inúmeras recentes contribuições neste tópico, muitas questões continuam em aberto. O objetivo deste trabalho é responder a alguns destes pontos, tanto de um ponto vista teórico, quanto computacional. Para este fim, esta tese inicia-se com um visão geral do tópico em questão, bem como se apresenta uma breve revisão de importantes conceitos relacionados à mecânica computacional. De seguida, um modelo de dano dúctil não-local termodinamicamente consistente e a grandes deformações é proposto no Capítulo 3. É demonstrado que o modelo não-local dispõe de muitas das vantagens do respectivo modelo local quando se assume que o operador não-local é independente da história da deformação. A implementação numérica do modelo proposto é apresentada em detalhe, cuja solução há de ser alcançada através de um algoritmo global, o que claramente leva a soluções independentes da malha. No Capítulo 4, os princípios teóricos e os desenvolvimentos numéricos do Capítulo 3 são utilizados em conjunto com um modelo de dano baseado na teoria de Gurson, sendo que no presente trabalho incluiu-se um mecanismo de danificação associado a estados de corte. Tal como para o modelo do Capítulo 3, os resultados mostram-se independentes do refino da malha. A fim de se garantir taxas de convergência quadráticas inerentes ao método de Newton-Raphson, um procedimento generalizado para a obtenção de operadores tangentes não-locais consistentes é apresentado no Capítulo 5. Exemplo demonstram que a abordagem é genérica, ao mesmo tempo que proporciona taxas quadráticas de convergência. No Capítulo 6, o uso de diferentes variáveis não-locais sugerem que o dano é a variável não-local ideal no caso de modelos implícitos de dano. Em seguida, uma aproximação do método não-local é proposta, no Capítulo 7, visando a sua utilização com esquemas explícitos de integração de códigos comerciais de elementos finitos. Encerra-se esta tese com alguns importanes comentários finais e sugestões de desenvolvimentos futuros.

Agradecimentos

Aos meus orientadores, Dr. José César de Sá e Dr. Francisco Andrade Pires, por terem me acolhido como aluno na Universidade do Porto, pelas valiosas sugestões e correções ao longo deste trabalho, pelo suporte nas questões burocráticas e também por me proporcionarem a oportunidade de participar em importantes congressos na área da Mecânica Computacional.

Aos meus antigos professores de graduação, Dr. Miguel de Vaz Jr. e Dr. Pablo Muñoz-Rojas, por acreditarem em mim e por me apoiarem em todos os momentos, além de terem aberto a porta que me permitiu iniciar este trabalho.

Ao Programa AlBan, *Programa de Bolsas de Alto Nível da União Europeia para a América Latina*, bolsa número E07D401751BR, pelo importante apoio financeiro disponibilizado para o desenvolvimento deste trabalho.

Aos meus amigos e também colegas de doutoramento, Lucival Malcher, Fábio Reis e Mariana Seabra, pelas nossas diversas discussões relacionadas à Mecânica Computacional, mas também pelos momentos de descontração com um bom café português ou ainda em algum dos excelentes restaurantes que a cidade do Porto tem a oferecer.

Ao meu colega e amigo Matthias Vogler, cujos conhecimentos do idioma português estão cada vez mais aprimorados, pelo seu empenho e dedicação ao trabalharmos juntos em novos desenvolvimentos e pelas diversas discussões no tema Modelamento Constitutivo, com as quais aprendi muito.

À minha família que, apesar da distância, apoiou-me e também me proporcionou importantes momentos de descontração em muitas das nossas conversas via Internet, além das visitas que fizeram durante a minha estadia em Portugal.

À minha esposa Katharina, por ter me apoiado firmemente desde o momento em que decidi me candidatar a uma vaga de doutoramento, e também por sua paciência e seu apoio incondicional ao longo destes últimos anos, sem os quais haveria sido muito mais difícil a realização deste trabalho.

Contents

List of Figures

List of Tables

Dedicated to my family and friends

Chapter 1

Introduction

A *ductile material* is characterised by the presence of moderate to large plastic deformations (i.e., permanent deformations) before failure takes place after a certain external load has been applied. Within this class of materials are most steel, aluminium and copper alloys, which are of crucial importance for the industrial scenario nowadays. Concerning the extraction and production of these materials, new techniques have been constantly brought to market in order to obtain metallic alloys that possess the desired properties regarding endurance, resistance, weight, wear and tear. Notwithstanding the importance of such production techniques, a comprehensive understanding of how ductile materials behave when subjected to mechanical loads is also necessary. In turn, this understanding allows the establishment of suitable constitutive laws that are capable of modelling the material behaviour and predicting material degradation and failure. The accurate modelling of materials plays a major role in product development, since the precise prediction of deformation and failure allows the efficient design and optimisation of a given product, preventing the use of unnecessary material and hence saving financial resources.

Along the past century, many researchers have attempted to develop material laws that have the ability of reproducing what is observed in experiments. Key contributions on this topic are the pioneering works of Tresca [111], Huber [63], von Mises [118] and Hencky [61]. These authors have proposed a mathematical approach to predict the onset of plastic behaviour through the establishment of *yield functions*. In their approach, when a given critical material-dependent parameter is reached, plasticity is assumed to take place. As a matter of fact, this kind of approach is still extensively used nowadays for which new enhanced yield loci have been constantly sought aiming to predict plastic initiation under complicated stress states and loading conditions.

After the first developments on the modelling of materials, it has soon become evident that also plastic straining as well as the material progressive degradation should be somehow taken into account for accurate predictions in practical engineering problems. In this context, three main approaches have been extensively used: (a) elasto-plastic models with post-processed failure criteria; (b) constitutive modelling within the so-called *Continuum Damage Mechanics* (CDM); (c) material laws established from micro-mechanical considerations.

The first approach is based on a purely elasto-plastic framework in which material internal degradation is uncoupled from plastic straining. Thus, it is very appealing from a practical point of view due to its relatively easiness of use (if compared to the other two approaches) for which many authors have made important contributions (e.g., [9, 60, 71], to cite a few).

The theory of CDM takes as main assumption the existence of internal material damage, which is regarded in a phenomenological fashion. Within the CDM framework, damage is treated as an internal variable that also participates in the dissipative inelastic process. Plasticity and damage are then strongly coupled within this approach. Key contributions within the CDM framework are due to Lemaitre [74, 75, 76], whose constitutive model has served as the base of many other material laws proposed in the literature.

Finally, the third approach assumes that material degradation is regarded through some kind of theoretical analysis at the micro-structure of the material. For instance, one possibility is the adoption of the postulate of mass conservation in the analysis of voids at the micro-structure. In turn, this micro-mechanical analysis delivers equations that can be employed at the macro-scale. In this context, Gurson [57] has proposed a pressure-sensitive yield function which is coupled with plastic flow and porosity. His model has been later extended by several researchers; perhaps, the most influential contribution has been given by Tvergaard and Needleman [113], who incorporated the effects of void nucleation and coalescence in Gurson's model. It is worth mentioning that, in this case, damage does not energetically contribute to dissipation[1] but it is rather a direct consequence of mass conservation, in sharp contrast to the premisses of CDM.

Within the scope of this thesis, we shall restrict ourselves to the modelling of ductile materials adopting the theoretical background provided by the second (b) and third (c) aforementioned approaches. However, several of the concepts presented

[1]Damage does influence plastic straining indirectly but has no explicit contribution in the Clausius-Duhem inequality.

and conclusions drawn in this thesis can be straightforwardly extended to models that are based on the first approach.

1.1 The issue of pathologically mesh-dependent solutions

Many constitutive models established with one of the aforementioned approaches have proved very effective in modelling material internal degradation and predicting failure within a reasonable range of applications. They are, nevertheless, most often based on the standard (local) continuum theory which inherently assumes that the material is homogeneous and continuous at any size scale. However, this assumption is not valid when deformation reaches a critical level. At this point, the internal degradation of the material has an important influence on the macro-structural response to external loads. Moreover, plastic strain tends to concentrate in a localised zone while the body experiences a global strain-softening regime. At this phase, heterogeneities in the micro-structure play a crucial role, being responsible for the onset of the failure phenomenon which will lead, eventually, to the appearance of a macro-crack.

Since classical local theories disregard important effects of the micro-structure of the material, they cannot correctly describe the aforementioned localised failure process. Likewise, the mathematical description of the failure phenomenon using the local theory is inappropriate since it inherently suffers from spurious instabilities. This can be explained as follows. In classical multi-variable calculus, the partial differential equilibrium equations which govern static (dynamic) problems are classified as elliptic (hyperbolic). As long as these equations remain elliptic (hyperbolic) the solution of the static (dynamic) IBVP is guaranteed to be unique. However, when the material tangent modulus becomes negative (that is, under softening regimes), the ellipticity (hyperbolicity) is lost and uniqueness of solution no longer exists. This lack of ellipticity (hyperbolicity) manifests itself through a pathological dependence of solution on the spatial discretisation when using numerical methods. Within a typical finite element framework, for instance, the localised zone will have the size of the elements at the critical zone. As the mesh is infinitely refined, plastic strain concentrates in an infinitely small layer of elements and, in this case, the total dissipated energy of the process unrealistically vanishes. In fact, it can be concluded that the problem of the local theory lies on its lack of information about the size of the localised zone. Thus, the mathematical interpretation of the problem implies that this missing information should

be, in some manner, incorporated into the continuum theory in order to obtain objective descriptions of the localised failure process. Looking now the problem from the physical point of view, it turns out to be quite clear that the actual size of the localised zone is related to the heterogeneous micro-structure of the material. Therefore, both mathematical and physical interpretations imply that the standard continuum theory must be somehow enriched in order to correctly describe strain-driven localisation.

Many strategies have been proposed over the last three decades attempting to overcome the issue of spurious localisation due to strain-softening. Among them, a simple approach, which preserves all the facilities of the standard local method, has been gaining good acceptance in the industry. We shall refer to this method herein as *adaptive hardening modulus strategy* (AHMS). In this method, the hardening modulus is systematically adjusted to the size of the element so that a certain prescribed ratio is kept. This ratio is in turn associated to the size of the damaging (or fracturing) zone or must fulfil some constraint related to the dissipated energy within the element. It is worth mentioning that, instead of adapting the hardening modulus, some researchers (see [52]) have chosen to compensate the effects of ill-posedness through other dissipative constitutive variables; the underlying idea of the method is, however, the same. As demonstrated in some contributions (e.g. [24, 25]), the AHMS is quite simple to implement and, for numerous cases, very effective as well. Furthermore, the size of the localising zone is very easily controlled through the prescribed ratio, so that it can be explicitly calibrated to match experiments. However, since the AHMS is merely an artificial compensation of the effects of spurious localisation, the ill-posedness of the structural problem still persists, which is a major disadvantage of the AHMS. For instance, this can be critical when the finite element mesh has small imperfections (e.g. due to round-off errors in the definition of the nodal positions in the input file). In this case, these imperfections within a given element may be far too small to activate the AHMS, but are large enough to capture non-physical solutions. In fact, to a larger extent, it is generally not possible to predict whether spurious results will take place with the AHMS or not; simply because ill-posedness is not eliminated at all. This fact motivates the pursuit for a more reliable strategy that can effectively avoid any kind of spurious mesh dependence.

This is the case of *viscoplastic regularisation* (VR). The VR effectively eliminates the mathematical problem of ill-posedness because it introduces, in an implicit fashion, the lacking information about the size of the localising zone into the structural problem, keeping the partial differential equations elliptic (or hyperbolic in

the case of transient regimes). A key contribution on the use of VR for the elimination of pathological mesh dependence is due to Needleman [84]. Notwithstanding its regularising properties, the VR is relatively simple to implement, especially because the constitutive law keeps its standard local-like behaviour. Furthermore, a variety of viscoplastic laws and the algorithms associated to their numerical implementation are given in great detail in many references (e.g. [42, 90, 92, 106]). However, in sharp contrast to the AHMS, the size of the localising zone (dictated by the *intrinsic length*) cannot be easily controlled in the VR. In fact, expressions correlating the material properties of the viscoplastic model and the intrinsic length can be established (see [92]); however, the intrinsic length itself cannot be defined in an explicit fashion, but rather through some other implicit parameters. As a consequence, controlling the size of the localising zone with the VR turns out to be quite difficult when compared to the AHMS.

Another suitable approach, which is the main subject of this thesis, is the so-called *non-local formulation* (NLF). The NLF incorporates an intrinsic length into the classical continuum by employing spatially weighted averages through an integral operator. In contrast to the VR, the intrinsic length can be explicitly controlled with the NLF. Moreover, it effectively eliminates ill-posedness, contrasting with the major disadvantage of the AHSM. Therefore, the NLF has got the properties that are expected from a good regularisation approach. Table 1.1 summarises, in a general fashion, the properties of each of the three regularisation methods described above.

Table 1.1: General properties of regularisation methods

	Elimination of ill-posedness?	Easy to implement?	Easy control of intrinsic length?
AHMS	No	Yes	Yes
VR	Yes	Yes	No
NLF	Yes	No	Yes

Remark 1.1. *The NLF has been classified as 'not easy to implement' based on a rather general, qualitative comparison with the other two strategies. As it will be shown in detail throughout this thesis, very efficient numerical algorithms, which require relatively minor implementation efforts, can be established within the non-local framework.*

1.2 Non-local modelling

The first non-local models were proposed in the elasticity context in the 1960s [48, 103]. Such models aimed to improve the description of micro-structural interactions in elastic-wave dominated problems. However, the theory was limited to the elastic domain and the first extension of the theory to the plastic domain has been done by Eringen [49, 50]. In his formulation, the total strain tensor was replaced by its non-local average; however, the model was not intended to act as localisation limiter.

In the context of CDM, the first non-local damage model was proposed by Pijaudier-Cabot and Bažant [93] where they applied a non-local averaging operator only to variables that were related to the inelastic process and that could only grow or remain constant [104]. This choice stemmed from the fact that the average of the total strain tensor as in Eringen's model could still lead to spurious instabilities in the IBVP, as previously shown by Bažant and Chang [13]. In the late 1980s, the first non-local plasticity model intended to serve as a localisation limiter was proposed by Bažant and Lin [15]. After these initial developments, a comprehensive number of relevant contributions have then rapidly emerged [14, 21, 22, 41, 67, 68, 69, 70, 96, 104, 110].

Another class of non-local approaches are the enhanced constitutive theories that incorporate the gradients of one or more variables into originally local models. The gradient-enhanced models are the differential counterpart of the non-local integral-type theory and have been developed as an alternative to the classical non-local theory. Over the last years, several researchers have brought significant developments comprising gradient-enhanced constitutive theories, plenty of them with detailed contributions on effective and efficient numerical implementations [2, 26, 35, 46, 55, 88, 123].

Despite the many advances accomplished in the non-local field over the last years, many questions still remain unanswered. For instance, there is no general guideline, in a broad sense, on how to employ the non-local theory for the mesh-insensitive description of ductile materials. In fact, most authors have adopted one of the two general non-local formulations (either integral or gradient-enhanced), employed it on their previously existing local model and shown, for a few examples, that pathological mesh sensitivity was, in their cases, circumvented. However, it has not been made clear if these models would still preserve their regularising properties if applied under several different stress states (i.e., tension, compression,

shear, combined stress states). As a matter of fact, the current main disadvantage of the NLF is that it is not clear enough how it should be used and implemented.

Therefore, the main goal of this thesis is to answer many of these questions and to provide a more general guideline on how the concepts of non-locality should be employed, both from a theoretical and numerical point of view, for the accurate and efficient description of ductile materials under strain-softening regimes.

1.3 Thesis organisation

In order to facilitate the readability and comprehension, it is outlined how this thesis has been organised and which are the main topics addressed in each chapter.

Chapter 2

In this chapter, the main concepts of the standard Continuum Mechanics and the Finite Element Method are reviewed. The intention of Chapter 2 is not to be exhaustive but rather to serve as the base for the developments addressed in the following chapters.

Chapter 3

This chapter is devoted to the formulation and numerical implementation of a ductile damage constitutive model enriched with a thermodynamically consistent non-local theory of integral-type. In order to describe ductile deformation, the model takes finite strains into account. To model elasticity, a Hencky-like hyper-elastic free energy potential coupled with non-local damage is adopted. The thermodynamic consistency of the model is ensured by applying the first and second thermodynamical principles in the global form and the dissipation inequality can be re-written in a local form by incorporating a non-local residual that accounts for energy exchanges between material points of the non-local medium. The thermodynamically consistent non-local model is compared with its associated classical formulation (in which non-locality is merely incorporated by averaging the damage variable without resorting to thermodynamic potentials) where the thermodynamical admissibility of the classical formulation is demonstrated. Within the computational scheme, the non-local constitutive initial boundary value problem is discretised over pseudo-time where it is shown that well-established numerical

integration strategies can be straightforwardly extended to the non-local integral formulation. A modified Newton-Raphson solution strategy is adopted to solve the non-linear complementarity problem and its numerical implementation, regarding the proposed non-local constitutive model, is presented in detail. The results of two- and three-dimensional finite element analyses show that the model is able to eliminate the pathological mesh dependence inherently present under the softening regime if the local theory is considered.

Chapter 4

In this chapter, we enhance with non-locality a Gurson-based model containing a phenomenologically defined shear mechanism similar to the one proposed by Nahshon and Hutchison. The numerical implementation of the model within a finite element framework is depicted in detail. It is shown that the solution of the non-local constitutive problem has to be pursued in a global fashion where a global system of equations containing other systems of equations, each one associated with each material integration point, is present. A full and a modified Newton-Raphson approach are proposed and assessed for the solution of the non-local material problem. The results are scrutinised and reveal a much more pronounced spurious mesh dependence of the local theory under shear stress states than in the axisymmetric case.

Chapter 5

In Chapter 5, we firstly present the general expression of the consistent tangent operator for elasto-plastic non-local models of integral-type, necessary for quadratic rates inherent to the Newton-Raphson method. It is demonstrated that a global compliance matrix needs to be inverted, in the general case, for the establishment of the consistent algorithmic modulus. As an application of the developed methodology, a classical J_2 plasticity model is enriched with the non-local theory, for which a closed-form tangent operator is obtained. This avoids the inversion of the global matrix, rendering a very efficient numerical implementation. The Lemaitre-based non-local model of Chapter 3 is also addressed in this chapter, for which a closed-form tangent operator is also provided. The analysis of some problems clearly demonstrates that the presented consistent linearisation is able to provide quadratic rates of asymptotic convergence.

Chapter 6

Aiming to answer the question of which non-local formulations effectively lead to mesh-insensitive results, we select, in Chapter 6, several constitutive variables to be non-local quantities by taking both Lemaitre and GTN models as the base for the non-local enhancement. The resulting non-local constitutive models are employed in the numerical simulation of various specimens which are subjected to different values of stress triaxiality and Lode angle at the fracture zone. The goal is to find which models present the best performance in the task of providing mesh-insensitive solutions. The results show that strain-softening mesh dependency is much stronger in plane strain and pure shear stress states than in the axisymmetric case. It is also found that the variables that regularise the solution in the axisymmetric case do not necessarily eliminate mesh sensitivity in the other cases.

Chapter 7

In Chapter 7, we adopt an approximation of the non-local theory that is suitable to easily transform existing local models in non-local, requiring only little modification. The technique is restricted to explicit finite element codes and has been designed to be easily incorporated as a user-defined feature in the commercial code LS-DYNA. The shortcoming of accessing the neighbour integration points at once, which is a major difficulty when implementing non-local models in FE commercial programs, is overcome by adopting an implementation strategy that saves information of the previous time step. In a general sense, the disadvantage of such approximated non-local formulation is the requirement of small time steps for enough accuracy, so that it is not practicable in implicit codes. However, this does not represent a problem in the present case since the explicit integration scheme of LS-DYNA naturally demands very small time steps in order to guarantee stable solutions. As a consequence, the results obtained with the present technique are sufficiently accurate to attenuate the mesh dependency issue. Numerical simulation shows that the non-local technique presented in Chapter 7 is able to avoid the spurious mesh dependency for a wide range of material models, proving that the proposed strategy is suitable for a wide spectrum of practical applications in engineering.

Chapter 8

Chapter 8 briefly summarises the main topics addressed in the thesis, emphasising the theoretical and numerical advances accomplished during this work. Furthermore, the conclusions drawn from the results obtained in the preceding chapters are highlighted and the contribution brought with the present work is discussed. This thesis is then finalised with some closing remarks and recommendations for future work in the topic of non-local modelling and regularisation approaches.

1.4 Related publications

Most of this thesis has been included in scientific contributions that have either been published, submitted or are currently in final preparation for submission. A list relating these publications is therefore given herein.

- F.X.C. Andrade, F.M. Andrade Pires, J.M.A. Cesar de Sa, L. Malcher. *Improvement of the Numerical Prediction of Ductile Failure with an Integral Nonlocal Damage Model*. International Journal of Material Forming, v. 2, pp. 439–442, 2009.
- J.M.A. Cesar de Sa, F.M. Andrade Pires, and F.X.C. Andrade. *Local and Nonlocal Modeling of Ductile Damage*. In M. Vaz Jr., E.A. De Souza Neto, and P.A. Muñoz-Rojas, editors, Advanced Computational Materials Modeling: From Classical to Multi-Scale Techniques, chapter 2, pp. 23–72. Wiley-VCH, 2010.
- J.M.A. Cesar de Sa, F.X.C. Andrade, and F.M. Andrade Pires. *Theoretical and Numerical Issues on Ductile Failure Prediction - An Overview*. Computer Methods in Materials Science, v. 10, No. 4, pp. 279–293, 2010.
- F.X.C. Andrade, J.M.A. Cesar de Sa, and F.M. Andrade Pires. *A Ductile Damage Nonlocal Model of Integral-type at Finite Strains: Formulation and Numerical Issues*. International Journal of Damage Mechanics, No. 20, pp. 515–557, 2011.
- F.X.C. Andrade, M. Vogler, J.M.A. Cesar de Sa, and F.M. Andrade Pires. *User-defined Nonlocal Models in LS-DYNA*. Full paper in Proceedings of the 8th LS-DYNA European Users Conference, Strasbourg, 2011.

- F.X.C. Andrade, J.M.A. Cesar de Sa, and F.M. Andrade Pires. *Consistent Linearisation of Non-local Elasto-plastic Models of Integral-type*. In preparation.

- F.X.C. Andrade, J.M.A. Cesar de Sa, and F.M. Andrade Pires. *Assessment and Comparison of Non-local Models for the Mesh-insensitive Description of Ductile Materials*. In Preparation.

- F.X.C. Andrade, J.M.A. Cesar de Sa, and F.M. Andrade Pires. *Finite Element Implementation of a Non-local Gurson-based Damage Model including a Shear Mechanism*. In Preparation.

Chapter 2

Standard Continuum Mechanics and the Finite Element Method

Before we can proceed to the definition of continuous media enriched with the non-local theory, a general review of the main concepts of the standard (local) continuum mechanics needs to be done. These concepts are necessary because many of the aspects of the non-local theory are direct extensions from the local case. Nonetheless, a suitable numerical method also needs to be defined so that solutions in practical engineering can be achieved for a large number of cases and applications. In view of that, we shall adopt the *Finite Element Method* (FEM) throughout this thesis as the general method for the analysis of solids. In the following chapters, we will very often make mention to the concepts presented in this chapter, where the differences between the local and non-local case will be highlighted.

It is important to remark that the present chapter has not the intention to be an exhaustive review neither on Continuum Mechanics nor on the FEM but rather a brief overview on these topics, which are comprehensively addressed in many well-established publications (e.g. [20, 40, 58, 62, 78, 112] in Continuum Mechanics and [12, 31, 33, 34, 65, 122] in FEM). Concerning the notation used, we will adopt most of the symbology used by De Souza Neto et al. [40].

2.1 Kinematics of deformation

Motion

Let $\boldsymbol{p}$ be a particle of a given body in a region Ω_0, delimited by a regular boundary $\partial\Omega_0$. After a given motion $\boldsymbol{\varphi}$, i.e. a deformation of the body within a certain time, the position $\boldsymbol{x}$ of the material particle $\boldsymbol{p}$ at time t is given by

$$\boldsymbol{x} = \boldsymbol{\varphi}(\boldsymbol{p}, t). \tag{2.1}$$

The *displacement* field, $\boldsymbol{u}$, of the material particle $\boldsymbol{p}$ is defined by

$$\boldsymbol{u}(\boldsymbol{p}, t) = \boldsymbol{\varphi}(\boldsymbol{p}, t) - \boldsymbol{p}. \tag{2.2}$$

Assuming that φ is invertible, the position $\boldsymbol{p}$ can be defined by

$$\boldsymbol{p} = \boldsymbol{\varphi}^{-1}(\boldsymbol{x}, t). \tag{2.3}$$

The material particle $\boldsymbol{p}$ is said to be at the *reference* or *undeformed* configuration meanwhile the position $\boldsymbol{x}$ is at the *deformed* configuration. The differences between reference and deformed configurations play a major role in the analysis of finite deformations and therefore will be very often mentioned in this thesis.

The velocity of the particle $\boldsymbol{p}$ is defined by

$$\dot{\boldsymbol{x}} = \frac{\partial \boldsymbol{\varphi}(\boldsymbol{p}, t)}{\partial t}. \tag{2.4}$$

Applying the definition of Eq. (2.3), one can write

$$\boldsymbol{v}(\boldsymbol{x}, t) \equiv \dot{\boldsymbol{x}}(\boldsymbol{\varphi}^{-1}(\boldsymbol{x}, t), t), \tag{2.5}$$

which corresponds to the velocity of the material particle $\boldsymbol{x}$ at time t.

The deformation gradient

The *deformation gradient*, $\boldsymbol{F}$, is a second order tensor that relates $\boldsymbol{p}$ and $\boldsymbol{x}$ through the following definition:

$$\boldsymbol{F}(\boldsymbol{p}, t) = \nabla_p \boldsymbol{\varphi}(\boldsymbol{p}, t) = \frac{\partial \boldsymbol{x}_t}{\partial \boldsymbol{p}}, \tag{2.6}$$

or, using the definition of displacement field of Eq. (2.2), we have

$$\boldsymbol{F} = \boldsymbol{I} + \nabla_p \boldsymbol{u}, \tag{2.7}$$

where $\boldsymbol{I}$ is the second order identity tensor. In the equations above, the deformation gradient has been defined as a function of the *reference* configuration, where the operator ∇_p is generally called *material gradient operator*. Alternatively, the deformation gradient, $\boldsymbol{F}$, can also be defined using the *spatial gradient operator*, ∇_x, that is,

$$\boldsymbol{F}(\boldsymbol{x}, t) = \left[\nabla_x \boldsymbol{\varphi}^{-1}(\boldsymbol{x}, t)\right]^{-1} = \left[\boldsymbol{I} - \nabla_x \boldsymbol{u}\right]^{-1}. \tag{2.8}$$

The *volume change ratio* is represented by the determinant of the deformation gradient, $\det \boldsymbol{F}$, for which the notation below will be adopted throughout this thesis:

$$J \equiv \det \boldsymbol{F}, \tag{2.9}$$

where J is called *Jacobian of deformation*.

To distinguish pure stretches from pure rotations, the *polar decomposition* can be applied to the deformation gradient, which gives

$$\boldsymbol{F} = \boldsymbol{R}\boldsymbol{U} = \boldsymbol{V}\boldsymbol{R}, \tag{2.10}$$

where $\boldsymbol{R}$ is a proper orthogonal tensor called *rotation tensor*. In Eq. (2.10), the symmetric positive definite tensors $\boldsymbol{U}$ and $\boldsymbol{V}$ are, respectively, the *right* and *left stretch tensors*, which can also be expressed as

$$\boldsymbol{U} = \sqrt{\boldsymbol{C}}, \qquad \boldsymbol{V} = \sqrt{\boldsymbol{B}}, \tag{2.11}$$

where $\boldsymbol{C}$ and $\boldsymbol{B}$ are, respectively, the *right* and *left Cauchy-Green strain tensors*, defined by

$$\boldsymbol{C} = \boldsymbol{U}^2 = \boldsymbol{F}^T\boldsymbol{F}, \qquad \boldsymbol{B} = \boldsymbol{V}^2 = \boldsymbol{F}\boldsymbol{F}^T. \tag{2.12}$$

Strain measures

If, after a given deformation, the material particles of a body occupy a different position in space, but the relative distance between them remain the same, it is said that a *pure rotation* has taken place. On the other hand, if the relative distance between two material points has been modified over deformation due to the action of stretching, the surrounding region is said to be *strained*. Straining is related to pure stretches, which in turn are characterised by the right and left

Cauchy-Green strain tensors, $\boldsymbol{C}$ and $\boldsymbol{B}$, defined in the last subsection. However, these quantities are not sufficient to properly quantify straining. Thus, a certain strain measure needs to be adopted.

In a broad sense, there are virtually infinite possibilities to measure straining, so the choice of a strain measure remains arbitrary. In practice, however, this choice is dictated by mathematical and physical convenience. An important class of strain measures is the so-called *Lagrangian strain tensors*, given by

$$\boldsymbol{E}^{(m)} = \begin{cases} \frac{1}{m}\left(\boldsymbol{U}^m - \boldsymbol{I}\right) & , \quad m \neq 0 \\ \ln\left[\boldsymbol{U}\right] & , \quad m = 0 \end{cases} \tag{2.13}$$

where m is a real number and $\ln[\cdot]$ represents the logarithm of a tensor.

In similar manner, another important family of strain tensors can be defined by using the left stretch tensor, $\boldsymbol{V}$. The *Eulerian strain tensors* are expressed as

$$\boldsymbol{\varepsilon}^{(m)} = \begin{cases} \frac{1}{m}\left(\boldsymbol{V}^m - \boldsymbol{I}\right) & , \quad m \neq 0 \\ \ln\left[\boldsymbol{V}\right] & , \quad m = 0. \end{cases} \tag{2.14}$$

In particular, the *logarithmic strain tensor* ($m = 0$) will be often adopted in the following chapters of this thesis.

It is important to remark that, under pure rotations (i.e., $\boldsymbol{F} = \boldsymbol{R}$), any of the strain measures defined above vanishes, that is,

$$\boldsymbol{U} = \boldsymbol{I} \implies \boldsymbol{E}^{(m)} = \boldsymbol{0}, \tag{2.15}$$

$$\boldsymbol{V} = \boldsymbol{I} \implies \boldsymbol{\varepsilon}^{(m)} = \boldsymbol{0}. \tag{2.16}$$

The velocity gradient

Similarly to the case of deformation, where an associated gradient has been defined, it is also possible to define a gradient related to the velocity. The spatial field $\boldsymbol{L}$, called *velocity gradient*, is then expressed as

$$\boldsymbol{L} = \nabla_x \boldsymbol{v}, \tag{2.17}$$

or, alternatively by

$$\boldsymbol{L} = \dot{\boldsymbol{F}}\boldsymbol{F}^{-1}. \tag{2.18}$$

The velocity gradient can be split into a symmetric and a skew part, that is,

$$\boldsymbol{D} = \mathrm{sym}(\boldsymbol{L}), \quad \boldsymbol{W} = \mathrm{skew}(\boldsymbol{L}), \tag{2.19}$$

respectively called *rate of deformation* (or *stretching*) and *spin tensors*. In a physical sense, $\boldsymbol{D}$ is associated with straining meanwhile $\boldsymbol{W}$ is associated with rigid velocities.

Stress measures

Two stress measures will be often used throughout this thesis. The first one is the *Cauchy* or *true stress tensor*, $\boldsymbol{\sigma}$, defined as

$$\boldsymbol{t} = \boldsymbol{\sigma}\boldsymbol{n}, \tag{2.20}$$

where $\boldsymbol{t}$ is the surface traction and $\boldsymbol{n}$ is its associated normal vector.

The Cauchy stress tensor can be split into two contributions

$$\boldsymbol{\sigma} = \boldsymbol{s} + p\boldsymbol{I}, \tag{2.21}$$

where $\boldsymbol{s} = \mathrm{dev}[\boldsymbol{\sigma}]$ is the *deviatoric* part of the true stress tensor and p is the *pressure*, a quantity related to the first invariant of the true stress tensor, defined as

$$p = \frac{1}{3}\mathrm{tr}[\boldsymbol{\sigma}]. \tag{2.22}$$

The second stress measure is the *Kirchhoff stress tensor*, denoted by $\boldsymbol{\tau}$, defined as

$$\boldsymbol{\tau} = J\boldsymbol{\sigma}. \tag{2.23}$$

Analogously to the Cauchy stress, the Kirchhoff stress tensor can also be split into two different parts, i.e.,

$$\boldsymbol{\tau} = \boldsymbol{\tau}_d + \tau_h\boldsymbol{I}, \tag{2.24}$$

where $\boldsymbol{\tau}_d = \mathrm{dev}[\boldsymbol{\tau}]$ and $\tau_h = \frac{1}{3}\mathrm{tr}[\boldsymbol{\tau}]$ are, respectively, the deviatoric and hydrostatic (or spherical) parts.

Another important stress measure is the *first Piola-Kirchhoff stress tensor*, denoted by $\boldsymbol{P}$, also often referred to as the *nominal stress*. This stress measure will be only sporadically used in this thesis and therefore no detailed definitions will be herein provided. The first Piola-Kirchhoff stress tensor relates to the other two

stress measures presented in this section through the following expressions [40]:

$$\boldsymbol{P} \equiv J\boldsymbol{\sigma}\boldsymbol{F}^{-T}, \tag{2.25}$$

$$\boldsymbol{P} \equiv \boldsymbol{\tau}\boldsymbol{F}^{-T}. \tag{2.26}$$

2.2 Fundamental laws

The quantities presented in the previous section are important for the mathematical representation of phenomena such as deformation, motion and straining. However, they cannot be used for predictions if no relation among them is made. Therefore, in this section, we briefly review some fundamental laws that govern the aforementioned physical phenomena and that will be important for the future developments addressed in this thesis.

Conservation of mass

The postulate of conservation of mass requires that

$$\dot{\rho} + \rho \, \mathrm{div}_x \dot{\boldsymbol{u}} = 0 \tag{2.27}$$

where ρ is the *density* at the deformed configuration.

Momentum balance

The *momentum balance*, also referred to as *strong form of the equilibrium equation*, of any given body can be expressed as

$$\mathrm{div}_x \boldsymbol{\sigma} + \boldsymbol{b} = \rho \ddot{\boldsymbol{u}}, \tag{2.28}$$

where $\boldsymbol{b}$ denotes the body force vector in the deformed configuration. The equilibrium equation (2.28) needs to fulfil the following boundary condition:

$$\boldsymbol{t} = \boldsymbol{\sigma}\boldsymbol{n}, \tag{2.29}$$

where $\boldsymbol{t}$ is a traction vector applied on the boundary of the body.

The first and second principles of thermodynamics

The first principle of thermodynamics postulates that the energy must be conserved. This can be mathematically expressed as

$$\rho\dot{e} = \boldsymbol{\sigma} : \boldsymbol{D} + \rho r - \mathrm{div}_x \boldsymbol{q}, \tag{2.30}$$

where e, r and q are, respectively, the *specific internal energy*, the *density of heat production* and the *heat flux*. Throughout this thesis, only processes with constant temperature will be considered. In this case, the first principle reduces to

$$\rho\dot{e} = \boldsymbol{\sigma} : \boldsymbol{D}. \tag{2.31}$$

The equation above states that the rate of internal energy per unit *deformed* volume must equal the stress power, $\boldsymbol{\sigma} : \boldsymbol{D}$, per unit *deformed* volume. Making use of the relation below,

$$\bar{\rho} = J\rho, \tag{2.32}$$

where $\bar{\rho}$ denotes the reference density, it is possible to re-write Equation (2.31) as

$$\bar{\rho}\dot{e} = \boldsymbol{\tau} : \boldsymbol{D}. \tag{2.33}$$

The second principle of thermodynamics is associated with the so-called *irreversibility of entropy production*, expressed by the following inequality:

$$\rho T\dot{s} + \mathrm{div}_x \boldsymbol{q} - \rho r \geq 0, \tag{2.34}$$

where s denotes the *entropy* and T the *temperature*. Similar to the case of the first principle of thermodynamics, if only isothermal processes are considered, Equation (2.34) is then given by

$$\rho T\dot{s} \geq 0. \tag{2.35}$$

Pre-multiplying Equation (2.35) by J, we have

$$\bar{\rho} T\dot{s} \geq 0. \tag{2.36}$$

The Clausius-Duhem inequality

Firstly, we introduce the *Helmholtz free energy*, ψ, defined by

$$\psi = e - Ts. \tag{2.37}$$

Re-arranging Equation (2.37) and differentiating with respect to time, we have

$$T\dot{s} = \dot{e} - \dot{\psi}. \tag{2.38}$$

We remark that the temperature has been assumed constant, thus, $\dot{T} = 0$. Using Equation (2.31), we conclude that

$$\bar{\rho}T\dot{s} = \boldsymbol{\tau} : \boldsymbol{D} - \bar{\rho}\dot{\psi}. \tag{2.39}$$

Finally, substituting Equation (2.39) gives

$$\boldsymbol{\tau} : \boldsymbol{D} - \bar{\rho}\dot{\psi} \geq 0. \tag{2.40}$$

The fundamental inequality above is called *Clausius-Duhem inequality*.

2.3 The quasi-static IBVP

The fundamental laws presented in the last section allow us to define an *Initial Boundary Value Problem* (IBVP) associated with the description of a given deformation process. The solution of the IBVP delivers the prediction of how a given solid will mechanically behave when subjected to certain boundary conditions. Within the scope of this thesis, only quasi-static problems will be addressed, hence, any inertial effects will be neglected[1]. Thus, the equilibrium equation (2.28), in the strong form, is re-written to be given by

$$\mathrm{div}_x\boldsymbol{\sigma} = \mathbf{0}. \tag{2.41}$$

Multiplying Equation (2.41) by a *virtual displacement*, $\boldsymbol{\eta}$, and integrating over the volume, we have

$$\int_{\varphi(\Omega)} (\mathrm{div}_x\boldsymbol{\sigma})^T\boldsymbol{\eta}\, dV = 0. \tag{2.42}$$

After some straightforward operations, Equation (2.42) becomes

$$\int_{\varphi(\Omega)} \left[\boldsymbol{\sigma} : \nabla_x\boldsymbol{\eta} - (\mathrm{div}_x\boldsymbol{\sigma}\cdot\boldsymbol{\eta})\right] dV = 0. \tag{2.43}$$

[1]In Chapter 7, an explicit finite element formulation will be addressed. Although also in that chapter only quasi-static problems will be analysed, the explicit framework requires the consideration of the inertial effects on its formulation. Such requirement will be recalled accordingly in Chapter 7, where the necessary equations will be properly reviewed.

Making use of the divergence theorem, we have

$$\int_{\varphi(\Omega)} \boldsymbol{\sigma} : \nabla_x \boldsymbol{\eta}\, dV - \int_{\varphi(\partial\Omega)} (\boldsymbol{\sigma} \cdot \boldsymbol{n})^T \boldsymbol{\eta}\, dA = 0. \tag{2.44}$$

Finally, substituting Equation (2.29) into Equation (2.44) leads to

$$\int_{\varphi(\Omega)} \boldsymbol{\sigma} : \nabla_x \boldsymbol{\eta}\, dV - \int_{\varphi(\partial\Omega)} \boldsymbol{t} \cdot \boldsymbol{\eta}\, dA = 0. \tag{2.45}$$

Equation (2.45) is called *weak form of the equilibrium equation*. The use of the weak form can significantly facilitate the use of efficient numerical methods for the solution of the structural IBVP. With the definition of weak equilibrium at hand, we can define the quasi-static IBVP, in the spatial description, as follows.

Problem 2.1. *Given a prescribed deformation gradient history,*

$$\boldsymbol{F}(t) = \boldsymbol{I} + \nabla_p \boldsymbol{u}(\boldsymbol{p}, t), \tag{2.46}$$

and the Cauchy stress, at each point of the body expressed as

$$\boldsymbol{\sigma}(t) = \boldsymbol{\sigma}\left(\boldsymbol{F}(t), \boldsymbol{\alpha}(t)\right), \tag{2.47}$$

obtained from the solution of the constitutive initial boundary value problem where $\boldsymbol{\alpha}$ *is the set of internal variables associated with the material, find a kinematically admissible displacement function,* $\boldsymbol{u} \in \mathcal{K}$*, such that the equation*

$$\int_{\varphi(\Omega)} \boldsymbol{\sigma}(t) : \nabla_x \boldsymbol{\eta}\, dV - \int_{\varphi(\partial\Omega)} \boldsymbol{t}(t) \cdot \boldsymbol{\eta}\, dA = 0 \tag{2.48}$$

is satisfied for all $t \in [t_0, t_n]$ *and for all* $\boldsymbol{\eta} \in \mathcal{V}_t$*.*

The set of kinematically admissible displacements, $\mathcal{K}$*, and the space of virtual displacements at time* t*,* $\mathcal{V}_t$*, are respectively given by*

$$\mathcal{K} = \left\{\boldsymbol{u} : \Omega \to \mathcal{U} | \boldsymbol{u}(\boldsymbol{p}, t) = \bar{\boldsymbol{u}}(\boldsymbol{p}, t), t \in [t_0, t_n], \boldsymbol{p} \in \partial\Omega_u\right\}, \tag{2.49}$$

$$\mathcal{V}_t = \left\{\boldsymbol{\eta} : \Omega \to \mathcal{U} | \boldsymbol{\eta} = \boldsymbol{0} \in \partial\Omega_u(t)\right\}. \tag{2.50}$$

Unfortunately, analytical solutions for the problem defined above exist only for a restricted set of special cases. For accurate predictions of the mechanical behaviour of solids in the general case, the use of numerical methods is therefore indispensable.

The material version

For reference, the material version of the weak form of the equilibrium equation is also herein provided, which reads

$$\int_{\Omega} \boldsymbol{P} : \nabla_p \boldsymbol{\eta} \, dV - \int_{\partial\Omega} \bar{\boldsymbol{t}} \cdot \boldsymbol{\eta} \, dA = 0, \tag{2.51}$$

where $\bar{\boldsymbol{t}}$ is the surface traction per unit reference area. In the context of this thesis, Equation (2.51) will be particularly useful for the linearisation of the equilibrium equation provided in Appendix A.

2.4 Displacement-based finite elements

In this section, the general concepts of the finite element method formulated with a displacement-based approach will be briefly addressed. The finite element method has been chosen in this thesis as the base numerical tool mainly due to its versatility and its high effectiveness when adopted for the simulation of deformation processes.

2.4.1 Spatial discretisation

As stressed out above, the solution of Problem 2.1 often requires the use of some sort of numerical strategy. Within a typical finite element framework, the field variables are discretised through the so-called *interpolation* or *shape* functions. In the case of displacement-based finite elements, the interpolated field variable are the displacements. Within a given element e, the interpolation is assumed to be

$$\boldsymbol{u}(\boldsymbol{x}) \equiv \sum_{i=1}^{n_{node}} N_i^{(e)}(\boldsymbol{x}) \mathbf{u}_i, \tag{2.52}$$

where $N_i^{(e)}(\boldsymbol{x})$ is the shape function associated with node i (evaluated at $\boldsymbol{x}$) and n_{node} is the number of nodes of the element. In similar manner, a global interpolation function can also be set, that is,

$$\boldsymbol{u}(\boldsymbol{x}) \equiv \sum_{i=1}^{n_{poin}} N_i^{g}(\boldsymbol{x}) \mathbf{u}_i, \tag{2.53}$$

where n_{poin} is the total number of nodes of the finite element mesh and $N_i^g(\boldsymbol{x})$ is the *global interpolation matrix*, which can be represented by

$$\mathbf{N}^g(\boldsymbol{x}) = \left[\begin{array}{cccc} \text{diag}[N_1^g(\boldsymbol{x})] & \text{diag}[N_2^g(\boldsymbol{x})] & \cdots & \text{diag}[N_{n_{poin}}^g(\boldsymbol{x})] \end{array} \right], \tag{2.54}$$

where $\text{diag}[N_i^g]$ denotes a $n_{dim} \times n_{dim}$ diagonal matrix defined as

$$\text{diag}[N_i^g] = \left[\begin{array}{cccc} N_i^g & 0 & \cdots & 0 \\ 0 & N_i^g & \cdots & 0 \\ \vdots & \vdots & \ddots & \vdots \\ 0 & 0 & \cdots & N_i^g \end{array} \right]. \tag{2.55}$$

At this point, it is also convenient to define the global vector of nodal displacements, given by

$$\mathbf{u} = \left[\begin{array}{cccccccc} \text{u}_1^1, & \cdots & \text{u}_{n_{dim}}^1, & \cdots\cdots & \text{u}_1^{n_{poin}}, & \cdots & \text{u}_{n_{dim}}^{n_{poin}} \end{array} \right]^T. \tag{2.56}$$

With the above matrix notation at hand, Equation (2.53) can be re-phrased to be given by

$$\boldsymbol{u}(\boldsymbol{x}) = \mathbf{N}^g(\boldsymbol{x})\mathbf{u} \tag{2.57}$$

where the equation above represents the interpolation of the displacement field by means of discrete functions. Analogously, we can write the field of virtual displacements to be given by

$$\boldsymbol{\eta}(\boldsymbol{x}) = \mathbf{N}^g(\boldsymbol{x})\boldsymbol{\eta}. \tag{2.58}$$

We also define the global *discrete symmetric gradient matrix*, $\mathbf{B}^g$, which in the case of plane stress and plane strain problems assumes the form

$$\mathbf{B}^g = \left[\begin{array}{cccccccc} N_{1,1}^g & 0 & N_{2,1}^g & 0 & \cdots & N_{n_{poin},1}^g & 0 \\ 0 & N_{1,2}^g & 0 & N_{2,2}^g & \cdots & 0 & N_{n_{poin},2}^g \\ N_{1,2}^g & N_{1,1}^g & N_{2,2}^g & N_{2,1}^g & \cdots & N_{n_{poin},2}^g & N_{n_{poin},1}^g \end{array} \right], \tag{2.59}$$

where use of the following notation has been made:

$$(\cdot)_{i,j} = \frac{\partial (\cdot)_i}{\partial x_j}. \tag{2.60}$$

For completeness, the *global discrete full gradient operator*, $\mathbf{G}^g$, is also provided herein, whose format in plane stress and plane strain analyses is given by

$$\mathbf{G}^g = \begin{bmatrix} N^g_{1,1} & 0 & N^g_{2,1} & 0 & \cdots & N^g_{n_{poin},1} & 0 \\ 0 & N^g_{1,1} & 0 & N^g_{2,1} & \cdots & 0 & N^g_{n_{poin},1} \\ N^g_{1,2} & 0 & N^g_{2,2} & 0 & \cdots & N^g_{n_{poin},2} & 0 \\ 0 & N^g_{1,2} & 0 & N^g_{2,2} & \cdots & 0 & N^g_{n_{poin},2} \end{bmatrix}. \tag{2.61}$$

2.4.2 Temporal discretisation. The non-linear incremental finite element procedure

In practical engineering applications, it is often required the modelling of materials that are dependent of the deformation history. Such materials are called *path-dependent* and, regardless whether they take strain rate effects into account or not, a suitable temporal discretisation needs to be performed. Within the context of most of this thesis, a pseudo-time discretisation between the time increments $[t_n, t_{n+1}]$ will be considered for which a fully implicit scheme is adopted[2].

For a generic path-dependent material model, an incremental constitutive function, $\hat{\boldsymbol{\sigma}}$, is assumed to exist, i.e.,

$$\boldsymbol{\sigma}_{n+1} = \hat{\boldsymbol{\sigma}}(\boldsymbol{F}_{n+1}, \boldsymbol{\alpha}_n). \tag{2.62}$$

In practice, the function $\hat{\boldsymbol{\sigma}}$ is associated with an integration algorithm that computes the material behaviour for a given deformation gradient $\boldsymbol{F}_{n+1}$ and set of internal variables, $\boldsymbol{\alpha}_n$, which remain constant within $[t_n, t_{n+1}]$. Accordingly, a similar incremental function for the set of internal variables is also defined:

$$\boldsymbol{\alpha}_{n+1} = \hat{\boldsymbol{\alpha}}(\boldsymbol{F}_{n+1}, \boldsymbol{\alpha}_n). \tag{2.63}$$

Up to this point, it suffices to leave the incremental constitutive functions $\hat{\boldsymbol{\sigma}}$ and $\hat{\boldsymbol{\alpha}}$ unspecified for the sake of generality. In the following chapters, these functions will be defined accordingly for the non-local case.

The non-linear incremental finite element equation

The definition of the incremental constitutive function of Section 2.4.2, combined with the spatial discretisation presented in Section 2.4.1, allows the definition of

[2]In Chapter 7, an FE explicit scheme will be adopted for which the proper time discretisation will be presented accordingly.

the *incremental finite element equilibrium equation*, obtained after some straightforward substitutions and re-arrangements from Equation (2.45):

$$\mathbf{r}(\mathbf{u}_{n+1}) \equiv \mathbf{f}^{int}(\mathbf{u}_{n+1}) - \mathbf{f}^{ext} = \mathbf{0}, \tag{2.64}$$

where $\mathbf{f}^{int}$ and $\mathbf{f}^{ext}$ are, respectively, the *internal* and *external force vectors*, defined for a given element e as

$$\mathbf{f}^{int}_{(e)} = \int_{\varphi_{n+1}(\Omega^{(e)})} \mathbf{B}^T \hat{\boldsymbol{\sigma}}(\boldsymbol{F}_{n+1}, \boldsymbol{\alpha}_n)\, dV, \tag{2.65}$$

$$\mathbf{f}^{ext}_{(e)} = \int_{\varphi_{n+1}(\partial\Omega^{(e)})} \mathbf{N}^T \boldsymbol{t}_{n+1}\, dA. \tag{2.66}$$

Within the scope of this thesis, Equation (2.64) will be generally non-linear and therefore requires an adequate (numerical) method for its solution. Considering an incremental scheme, in which a given fraction of the external prescribed load is applied at each increment, Equation (2.64) is solved as summarised in Box 1.

Remark 2.1. *In practice, the external force is computed by the expression*

$$\mathbf{f}^{ext}_{n+1} = \lambda_{n+1} \bar{\mathbf{f}}^{ext}, \tag{2.67}$$

where $lambda_{n+1}$ *is the prescribed load factor at time* t_{n+1} *and* $\bar{\mathbf{f}}^{ext}$ *is computed only once at the first iteration of the incremental procedure through the expression*

$$\bar{\mathbf{f}}^{ext}_{(e)} = \int_{\varphi_{n+1}(\partial\Omega^{(e)})} \mathbf{N}^T \bar{\boldsymbol{t}}\, dA, \tag{2.68}$$

where $\bar{\boldsymbol{t}}$ *is a prescribed field which remains constant through the incremental procedure.*

Numerical integration of $\mathbf{f}^{int}$ and $\mathbf{f}^{ext}$

One important aspect of the finite element implementation is the substitution of the exact integrals of Equations (2.65) and (2.66) by some sort of numerical procedure. In this thesis, both the internal and external force vectors will be integrated using standard Gaussian quadratures. For instance, in the case of the internal force vector, $\mathbf{f}^{int}$ is approximated by the following expression:

$$\mathbf{f}^{int}_{(e)} = \int_{\varphi_{n+1}(\Omega^{(e)})} \mathbf{B}^T \hat{\boldsymbol{\sigma}}\, dV \approx \sum_{i=1}^{ngp} w_i J_i \mathbf{B}_i^T \hat{\boldsymbol{\sigma}}_i, \tag{2.69}$$

Box 1: The incremental non-linear finite element scheme – implicit solution.

(i) Assemble the global external force vector, $\bar{\mathbf{f}}^{ext}$

(ii) Initialise increment counter $i = 1$

(iii) Set load factor λ_i

(iv) Solve the non-linear equilibrium equation

$$\mathbf{r}(\mathbf{u}_i) = \mathbf{f}^{int}(\mathbf{u}_i) - \lambda_i \bar{\mathbf{f}}^{ext} = \mathbf{0}$$

(v) Update increment counter $i = i + 1$

(vi) Check if prescribed number of increments has been achieved

```
IF i > NINCR  THEN
     EXIT
ELSE
     GOTO (iii)
ENDIF
```

where w_i and J_i are, respectively, the Gaussian weight and the Jacobian at the i^{th} integration point. A similar procedure is carried out for the external force vector. The use of the Gaussian quadrature will be particularly important in the numerical implementation of the non-local models developed in this thesis as it will become clear in the following chapters.

The Newton-Raphson method

As stressed out before, the equilibrium equation (2.64) is generally non-linear and demands an appropriate solution method. We will adopt herein the Newton-Raphson method, which is particularly attractive due its quadratic rates of convergence. Following standard procedures of the method and particularising for the case of the finite element framework presented in this chapter, the displacements are updated as

$$\mathbf{u}_{n+1}^{k+1} = \mathbf{u}_{n+1}^{k} - \left(\frac{\partial \mathbf{r}}{\partial \mathbf{u}_{n+1}} \bigg|_{\mathbf{u}_{n+1}^{k}} \right)^{-1} \mathbf{r}(\mathbf{u}_{n+1}^{k}). \tag{2.70}$$

Equation (2.70) can be more conveniently written as

$$\mathbf{K}_T \delta \mathbf{u} = -\mathbf{r}(\mathbf{u}_{n+1}^{k}), \tag{2.71}$$

where

$$\mathbf{u} = \mathbf{u}_{n+1}^{k+1} - \mathbf{u}_{n+1}^{k}, \tag{2.72}$$

and $\mathbf{K}_T$ is called *global tangent stiffness matrix*, given by

$$\mathbf{K}_T = \left.\frac{\partial \mathbf{r}}{\partial \mathbf{u}_{n+1}}\right|_{\mathbf{u}_{n+1}^{k}}. \tag{2.73}$$

The correct derivation of the tangent stiffness is crucial to guarantee the quadratic rates of convergence of the Newton-Raphson method. In the case of finite strains within a spatial description, the expression for Equation (2.73) arises quite naturally from the linearisation of the equilibrium equation in its weak form, given in detail in Appendix A. Recalling that the internal force vector is integrated using a Gaussian quadrature (Equation 2.69), the element stiffness matrix is then given by

$$\mathbf{K}_T^{(e)} = \sum_{i=1}^{ngp} w_i J_i \mathbf{G}_i^T \hat{\mathbf{a}}_i \mathbf{G}_i, \tag{2.74}$$

where $\mathbf{a}_i$ is the *spatial tangent modulus* whose components are given by

$$\mathsf{a}^{ijkl} = \frac{1}{J}\frac{\partial \tau^{ij}}{\partial F^{km}} F^{lm} - \sigma^{il}\delta^{jk}. \tag{2.75}$$

For convenience, the full Newton-Raphson procedure associated with the present finite element framework at finite strains is summarised in Box 2.

Remark 2.2. *In this thesis, superscripts in tensors will generally correspond to their tensorial components, meanwhile subscripts correspond to the integration point at which the tensor is evaluated. This notation will be particularly useful in the following chapters, where distinction between constitutive quantities associated with different integration points is crucial in the non-local case.*

2.5 Conclusions

In this chapter, the general concepts of continuum mechanics and of the finite element method have been briefly reviewed. It is important to remark that the concepts presented so far are well-established and widely accepted either by academic researchers or by the industry. Many of the concepts presented herein will be used as base for comparison with the non-local theory and its associated numerical treatment.

Box 2: Newton-Raphson scheme for the solution of the incremental non-linear finite element equilibrium equation – implicit solution.

(i) Set $k = 1$, initial guess and residual function array

$$\mathbf{u}_{n+1}^{k} = \mathbf{u}_n; \qquad \mathbf{r}^{k} = \mathbf{f}^{\text{int}}(\mathbf{u}_n) - \lambda_{n+1}\overline{\mathbf{f}}^{\text{ext}}$$

(ii) Compute the consistent spatial tangent moduli

$$\mathsf{a}^{ijkl} = \frac{1}{J}\frac{\partial \hat{\tau}^{ij}}{\partial F^{km}}F^{lm} - \sigma^{il}\delta^{jk}$$

(iii) Assemble element tangent stiffness matrices

$$\mathbf{K}_T^{(e)} = \sum_{i=1}^{ngp} w_i J_i \mathbf{G}_i^T \hat{\mathbf{a}}_i \mathbf{G}_i$$

(iv) Assemble global stiffness and solve for $\delta\mathbf{u}^{k+1}$

$$\mathbf{K}_T \delta\mathbf{u}^{k+1} = -\mathbf{r}^{k}$$

(v) Update displacements

$$\mathbf{u}_{n+1}^{k+1} = \mathbf{u}_{n+1}^{k} + \delta\mathbf{u}^{k+1}$$

(vi) Update the deformation gradient

$$\boldsymbol{F}_{n+1}^{k+1} = \left(\boldsymbol{I} - \nabla_x \mathbf{u}_{n+1}^{k+1}\right)^{-1}$$

(vii) Update stresses and internal variables

$$\boldsymbol{\sigma}_{n+1}^{k+1} = \hat{\boldsymbol{\sigma}}(\boldsymbol{F}_{n+1}^{k+1}, \boldsymbol{\alpha}_n); \qquad \boldsymbol{\alpha}_{n+1}^{k+1} = \hat{\boldsymbol{\alpha}}(\boldsymbol{F}_{n+1}^{k+1}, \boldsymbol{\alpha}_n)$$

(viii) Compute element internal force

$$\mathbf{f}_{(e)}^{\text{int}} = \sum_{i=1}^{ngp} w_i J_i \mathbf{B}_i^T \boldsymbol{\sigma}_{n+1}^{k+1}$$

(ix) Assemble the global internal force array and re-compute the residual function

$$\mathbf{r}^{k+1} = \mathbf{f}^{\text{int}} - \lambda_{n+1}\overline{\mathbf{f}}^{\text{ext}}$$

(x) Check convergence

$$\texttt{IF } \left\|\mathbf{r}^{k+1}\right\| < TOL \quad \texttt{EXIT}$$

(xi) Set $k = k + 1$ and go to (ii).

Chapter 3

A Lemaitre-based Non-local Ductile Damage Model of Integral-type at Finite strains

The appropriate modelling of plastic straining and ductile damage, which is crucial to describe the deformation of metals undergoing large deformations, has been the focus of extensive research effort over the last decades. Since the pioneering work of Kachanov [72] and Rabotnov [97], when initial concepts of Continuum Damage Mechanics (CDM) were developed, several significant contributions have emerged and new theories proposed for the description of material progressive internal degradation [e.g., 57, 74, 75, 76, 113]. Likewise, numerical methods have rapidly evolved and many authors have proposed efficient algorithms that are able to simulate material deformation at finite strains [e.g., 91, 107, 119] and predict ductile fracture onset [e.g., 5, 36, 38].

However, a large number of models within the CDM theory are rooted on the assumption of the so-called *local continuum*. In local media, the behaviour of the material is completely represented by a point-wise constitutive law, which is independent of the influence of surrounding material points. As a matter of fact, the local theory assumes that the material is continuous at any scale and, therefore, size effects are inherently neglected. Nevertheless, when a structural problem formulated within the local theory experiences softening regimes, it becomes inobjective since the equilibrium partial differential equations lose ellipticity (or hyperbolicity, in transient problems). As a consequence, the IBVP has no longer a unique solution as it is dependent upon spatial discretisation [94]. This adversity, often referred to as *pathological mesh dependency*, causes plastic strain (and other

dissipative variables such as damage) to concentrate into a single element (or a layer of elements) as the mesh is subsequently refined in a typical finite element analysis.

To circumvent this pathology, the non-local theory has emerged as an alternative approach which incorporates an intrinsic length into the traditional continuum theory. If properly formulated, the theory overcomes the problem of pathological mesh dependency and acts as a localisation limiter for both plasticity and damage, either by means of gradient-enhanced or integral-type formulations.

Despite the fact that some contributions have shown that both integral-type and implicit gradient-dependent non-local models are, in general, equivalent[1] and present similar characteristics [89, 109], these two competitive approaches have been most commonly adopted to model distinct material behaviour. In particular, ductile materials have been enhanced, almost exclusively, by means of gradient-dependent constitutive models. In this case, numerical implementation issues and extension to finite strains have been extensively addressed by many authors [e.g., 26, 47, 55, 81, 101, amongst several others]. On the other hand, non-local formulations of integral-type have been usually employed in cojunction with material laws that are typically adopted for the description of quasi-brittle materials like concrete and soil [e.g., 18, 22, 30, 41, 56, 87, 93, amongst many others]. Despite significant advances both in theoretical and computational fields concerning the integral-type formulation, only a limited number of works have been devoted to model ductile deformation with this kind of non-local theory [e.g. 114].

The integral-type of non-local theory has been mainly avoided due to the integral averaging which, by definition, prevents the material model to be formulated in a point-wise manner. Some authors claim [e.g. 88] that this approach can be prohibitive, especially for elasto-plastic damage models which are, in the great majority of cases, highly non-linear. Instead, if an implicit gradient-dependent theory is used, a diffusive equation is added to the structural problem and the non-local variable is treated as an additional degree of freedom. The main advantage of the gradient approach is that the problem keeps a local-like format; however, additional FE discretisation is necessary and, since the non-local variable is considered to be an additional degree of freedom of the structural problem rather than a purely constitutive quantity, its physical interpretation becomes, to some extent, abstract.

The integral-type formulation, on the other hand, keeps non-locality entirely at the material level. This means that neither additional degrees of freedom nor

[1]The models are equivalent in the sense that they are both *strongly non-local*.

extra diffusive equations are necessary within the integral-type framework. In fact, its main attribute, when compared to the local approach, is that the non-local constitutive problem has an extra degree of non-linearity since it depends on neighbouring material points. As a consequence, the typical loading-unloading conditions cannot be fulfilled point-wisely. Most recent gradient-enhanced theories have tackled this shortcoming (which is also present in the gradient counterpart of the non-local theory) by satisfying the loading-unloading conditions only in a weak sense [e.g. 35, 55, 88], a direct consequence of the additional diffusive equation embedded in the global structural problem. The integral-type theory, on the other hand, needs to ensure these conditions on the material level and this has been regarded as a major drawback. However, iterative methods can be used in order to fulfil the loading-unloading conditions. For instance, Strömberg and Ristinmaa [110] have proposed a strategy to solve a hybrid local/non-local elasto-plastic model by means of a modified Newton-Raphson method. More recently, Benvenuti and Borino [18] have solved a thermodynamically consistent non-local model for quasi-brittle materials using a projected Jacobi method. Later, Benvenuti and Tralli [19] have assessed different iterative solution methods for non-local models of integral-type with linear hardening. As a matter of fact, elasto-plastic damage models with complex non-linear evolution laws can also be efficiently integrated by using these techniques.

With regard to the theoretical formulation of non-local constitutive models, the works of Polizzotto et al. [96], Borino et al. [21] and Borino et al. [22] have, amongst others, provided a consistent thermodynamic framework for the non-local theory. These authors have made use of the concept of a non-local residual which accounts for energy exchanges between material particles in non-local media. Hence, the dissipation inequality, which has to be written in a global integral form due to the nature of the non-local constitutive model, could be re-written in a convenient local form. However, they have limited their theory to small-strain plasticity and elastic-damage frameworks. More recently, some authors have extended these concepts to finite strain plasticity but, to the author's knowledge, exclusively for gradient-enhanced theories (for instance in [95]).

The main goal of this chapter is to propose a non-local theory of integral-type suitable for finite strain analysis which incorporates many of the aforementioned advances. By adopting the well established multiplicative hyperelasto-plastic framework [91, 107, 119], we can derive a straightforward numerical implementation of the non-local constitutive model, which requires minor modifications to existing finite element codes.

This chapter is organised in the following fashion. In the first section, we briefly revise some general concepts and definitions of the multiplicative hyperelasto-plasticity framework. Then, we present the non-local theory and its underlying assumptions together with the implications of extending the theory to finite strains. The following section highlights the definition of the constitutive model within a consistent thermodynamical framework which is followed by the establishment of the constitutive equations starting from the generalised normality rule. Subsequently, the numerical implementation of the non-local model is described in detail where an efficient material integration algorithm is provided. Finally, some numerical examples show the ability of the proposed model to eliminate the pathological mesh dependence, followed by general final conclusions.

3.1 General kinematics of multiplicative hyper-elasto-plasticity

The intention of this section is to provide a brief review of some important definitions that will be employed in further developments rather than to provide a detailed review on the multiplicative hyperlasto-plasticity framework which is already well established [see 40, 91, 106, 107, 119, for a more detailed discussion]. The deformation gradient, $\boldsymbol{F}$, can be decomposed in the product

$$\boldsymbol{F} = \boldsymbol{F}^e \boldsymbol{F}^p, \tag{3.1}$$

where $\boldsymbol{F}^e$ and $\boldsymbol{F}^p$ are, respectively, the elastic and plastic deformation gradients. The multiplicative split of $\boldsymbol{F}$ assumes the existence of a local unstressed intermediate configuration that corresponds to a deformed configuration which has been elastically unloaded.

The polar decomposition can be straightforwardly employed within the multiplicative framework and we obtain the following useful relations:

$$\boldsymbol{F}^e = \boldsymbol{R}^e \boldsymbol{U}^e = \boldsymbol{V}^e \boldsymbol{R}^e, \tag{3.2}$$

$$\boldsymbol{F}^p = \boldsymbol{R}^p \boldsymbol{U}^p = \boldsymbol{V}^p \boldsymbol{R}^p, \tag{3.3}$$

where $\boldsymbol{R}^e$, $\boldsymbol{U}^e$ and $\boldsymbol{V}^e$ are the elastic rotation, right and left elastic stretch tensors, respectively. Likewise, $\boldsymbol{R}^p$, $\boldsymbol{U}^p$ and $\boldsymbol{V}^p$ are named the plastic rotation, right and left plastic stretch tensors.

The velocity gradient, which can be defined as

$$\boldsymbol{L} \equiv \dot{\boldsymbol{F}}\boldsymbol{F}^{-1}, \tag{3.4}$$

may also be expressed in terms of $\boldsymbol{F}^e$ and $\boldsymbol{F}^p$:

$$\boldsymbol{L} = \boldsymbol{L}^e + \boldsymbol{F}^e\boldsymbol{L}^p\left(\boldsymbol{F}^e\right)^{-1}, \tag{3.5}$$

where we have defined

$$\boldsymbol{L}^e \equiv \dot{\boldsymbol{F}}^e\left(\boldsymbol{F}^e\right)^{-1}, \qquad \boldsymbol{L}^p \equiv \dot{\boldsymbol{F}}^p\left(\boldsymbol{F}^p\right)^{-1}. \tag{3.6}$$

We can also define the plastic stretch and plastic spin as

$$\boldsymbol{D}^p \equiv \mathrm{sym}\left[\boldsymbol{L}^p\right], \qquad \boldsymbol{W}^p \equiv \mathrm{skew}\left[\boldsymbol{L}^p\right]. \tag{3.7}$$

The plastic stretch, $\boldsymbol{D}^p$, which is defined at the intermediate configuration, can be rotated into the deformed configuration by:

$$\tilde{\boldsymbol{D}}^p = \boldsymbol{R}^e\boldsymbol{D}^p\boldsymbol{R}^{e^T} = \boldsymbol{R}^e\mathrm{sym}\left[\dot{\boldsymbol{F}}^p\boldsymbol{F}^{p-1}\right]\boldsymbol{R}^{e^T}. \tag{3.8}$$

The strain tensor adopted to measure elastic deformations will be the *logarithmic elastic strain tensor*, which is expressed as

$$\boldsymbol{\varepsilon}^e = \ln\boldsymbol{V}^e = \frac{1}{2}\ln\boldsymbol{B}^e, \tag{3.9}$$

where $\boldsymbol{B}^e = \left(\boldsymbol{V}^e\right)^2 = \boldsymbol{F}^e\boldsymbol{F}^{e^T}$ is the *elastic left Cauchy-Green tensor*.

3.2 Non-local theory

The derivation of any non-local theory starts from the choice of the variable to be enhanced by non-locality. Typical choices are, amongst others, the regularisation of variables related to kinematics (such as the strain tensor), regularisation of internal variables (e.g. scalar measurements of the amount of plastic strain or damage) or regularisation of thermodynamic forces power-conjugated with internal variables (for instance, the elastic energy release rate in damage models). With this wide range of possibilities, it is difficult at first glance to decide which option is more effective and which one should be used. In fact, the choice of the non-local variable depends on the kind of material to be modelled and on the nature of the problem to be solved. In the particular case of elasto-plastic damaging ductile

solids, the internal degradation of the material, which in the CDM theory is usually treated by means of some damage measurement as an internal variable, is closely linked to the localisation phenomenon. Therefore, the choice of damage as the non-local variable is quite natural if we are trying to model ductile deformation and this option[2] will be used in all the developments of this chapter. We remark, however, that the developments presented here are limited to a scalar isotropic damage variable, although many of the general concepts of the non-local theory presented may be extended to more sophisticated measurements of damage.

Once the non-local variable is chosen, its non-local counterpart can be expressed, in the integral-type formulation, by means of the spatially weighted averaging integral as

$$\bar{D}(\boldsymbol{x}) = \int_V \beta(\boldsymbol{x}, \boldsymbol{\xi}) D(\boldsymbol{\xi})\, dV(\boldsymbol{\xi}), \tag{3.10}$$

where D and $\bar{D}$ are, respectively, the local and non-local damage variables and $\beta(\boldsymbol{x}, \boldsymbol{\xi})$ is a weighted averaging operator. It is important to remark that $\bar{D}(\boldsymbol{x})$ represents the measurement of non-local damage at a generic material point denoted by $\boldsymbol{x}$, which has been averaged over a finite volume V. The size of the non-local volume is dictated by a constitutive parameter generally called *intrinsic length* which has a physical dimension of length and takes, in an averaged sense, the influence of the micro-structure into account.

The averaging operator, $\beta(\boldsymbol{x}, \boldsymbol{\xi})$, must satisfy the normalising condition

$$\int_V \beta(\boldsymbol{x}, \boldsymbol{\xi})\, dV(\boldsymbol{\xi}) = 1, \tag{3.11}$$

in order to keep uniform fields. Usually, the normalisation is done by means of a penalisation as [14, 68]

$$\beta(\boldsymbol{x}, \boldsymbol{\xi}) = \frac{\alpha(\boldsymbol{x}, \boldsymbol{\xi})}{\Omega_r(\boldsymbol{x})}, \tag{3.12}$$

where Ω_r is commonly referred to as *representative volume* [22, 110] and is given by

$$\Omega_r(\boldsymbol{x}) = \int_V \alpha(\boldsymbol{x}, \boldsymbol{\xi})\, dV(\boldsymbol{\xi}), \tag{3.13}$$

and $\alpha(\boldsymbol{x}, \boldsymbol{\xi})$ is a prescribed weighting function. The disadvantage of this method is that the averaging operator is not symmetric, i.e., $\beta(\boldsymbol{x}, \boldsymbol{\xi}) \neq \beta(\boldsymbol{\xi}, \boldsymbol{x})$. The lack of symmetry stems from the fact that $\Omega_r(\boldsymbol{x})$ varies near boundaries. This characteristic is schematically illustrated in Figure 3.1. Evaluating the weighting function for the points located at $\boldsymbol{x}_1$ and $\boldsymbol{x}_2$, we easily conclude that $\alpha(\boldsymbol{x}_1, \boldsymbol{x}_2) =$

[2] A comprehensive comparison of different non-local variables in Chapter 6 will make clear that the choice of damage as the non-local variable is preferred.

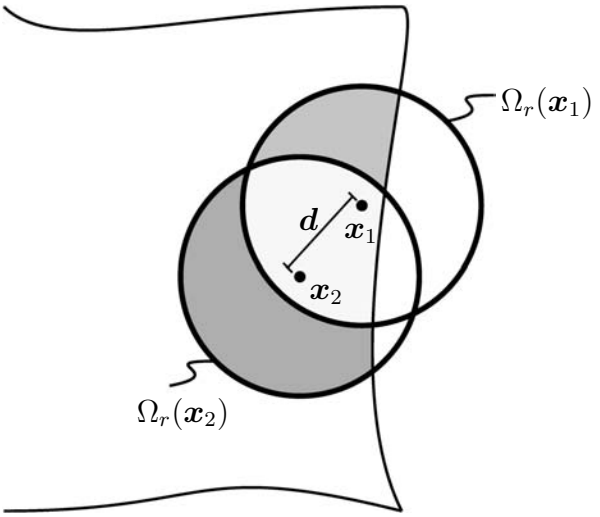

FIGURE 3.1: Schematic illustration of the lack of symmetry of the non-symmetric averaging operator $\beta(\boldsymbol{x}, \boldsymbol{\xi})$ of Equation (3.12).

$\alpha(\boldsymbol{x}_2, \boldsymbol{x}_1)$ since the distance between these points is the same, regardless the point from which it is measured. However, the representative volumes measured from both points will be distinct, that is, $\Omega_r(\boldsymbol{x}_1) \neq \Omega_r(\boldsymbol{x}_2)$. Thus,

$$\frac{\alpha(\boldsymbol{x}_1, \boldsymbol{x}_2)}{\Omega_r(\boldsymbol{x}_1)} \neq \frac{\alpha(\boldsymbol{x}_2, \boldsymbol{x}_1)}{\Omega_r(\boldsymbol{x}_2)}, \tag{3.14}$$

and, consequently, using the definition of the non-symmetric averaging operator of Equation (3.12), we conclude that $\beta(\boldsymbol{x}_1, \boldsymbol{x}_2) \neq \beta(\boldsymbol{x}_2, \boldsymbol{x}_1)$.

It is worth mentioning that, for a material point sufficiently far from the boundary, $\Omega_r(\boldsymbol{x})$ becomes constant and is usually denoted by Ω_∞. In practice, Ω_∞ is computed as the area of a circle (2D problems) or the volume of a sphere (3D problems).

From a purely computational point of view, the use of a non-symmetric operator is disadvantageous due to the additional amount of memory necessary for storage if compared to the case of a symmetric operator (where the entries of the matrix are equal with respect to the main diagonal and need not be stored twice). Beside the advantages concerning memory management, the definition and use of a symmetric averaging operator is also appealing for the concise theoretical elaboration of non-local models which are consistent with thermodynamics [22]. For this purpose, Borino et al. [22] have proposed a symmetric averaging operator, which is written as

$$\beta(\boldsymbol{x}, \boldsymbol{\xi}) = \left(1 - \frac{\Omega_r(\boldsymbol{x})}{\Omega_\infty}\right) \delta(\boldsymbol{x}, \boldsymbol{\xi}) + \frac{1}{\Omega_\infty} \alpha(\boldsymbol{x}, \boldsymbol{\xi}), \tag{3.15}$$

where $\delta(\boldsymbol{x}, \boldsymbol{\xi})$ is the Kronecker delta.

Some authors [22, 96] have also adopted the following notation to define a non-local variable

$$\mathcal{R}(D) = \bar{D}(\boldsymbol{x}) = \int_V \beta(\boldsymbol{x}, \boldsymbol{\xi}) D(\boldsymbol{\xi})\, dV(\boldsymbol{\xi}) \tag{3.16}$$

where $\mathcal{R}(\cdot)$ denotes an integral regularisation operator. In some developments carried out throughout this thesis, this alternative notation will be useful for the sake of clarity.

3.2.1 Weighting function

As pointed out before, the averaging operator contains a prescribed weighting function which, in turn, depends on an intrinsic parameter with the physical dimension of length. The definition of the weighting function is, to some extent, arbitrary. However, in order to obtain the diffusive effect expected from the non-local theory, it should satisfy some basic characteristics. For instance, the function should have its maximum at the origin and the decrease around it as the distance of neighbouring points increases.

We will adopt in this thesis the bell-shaped function, which is frequently employed in non-local theories of integral-type [e.g. 14, 68], that is given by

$$\alpha(\boldsymbol{x}, \boldsymbol{\xi}) = \left\langle 1 - \frac{\|\boldsymbol{x} - \boldsymbol{\xi}\|^2}{\ell_r^2} \right\rangle^2, \tag{3.17}$$

where $\langle \cdot \rangle$ are the Macauley brackets. The intrinsic parameter is incorporated through the quantity ℓ_r that will be hereinafter referred to as *non-local intrinsic length*.

Remark 3.1. *The non-local intrinsic length cannot be directly measured from experiments but rather obtained through inverse analysis based on experimental evidence [14]. The determination of ℓ_r is therefore intricate and demands, in a general sense, a suitable numerical strategy. The intention in this chapter is to propose a non-local constitutive theory for ductile materials and to describe its associated computational implementation considering ℓ_r as a numerical parameter. Thus, the results and conclusions obtained herein would need to be experimentally validated. Nonetheless, as it will be shown in the following sections, the model presented in this contribution is able to avoid the pathological mesh dependency and can be conveniently used as a localisation limiter.*

3.2.2 Non-local averaging strategy

Under the assumption of infinitesimal strains, non-local averaging is independent of the configuration since the difference between the undeformed and deformed configurations can be neglected. However, this is clearly not true when finite strains are present. In this case, the definition of the non-local averaging integral on different configurations will lead to distinct results.

Inspired by the assessment carried out by Steinmann [108] and Geers et al. [55], we will consider three different strategies for the non-local averaging: (a) Eulerian-type; (b) total Lagrangian-type; (c) updated Lagrangian-type.

In the non-local averaging of Eulerian-type (see Figure 3.2), the weighted integral is evaluated at the *deformed* configuration. With such a strategy, the non-local volume of influence associated with the material point P is forced to remain the same (a circle or a sphere in the three-dimensional case) as the body undergoes deformation. As a consequence, material particles may enter or leave the representative volume Ω_r which remains undeformed throughout deformation.

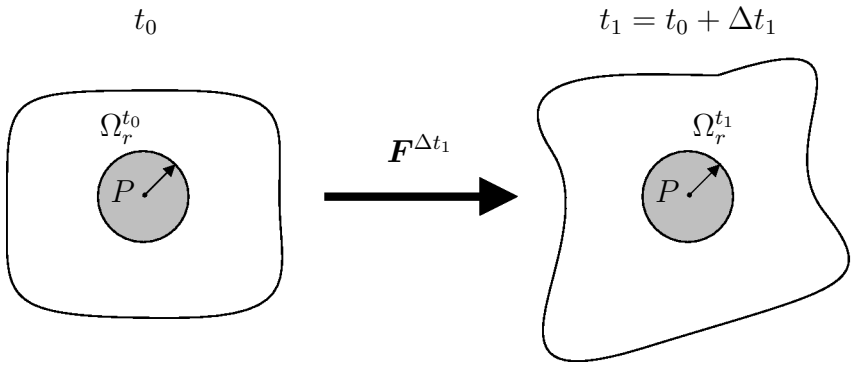

FIGURE 3.2: Non-local averaging of Eulerian-type.

In the total Lagrangian-type of non-local averaging, the weighted integral is evaluated at the *undeformed* configuration (see Figure 3.3). Thus, according to this concept, the final non-local influence volume will be distorted[3] from the original circle-shaped one in a two-dimensional analysis. This stems from the fact that the material points that exert influence over P remain the same ones throughout deformation.

[3]It it worth mentioning that the non-local volume of influence is not actually deformed but rather its shape looks distorted when evaluated at the deformed configuration. This stems from the fact that the averaging operator is independent of the history of deformation as alluded in Section 3.2.3.

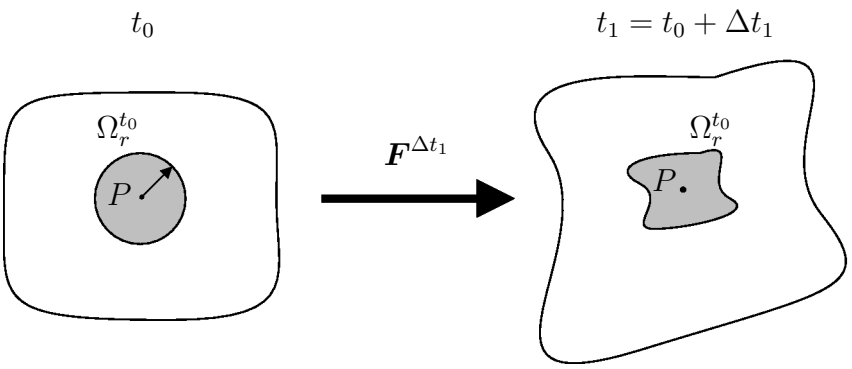

FIGURE 3.3: Non-local averaging of total Lagrangian-type.

Finally, the updated Lagrangian-type of non-local averaging is defined by mixing the two other strategies as the material points that influence P are kept the same but only over the increment of deformation. Before a new increment is applied, the non-local volume of influence is recomputed and different points may now exert influence on P (see Figure 3.4). As a matter of fact, this strategy only makes sense when working within an incremental framework. The updated Lagrangian-type of non-local averaging recovers the total Lagrangian-type if only one increment of deformation is applied. Likewise, if the size of the deformation increment tends to be infinitesimal, the non-local averaging of Eulerian-type is recovered.

From a computational point of view, the different strategies for the evaluation of the non-local averaging have a significant effect on the overall efficiency. If the Eulerian concept is chosen, for instance, the computation of the averaging operator $\beta(\boldsymbol{x}, \boldsymbol{\xi})$ has to be performed at every equilibrium iteration demanding additional CPU time for this task. On the other hand, when the total Lagrangian-type of non-local averaging is adopted, the evaluation of $\beta(\boldsymbol{x}, \boldsymbol{\xi})$ only needs to be carried out once, saving significant computational time.

With regard to the theoretical implications, the distinct non-local averaging strategies will behave quite differently under different stress states [55]. For example, let us consider the necking of a bar subjected to axial tension. As the area in the central section of the bar decreases due to necking, the Eulerian-type of non-local averaging will have progressively less material points to account for the non-local influence. The total Lagrangian strategy, on the other hand, preserves the same number of materials points for the non-local averaging throughout deformation. Conversely, if the bar is subjected to a compressive loading, more influence points may enter the representative volume defined with the Eulerian-type of non-local averaging. In the total Lagrangian strategy, however, no additional material points will be used in the non-local averaging. In the section of numerical results, we will

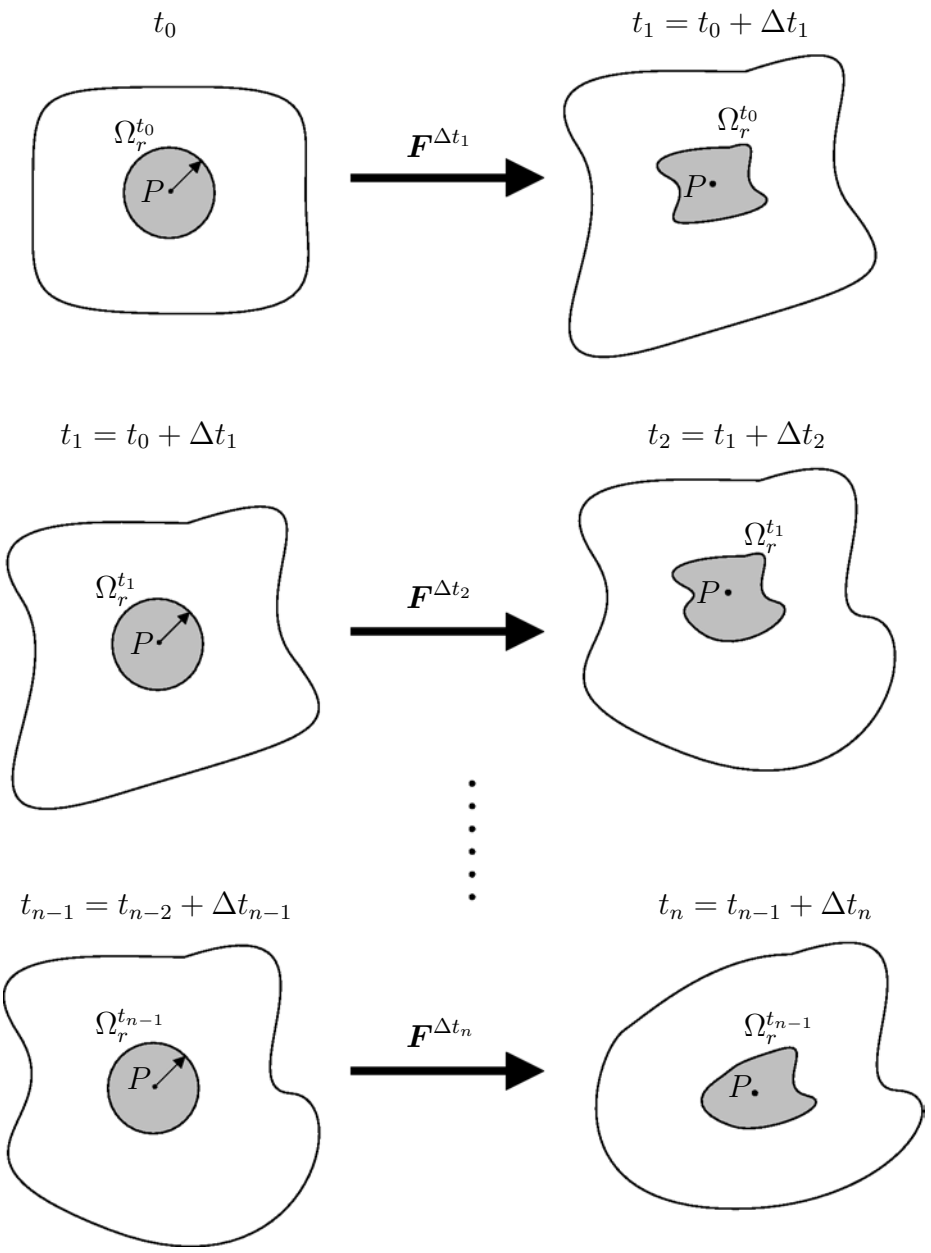

FIGURE 3.4: Non-local averaging of updated Lagrangian-type.

employ the different averaging strategies in order to better understand their differences.

3.2.3 Assumptions behind the non-local theory

One important assumption of the present non-local theory is that both the non-local intrinsic length, ℓ_r, and the averaging operator, $\beta(\boldsymbol{x}, \boldsymbol{\xi})$, are completely independent of the deformation history. In computational terms, this means that

$\beta(\boldsymbol{x}, \boldsymbol{\xi})$ is not altered when the body is subjected to a given deformation over (pseudo-)time but it is simply evaluated at different configurations as described in the last section. With this in mind, we can now evaluate the rate of the non-local variable:

$$\frac{\partial}{\partial t}\left[\bar{D}(\boldsymbol{x})\right] = \frac{\partial}{\partial t}\left[\int_V \beta(\boldsymbol{x}, \boldsymbol{\xi}) D(\boldsymbol{\xi})\, dV(\boldsymbol{\xi})\right]. \tag{3.18}$$

Under the hypothesis that $\beta(\boldsymbol{x}, \boldsymbol{\xi})$ is independent of the deformation history, the volume of the integral of Equation (3.18) does not vary, which allows us to write

$$\dot{\bar{D}}(\boldsymbol{x}) = \int_V \left[\dot{\beta}(\boldsymbol{x}, \boldsymbol{\xi}) D(\boldsymbol{\xi}) + \beta(\boldsymbol{x}, \boldsymbol{\xi}) \dot{D}(\boldsymbol{\xi})\right] dV(\boldsymbol{\xi}). \tag{3.19}$$

where the notation $\dot{(\cdot)}$ to denote rates has been adopted and the chain rule has been applied. Since $\beta(\boldsymbol{x}, \boldsymbol{\xi})$ does not vary over (pseudo-)time, it is straightforward to conclude that

$$\dot{\beta}(\boldsymbol{x}, \boldsymbol{\xi}) = 0, \tag{3.20}$$

which leads to the important relation:

$$\dot{\bar{D}}(\boldsymbol{x}) = \int_V \beta(\boldsymbol{x}, \boldsymbol{\xi}) \dot{D}(\boldsymbol{\xi})\, dV(\boldsymbol{\xi}). \tag{3.21}$$

From a numerical point of view, the format of the equation above is crucial. If $\beta(\boldsymbol{x}, \boldsymbol{\xi})$ is assumed to be dependent of the deformation history or of any other constitutive quantity, its rate might be different than zero, leading to a more complicated expression to be worked out when developing the numerical implementation of the constitutive model.

Finally, another consequence of the independence of $\beta(\boldsymbol{x}, \boldsymbol{\xi})$ on the history of deformation is that the formulation of the non-local constitutive model is not altered when a different averaging strategy is adopted.

3.3 Thermodynamic framework

Some local constitutive models are very appealing from a theoretical point of view due to their thermodynamically consistent formulations [e.g., 28, 29, 74, 75, 76]. Therefore, we will provide herein the derivation of the non-local constitutive model with the recourse of the theory of thermodynamics of irreversible processes. We remark that the thermodynamical implications regarding the use of the logarithmic strain tensor (which have already been developed for local models at finite strains) can be directly extended to the non-local case since we have chosen damage to

be the non-local variable. It is also important to mention that the theory will be limited to the purely mechanical case, i.e., thermal effects are completely neglected.

To start with, let us recall the first principle of thermodynamics, which can be given by

$$\int_V \bar{\rho}\dot{e}\, dV = \int_V \boldsymbol{\tau} : \boldsymbol{D}\, dV, \tag{3.22}$$

where $\bar{\rho}$ is the density at the deformed configuration, $\dot{e}$ is the rate of the internal energy and $\boldsymbol{\tau}$ is the Kirchhoff stress tensor. The quantity $\boldsymbol{D}$ is the stretching tensor defined by

$$\boldsymbol{D} \equiv \mathrm{sym}\left[\boldsymbol{L}\right]. \tag{3.23}$$

In the standard local continuum theory, the volume V can be considered infinitesimal. However, this is not the case of the non-local theory since V cannot be smaller than a given finite volume size dictated by the intrinsic length of the material [21, 22, 85, 96].

The integral format of Equation (3.22) can be conveniently re-written in a local form:

$$\bar{\rho}\dot{e} = \boldsymbol{\tau} : \boldsymbol{D} + P, \tag{3.24}$$

where P is called *non-local residual*. The use of a non-local residual has been firstly introduced by Edelen and Laws [43] and Edelen et al. [44] in the elasticity context and later exploited in small-strain plasticity and damage by others [21, 22, 85, 96]. More recently, Polizzotto [95] used the same concept in a strain gradient theory at finite strains.

The residual P accounts for the energy exchanges among non-local material particles, which is tacitly considered if the integral form in Equation (3.22) is used instead. Since it is reasonable to neglect energy exchanges with the exterior, the following insulation condition [96] holds:

$$\int_V P\, dV = 0. \tag{3.25}$$

We recall the expression for the Helmholtz free energy, which reads

$$\psi = e - Ts, \tag{3.26}$$

where T is the absolute temperature and s is the entropy. Since in the present model we consider isothermal processes only, then $\dot{T} = 0$. With the expression of

the Helmholtz free energy at hand (Equation 3.26), we know that

$$\bar{\rho} T \dot{s} = \bar{\rho} \dot{e} - \bar{\rho} \dot{\psi} \tag{3.27}$$

thus,

$$\bar{\rho} T \dot{s} = \boldsymbol{\tau} : \boldsymbol{D} + P - \bar{\rho} \dot{\psi}. \tag{3.28}$$

Invoking now the second principle of thermodynamics, we have

$$\int_V \bar{\rho} T \dot{s} \, dV \geq 0. \tag{3.29}$$

Equation (3.29) can be re-written in its local form as

$$\bar{\rho} T \dot{s} \geq 0, \tag{3.30}$$

which can be substituted in Equation (3.28), leading to the Clausius-Duhem inequality, given by

$$\boldsymbol{\tau} : \boldsymbol{D} + P - \bar{\rho} \dot{\psi} \geq 0. \tag{3.31}$$

We remark that a non-local residual is not necessary in Equation (3.30) since it has already been considered in Equation (3.28).

3.3.1 Determination of $\bar{\rho}\dot{\psi}$

Firstly, we assume that the specific free energy function is given by

$$\bar{\rho}\psi\left(\boldsymbol{\varepsilon}^e, R, \mathcal{R}(D)\right) \equiv \bar{\rho}\psi^{e,d}\left(\boldsymbol{\varepsilon}^e, \mathcal{R}(D)\right) + \bar{\rho}\psi^{p}\left(R\right), \tag{3.32}$$

where $\bar{\rho}\psi^{e,d}\left(\boldsymbol{\varepsilon}^e, \mathcal{R}(D)\right)$ and $\bar{\rho}\psi^{p}\left(R\right)$ are respectively the specific free energy functions associated with elastic-damage and plasticity. The potential $\psi\left(\boldsymbol{\varepsilon}^e, R, \mathcal{R}(D)\right)$ is associated with a generic material point located at $\boldsymbol{x}$ and depends on the potentials of other surrounding points due to non-locality. Therefore, this potential does not hold alone as the energy exchanges among neighbour material particles must be taken into account. Nevertheless, such energy exchanges have already been considered through the non-local residual P in Equation (3.31).

At this point, it is necessary to define the elastic-damage specific free energy potential. Considering a Hencky hyperelastic potential, we have

$$\bar{\rho}\psi^{e,d}\left(\boldsymbol{\varepsilon}^e, \mathcal{R}(D)\right) = \frac{1}{2}\boldsymbol{\varepsilon}^e : \left(1 - \mathcal{R}(D)\right)\mathbf{D}^e : \boldsymbol{\varepsilon}^e, \tag{3.33}$$

where $\mathbf{D}^e$ is the typical linear elasticity fourth-order tensor. The rate of $\bar{\rho}\psi$ is then given by

$$\bar{\rho}\dot{\psi} = \bar{\rho}\frac{\partial \psi}{\partial \boldsymbol{\varepsilon}^e} : \dot{\boldsymbol{\varepsilon}}^e + \bar{\rho}\frac{\partial \psi}{\partial \mathcal{R}(D)}\mathcal{R}(\dot{D}) + \bar{\rho}\frac{\partial \psi}{\partial R}\dot{R}, \tag{3.34}$$

where the thermodynamic forces conjugated with isotropic hardening and non-local damage read, respectively,

$$\chi = \bar{\rho}\frac{\partial \psi}{\partial R}, \tag{3.35}$$

$$Y = \bar{\rho}\frac{\partial \psi}{\partial \mathcal{R}(D)} = -\frac{1}{2}\boldsymbol{\varepsilon}^e : \mathbf{D}^e : \boldsymbol{\varepsilon}^e. \tag{3.36}$$

For the determination of the first term of the right-hand side of Equation (3.34), we apply the chain rule, which, together with the definition of the logarithmic elastic strain tensor of Equation (3.9), gives

$$\frac{\partial \psi}{\partial \boldsymbol{\varepsilon}^e} : \dot{\boldsymbol{\varepsilon}}^e = \frac{1}{2}\frac{\partial \psi}{\partial \boldsymbol{\varepsilon}^e} : \frac{\partial \left(\ln \boldsymbol{B}^e\right)}{\partial \boldsymbol{B}^e} : \dot{\boldsymbol{B}}^e \tag{3.37}$$

$$= \frac{1}{2}\left[\frac{\partial \psi}{\partial \boldsymbol{\varepsilon}^e} : \frac{\partial \left(\ln \boldsymbol{B}^e\right)}{\partial \boldsymbol{B}^e}\right]\boldsymbol{B}^e : \dot{\boldsymbol{B}}^e\boldsymbol{B}^{e-1}. \tag{3.38}$$

The function $\ln \boldsymbol{B}^e$ belongs to the class of functions called isotropic tensor functions with a single argument. By the definition of $\boldsymbol{\varepsilon}^e$ and due to the isotropy of ψ, the tensors $\boldsymbol{\varepsilon}^e$, $\boldsymbol{B}^e$ and $\partial\psi/\partial\boldsymbol{\varepsilon}^e$ have the same principal axes. In view of that and using closed-form formulas for the evaluation of isotropic tensor functions with single argument [37, 82], we obtain (after some algebra) the following identity

$$\frac{\partial \psi}{\partial \boldsymbol{\varepsilon}^e} : \frac{\partial \left(\ln \boldsymbol{B}^e\right)}{\partial \boldsymbol{B}^e}\boldsymbol{B}^e = \frac{\partial \psi}{\partial \boldsymbol{\varepsilon}^e}. \tag{3.39}$$

Therefore, we have

$$\frac{\partial \psi}{\partial \boldsymbol{\varepsilon}^e} : \dot{\boldsymbol{\varepsilon}}^e = \frac{1}{2}\frac{\partial \psi}{\partial \boldsymbol{\varepsilon}^e} : \dot{\boldsymbol{B}}^e\boldsymbol{B}^{e-1}. \tag{3.40}$$

Using the multiplicative elasto-plastic decomposition of the deformation gradient (Equation 3.1) in conjunction with the definition of the left elastic Cauchy-Green strain tensor, $\boldsymbol{B}^e = \boldsymbol{F}^e\boldsymbol{F}^{e^T}$, leads to

$$\boldsymbol{B}^e = \boldsymbol{F}\left(\boldsymbol{F}^p\right)^{-1}\left(\boldsymbol{F}^p\right)^{-T}\boldsymbol{F}^T. \tag{3.41}$$

Using the rate of the above expression and substituting in Equation (3.40) yields, after some algebraic manipulation and by taking into account the elastic isotropy, on

$$\frac{\partial \psi}{\partial \boldsymbol{\varepsilon}^e} : \dot{\boldsymbol{\varepsilon}}^e = \frac{\partial \psi}{\partial \boldsymbol{\varepsilon}^e} : \left(\boldsymbol{D} - \boldsymbol{R}^e \boldsymbol{D}^p \boldsymbol{R}^{e^T} \right). \tag{3.42}$$

Finally, with the definition of the plastic stretch rotated to the deformed configuration (Equation 3.8), we get

$$\frac{\partial \psi}{\partial \boldsymbol{\varepsilon}^e} : \dot{\boldsymbol{\varepsilon}}^e = \frac{\partial \psi}{\partial \boldsymbol{\varepsilon}^e} : \left(\boldsymbol{D} - \tilde{\boldsymbol{D}}^p \right). \tag{3.43}$$

Hence, Equation (3.34) becomes

$$\bar{\rho}\dot{\psi} = \bar{\rho}\frac{\partial \psi}{\partial \boldsymbol{\varepsilon}^e} : \left(\boldsymbol{D} - \tilde{\boldsymbol{D}}^p \right) + Y\mathcal{R}(\dot{D}) + \chi \dot{R}. \tag{3.44}$$

Substituting into the Clausius-Duhem inequality (Equation 3.31), we have

$$\left(\boldsymbol{\tau} - \bar{\rho}\frac{\partial \psi}{\partial \boldsymbol{\varepsilon}^e} \right) : \boldsymbol{D} + \bar{\rho}\frac{\partial \psi}{\partial \boldsymbol{\varepsilon}^e} : \tilde{\boldsymbol{D}}^p + P - Y\mathcal{R}(\dot{D}) - \chi \dot{R} \geq 0, \tag{3.45}$$

from which the following constitutive relation applies since Equation (3.45) must hold for any motion:

$$\boldsymbol{\tau} = \bar{\rho}\frac{\partial \psi}{\partial \boldsymbol{\varepsilon}^e} = (1 - \mathcal{R}(D))\, \mathbf{D}^e : \boldsymbol{\varepsilon}^e. \tag{3.46}$$

The Clausius-Duhem inequality then reads

$$\boldsymbol{\tau} : \tilde{\boldsymbol{D}}^p + P - Y\mathcal{R}(\dot{D}) - \chi \dot{R} \geq 0. \tag{3.47}$$

3.3.2 Determination of P

Since we have substituted the global integral version of the first and second principles of thermodynamics by a local form which accounts for a non-local residual, we can alternatively write the inequality of Clausius-Duhem in a purely local form as

$$\boldsymbol{\tau} : \tilde{\boldsymbol{D}}^p - X\dot{D} - \chi \dot{R} \geq 0, \tag{3.48}$$

where X is a thermodynamic force conjugated to local damage which inherently takes into account the non-local energy exchanges among several material particles.

Of course, the definition of X is not clear. Nevertheless, since the inequalities (3.47) and (3.48) have to be equivalent, we can compare both expressions as

$$\boldsymbol{\tau} : \tilde{\boldsymbol{D}}^p + P - Y\mathcal{R}(\dot{D}) - \chi\dot{R} = \boldsymbol{\tau} : \tilde{\boldsymbol{D}}^p - X\dot{D} - \chi\dot{R}, \tag{3.49}$$

which straightforwardly leads to

$$P = Y\mathcal{R}(\dot{D}) - X\dot{D}. \tag{3.50}$$

Finally, we can apply the insulation condition from Equation (3.25):

$$\int_V P\, dV = \int_V \left(Y\mathcal{R}(\dot{D}) - X\dot{D}\right)\, dV = 0, \tag{3.51}$$

which results in

$$\int_V X\dot{D}\, dV = \int_V Y\mathcal{R}(\dot{D})\, dV. \tag{3.52}$$

Since $\beta(\boldsymbol{x}, \boldsymbol{\xi})$ is symmetric, the following Green-type identity holds [22]:

$$\int_V Y\mathcal{R}(\dot{D})\, dV = \int_V \mathcal{R}(Y)\dot{D}\, dV. \tag{3.53}$$

Therefore, we conclude that

$$X = \mathcal{R}(Y), \tag{3.54}$$

hence,

$$P = Y\mathcal{R}(\dot{D}) - \mathcal{R}(Y)\dot{D}. \tag{3.55}$$

Finally, with Equation (3.55), the Clausius-Duhem inequality becomes

$$\boldsymbol{\tau} : \tilde{\boldsymbol{D}}^p - \mathcal{R}(Y)\dot{D} - \chi\dot{R} \geq 0, \tag{3.56}$$

or, equivalently,

$$\boldsymbol{\tau} : \tilde{\boldsymbol{D}}^p + \mathcal{R}(-Y)\dot{D} - \chi\dot{R} \geq 0. \tag{3.57}$$

The local form of the Clausius-Duhem inequality including the non-local residual facilitates the definition of the plastic and damage dissipation potentials which now may also be defined in a local form (local in the sense that the potential is the one associated with a generic material point).

3.4 Constitutive equations

In order to derive the constitutive equations of the model, we first define a dissipation potential, F, to be given by

$$F = F_p + F_d, \tag{3.58}$$

where F_p and F_d are, respectively, the dissipation potentials associated with plasticity and damage. By assuming plastic isotropy (which leads to a zero plastic spin, i.e., $\boldsymbol{W}^p = \boldsymbol{0}$) and applying the generalised normality rule, we have

$$\tilde{\boldsymbol{D}}^p = \dot{\gamma}\frac{\partial F}{\partial \boldsymbol{\tau}}, \tag{3.59}$$

and

$$\dot{R} = -\dot{\gamma}\frac{\partial F}{\partial \chi}. \tag{3.60}$$

We know from Equation (3.21) that the rate of non-local damage, which is the internal variable that accounts for internal degradation in the present formulation, is by definition given by

$$\dot{\bar{D}} = \mathcal{R}\left(\dot{D}\right), \tag{3.61}$$

i.e., it is a regularisation applied on the rate of local damage, which, following the generalised normality rule, reads

$$\dot{D} = \dot{\gamma}\frac{\partial F}{\partial \mathcal{R}(-Y)}. \tag{3.62}$$

In order to get the evolution equations that define the non-local constitutive model, functions for the plastic and damage dissipation potentials must be defined. For the former, we adopt the *undamaged* von Mises yield function [75], given by

$$F_p \equiv \frac{q(\boldsymbol{\tau})}{\left(1-\bar{D}\right)} - \tau_y\left(R\right), \tag{3.63}$$

where τ_y is the uniaxial yield stress and $q = q(\boldsymbol{\tau})$ is the von Mises equivalent stress evaluated using the Kirchhoff stress tensor, defined as:

$$q(\boldsymbol{\xi}) = \sqrt{3J_2(\boldsymbol{\tau}_d(\boldsymbol{\xi}))} = \sqrt{\frac{3}{2}\boldsymbol{\tau}_d(\boldsymbol{\xi}) : \boldsymbol{\tau}_d(\boldsymbol{\xi})}. \tag{3.64}$$

For the dissipation potential associated with local damage, we define

$$F_d \equiv \frac{r}{(s+1)(1-D)} \left[\frac{\mathcal{R}(-Y)}{r} \right]^{s+1}, \tag{3.65}$$

where r and s are scalar parameters for damage evolution. Equation (3.65) is based on the damage dissipation potential proposed by Lemaitre [75]. The only difference is that we have considered the averaging of the energy release rate, $-Y$. This choice is based on the implications from thermodynamics, addressed in the last section, where the thermodynamic force conjugated with local damage should be $\mathcal{R}(-Y)$. By rearranging Equation (3.59) using the relations from Equation (3.8), the non-local constitutive model can be derived from the following set of equations:

$$\dot{\boldsymbol{F}}^p \boldsymbol{F}^{p-1} = \dot{\gamma} \boldsymbol{R}^{e\,T} \frac{\partial F}{\partial \boldsymbol{\tau}} \boldsymbol{R}^e, \tag{3.66}$$

$$\dot{R} = -\dot{\gamma} \frac{\partial F}{\partial \chi}, \tag{3.67}$$

$$\dot{\bar{D}} = \mathcal{R}\left[\dot{\gamma} \frac{\partial F}{\partial \mathcal{R}(-Y)} \right]. \tag{3.68}$$

Straightforward multi-variable calculus operations lead to

$$\dot{\boldsymbol{F}}^p \boldsymbol{F}^{p-1} = \frac{\dot{\gamma}}{\left(1-\bar{D}\right)} \boldsymbol{R}^{e\,T} \left(\frac{3}{2} \frac{\boldsymbol{\tau}_d}{q} \right) \boldsymbol{R}^e, \tag{3.69}$$

$$\dot{R} = \dot{\gamma}, \tag{3.70}$$

$$\dot{\bar{D}} = \mathcal{R}\left\{ \frac{\dot{\gamma}}{(1-D)} \left[\frac{\mathcal{R}(-Y)}{r} \right]^s \right\}. \tag{3.71}$$

Alternatively, Equation (3.71) can be more explicitly written as

$$\dot{\bar{D}}(\boldsymbol{x}) = \int_V \beta(\boldsymbol{x}, \boldsymbol{\xi}) \frac{\dot{\gamma}(\boldsymbol{\xi})}{(1 - D(\boldsymbol{\xi}))} \left[\frac{1}{r} \int_V \beta(\boldsymbol{\xi}, \boldsymbol{\eta}) \left(-Y(\boldsymbol{\eta})\right) \, dV(\boldsymbol{\eta}) \right]^s dV(\boldsymbol{\xi}). \tag{3.72}$$

It is worth mentioning that the non-local constitutive model is by no means dependent of a single point only. In fact, the equations above are simply those associated with the generic material point located at $\boldsymbol{x}$. Likewise, the Kuhn-Tucker conditions associated with the material point at $\boldsymbol{x}$ read

$$\dot{\gamma}(\boldsymbol{x}) \geq 0; \quad F_p(\boldsymbol{x}) \leq 0; \quad \dot{\gamma}(\boldsymbol{x}) F_p(\boldsymbol{x}) = 0 \quad \forall \, \boldsymbol{x} \in V. \tag{3.73}$$

and must hold globally in V.

3.4.1 Relation to classical non-local formulation

Most non-local theories are formulated within a classical approach [27], i.e., they are merely ad-hoc extensions of previously existing local constitutive models for which one or more local variables are replaced by their non-local counterparts. Accordingly, the non-local theory presented above can also be defined in an ad-hoc fashion by simply replacing local damage by its non-local counterpart. In this case, the evolution of non-local damage is given by

$$\dot{\bar{D}} = \mathcal{R}\left[\frac{\dot{\gamma}}{(1-D)}\left(\frac{-Y}{r}\right)^{s}\right], \tag{3.74}$$

which clearly differs from Equation (3.71) only due to the absence of regularisation on $-Y$. Although less theoretically appealing, the classical version of the present non-local damage model is thermodynamically admissible, i.e., it does not generate negative dissipations. This can be straightforwardly demonstrated as follows. Recalling the Clausius-Duhem inequality in the global form, the dissipation for the classical formulation reads

$$\int_V \left(\boldsymbol{\tau} : \tilde{\boldsymbol{D}}^p - Y\dot{\bar{D}} - \chi\dot{R}\right) dV \geq 0. \tag{3.75}$$

The equation above can be split into two dissipative contributions, the first one due to plasticity and the other one associated with damage, respectively given by

$$\int_V \left(\boldsymbol{\tau} : \tilde{\boldsymbol{D}}^p - \chi\dot{R}\right) dV \;\geq\; 0, \tag{3.76}$$

$$\int_V -Y\dot{\bar{D}}\, dV \;\geq\; 0. \tag{3.77}$$

As a matter of fact, the dissipation associated with plasticity (Equation 3.76) is always positive. This is rooted on the fact that, like in the local case, the plastic potential, F_p, is a convex function that is zero-valued at the origin and for which $\dot{F}_p \geq 0$. These properties tacitly fulfil the second principle of thermodynamics 'a priori' for which positiveness of dissipation must hold for any deformation [40, 76].

In order to verify the thermodynamical admissibility of Equation (3.77), we first examine the expression for the damage energy release rate, which can be alternatively written as

$$-Y = \frac{q^2}{6G(1-D)^2} + \frac{\tau_h^2}{2K(1-D)^2}, \tag{3.78}$$

where G and K are respectively the shear and bulk modulus. Clearly, $-Y$ is always positive. Subsequently, close inspection of the rate of local damage, $\dot{D}$,

which is given by

$$\dot{D} = \frac{\dot{\gamma}}{(1-D)} \left(\frac{-Y}{r} \right)^s , \tag{3.79}$$

demonstrates that $\dot{D}$ is also always positive. In order to obtain the rate of non-local damage, $\dot{D}$ is averaged as in Equation (3.21) where the averaging function $\beta(\boldsymbol{x}, \boldsymbol{\xi})$ is by definition always non-negative, leading us to the conclusion that $\dot{\bar{D}} \geq 0$ for any deformation. Therefore, since the product $-Y\dot{\bar{D}}$ is always positive, we state that the inequality in Equation (3.75) holds under any circumstance and we conclude that the classical non-local model is thermodynamically admissible.

3.5 Numerical implementation

The constitutive equations defined in the last section lead to an IBVP that needs to be solved in order to describe the behaviour of the material when subjected to a given history of deformation gradient. The constitutive behaviour of a generic material point located at $\boldsymbol{x}$ is given by the functions $\boldsymbol{F}^p(\boldsymbol{x}, t)$, $R(\boldsymbol{x}, t)$ and $\bar{D}(\boldsymbol{x}, t)$ that satisfy

$$\begin{cases} \dot{\boldsymbol{F}}^p(\boldsymbol{x}, t)\boldsymbol{F}^{p-1}(\boldsymbol{x}, t) = \dfrac{\dot{\gamma}(\boldsymbol{x}, t)}{\left(1 - \bar{D}(\boldsymbol{x}, t)\right)} \boldsymbol{R}^{e\,T}(\boldsymbol{x}, t) \dfrac{3}{2} \dfrac{\boldsymbol{\tau}_d(\boldsymbol{x}, t)}{q(\boldsymbol{x}, t)} \boldsymbol{R}^e(\boldsymbol{x}, t) \\ \\ \dot{R}(\boldsymbol{x}, t) = \dot{\gamma}(\boldsymbol{x}, t) \\ \\ \dot{\bar{D}}(\boldsymbol{x}, t) = \mathcal{R} \left\{ \dfrac{\dot{\gamma}(\boldsymbol{x}, t)}{(1 - D(\boldsymbol{x}, t))} \left[\dfrac{\mathcal{R}(-Y(\boldsymbol{x}, t))}{r} \right]^s \right\} \end{cases} \tag{3.80}$$

subjected to the Kuhn-Tucker conditions:

$$\dot{\gamma}(\boldsymbol{x}, t) \geq 0 \quad F_p(\boldsymbol{x}, t) \leq 0 \quad \dot{\gamma}(\boldsymbol{x}, t) F_p(\boldsymbol{x}, t) = 0 \tag{3.81}$$

for the given initial values $\boldsymbol{F}^p(\boldsymbol{x}, t_0)$, $R(\boldsymbol{x}, t_0)$ and $\bar{D}(\boldsymbol{x}, t_0)$, and given history of the deformation gradient $\boldsymbol{F}(\boldsymbol{x}, t)$ for any $t \in [t_0, t_n]$.

Since an enriched non-local continuum has been considered, the constitutive IBVP depends on other material points which implies that the consistency condition $F_p(\boldsymbol{x}, t) \leq 0$ cannot be fulfilled in a point-wise fashion. In fact, an additional degree of non-linearity is inherently incorporated by the non-local formulation due to the integral averaging. Consequently, analytical solutions for the non-local constitutive IBVP problem are only possible for a limited number of special cases.

Nevertheless, the constitutive problem can be solved by using iterative solution methods as it will be discussed in the following sections.

3.5.1 Numerical evaluation of the averaging integral

In a typical finite element framework, the well established Gaussian quadrature is very often employed to numerically integrate the equations associated with the elements of the mesh. As a consequence, all constitutive quantities are computed at the Gauss points which are, in fact, the discrete version of the infinitesimal material points at the continuum level. Likewise, the non-local averaging integral can be worked out using the same method, keeping all constitutive quantities computed at the Gauss points. This strategy has been often adopted in non-local formulations of integral-type [e.g. 68, 85] and the integral of Equation (3.10) can be expressed in its discrete form as

$$\bar{D}_i = \sum_{j=1}^{ngp_i} w_j J_j \beta_{ij} D_j, \tag{3.82}$$

where $\beta_{ij} \equiv \beta(\boldsymbol{x}, \boldsymbol{\xi})$ is the averaging factor that relates the Gauss points i and j respectively located at global coordinates $\boldsymbol{x}$ and $\boldsymbol{\xi}$. $\bar{D}_i$ and D_j are the damage variables associated to the Gauss points i and j, respectively. The quantity w_j is the Gaussian weight and J_j is the Jacobian, both evaluated at the Gauss point j. Finally, ngp_i is the number of Gauss points that lie inside the non-local volume of interaction measured from point i.

In similar manner, Equation (3.72) is re-phrased as

$$\dot{\bar{D}}_i = \sum_{j=1}^{ngp_i} \left\{ w_j J_j \beta_{ij} \frac{\dot{\gamma}_j}{(1-D_j)} \left[\frac{1}{r} \sum_{k=1}^{ngp_j} w_k J_k \beta_{jk} \left(-Y_k\right) \right]^s \right\}, \tag{3.83}$$

where $\beta_{jk} \equiv \beta(\boldsymbol{\xi}, \boldsymbol{\eta})$ is the averaging factor that relates the Gauss points j and k located at global coordinates $\boldsymbol{\xi}$ and $\boldsymbol{\eta}$, respectively, and ngp_j is the number of Gauss points that have non-local influence over the j^{th} Gauss point.

Remark 3.2. *As typically observed in finite elements, element distortion will inevitably affect the quality of the Gauss quadrature since it only guarantees exact solutions for polynomial functions. As the elements of the mesh become distorted, their polynomial character is gradually lost and the integration tends to have poorer results. As a matter of fact, this will also influence the results of the non-local problem, therefore creating some dependence on the quality of the mesh. However,*

this 'mesh dependence' is of a different kind and absolutely not associated with the pathological mesh dependence caused by the softening regime. In other words, if a sufficient number of non-local interaction points are present, even if the elements are heavily distorted, the ill-posedness of the structural problem will be avoided. The numerical predictions may render poor results but uniquely due to inaccurate numerical integration over the spatial domain.

Remark 3.3. *Throughout this thesis, the subscripts i, j, k and l will be in the majority of the cases employed to denote different Gauss points of the finite element mesh. Therefore, they generally do not correspond to the components of vectors or tensors, neither summations are implied, unless otherwise specified.*

3.5.2 The global elastic predictor/return mapping scheme

As previously pointed out, the main difficulty of the solution of the non-local constitutive problem is the fulfilment of the consistency condition. In fact, the constitutive problem has a global character since one material point depends on other points that, in turn, depend on other ones and so on.

A suitable manner to solve the non-local material problem is by adopting the general concepts of the well known elastic predictor/return mapping scheme very often used in numerical implementations of local constitutive models. Our intention here is not to provide a detailed description of this strategy which is extensively documented elsewhere [e.g., 40, 106]. Instead, we aim to demonstrate how to employ it with the constitutive model presented in the preceding sections leading to an efficient numerical implementation.

To start with, we first discretise the constitutive IVBP of Equation (3.80) over a (pseudo-)time increment. Following standard procedures of the implementation of hyperelasto-plastic theories based on the multiplicative decomposition, we employ the *exponential map backward scheme* for the discretisation of the plastic flow which leads to

$$\boldsymbol{F}^{p}_{i_{n+1}} = \exp\left[\frac{3}{2}\frac{\Delta\gamma_i}{\left(1-\bar{D}_{i_{n+1}}\right)}\boldsymbol{R}^{e^T}_{i_{n+1}}\frac{\mathrm{dev}(\boldsymbol{\tau}_{i_{n+1}})}{\sqrt{3J_2(\boldsymbol{\tau}_{i_{n+1}})}}\boldsymbol{R}^{e}_{i_{n+1}}\right]\boldsymbol{F}^{p}_{i_n}. \tag{3.84}$$

Due to the isotropy of the tensor exponential function, Equation (3.84) can be re-written as

$$\boldsymbol{F}^{p}_{i_{n+1}} = \boldsymbol{R}^{e^T}_{i_{n+1}}\exp\left[\frac{3}{2}\frac{\Delta\gamma_i}{\left(1-\bar{D}_{i_{n+1}}\right)}\frac{\mathrm{dev}(\boldsymbol{\tau}_{i_{n+1}})}{\sqrt{3J_2(\boldsymbol{\tau}_{i_{n+1}})}}\right]\boldsymbol{R}^{e}_{i_{n+1}}\boldsymbol{F}^{p}_{i_n}, \tag{3.85}$$

which represents the update of the plastic deformation gradient. Equivalently, we can define the update of the elastic deformation gradient, which in view of Equation (3.1), is straightforwardly obtained as

$$\boldsymbol{F}^{e}_{i_{n+1}} = \boldsymbol{F}^{e\,trial}_{i_{n+1}} \boldsymbol{R}^{e^T}_{i_{n+1}} \exp\left[-\frac{3}{2}\frac{\Delta\gamma_i}{\left(1-\bar{D}_{i_{n+1}}\right)}\frac{\mathrm{dev}(\boldsymbol{\tau}_{i_{n+1}})}{\sqrt{3J_2(\boldsymbol{\tau}_{i_{n+1}})}}\right]\boldsymbol{R}^{e}_{i_{n+1}}, \tag{3.86}$$

where $\boldsymbol{F}^{e\,trial}_{i_{n+1}}$ is the elastic trial deformation gradient, given by

$$\boldsymbol{F}^{e\,trial}_{i_{n+1}} = \boldsymbol{F}_{i_\Delta}\boldsymbol{F}^{e}_{i_n}, \tag{3.87}$$

and $\boldsymbol{F}_{i_\Delta}$ is the incremental deformation gradient defined as

$$\boldsymbol{F}_{i_\Delta} = \boldsymbol{I} + \nabla_n\left[\Delta\boldsymbol{u}_i\right], \tag{3.88}$$

where $\Delta\boldsymbol{u}_i$ corresponds to the incremental displacement field of Gauss point i.

The use of the logarithmic strain as a strain measure is substantially beneficial since it allows to re-write the plastic flow equation as [40]

$$\boldsymbol{\varepsilon}^{e}_{i_{n+1}} = \boldsymbol{\varepsilon}^{e\,trial}_{i_{n+1}} - \frac{3}{2}\frac{\Delta\gamma_i}{\left(1-\bar{D}_{i_{n+1}}\right)}\frac{\mathrm{dev}(\boldsymbol{\tau}_{i_{n+1}})}{\sqrt{3J_2(\boldsymbol{\tau}_{i_{n+1}})}}, \tag{3.89}$$

which remarkably retrieves the same format of equation as if the model were under the hypothesis of infinitesimal strains, facilitating its numerical implementation.

The integration of the evolution of the internal variables R and $\bar{D}$, respectively given in $(3.80)_2$ and $(3.80)_3$, is done by using the conventional backward Euler scheme. Thus, following the typical procedures of return mapping schemes, the final system of equations to be solved when the material is on the plastic damage

domain is given by

$$\begin{cases} \boldsymbol{\varepsilon}^{e}_{i_{n+1}} = \boldsymbol{\varepsilon}^{e\,trial}_{i_{n+1}} - \dfrac{3}{2}\dfrac{\Delta\gamma_i}{\left(1-\bar{D}_{i_{n+1}}\right)}\dfrac{\mathrm{dev}(\boldsymbol{\tau}_{i_{n+1}})}{\sqrt{3J_2(\boldsymbol{\tau}_{i_{n+1}})}} \\ \\ R_{i_{n+1}} = R_{i_n} + \Delta\gamma_i \\ \\ \bar{D}_{i_{n+1}} = \bar{D}_{i_n} + \displaystyle\sum_{j=1}^{ngp_i}\left\{ w_j J_j \beta_{ij} \dfrac{\Delta\gamma_j}{\left(1-D_{j_{n+1}}\right)} \left[\dfrac{1}{r}\sum_{k=1}^{ngp_j} w_k J_k \beta_{jk}\left(-Y_{k_{n+1}}\right)\right]^s \right\} \\ \\ \dfrac{\sqrt{3J_2(\boldsymbol{\tau}_{i_{n+1}})}}{\left(1-\bar{D}_{i_{n+1}}\right)} - \tau_y\left(R_{i_{n+1}}\right) = 0 \end{cases} \tag{3.90}$$

Otherwise, the point is elastic and no return mapping is necessary.

We remark that the system above is by no means point-wise, i.e., its solution is coupled to the solution of other material points. Before proceeding to the description of the solution of the constitutive problem, we can algebraically manipulate the system of equations (3.90) and reduce the problem to the solution of a system of equations where there is only one equation associated with each Gauss point of the mesh. This simplification remarkably increases the efficiency of the algorithm, to be defined in the following, where the single residual equation associated with the generic Gauss point i, is given by

$$\begin{aligned} \bar{f}_i &= 3G\Delta\gamma_i - \left(1-\bar{D}_{i_n}\right)\left(\tilde{q}^{trial}_{i_{n+1}} - \tau_{y_i}\right) \\ &+ \left(\tilde{q}^{trial}_{i_{n+1}} - \tau_{y_i}\right)\sum_{j=1}^{ngp_i}\left\{ w_j J_j \beta_{ij} \frac{\left(\tilde{q}^{trial}_{i_{n+1}} - \tau_{y_i}\right)}{3G} \left[\frac{1}{r}\sum_{k=1}^{ngp_j} w_k J_k \beta_{jk}\left(-Y_{k_{n+1}}\right)\right]^s \right\}, \end{aligned} \tag{3.91}$$

where $\tilde{q}^{trial}_{i_{n+1}}$ is the *undamaged* trial von Mises equivalent stress, which is given by

$$\tilde{q}^{trial}_{i_{n+1}} = \sqrt{\frac{3}{2}}\left\| 2G\mathrm{dev}\left(\boldsymbol{\varepsilon}^{e\,trial}_{i_{n+1}}\right)\right\|. \tag{3.92}$$

Despite the reduction from a system to a single equation associated with each Gauss point, the solution of the non-local constitutive problem still must be sought globally in order to ensure the fulfilment of the consistency condition. In fact, the problem at hand belongs to the family of non-linear complementarity problems (NCP) [19]. We can define $\bar{\boldsymbol{f}}$ to be a vector containing all the residual functions associated with the Gauss points of the mesh. Likewise, the vector $\Delta\boldsymbol{\gamma}$ corresponds

to all the unknowns of the global problem. Using the Newton-Raphson solution method to solve the NCP, we get

$$\Delta\boldsymbol{\gamma}^{k+1} = \Delta\boldsymbol{\gamma}^{k} - \left(\frac{\partial \bar{\boldsymbol{f}}}{\partial \Delta\boldsymbol{\gamma}}\bigg|_{\Delta\boldsymbol{\gamma}^{k}} \right)^{-1} \bar{\boldsymbol{f}}\left(\Delta\boldsymbol{\gamma}^{k}\right), \tag{3.93}$$

which can be more conveniently written as

$$\left(\frac{\partial \bar{\boldsymbol{f}}}{\partial \Delta\boldsymbol{\gamma}}\bigg|_{\Delta\boldsymbol{\gamma}^{k}} \right) \delta\boldsymbol{\gamma} = -\bar{\boldsymbol{f}}\left(\Delta\boldsymbol{\gamma}^{k}\right), \tag{3.94}$$

where

$$\delta\boldsymbol{\gamma} = \Delta\boldsymbol{\gamma}^{k+1} - \Delta\boldsymbol{\gamma}^{k}, \tag{3.95}$$

$$\frac{\partial \bar{\boldsymbol{f}}}{\partial \Delta\boldsymbol{\gamma}} = \begin{bmatrix} \dfrac{\partial \bar{f}_1}{\partial \Delta\gamma_1} & \dfrac{\partial \bar{f}_1}{\partial \Delta\gamma_2} & \cdots & \dfrac{\partial \bar{f}_1}{\partial \Delta\gamma_{ngp}} \\ \dfrac{\partial \bar{f}_2}{\partial \Delta\gamma_1} & \dfrac{\partial \bar{f}_2}{\partial \Delta\gamma_2} & \cdots & \dfrac{\partial \bar{f}_2}{\partial \Delta\gamma_{ngp}} \\ \vdots & \vdots & \ddots & \vdots \\ \dfrac{\partial \bar{f}_{ngp}}{\partial \Delta\gamma_1} & \dfrac{\partial \bar{f}_{ngp}}{\partial \Delta\gamma_2} & \cdots & \dfrac{\partial \bar{f}_{ngp}}{\partial \Delta\gamma_{ngp}} \end{bmatrix}. \tag{3.96}$$

We remark that, in the general case, the matrix $\frac{\partial \bar{\boldsymbol{f}}}{\partial \Delta\boldsymbol{\gamma}}$ is unsymmetric. A modified Newton-Raphson strategy can be achieved if we replace the matrix above by the following approximation that includes the diagonal terms and neglects all off-diagonal ones:

$$\frac{\partial \bar{\boldsymbol{f}}}{\partial \Delta\boldsymbol{\gamma}}^{\star} = \begin{bmatrix} \dfrac{\partial \bar{f}_1}{\partial \Delta\gamma_1} & 0 & \cdots & 0 \\ 0 & \dfrac{\partial \bar{f}_2}{\partial \Delta\gamma_2} & \cdots & 0 \\ \vdots & \vdots & \ddots & \vdots \\ 0 & 0 & \cdots & \dfrac{\partial \bar{f}_{ngp}}{\partial \Delta\gamma_{ngp}} \end{bmatrix} \tag{3.97}$$

which is the matrix corresponding to the local case for which the following useful relation applies:

$$\Delta\gamma_i^{k+1} = \Delta\gamma_i^k - \left(\frac{\partial \bar{f}_i^k}{\partial \Delta\gamma_i^k}^{\star}\right)^{-1} \bar{f}_i^k. \tag{3.98}$$

Therefore, according to this strategy, there is neither the need to assemble a global matrix nor to solve a linear system of equations per iteration since each equation can be updated independently, which saves significant CPU time.

Finally, we can establish the algorithm for the integration of the non-local constitutive model as depicted in pseudo-code format in Box 3. Remarkably, the algorithm is very similar to those employed in local models within a multiplicative hyperlasto-plasticity framework. The major difference is that the integration of the constitutive problem has to be done in a global fashion, firstly by computing and storing the elastic trial state for all integration points, then by solving the global problem by means of a modified Newton-Raphson algorithm and finally by updating the stress state for all Gauss points. Afterwards, the internal force vector is computed as usual and the analysis is undertaken as in the local case.

3.5.3 The consistent tangent stiffness

In order to ensure quadratic rates of convergence when using the full Newton-Raphson method, the use of the exact tangent stiffness is highly desired. It has been often advocated that the derivation of the consistent tangent stiffness within a non-local framework of integral-type requires non-standard procedures that are not practicable. This argument has motivated many researchers to develop strong non-local models through gradient-enhanced theories at the cost of having additional degrees of freedom at each node of the finite element mesh. As pointed out in the beginning of this chapter, gradient-dependent non-local formulations keep a local-like format, for which the consistent tangent can be determined in a relatively straightforward manner.

This aspect of the non-local formulation of integral-type has been, up to this date and to the author's knowledge, very little addressed in the literature. However, it is in fact possible to obtain closed-form expressions for the tangent stiffness for the integral case as well. During the course of this work, a general methodology for the derivation of the consistent stiffness for elasto-plastic constitutive models has been developed. This advance will be presented in detail in Chapter 5, together with a closed-form expression of the consistent tangent operator associated with the non-local constitutive model presented in this chapter.

Box 3: Algorithm for the solution of the non-local constitutive problem.

(i) Update the deformation gradient of all Gauss points for given incremental displacement $\Delta \boldsymbol{u}_i$

```
DO I=1,NGP
```

$$\boldsymbol{F}_{i_\Delta} = \boldsymbol{I} + \nabla_n \left[\Delta \boldsymbol{u}_i\right]; \qquad \boldsymbol{F}_{i_{n+1}} = \boldsymbol{F}_{i_\Delta} \boldsymbol{F}_{i_n}$$

```
END DO
```

(ii) Compute the elastic trial state for all Gauss points

```
DO I=1,NGP
```

$$\begin{aligned}
\boldsymbol{B}^e_{i_n} &= \exp\left[2\boldsymbol{\varepsilon}^e_{i_n}\right] \\
\boldsymbol{B}^{e\,trial}_{i_{n+1}} &= \boldsymbol{F}_{i_\Delta} \boldsymbol{B}^e_{i_n} \left(\boldsymbol{F}_{i_\Delta}\right)^T \\
\boldsymbol{\varepsilon}^{e\,trial}_{i_{n+1}} &= \frac{1}{2} \ln\left[\boldsymbol{B}^{e\,trial}_{i_{n+1}}\right] \\
R^{trial}_{i_{n+1}} &= R_{i_n} \\
\tilde{q}^{trial}_{i_{n+1}} &= \sqrt{\frac{3}{2}} \left\| 2G \mathrm{dev}\left(\boldsymbol{\varepsilon}^{e\,trial}_{i_{n+1}}\right) \right\|
\end{aligned}$$

```
END DO
```

(iii) Solve the non-linear complementarity problem for $\Delta \boldsymbol{\gamma}$ with the algorithm in Box 4:

$$\bar{\boldsymbol{f}}\left(\Delta \boldsymbol{\gamma}\right) = \boldsymbol{0}$$

(iv) Update stress state and constitutive variables for all Gauss points

```
DO I=1,NGP
  IF Δγ_i = 0 THEN
```

$$\bar{D}_{i_{n+1}} = \bar{D}_{i_n}$$

```
  ELSE
```

$$\bar{D}_{i_{n+1}} = 1 - \left(\frac{3G\Delta\gamma_i}{\tilde{q}^{trial}_{i_{n+1}} - \tau_y\left(R_{i_{n+1}}\right)} \right)$$

```
  END IF
```

$$\begin{aligned}
\boldsymbol{\varepsilon}^e_{i_{n+1}} &= \boldsymbol{\varepsilon}^{e\,trial}_{i_{n+1}} - \sqrt{\frac{3}{2}} \frac{\Delta\gamma_i}{\left(1 - \bar{D}_{i_{n+1}}\right)} \frac{\mathrm{dev}\left(\boldsymbol{\varepsilon}^{e\,trial}_{i_{n+1}}\right)}{\left\| \mathrm{dev}\left(\boldsymbol{\varepsilon}^{e\,trial}_{i_{n+1}}\right) \right\|} \\
\boldsymbol{\tau}_{i_{n+1}} &= \left(1 - \bar{D}_{i_{n+1}}\right) \mathbf{D}^e : \boldsymbol{\varepsilon}^e_{i_{n+1}} \\
\boldsymbol{\sigma}_{i_{n+1}} &= \frac{1}{\det \boldsymbol{F}_{i_{n+1}}} \boldsymbol{\tau}_{i_{n+1}}
\end{aligned}$$

```
END DO
```

Box 4: Algorithm for the solution of the NCP.

1. Initialise $k = 0$ and $\Delta\boldsymbol{\gamma}^{k+1} = \mathbf{0}$

2. Loop over Gauss points and evaluate residual function

```
DO I=1,NGP
```

IF $F_{p\,i}^{k+1} = \tilde{q}_{i_{n+1}}^{trial} - \tau_y(R_{i_{n+1}}^{k+1}) \leq 0$ AND $\Delta\gamma_i^{k+1} = 0$ THEN

$$\bar{f}_i\left(\Delta\boldsymbol{\gamma}^{k+1}\right) = 0$$

ELSE

$$\bar{f}_i\left(\Delta\boldsymbol{\gamma}^{k+1}\right) = \text{Equation (3.91)}$$

END IF

```
END DO
```

3. Check convergence

IF $\left\|\bar{\boldsymbol{f}}\right\| < TOL$ EXIT

4. Update and switch incremental plastic multiplier vector

```
DO I=1,NGP
```

$$\Delta\gamma_i^k = \Delta\gamma_i^{k+1}$$

$$\Delta\gamma_i^{k+1} = \Delta\gamma_i^k - \left(\frac{\partial \bar{f}_i^k}{\partial \Delta\gamma_i^k}^{\star}\right)^{-1} \bar{f}_i^k$$

```
END DO
```

5. Go to Box **2.**

3.6 Numerical results

3.6.1 Necking of a cylindrical bar

In the present section, we assess the effectiveness of the non-local model by simulating the necking of a cylindrical bar. This is a widely known benchmark commonly employed in the assessment of finite strain theories. As schematically depicted in Figure 3.5, only a quarter of the bar is simulated due to symmetry. An imperfection to trigger necking is introduced by decreasing the cross-sectional area at the centre of the bar by 1.8%. Eight-noded quadrilateral elements with reduced integration have been employed in all simulations. The material properties are listed in Table 3.1 and a reference value of $\ell_r = \sqrt{c} = 0.6325$ mm for the intrinsic length has been adopted following [26] who used a value of $c = 0.4$ mm^2 in the context of a non-local implicit gradient model. The bar has been subjected to a prescribed vertical displacement of $u_y = 2.756$ mm. In order to capture the mesh dependency of the local theory as well as to illustrate the regularising effect of the non-local enrichment, different mesh refinements have been considered as shown in Figure 3.5.

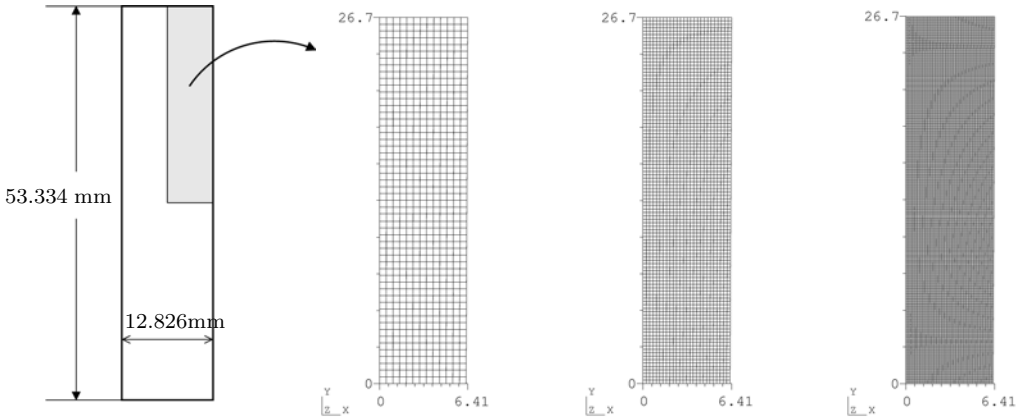

FIGURE 3.5: Necking of a Cylindrical bar: geometry and mesh refinement.

The results with the local model, depicted in Figure 3.6, clearly show the tendency of damage to concentrate into a single element upon mesh refinement. In Figure 3.6c, damage attained the critical value of 1.0 before the prescribed displacement reached its total value and the simulation was stopped.

When the non-local theory is adopted, damage converges to a stabilised value after some subsequent mesh refinement as one can conclude after a close inspection of Figures 3.7, 3.8 and 3.9. The results demonstrate that the pathological

TABLE 3.1: Material properties for the cylindrical bar.

Property	**Value**
Elastic modulus	$E = 206.9$ GPa
Poisson's ratio	$\nu = 0.29$
Damage exponent	$s = 1.0$
Damage denominator	$r = 1.25$ MPa
Hardening function	$\tau_y(R) = (715 - 450)[1 - \exp(16.93R)]$ $+129.24R$ MPa
Non-local intrinsic length	$\ell_r = 0.6325$ mm

mesh dependency has been eliminated with any of the three non-local averaging strategies alluded in the third section of this chapter with slight differences on the maximum damage value reached. As one could expect, the Eulerian and updated Lagrangian-type of non-local averaging have remarkably lead to quite similar results since the time-steps employed were not too large. Moreover, the total Lagrangian-type converged to a slightly lower value of maximum damage, demonstrating a similar behaviour as the one reported by Geers et al. [55] who used a gradient-enhanced elasto-plastic model coupled with damage.

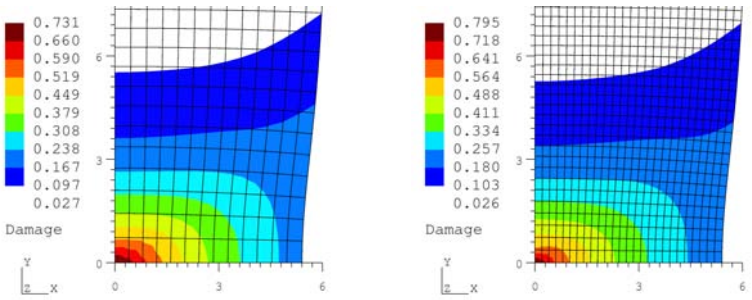

(A) (B)

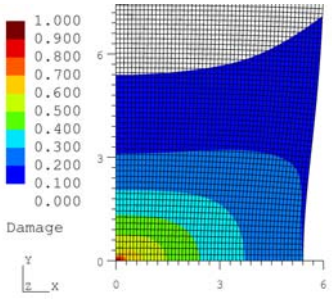

(C)

FIGURE 3.6: Damage contours at the critical region for the local case.

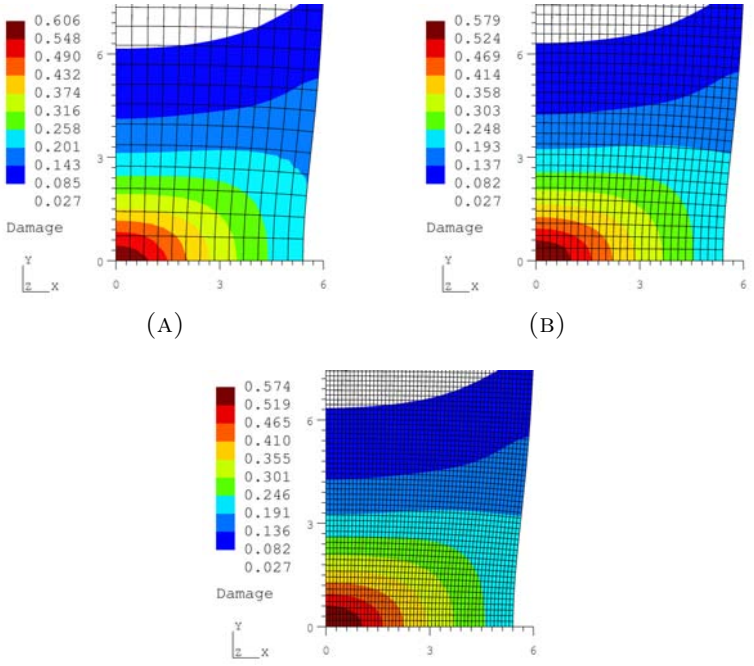

(A) (B)

(C)

FIGURE 3.7: Damage contours at the critical region for the non-local case: non-local averaging of Eulerian-type.

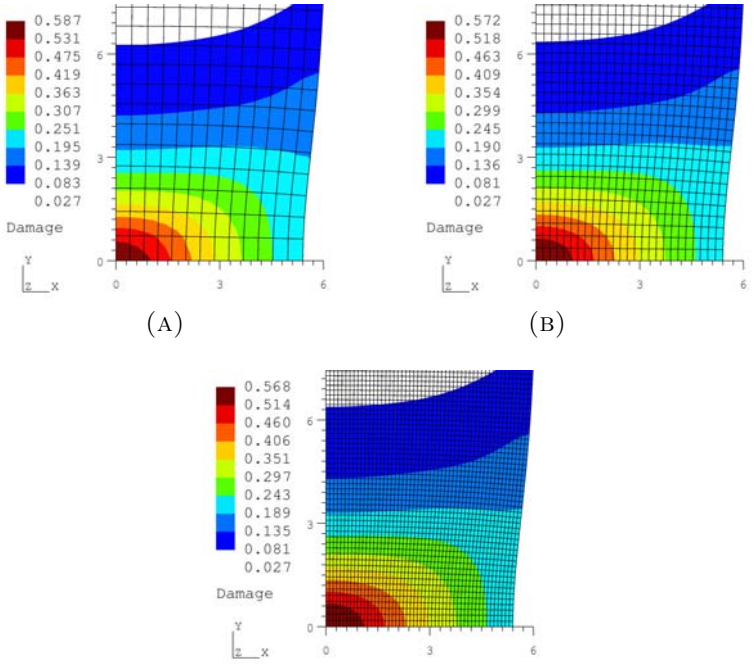

(A) (B)

(C)

FIGURE 3.8: Damage contours at the critical region for the non-local case: non-local averaging of total Lagrangian-type.

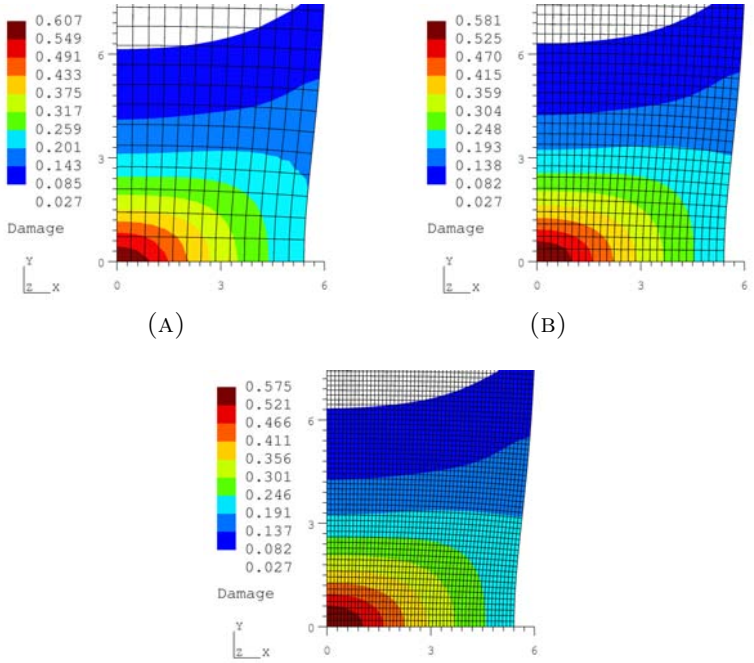

(A) (B)

(C)

FIGURE 3.9: Damage contours at the critical region for the non-local case: non-local averaging of updated Lagrangian-type.

The efficiency of the material integration algorithm has also been assessed for the present example. As depicted in Table 3.2, the typical convergence exhibits a remarkably high rate although we have neglected the off-diagonal terms in Equation (3.96). It is important to mention that, within one equilibrium iteration, the material problem has been solved for the *whole body* in just 4 iterations.

TABLE 3.2: Typical convergence of the projected modified Newton-Raphson algorithm: simulation of the necking of a cylindrical bar.

Iteration	**Residual Norm**
1	$6.70 \times 10^{+04}$
2	$3.43 \times 10^{+00}$
3	6.17×10^{-06}
4	1.55×10^{-11}

3.6.2 Damaging of a notched bar

In order to further illustrate the regularising properties of the proposed non-local model, we simulate the damaging of a notched bar. The geometry has been discretised by three meshes with different refinements (see Figure 3.10) with 8-noded quadratic elements with reduced integration. The material properties are given in Table 3.3.

The specimen has been subjected to a vertical prescribed displacement of $u_y = 0.555$ mm. This example has also been carried out by Vaz Jr. and Owen [115] in the context of local elasto-plastic damage model where it has been shown that the fracture location has been correctly predicted since the damage evolution law was a function of the triaxiality ratio, $\eta = \tau_h/q$, as it is in the case of the present model.

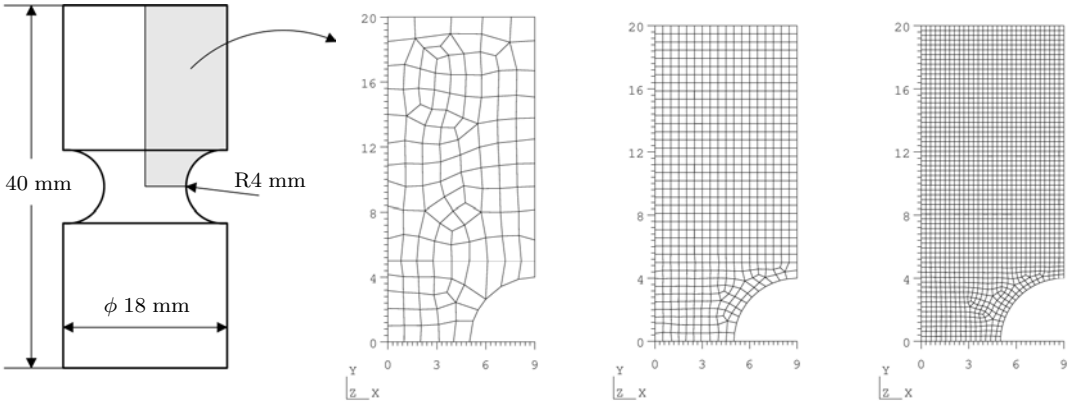

FIGURE 3.10: Damaging of a notched bar: geometry and meshes.

TABLE 3.3: Material properties for the notched bar.

Property	**Value**
Elastic modulus	$E = 69$ GPa
Poisson's ratio	$\nu = 0.3$
Damage exponent	$s = 1.0$
Damage denominator	$r = 1.25$ MPa
Hardening function	$\tau_y(R) = 589(10^{-4} + R)^{0.216}$ MPa
Non-local intrinsic length	$\ell_r = 0.6325$ mm

Figure 3.11 shows the contours for damage in the local case. Noticeably, damage shrinks to a single element upon mesh refinement. In Figure 3.11c, damage has attained the value 1.0 before the total displacement was applied and the simulation was stopped. Conversely, Figures 3.12 and 3.13 highlight the results for the thermodynamically consistent and classical non-local models, respectively. Both formulations lead to a regularised solution where pathological mesh dependency was significantly alleviated. In Figure 3.14, we can observe a direct comparison between the formulations. We conclude after a close inspection that the thermodynamically consistent non-local model has demonstrated a higher diffusive effect than the associated classical theory. This is due to the additional regularisation on the energy release rate, $-Y$, which is a function of the triaxiality ratio, $\eta = \tau_h/q$.

Finally, we observe again the convergence of the material integration algorithm. As Table 3.4 clearly demonstrates, convergence has been attained very quickly and the constitutive solution has been computed for the whole body in a few iterations.

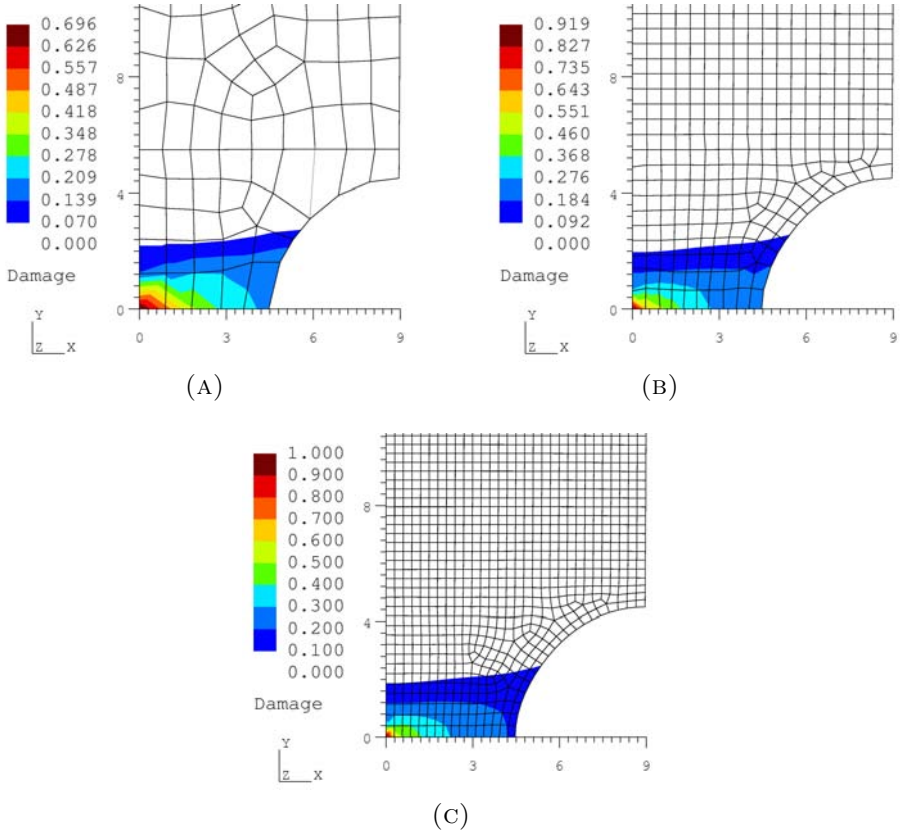

(A) (B)

(C)

FIGURE 3.11: Damage contours at the critical region for the local case.

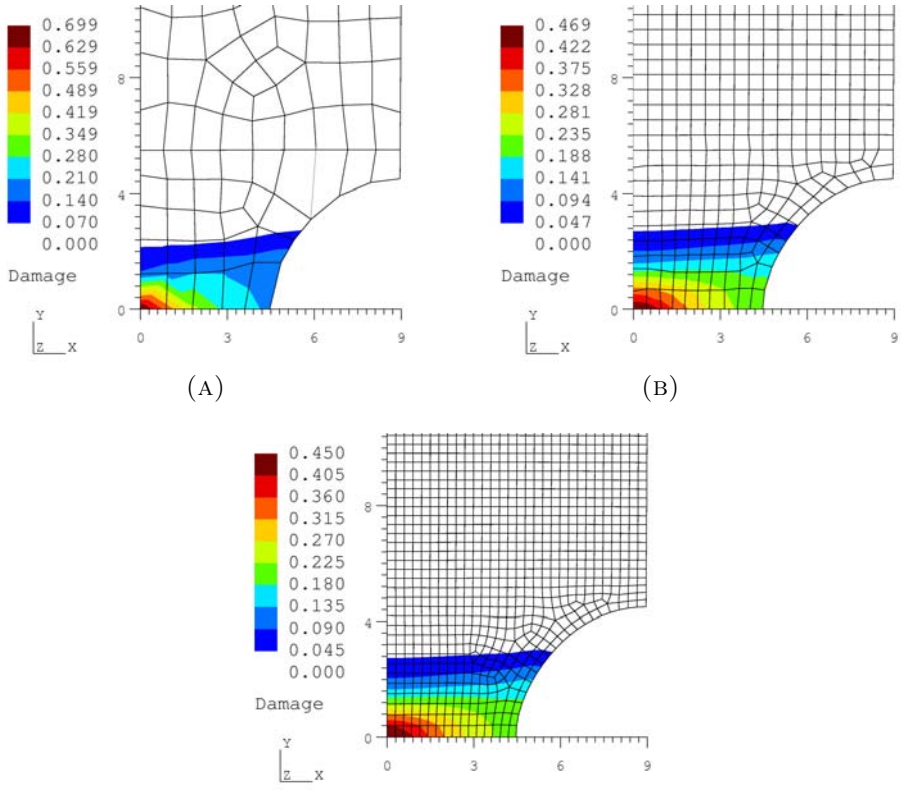

(A) (B)

(C)

FIGURE 3.12: Damage contours at the critical region for the thermodynamically consistent non-local formulation.

TABLE 3.4: Typical convergence of the projected modified Newton-Raphson algorithm: simulation of the damaging of a notched specimen.

Iteration	**Residual Norm**
1	$1.65 \times 10^{+08}$
2	$1.53 \times 10^{+04}$
3	1.31×10^{-02}
4	4.47×10^{-11}

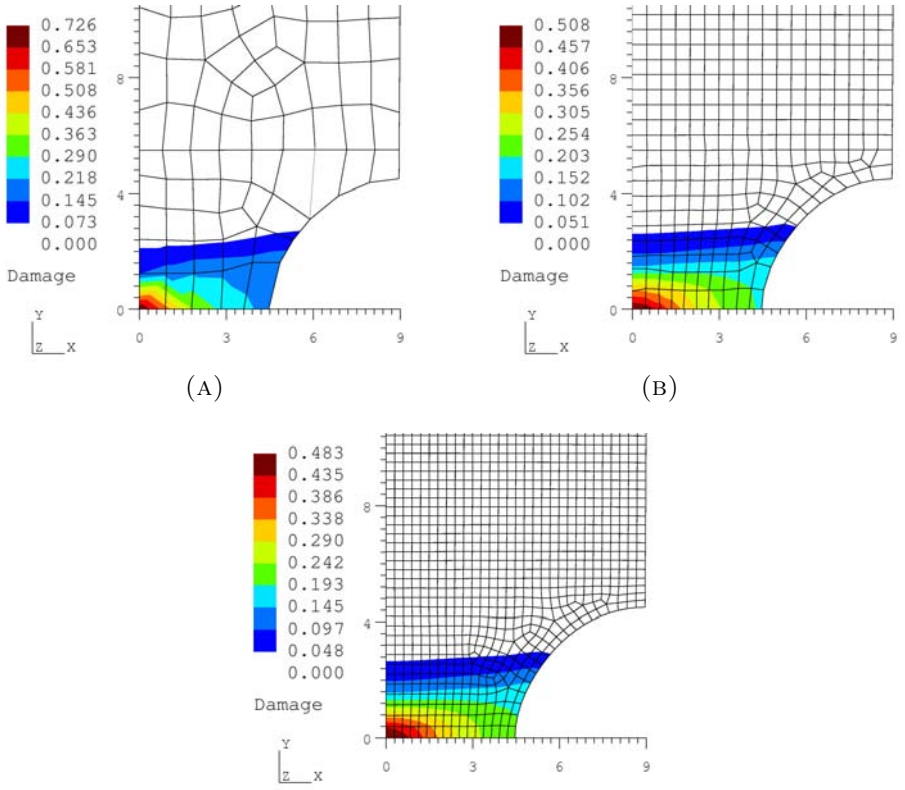

(A) (B)

(C)

FIGURE 3.13: Damage contours at the critical region for the classical non-local formulation.

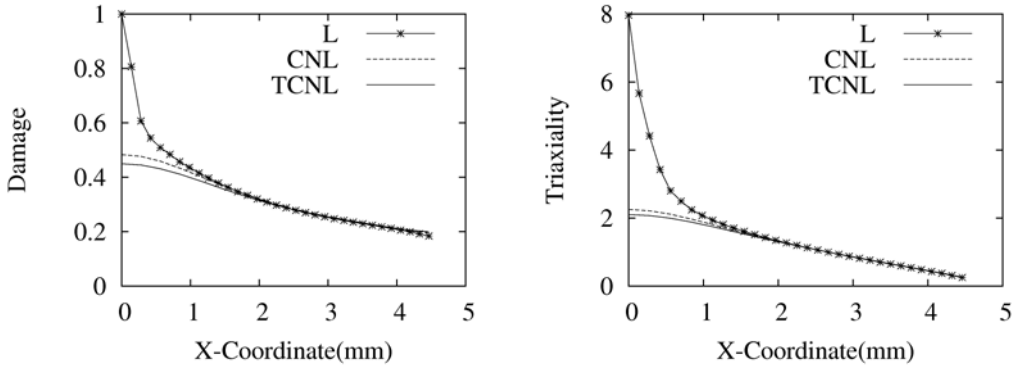

(A) (B)

FIGURE 3.14: Damage (A) and triaxiality (B) distributions along the central section of the specimen: comparison among the local (L), classical non-local (CNL) and thermodynamically consistent non-local (TCNL) formulations.

3.6.3 Stretching of a perforated plate

This last example illustrates the regularising properties of the proposed non-local model when applied in the three-dimensional simulation of a perforated plate (Figure 3.15(a)). This case has been subjected of experimental testing by Bao [7] especially due to the mid-range triaxiality value of $\eta = 1/3$ achieved at the critical region of the specimen. The plate has been discretised with 8-noded linear hexahedra as depicted in Figure 3.15.

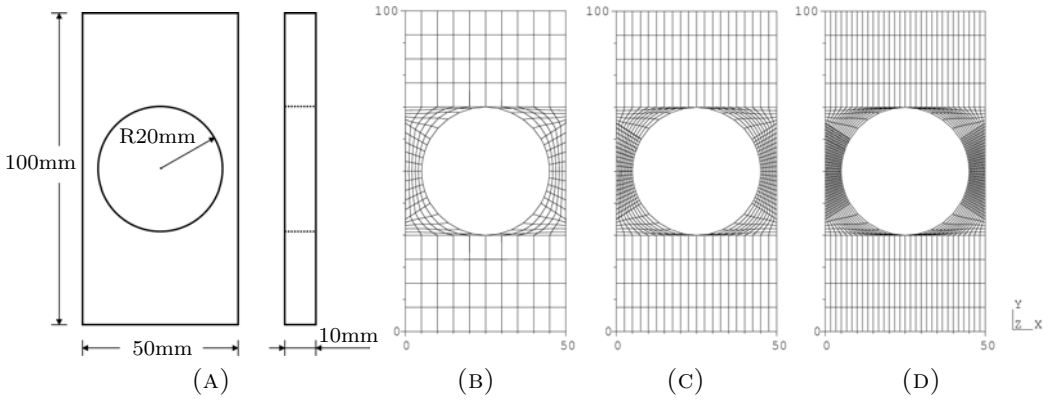

FIGURE 3.15: Geometry and different mesh refinements for the perforated plate.

TABLE 3.5: Material properties for the perforated plate.

Property	**Value**
Elastic modulus	$E = 71.5$ GPa
Poisson's ratio	$\nu = 0.3$
Damage exponent	$s = 1.0$
Damage denominator	$r = 6.0$ MPa
Hardening function	$\tau_y(R) = 908(0.0058 + R)^{0.1742}$ MPa
Non-local intrinsic length	$\ell_r = 2.0$ mm

In order to avoid spurious results due to element locking, the *F-bar formulation* [39] has been adopted. F-bar elements can be seen as a finite strain counterpart of the well-known B-bar methodology [64]. Since the intention of this example is to demonstrate how the non-local model can effectively eliminate spurious mesh dependence rather than to review an already well-established methodology, we shall limit ourselves to directly employ the F-bar formulation and the reader is referred to references [39, 40] for a comprehensive discussion on this topic. It is important to remark that the use of F-bar elements is *straightforward* with the

present non-local model. This stems from the fact that the non-local formulation proposed herein exclusively incorporates the non-local enhancement *on the material level*. Therefore, all implications demanded by the F-bar formulation keep exactly the same format as in local theories since the F-bar methodology is an element formulation that is independent of the constitutive model.

A prescribed displacement of $u_y = 0.5$ mm has been applied at one of the end surfaces of the plate while the other one has been kept fixed. As reported by Bao [7], experiments with an aluminium 2024-T351 have shown that fracture initiation takes place at the middle of the circumferential surface of the hole. Most of the material properties (Table 3.5) adopted in the present example are similar to those reported by Bao [7]. The internal length has been arbitrarily chosen to better represent the effects of the non-local model with the present discretisations. We remark again that the main goal of this chapter is to investigate the properties of the non-local model in a rather numerical fashion.

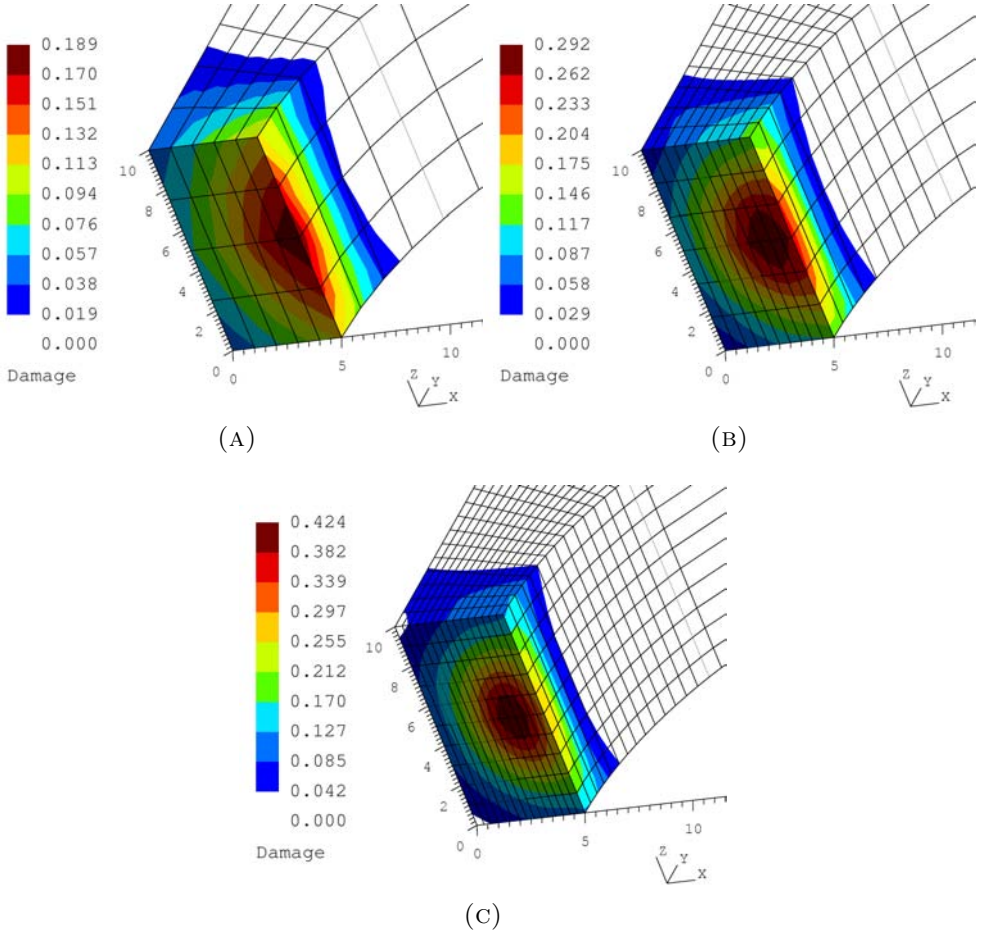

(A) (B)

(C)

FIGURE 3.16: Damage contours for the local case at the critical region.

The results obtained when the local case is considered are given in Figure 3.16[4]. Clearly, not only damage tends to concentrate in a narrow region upon mesh refinement, but also its magnitude tends to grow unlimitedly. When the non-local model is activated, this spurious result is significantly diminished as it can be concluded from Figure 3.17.

Finally, the convergence of the material algorithm is once again verified. Table 3.6 clearly shows that the algorithm has exhibited very high convergence rates, only requiring few iterations for the solution of the non-local constitutive problem.

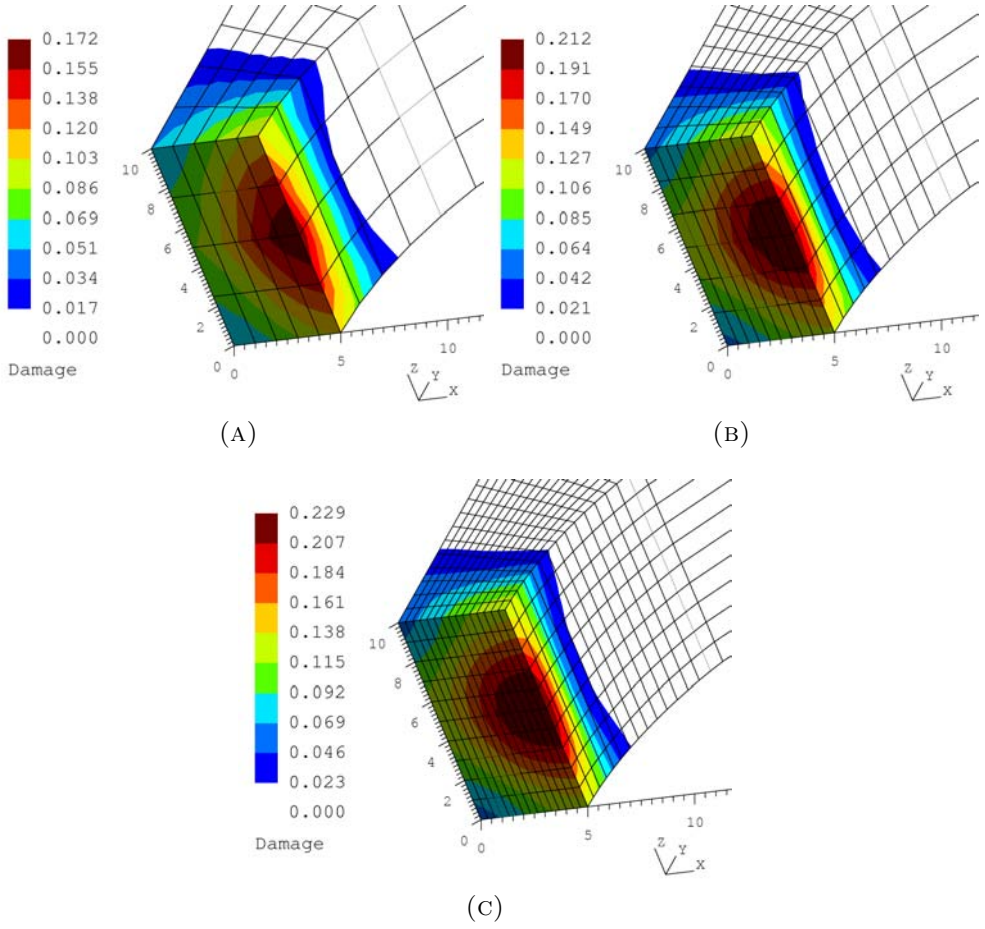

(A) (B)

(C)

FIGURE 3.17: Damage contours for the non-local case at the critical region.

3.7 Conclusions

In this chapter, a non-local constitutive model of integral-type for the description of ductile materials has been presented. The model has been formulated at finite strains where it has been shown that the well-established hyperelastic-based

[4]In the visualisations of this example, the results have been plotted on the undeformed mesh.

TABLE 3.6: Typical convergence of the projected modified Newton-Raphson algorithm: stretching of a perforated plate.

Iteration	**Residual Norm**
1	$2.35 \times 10^{+08}$
2	$1.82 \times 10^{+03}$
3	2.75×10^{-02}
4	5.89×10^{-11}

multiplicative plasticity framework can be efficiently employed in a straightforward manner in conjunction with the non-local formulation of integral-type. The exponential map backward integration scheme together with the use of the logarithmic strain measure has allowed the constitutive problem to be written in a small strain-like format for which the non-local solution is achieved by means of a projected modified Newton-Raphson strategy. Although the off-diagonal terms of Equation (3.96) have been disregarded, the material integration algorithm has exhibited remarkably high convergence rates.

Moreover, the derivation of the non-local model from thermodynamic potentials has been shown. The use of a non-local residual, as proposed by other authors for the description of small strain plasticity and damage of quasi-brittle materials, has been employed in order to write the dissipation inequality in a local fashion. The thermodynamical framework has implied the regularisation of the thermodynamic force conjugated with damage, resulting in a dual averaging character. The thermodynamically consistent model has been compared with its associated classical, ad-hoc formulated counterpart. The thermodynamical admissibility of the classical model has been demonstrated by re-writing the dissipation inequality in a global form. Representative results have shown that the thermodynamically consistent model tends to produce a higher diffusive effect on damage evolution than the classical model due to the additional averaging of the energy release rate, which in turn is directly associated with the triaxiality.

Finally, different averaging strategies evaluated at different configurations have been defined and assessed. The results have shown that all the three definitions, Eulerian-type, total Lagrangian-type and updated Lagrangian-type lead to distinct but regularised solutions for the case analysed in the present contribution.

As a main final conclusion, the proposed non-local model and its associated numerical implementation have proven to be a suitable tool to circumvent the pathological mesh sensitivity inherently present in the local formulation for softening ductile solids. Moreover, due to its straightforward implementation, the non-local model

of integral-type can be seen as a competitive alternative to gradient-enhanced models.

Chapter 4

Non-local Formulation of a Gurson-like Damage Model including a Shear Mechanism

The constitutive framework proposed by Gurson [57] is one of the pioneering works that attempted to describe material degradation based on micro-mechanical grounds. In his approach, material degradation, which is in a general sense characterised by the presence of micro-voids, is regarded through a constitutive variable denoted as *porosity*. The evolution of the porosity predicted by Gurson's model follows a direct consequence of the requirement for mass conservation of a rigid plastic material assuming plastic incompressibility. The theory of Gurson has then been very often adopted by many researchers in the prediction of ductile fracture. However, his model was restrictive in the sense that it considered that only existing spherical micro-voids could growth. This means that no porosity evolution would be predicted if the initial porosity were zero. Many authors have tried to overcome this limitation by incorporating in the theory other constitutive mechanisms that would better describe observable phenomena such as the nucleation and coalescence of voids. Perhaps, the most popular modification of Gurson's theory has been proposed by Tvergaard and Needleman [113] who modified the yield function of Gurson to account for the coalescence effect and also introduced in the evolution of porosity a term for micro-void nucleation.

It is interesting to observe that the phenomena described above (nucleation, growth and coalescence of voids) are very closely linked to fracture at high stress triaxialities. Thus, its very conception implies that they might fail when subjected to other stress triaxialities. In fact, recent research effort has precisely shown that neither

Gurson's nor Tvergaard-Needleman's model could predict material degradation under pure shear stress states, that is, when the triaxiality stress ratio is around zero [53, 83, 121]. In particular, Feucht et al. [53] have carried out the simulation of the so-called Iosipescu shear specimen where it has been shown that fracture could not be correctly predicted by the Gurson model with the Tvergaard-Needleman modification. In order to overcome this limitation, they have adopted a Johnson-Cook-like 'a posteriori' failure criterion. When the critical value of plastic strain was reached through the application of the criterion, the corresponding element was deleted from the finite element mesh, which rendered significantly improved numerical predictions. However, the constitutive model itself has not been altered, which means that failure was not predicted by a corrected evolution of porosity.

Nahshon and Hutchinson [83] and Xue [121] have instead sought to incorporate into the constitutive law an additional damaging mechanism to account for the material degradation under shear-dominated stress states. Both contributions have proposed modifications based on experimental findings. As reported by many authors [e.g. 10], under pure shear (i.e., when triaxiality is zero), the dominant fracture mechanism is the so-called *void-shearing*, in which the micro-cavities present in the matrix material tend to shear between themselves. In order to describe such phenomenon, Nahshon and Hutchinson [83] proposed an additional term, phenomenologically defined and dependent on the third invariant of the stress tensor, to be introduced in the evolution of porosity. Conversely, Xue [121] developed the definition of the shear mechanism based on a theoretical analysis of micro-voids. Both mechanisms share the property of being dependent on the third stress invariant. Recently, Reis et al. [98] have carried out a comprehensive numerical comparison of both mechanisms when subjected to pure shear, combined tensile/shear and combined compression/shear stress states. They have found that the shear mechanism proposed by Nahshon and Hutchinson presents an overall better performance than Xue's mechanism, although their results have suggested that the material parameter of Nahshon-Hutchinson's model needed to be changed according to the stress state.

In spite of these significant advances on Gurson-based models, most of the proposed constitutive theories have been conceived under the hypothesis of local continuum, that is, the material law is independent of the surrounding points. It is widely recognised that this inevitably leads to spurious mesh dependence on the finite element solution due to the loss of ellipticity of the equilibrium equations under the softening regime. Nonetheless, some contributions have tried to tackle this issue aiming to provide mesh-insensitive Gurson-based constitutive models. For instance, Tvergaard and Needleman [114] have proposed a non-local model of

integral-type by regularising the porosity variable. In their approach, they have avoided the definition of an 'exact' non-local formulation by only approximating the non-local rate equation. This approach has also been adopted by Feucht [51] who has also enriched Gurson's model with a gradient-dependent theory. Reusch et al. [99] have also employed a gradient-enhanced non-local formulation where a new damage variable, which was related to the local porosity through a gradient equation, has been incorporated in the yield function proposed by Tvergaard and Needleman [113]. The model was later extended to finite strains [100]. Hakansson et al. [59] provided a thermomechanical constitutive theory for porous materials by including an additional equilibrium equation containing the gradient of the porosity variable. In their formulation, the local mechanical, the thermal and the non-local problem were solved in an uncoupled fashion. Enakousta et al. [45] have considered a non-local porosity rate, defined through an averaging integral, which was explicitly integrated. In their numerical strategy, the non-local porosity was computed only after the material problem was solved for a fixed value of porosity. More recently, Samal et al. [105] have enhanced Rousselier's constitutive model by adopting a similar approach to the one proposed by Reusch et al. [99], i.e., a new damage variable has been incorporated through a gradient implicit formulation.

However, none of the aforementioned contributions has focused in developing a Gurson-based non-local model within a 'full' integral framework. As discussed in Chapter 3, the integral-type non-local formulation has the advantage of being completely defined on the material level, avoiding the definition of additional structural variables in the global system of equations. Besides, as demonstrated in Chapter 3, many of the advantages of the constitutive modelling at finite strains within the local framework can be straightforward extended to the non-local case. Therefore, the goal of this chapter is to propose a non-local Gurson-based damage model based on the integral approach. We adopt herein a shear mechanism, similar to the one proposed by Nahshon and Hutchinson [83], to take into account the degradation effects that take place whenever shear deformation is dominant. A non-local theory associated with the constitutive model is proposed where the damage variable is enhanced with non-locality. The numerical implementation of the non-local model is presented in detail. The need for a global material integration scheme when the 'exact' non-local formulation is adopted is highlighted. The solution of the material problem through either a full and a modified Newton-Raphson strategy is undertaken their efficiency is discussed. Furthermore, it is shown that the non-local theory is able to attenuate the unlimited localisation behaviour of the associated local theory.

4.1 Non-local constitutive model

As discussed in Chapter 3, Section 3.2, the establishment of the non-local constitutive model starts with the definition of the non-local quantity. Most Gurson-based non-local models available in the literature have introduced non-locality through some quantity related to the local porosity, f. This choice can be justified by the fact that the porosity is the variable that triggers the softening regime in Gurson-based constitutive models. Therefore, it sounds reasonable to regularise this variable in order to avoid excessive and unlimited localisation[1]. Adopting a non-local formulation of integral-type, we define

$$\bar{f}(\boldsymbol{x}) = \int_V \beta(\boldsymbol{x}, \boldsymbol{\xi}) f(\boldsymbol{\xi})\, dV(\boldsymbol{\xi}), \tag{4.1}$$

where $\bar{f}$ is the non-local damage variable defined at spatial point $\boldsymbol{x}$ and f is its associated local counter-part. We remark that f is herein regarded as a *damage variable* instead of *porosity* due to its phenomenological definition, yet to be presented in this chapter. In Equation (4.1), $\beta(\boldsymbol{x}, \boldsymbol{\xi})$ is the non-local averaging operator, which has to respect the normalising condition of Equation (3.11). Unlike the constitutive framework of Chapter 3, the use of a symmetric non-local averaging operator is, in the present case, only advantageous from a numerical point of view, for which less memory is required as pointed out in Chapter 3, Section 3.2.

One important assumption of the non-local theory adopted here is the independence of the non-local operator on the deformation history. As discussed in Chapter 3, this hypothesis leads us to draw the important conclusion that the rate of the non-local operator vanishes, i.e., $\dot{\beta}(\boldsymbol{x}, \boldsymbol{\xi}) = 0$. Hence, the following relation holds:

$$\dot{\bar{f}}(\boldsymbol{x}) = \int_V \beta(\boldsymbol{x}, \boldsymbol{\xi}) \dot{f}(\boldsymbol{\xi})\, dV(\boldsymbol{\xi}). \tag{4.2}$$

It is worth mentioning that the consideration of Equation (4.2) renders an 'exact' or 'fully coupled' non-local model. This kind of formulation has been generally avoided by many authors in the field who have either employed gradient-enhanced formulations [e.g. 59, 99, 105, amongst others] or adopted an approximation of the rate of the non-local variable [e.g. 51, 114]. The latter strategy, as also pointed out by its authors, has an increased dependency on the size of the time step used in the calculations when compared to general fully implicit material integration schemes (such as the typical return-mapping algorithm). Conversely, the present

[1] Similar to the case of the Lemaitre-based model of Chapter 3, where damage was adopted as the non-local quantity, the choice of f as non-local variable will be more clearly justified in Chapter 6.

non-local formulation avoids the errors associated with the approximation of the non-local rate[2]. Furthermore, in contrast to gradient-dependent non-local theories, no additional degrees-of-freedom are necessary in the structural problem since non-locality is herein strictly kept on the material level.

Before proceeding in the definition of the local evolution of the damage variable, $\dot{f}(\boldsymbol{\xi})$, we need to define some equations of the constitutive model first. This stems from the fact that the evolution of local damage will be a function of plastic straining. Firstly, we define the yield function to be given by

$$F_p(\boldsymbol{x}) = J_2(\boldsymbol{\tau}_d(\boldsymbol{x})) - \frac{1}{3}\left[1 + q_3 f^{*^2}(\boldsymbol{x}) - 2q_1 f^*(\boldsymbol{x}) \cosh\left(\frac{q_2 3\tau_h(\boldsymbol{x})}{2\tau_y(\boldsymbol{x})}\right)\right]\tau_y^2(\boldsymbol{x}), \quad (4.3)$$

where f^* is the *effective damage* given by

$$f^*(\boldsymbol{x}) = \begin{cases} \bar{f}(\boldsymbol{x}) & , \quad \bar{f}(\boldsymbol{x}) < f_c, \\ f_c + \left(\dfrac{1}{q_1} - f_c\right)\dfrac{\left(\bar{f}(\boldsymbol{x}) - f_c\right)}{(f_f - f_c)} & , \quad \bar{f}(\boldsymbol{x}) \geq f_c. \end{cases} \quad (4.4)$$

In the equations above, $J_2(\boldsymbol{\tau}_d(\boldsymbol{x}))$ denotes the second invariant of the deviatoric stress tensor; q_1, q_2 and q_3 are material parameters; f_c is the critical damage (which triggers the mechanism associated with coalescence of voids) and f_f is the damage at complete failure. The use of the effective damage f^* has been introduced by Tvergaard and Needleman [113] in order to capture the effects of coalescence of voids and is also adopted here. Note that the only difference between the yield function proposed by Tvergaard and Needleman [113] and the one adopted here is the presence of the non-local damage, $\bar{f}(\boldsymbol{x})$.

Plastic isotropy[3] and associative plasticity are assumed and, therefore, plastic flow is given by

$$\dot{\boldsymbol{F}}^p(\boldsymbol{x})\boldsymbol{F}^{p-1}(\boldsymbol{x}) = \dot{\gamma}(\boldsymbol{x})\boldsymbol{R}^{e^T}\left[\frac{\partial F_p(\boldsymbol{x})}{\partial \boldsymbol{\tau}(\boldsymbol{x})}\right]\boldsymbol{R}^e, \quad (4.5)$$

where

$$\frac{\partial F_p(\boldsymbol{x})}{\partial \boldsymbol{\tau}(\boldsymbol{x})} = \boldsymbol{\tau}_d(\boldsymbol{x}) + \frac{1}{3}q_1 q_2 \bar{f}(\boldsymbol{x})\tau_y(\boldsymbol{x}) \sinh\left(\frac{q_2 3\tau_h(\boldsymbol{x})}{2\tau_y(\boldsymbol{x})}\right)\boldsymbol{I}. \quad (4.6)$$

[2]In Chapter 7, we will conversely adopt an approximation of the rate of the non-local variable in the context of an explicit finite element formulation. In that case, the issue of the time step dependency is considerably alleviated due to the small critical time steps inherently required by the explicit formulation.

[3]The hypothesis of plastic isotropy leads to a zero plastic spin (i.e. $\boldsymbol{W}^p = \boldsymbol{0}$), which, associated with the multiplicative hyperelastic plasticity framework presented in Chapter 3, allows the plastic flow to be written in the form of Equation (4.5).

The evolution equation of the isotropic hardening variable, R, is given by

$$\begin{aligned}\dot{R}(\boldsymbol{x}) &= \frac{\dot{\gamma}(\boldsymbol{x})}{1-\bar{f}(\boldsymbol{x})}\left\{q_1\, q_2\, \bar{f}(\boldsymbol{x})\, \tau_h(\boldsymbol{x})\, \sinh\left(\frac{q_2 3\tau_h(\boldsymbol{x})}{2\tau_y(\boldsymbol{x})}\right)\right. \\ &+ \left.\frac{2}{3}\left[1+q_3\bar{f}^2(\boldsymbol{x})-2q_1\bar{f}(\boldsymbol{x})\cosh\left(\frac{q_2 3\tau_h(\boldsymbol{x})}{2\tau_y(\boldsymbol{x})}\right)\right]\tau_y(\boldsymbol{x})\right\}. \qquad (4.7)\end{aligned}$$

Finally, we define the evolution of local damage to be given by

$$\dot{f}(\boldsymbol{\xi}) = \dot{f}^N(\boldsymbol{\xi}) + \dot{f}^G(\boldsymbol{\xi}) + \dot{f}^S(\boldsymbol{\xi}), \qquad (4.8)$$

where $\dot{f}^N(\boldsymbol{\xi})$ and $\dot{f}^G(\boldsymbol{\xi})$ represent the local evolution of damage respectively associated with the nucleation and growth of micro-voids. Following the works of Gurson [57] and Tvergaard and Needleman [113], these mechanisms are defined as

$$\dot{f}^N(\boldsymbol{\xi}) = \mathcal{A}(\boldsymbol{\xi})\dot{\varepsilon}^p_{eq}(\boldsymbol{\xi}), \qquad (4.9)$$

$$\dot{f}^G(\boldsymbol{\xi}) = (1-f(\boldsymbol{\xi}))\dot{\varepsilon}^p_{v}(\boldsymbol{\xi}), \qquad (4.10)$$

where

$$\mathcal{A}(\boldsymbol{\xi}) = \frac{f_N}{s_N\sqrt{2\pi}}\exp\left[-\frac{1}{2}\left(\frac{\varepsilon^p_{eq}(\boldsymbol{\xi})-\varepsilon_N}{s_N}\right)^2\right]. \qquad (4.11)$$

The quantity $\dot{\varepsilon}^p_{eq}(\boldsymbol{\xi})$ is the local evolution of the equivalent plastic strain, given by

$$\begin{aligned}\dot{\varepsilon}^p_{eq}(\boldsymbol{\xi}) &= \sqrt{\frac{2}{3}}\|\tilde{\boldsymbol{D}}^p(\boldsymbol{\xi})\| \\ &= \dot{\gamma}(\boldsymbol{\xi})\sqrt{\frac{2}{3}\left\{\boldsymbol{\tau}_d(\boldsymbol{\xi}):\boldsymbol{\tau}_d(\boldsymbol{\xi})+\frac{1}{3}\left[q_1q_2f(\boldsymbol{\xi})\tau_y(\boldsymbol{\xi})\sinh\left(\frac{q_2 3\tau_h(\boldsymbol{\xi})}{2\tau_y(\boldsymbol{\xi})}\right)\right]^2\right\}}, \qquad (4.12)\end{aligned}$$

and $\dot{\varepsilon}^p_v(\boldsymbol{\xi})$ is the local evolution of the volumetric plastic strain:

$$\dot{\varepsilon}^p_v(\boldsymbol{\xi}) = \tilde{\boldsymbol{D}}^p(\boldsymbol{\xi}):\boldsymbol{I} = \dot{\gamma}(\boldsymbol{\xi})q_1q_2f(\boldsymbol{\xi})\tau_y(\boldsymbol{\xi})\sinh\left(\frac{q_2 3\tau_h(\boldsymbol{\xi})}{2\tau_y(\boldsymbol{\xi})}\right). \qquad (4.13)$$

The last term in the right-hand side of Equation (4.8), $\dot{f}^S(\boldsymbol{\xi})$, incorporates, in a phenomenological fashion, the effects of void shearing experimentally observed when the material is subjected to low triaxialities, here assumed to be given by

$$\dot{f}^S(\boldsymbol{\xi}) = kg_\xi f(\boldsymbol{\xi})\dot{\varepsilon}^p_{eq}(\boldsymbol{\xi}), \qquad (4.14)$$

where

$$g_\xi = 1 - \left[\frac{27}{2}\frac{J_3(\boldsymbol{\tau}_d(\boldsymbol{\xi}))}{q^3(\boldsymbol{\xi})}\right]^2, \tag{4.15}$$

and k is a material parameter that has to be experimentally calibrated. Equation (4.14) is in fact a slightly modified version of the shear mechanism proposed by Nahshon and Hutchinson [83]:

$$\dot{f}^S(\boldsymbol{\xi}) = k g_\xi f(\boldsymbol{\xi}) \frac{\boldsymbol{\tau}_d(\boldsymbol{\xi}) : \tilde{\boldsymbol{D}}^p(\boldsymbol{\xi})}{q(\boldsymbol{\xi})}. \tag{4.16}$$

During this study, it has been observed that the modified version (Equation 4.14) provides, in general, a more stable numerical algorithm and therefore it has been adopted. In the equations above, $q(\boldsymbol{\xi})$ denotes the equivalent von Mises stress, defined in Equation (3.64).

In Equation (4.14), g_ξ can assume values within the range of $0 \leq g_\xi \leq 1$. In the case of axisymmetric stress states, g_ξ has a value near zero and therefore the shear mechanism is inactive. Conversely, if the body is under pure shear, g_ξ equals to the unity and then the damaging mechanism due to void shearing is fully active. Any combined stress state, either tensile/shear or compression/shear, will render an intermediate value that will only partially activate the shear mechanism. As a matter of fact, experimental evidence has shown that, under combined stress states, different fracture mechanisms will take place simultaneously or even compete [10] and, therefore, Equation (4.14) remains physically sound.

It is also interesting to observe that Equation (4.14) is a linear function of the damage variable itself. Thus, the shear mechanism can only contribute to overall damage after some initial value of damage has already taken place. In fact, this can be physically supported by the fact that the shearing effect only occurs to existing voids, or, in other words, the void shearing phenomenon takes place only after micro-voids have nucleated.

The constitutive model is complete with the loading/unloading (or Kuhn-Tucker) conditions:

$$\dot{\gamma}(\boldsymbol{x}) \geq 0; \quad F_p(\boldsymbol{x}) \leq 0; \quad \dot{\gamma}(\boldsymbol{x}) F_p(\boldsymbol{x}) = 0 \quad \forall\, \boldsymbol{x} \in V. \tag{4.17}$$

The above equations are those associated with the material point located at $\boldsymbol{x}$. However, as discussed in Chapter 3 in detail, the Kuhn-Tucker conditions must hold globally. Therefore, a suitable global material integration strategy will be employed in the following.

4.2 Numerical implementation

4.2.1 Discretisation of the averaging integral

Within a typical local finite element framework, the material problem is computed at each Gauss point separately. Afterwards, the resulting stress is employed in the element integration which is, in turn, carried out over the Gauss points. In the local scheme, the spatial position of the integration point is not of importance since only the strain increment and the values of the internal variables at the previous iteration are needed for the solution of the material problem. However, in the case of the non-local material model, the geometric location of the material point plays a major role in the update of the stress state. In practice, this means that the non-local averaging integral in Equation (4.2) needs to be spatially discretised due to the non-local averaging operator. It is therefore very convenient to adopt the Gaussian quadrature scheme to integrate the non-local equation. Hence, Equation (4.2) becomes

$$\dot{\bar{f}}_i = \sum_{j=1}^{npg_i} w_j J_j \beta_{ij} \dot{f}_j, \tag{4.18}$$

where $\beta_{ij} \equiv \beta(\boldsymbol{x}, \boldsymbol{\xi})$ is the averaging factor that relates the Gauss points i and j respectively located at global coordinates $\boldsymbol{x}$ and $\boldsymbol{\xi}$. $\bar{f}_i$ and f_j are the damage variables associated to the Gauss points i and j, respectively. The quantity w_j is the Gaussian weight and J_j is the Jacobian, both evaluated at the Gauss point j. Finally, npg_i is the number of Gauss points that lie inside the non-local volume of interaction measured from point i.

4.2.2 Integration of the material problem

In the previous subsection, the non-local averaging integral has been spatially discretised. However, the material problem still needs to be integrated over a pseudo-time increment from t_n to t_{n+1}. Employing the exponential map backward scheme [3] for the time-discretisation of the plastic flow rule, defined in equation (4.5), we have

$$\boldsymbol{F}^p_{i_{n+1}} = \exp\left\{\Delta\gamma_i \boldsymbol{R}^{e^T}_{i_{n+1}} \left[\boldsymbol{\tau}_{d_i\, n+1} + \frac{1}{3} q_1 q_2 \bar{f}_{i_{n+1}} \tau_{y_i\, n+1} \sinh\left(\frac{q_2 3\tau_{h_i\, n+1}}{2\tau_{y_i\, n+1}}\right) \boldsymbol{I}\right] \boldsymbol{R}^e_{i_{n+1}}\right\} \boldsymbol{F}^p_{i_n}. \tag{4.19}$$

The isotropy of the exponential tensor function ensures that the following holds:

$$\boldsymbol{F}^{p}_{i_{n+1}} = \boldsymbol{R}^{e^T}_{i_{n+1}} \exp\left\{\Delta\gamma_i \left[\boldsymbol{\tau}_{d_i\, n+1} + \frac{1}{3} q_1 q_2 \bar{f}_{i_{n+1}} \tau_{y_i\, n+1} \sinh\left(\frac{q_2 3\tau_{h_i\, n+1}}{2\tau_{y_i\, n+1}}\right) \boldsymbol{I}\right]\right\} \boldsymbol{R}^{e}_{i_{n+1}} \boldsymbol{F}^{p}_{i_n}. \tag{4.20}$$

At this point, it is convenient to define the elastic trial deformation gradient:

$$\boldsymbol{F}^{e\,trial}_{i_{n+1}} = \boldsymbol{F}_{i_\Delta} \boldsymbol{F}^{e}_{i_n}, \tag{4.21}$$

where $\boldsymbol{F}_{i_\Delta}$ is the incremental deformation gradient given by

$$\boldsymbol{F}_{i_\Delta} = \boldsymbol{I} + \nabla_n \left[\Delta \boldsymbol{u}_i\right], \tag{4.22}$$

and $\Delta\boldsymbol{u}_i$ corresponds to the incremental displacement field of Gauss point i.

Making use of Equation (4.21), we can define the update of the elastic deformation gradient as

$$\begin{aligned} \boldsymbol{F}^{e}_{i_{n+1}} &= \boldsymbol{F}^{e\,trial}_{i_{n+1}} \boldsymbol{R}^{e^T}_{i_{n+1}} \exp\left\{\Delta\gamma_i \left[\boldsymbol{\tau}_{d_i\, n+1}\right.\right. \\ &+ \left.\left. \frac{1}{3} q_1 q_2 \bar{f}_{i_{n+1}} \tau_{y_i\, n+1} \sinh\left(\frac{q_2 3\tau_{h_i\, n+1}}{2\tau_{y_i\, n+1}}\right) \boldsymbol{I}\right]\right\} \boldsymbol{R}^{e}_{i_{n+1}}. \end{aligned} \tag{4.23}$$

Finally, the use of the logarithmic elastic strain tensor allows us to rewrite the equation above as

$$\boldsymbol{\varepsilon}^{e}_{i_{n+1}} = \boldsymbol{\varepsilon}^{e\,trial}_{i_{n+1}} - \Delta\gamma_i \left[\boldsymbol{\tau}_{d_i\, n+1} + \frac{1}{3} q_1 q_2 \bar{f}_{i_{n+1}} \tau_{y_i\, n+1} \sinh\left(\frac{q_2 3\tau_{h_i\, n+1}}{2\tau_{y_i\, n+1}}\right) \boldsymbol{I}\right], \tag{4.24}$$

which clearly resembles a small strains format that makes easier its numerical implementation.

Recalling that the strain tensor can be split into a deviatoric and a volumetric contribution, Equation (4.24) can be rewritten in two independent equations, that is,

$$\boldsymbol{\varepsilon}^{e}_{d\, i_{n+1}} = \boldsymbol{\varepsilon}^{e\,trial}_{d\, i_{n+1}} - \Delta\gamma_i \boldsymbol{\tau}_{d_i\, n+1}, \tag{4.25}$$

$$\varepsilon^{e}_{v\, i_{n+1}} = \varepsilon^{e\,trial}_{v\, i_{n+1}} - \Delta\gamma_i q_1 q_2 \bar{f}_{i_{n+1}} \tau_{y_i\, n+1} \sinh\left(\frac{q_2 3\tau_{h_i\, n+1}}{2\tau_{y_i\, n+1}}\right). \tag{4.26}$$

Using the relation $\tau_h = K\varepsilon^{e}_{v}$, Equation (4.26) can be written in a residual form:

$$r_{\tau_h\, i} = \tau_{h_{i_{n+1}}} - \tau^{e\,trial}_{h_{i_{n+1}}} + \Delta\gamma_i K q_1 q_2 \bar{f}_{i_{n+1}} \tau_{y_i\, n+1} \sinh\left(\frac{q_2 3\tau_{h_i\, n+1}}{2\tau_{y_i\, n+1}}\right). \tag{4.27}$$

Similarly, knowning that $\boldsymbol{\tau}_d = 2G\varepsilon_d^e$, we get the following relation after some algebraic manipulations:

$$\boldsymbol{\tau}_{d_{i\,n+1}} = \frac{1}{1+2G\Delta\gamma_i}\boldsymbol{\tau}^{trial}_{d_{i\,n+1}}. \tag{4.28}$$

The relation above prevents $\boldsymbol{\tau}_{d_{i\,n+1}}$ to be an unknown of the constitutive problem since it can be expressed by known quantities (G and $\boldsymbol{\tau}^{trial}_{d_{i\,n+1}}$) and also by the unknown $\Delta\gamma_i$, which is present in all residual equations.

Attention is focused now on the time integration of the internal variables. In contrast with the case of plastic flow, the conventional backward Euler scheme will be adopted. Therefore, the discretised evolution of the isotropic hardening variable and non-local damage are respectively given, in a residual form, by

$$\begin{aligned} r_{Ri} &= R_{i_{n+1}} - R_{i_n} - \frac{\Delta\gamma_i}{1-\bar{f}_{i_{n+1}}}\left\{q_1q_2\bar{f}_{i_{n+1}}\tau_{h_{i\,n+1}}\sinh\left(\frac{q_2 3\tau_{h_{i\,n+1}}}{2\tau_{y_{i\,n+1}}}\right)\right. \\ &+ \left.\frac{2}{3}\left[1+q_3\bar{f}^2_{i_{n+1}} - 2q_1\bar{f}_{i_{n+1}}\cosh\left(\frac{q_2 3\tau_{h_{i\,n+1}}}{2\tau_{y_{i\,n+1}}}\right)\right]\tau_{y_{i\,n+1}}\right\}, \end{aligned} \tag{4.29}$$

and

$$r_{\bar{f}\,i} = \bar{f}_{i_{n+1}} - \bar{f}_{i_n} - \sum_{j=1}^{npg_i} w_j J_j \beta_{ij}\Delta f_j, \tag{4.30}$$

where

$$\Delta f_j = \Delta f_j^N + \Delta f_j^G + \Delta f_j^S. \tag{4.31}$$

Clearly, Equation (4.30) has terms that belong to other Gauss points. Thus, the solution of the material problem at Gauss point i depends on many points that are whithin the interaction radius, dictated by the non-local characteristic length.

In the equation above, Δf_j^N, Δf_j^G and Δf_j^S represent, respectively the discrete version of the damage mechanisms associated with void nucleation, void growth and void shearing. The first one is defined as

$$\Delta f_j^N = \mathcal{A}_{j_{n+1}}\Delta\varepsilon^p_{eq_j}, \tag{4.32}$$

where

$$\mathcal{A}_{j_{n+1}} = \frac{f_N}{s_N\sqrt{2\pi}}\exp\left[-\frac{1}{2}\left(\frac{\varepsilon^p_{eq_{j\,n+1}} - \varepsilon_N}{s_N}\right)^2\right], \tag{4.33}$$

and

$$\Delta\varepsilon^p_{eq_j} = \Delta\gamma_{j_{n+1}}\sqrt{\frac{2}{3}\left\{\boldsymbol{\tau}_{d_{j\,n+1}} : \boldsymbol{\tau}_{d_{j\,n+1}} + \frac{1}{3}\left[q_1 q_2 f_{j_{n+1}}\tau_{y_{j\,n+1}}\sinh\left(\frac{q_2 3\tau_{h_{j\,n+1}}}{2\tau_{y_{j\,n+1}}}\right)\right]^2\right.}. \tag{4.34}$$

The term Δf_j^G is associated with the growth mechanism and is given by

$$\Delta f_j^G = (1 - f_{j_{n+1}})\Delta\varepsilon^p_{v_j}, \tag{4.35}$$

where

$$\Delta\varepsilon^p_{v_j} = \Delta\gamma_j q_1 q_2 f_{j_{n+1}}\tau_{y_{j\,n+1}}\sinh\left(\frac{q_2 3\tau_{h_{i\,n+1}}}{2\tau_{y_{j\,n+1}}}\right). \tag{4.36}$$

Finally, the (discretised) evolution of the mechanism associated with void shearing reads

$$\Delta f_j^S = k g_{j_{n+1}} f_{j_{n+1}}\Delta\varepsilon^p_{eq_j}, \tag{4.37}$$

where

$$g_{j_{n+1}} = 1 - \left[\frac{27}{2}\frac{J_3(\boldsymbol{\tau}_{d_{j\,n+1}})}{q^3_{j_{n+1}}}\right]^2. \tag{4.38}$$

It is worth to recall that, in the equations above, $\boldsymbol{\tau}_{d_{j\,n+1}}$ is replaced by the relation of Equation (4.28) in the numerical implementation.

The yield function, given in its non-discretised form in Equation (4.3), constrains the constitutive problem in such manner that it determines whether the material response is elastic or plastic. For the i^{th} integration point, the residual equation associated with the yield function is given by

$$r_{\Delta\gamma_i} = J_2(\boldsymbol{\tau}_{d_{i\,n+1}}) - \frac{1}{3}\left[1 + q_3 f^{*^2}_{i_{n+1}} - 2q_1 f^*_{i_{n+1}}\cosh\left(\frac{q_2 3\tau_{h_{i\,n+1}}}{2\tau_{y_{i\,n+1}}}\right)\right]\tau^2_{y_{i\,n+1}}. \tag{4.39}$$

The four residual equations defined above are associated with a given i^{th} integration point. In the local case, the solution of a system of equations containing these residual equations would suffice to provide the constitutive behaviour. However, in the non-local case, the solution of the system of equations associated with the i^{th} integration point is in fact coupled with the solution of other system of equations which are, in turn, associated with neighbour integration points. This is completely analogous to the Lemaitre-based constitutive model of Chapter 3 whose solution of the associated non-local constitutive model had to be pursued in a global fashion. In sharp contrast to the Lemaitre-based material model of Chapter 3, the system of equations cannot be reduced to a single non-linear equation per Gauss point. Therefore, we will adopt henceforth the following notation

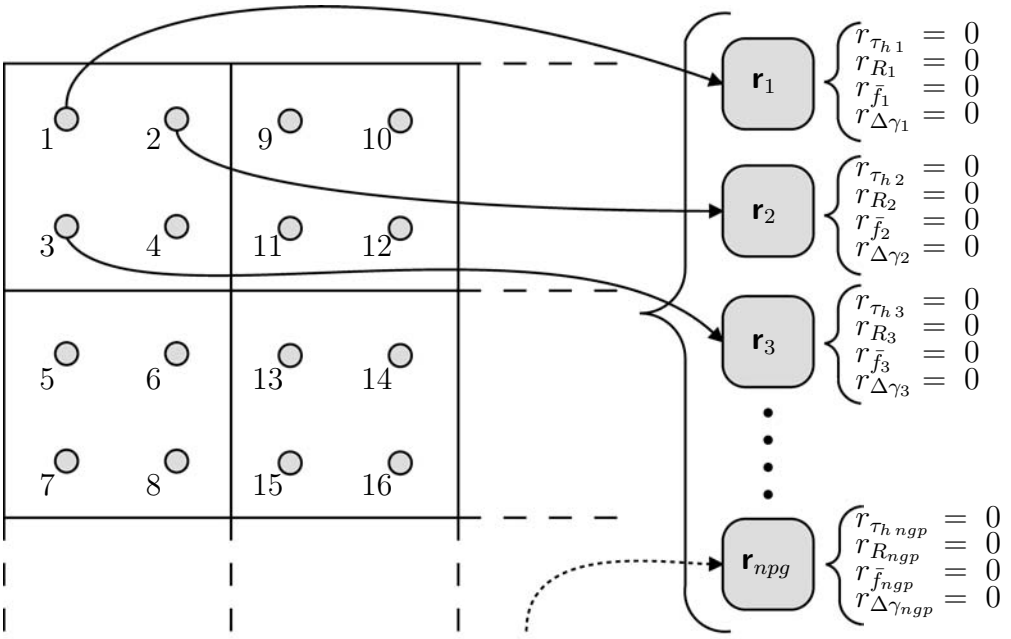

FIGURE 4.1: Schematic representation of the global non-local system.

to denote the system of equations associated with the i^{th} integration point:

$$\mathbf{r}_i = \begin{cases} r_{\tau_{h\,i}} = 0 \\ r_{R\,i} = 0 \\ r_{\bar{f}\,i} = 0 \\ r_{\Delta\gamma_i} = 0 \end{cases} \tag{4.40}$$

We recall that, in the non-local enhancement, the elastic counter-part of the constitutive model remains local. Therefore, the system above needs to be solved for $\tau_{h_i\,n+1}$, $R_{i_{n+1}}$, $\bar{f}_{i_{n+1}}$ and $\Delta\gamma_i$ only for plastic points and for all the Gauss points of the body simultaneously. A schematic representation of the global system of equations is given in Figure 4.1 where an excerpt of a finite element mesh containing quadrilateral elements with 4 integration points has been used for illustration purposes. For the sake of clarity, we will also adopt henceforth the following notation

to denote the group of unknowns associated with the i^{th} Gauss point:

$$\mathbf{x}_{i_{n+1}} = \left\{ \begin{array}{c} \tau_{h_{i\ n+1}} \\ \\ R_{i_{n+1}} \\ \\ \bar{f}_{i_{n+1}} \\ \\ \Delta\gamma_i \end{array} \right\}. \tag{4.41}$$

The non-local constitutive model has to be solved in a global fashion since every system of equation is in fact coupled with the ones associated with other integration points within its vicinity. Adopting the Newton-Raphson method, we have

$$\mathbf{x}_{n+1} = \mathbf{x}_n - \left[\left. \frac{\partial \mathbf{r}}{\partial \mathbf{x}} \right|_{\mathbf{x}_n} \right]^{-1} \mathbf{r}(\mathbf{x}_n), \tag{4.42}$$

which can be conveniently re-arranged to be given by

$$\left[\left. \frac{\partial \mathbf{r}}{\partial \mathbf{x}} \right|_{\mathbf{x}_n} \right] \delta\mathbf{x} = -\mathbf{r}(\mathbf{x}_n), \tag{4.43}$$

where

$$\delta\mathbf{x} = \mathbf{x}_{n+1} - \mathbf{x}_n. \tag{4.44}$$

If the full Newton-Raphson method is used, the matrix $\frac{\partial \mathbf{r}}{\partial \mathbf{x}}$ is given by

$$\frac{\partial \mathbf{r}}{\partial \mathbf{x}} = \left[\begin{array}{cccc} \frac{\partial \mathbf{r}_1}{\partial \mathbf{x}_1} & \frac{\partial \mathbf{r}_1}{\partial \mathbf{x}_2} & \cdots & \frac{\partial \mathbf{r}_1}{\partial \mathbf{x}_{ngp}} \\ \\ \frac{\partial \mathbf{r}_2}{\partial \mathbf{x}_1} & \frac{\partial \mathbf{r}_2}{\partial \mathbf{x}_2} & \cdots & \frac{\partial \mathbf{r}_2}{\partial \mathbf{x}_{ngp}} \\ \\ \vdots & \vdots & \ddots & \vdots \\ \\ \frac{\partial \mathbf{r}_{ngp}}{\partial \mathbf{x}_1} & \frac{\partial \mathbf{r}_{ngp}}{\partial \mathbf{x}_2} & \cdots & \frac{\partial \mathbf{r}_{ngp}}{\partial \mathbf{x}_{ngp}} \end{array} \right]. \tag{4.45}$$

As a matter of fact, the use of the full Newton method, necessary for quadratic convergence rates, requires the solution of a linear system with *ngp* equations. Nevertheless, an approximation can be adopted by disregarding the off-diagonal

terms, which leads to the following point-wise update:

$$\frac{\partial \mathbf{r}}{\partial \mathbf{x}} = \begin{bmatrix} \frac{\partial \mathbf{r}_1}{\partial \mathbf{x}_1} & \mathbf{0} & \cdots & \mathbf{0} \\ \mathbf{0} & \frac{\partial \mathbf{r}_2}{\partial \mathbf{x}_2} & \cdots & \mathbf{0} \\ \vdots & \vdots & \ddots & \vdots \\ \mathbf{0} & \mathbf{0} & \cdots & \frac{\partial \mathbf{r}_{ngp}}{\partial \mathbf{x}_{ngp}} \end{bmatrix}. \tag{4.46}$$

Recall that such approximation has been adopted for the Lemaitre-based model in Chapter 3 where, for that particular case, the state update procedure exhibited remarkably high convergence rates. Such convergence rates have persisted regardless of the stress state, which has greatly minimised the need of using the full Newton-Raphson method. However, Gurson-based models may be more non-linear that Lemaitre-based ones. Therefore, in the present case, both approaches, full and modified Newton-Raphson, will be compared in the next section.

4.2.3 Consistent tangent stiffness

In order to achieve the quadratic rates of convergence inherent to the Newton-Raphson solution method, a consistent linearisation of the constitutive integration procedure is necessary. As pointed out in Chapter 3, the use of consistent tangent operators within a non-local framework of integral-type is often said to be impracticable. However, as it will be shown in detail in Chapter 5, it is indeed possible to establish efficient tangent operators that are consistent with the non-local scheme. In the present case, numerical derivatives have been used to determine the terms $\partial \boldsymbol{\sigma}_i / \partial \boldsymbol{\varepsilon}_j$ in Equation (5.25). Note that, as it will be more clearly addressed in Chapter 5, the numerical derivation of the associated local derivative $\partial \boldsymbol{\sigma}_i / \partial \boldsymbol{\varepsilon}_i$ *does not* guarantee quadratic convergences, which can only be achieved if the non-local cross terms are consistently considered when assembling the global tangent operator, even with the use of numerical derivatives.

4.3 Numerical results

4.3.1 Axisymmetric specimen

In this first example, we simulate the notched cylindrical specimen of Chapter 3, Section 3.6.2, with the difference that in the present case we adopt the Gurson-based non-local model addressed in this chapter. The geometry and mesh refinement adopted are depicted in Figure 4.2. Once again, quadratic quadrilateral elements have been used where reduced integration has been employed to avoid spurious element locking. The material properties of this example, which are different from the ones employed in Section 3.6.2, are summarised in Table 4.1. It is worth mentioning that the effects of the shear mechanism do not take place in the axisymmetric specimen. This stems from the fact that the normalised third invariant remains constant and with the value of $\xi = 1.0$ during deformation. Therefore, the underlying local constitutive model reduces to the one proposed by Tvergaard and Needleman [113].

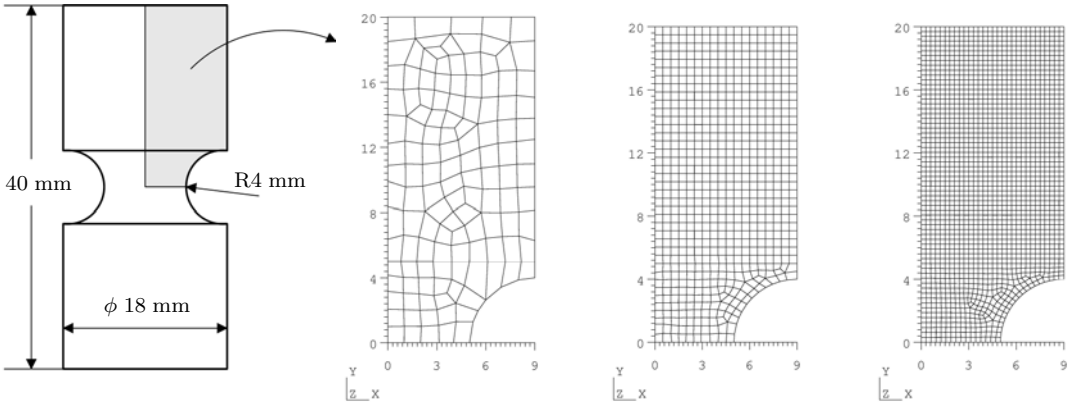

FIGURE 4.2: Geometry and discretisation of the axisymmetric specimen.

In Figure 4.3, we have the damage contours for the local case, that is, when the non-local intrinsic length is set to $\ell_r = 0.0$ mm. As expected, damage tends to unreallistically concentrate into a single element as it can be concluded after carefully inspecting Figure 4.3. This spurious mesh dependency is eliminated when the non-local theory is used instead. Observing Figure 4.4, it is quite clear that damage tends to converge to a given value upon mesh refinement. This is only possible because the non-local formulation has been consistently formulated and, therefore, its dissipative effects have taken place, preventing damage to unlimitedly localise into a single element.

TABLE 4.1: Material properties.

Property	**Value**
Elastic modulus	$E = 71.15$ GPa
Poisson's ratio	$\nu = 0.3$
Hardening function	$\tau_y(R) = 350 + 300R^{0.2}$ MPa
Micro-void volumetric fraction for nucleation	$f_N = 0.04$
Mean strain for void nucleation	$\varepsilon_N = 0.1$
Deviatoric strain for nucleation	$s_N = 0.05$
Critical damage	$f_c = 0.04$
Damage at fracture	$f_f = 0.18$
Shear-damage factor	$k = 1.0$
Non-local intrinsic length	$\ell_r = 0.6$ mm

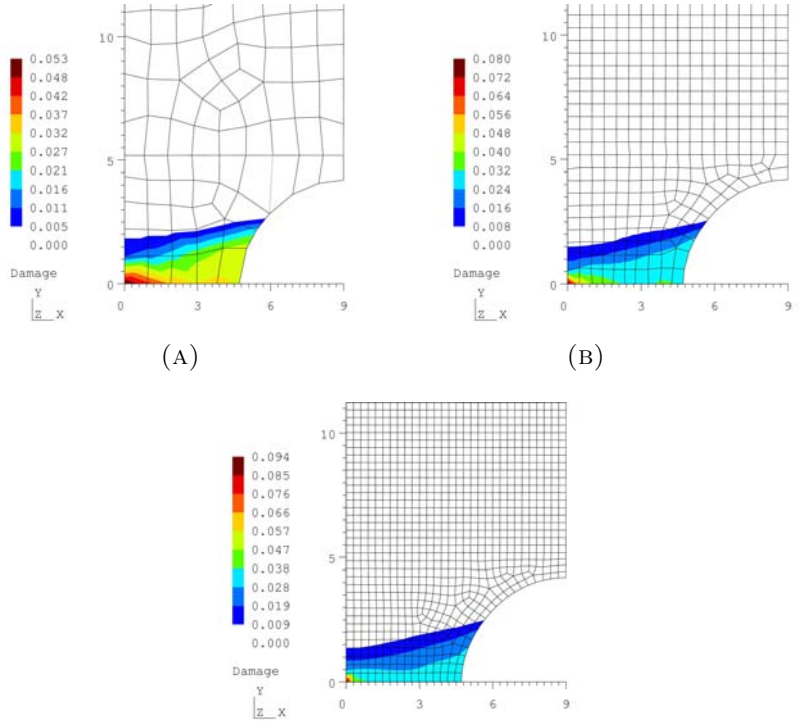

(A) (B)

(C)

FIGURE 4.3: Damage contours at the critical region: local case.

We also observe the convergence of the material integration algorithm, given in Table 4.2. When the modified Newton-Raphson method is adopted, the residual

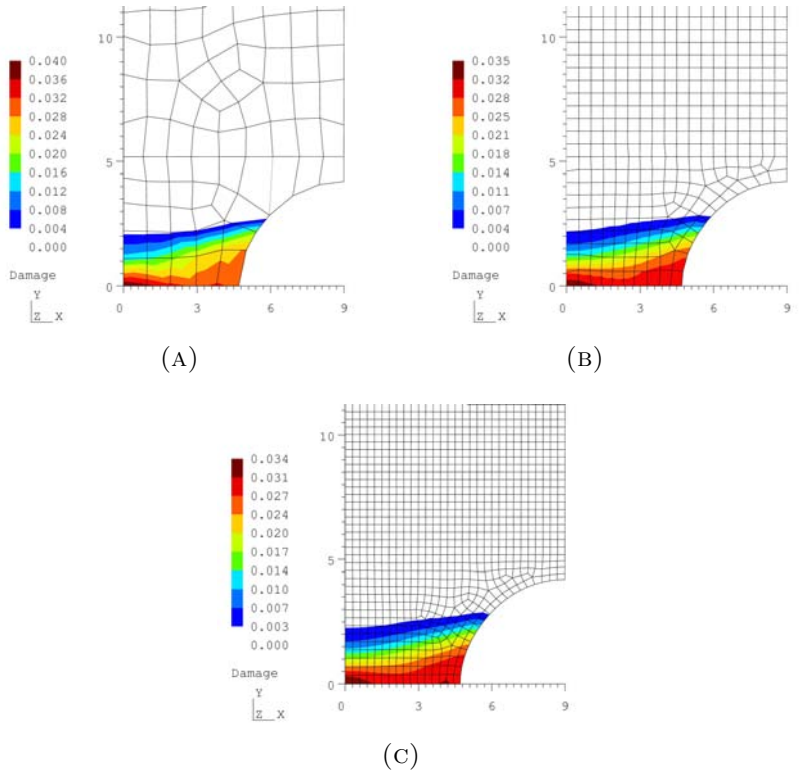

(A) (B)

(C)

FIGURE 4.4: Damage contours at the critical region: non-local case.

norm decreases relatively fast in the first 4 iterations. However, when approaching the solution, the convergence rate tends to be linear, demanding extra iterations until the convergence criterion is reached. In the first 4 iterations, the full Newton-Raphson strategy delivers similar convergence rates; however, when near the solution, the residual norm rapidly decreases to zero in a clearly quadratic convergence rate. Although the full Newton-Raphson method provides by far much better convergence rates, it is much more costly than the simple iterative update required by the modified N-R scheme. The additional computational burden stems from the fact that a global system of equations has to be solved. In fact, the computational cost increases exponentially with the number of elements of the finite element mesh. A mixed approach seems therefore appropriate, in which in the first iterations the modified scheme would be used and then, only when the residual norm had reached relatively low values (e.g. around 1.00×10^{-03}), the full Newton-Raphson method would be then adopted to obtain the final solution. However, such strategy has not been considered in the present investigation and is left here as a suggestion of future work.

TABLE 4.2: Typical convergence of the material algorithm: Residual norm.

Iteration	**Full N-R**	**Modified N-R**
1	$7.61 \times 10^{+01}$	$7.62 \times 10^{+01}$
2	$5.93 \times 10^{+00}$	$6.07 \times 10^{+00}$
3	1.83×10^{-01}	1.94×10^{-01}
4	5.77×10^{-03}	5.92×10^{-03}
5	3.15×10^{-09}	4.03×10^{-04}
⋮		⋮
10		2.42×10^{-09}

4.3.2 3D shear specimen

The second example of this chapter is the analysis of a three-dimensional specimen subjected to pure shear at the critical region. This specimen has been the subject of investigation by Brünig et al. [23] and is adopted here to assess the Gurson-based non-local model proposed in this chapter. In Figure 4.5, the geometry of the shear specimen is given with its associated dimensions. In order to capture the effects of spurious mesh dependency, three mesh refinements have been considered in the spatial discretisation of the specimen (see Figure 4.6), where quadratic hexahedra with reduced integration have been adopted. The material properties are the same of the last example (see Table 4.1).

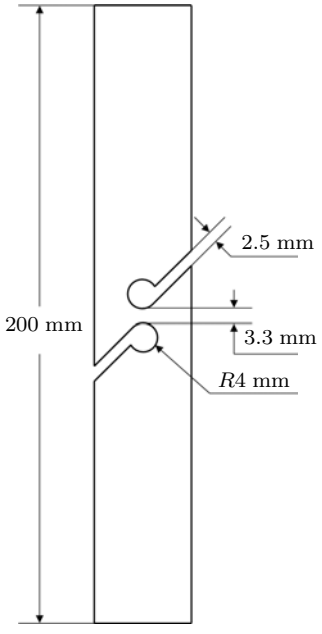

FIGURE 4.5: Geometry of the shear specimen.

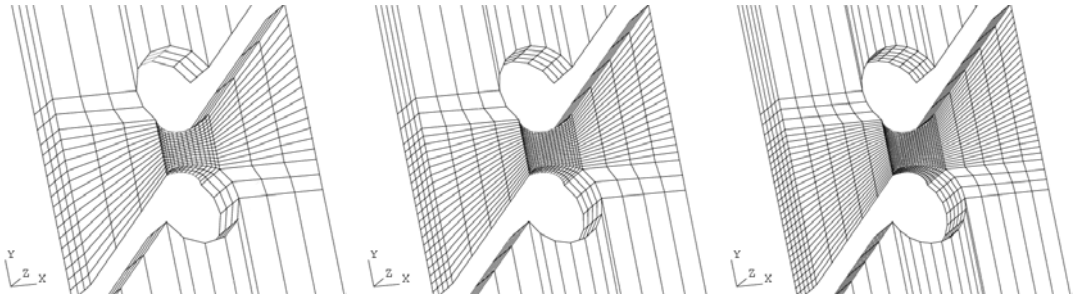

FIGURE 4.6: Shear specimen: different mesh refinements at the critical region.

The contours of damage for the local case are given in Figure 4.7. Once again, damage has the tendency of concentrating into a single element as the finite element mesh is refined. This effect is a direct consequence of the loss of ellipticity of the equilibrium equation when a material softening regime is present as it is in the present case. This pathological dependency on spatial discretisation can be significantly alleviated with the application of the non-local formulation. In Figure 4.8, the contours of damage now present a certain convergence as the mesh is refined. In other words, the spurious effects of pathological mesh dependency have been completely eliminated when the non-local model, presented in this chapter, was activated. In particular, damage tends to spread over a finite area at the critical region of the specimen, contrary to what has been observed in the local case (see Figure 4.7).

Remark 4.1. *It is worth mentioning that, although clearly present, pathological mesh dependency is, in the present example, not as intense as in other simulations presented in this thesis. This behaviour probably stems from the fact that the use of the present shear mechanism delivers a more realistic description of damaging when subjected to shear stress states, for which experimental evidence has shown that localisation plays, to some extent, a less important role when compared to tension stress states. In Chapter 6, where a comprehensive comparison of non-local models will be undertaken, it is shown that Lemaitre-based models present much more mesh sensitivity under shear than Gurson-based models enhanced with the present shear mechanism, which seems to support the aforementioned idea. However, it seems that in the specialised literature very little has been addressed on this topic, for which further research is necessary.*

Once again, the convergence of the material integration algorithm is subject of investigation. In Table 4.3, the norm of the residual vector, $\mathbf{r}$, is listed over the iterations. As it can be clearly concluded after a close inspection of Table 4.3, the full Newton-Raphson method was able to provide quadratic rates of convergence, since the residual norm has very quickly decreased towards zero when close to the

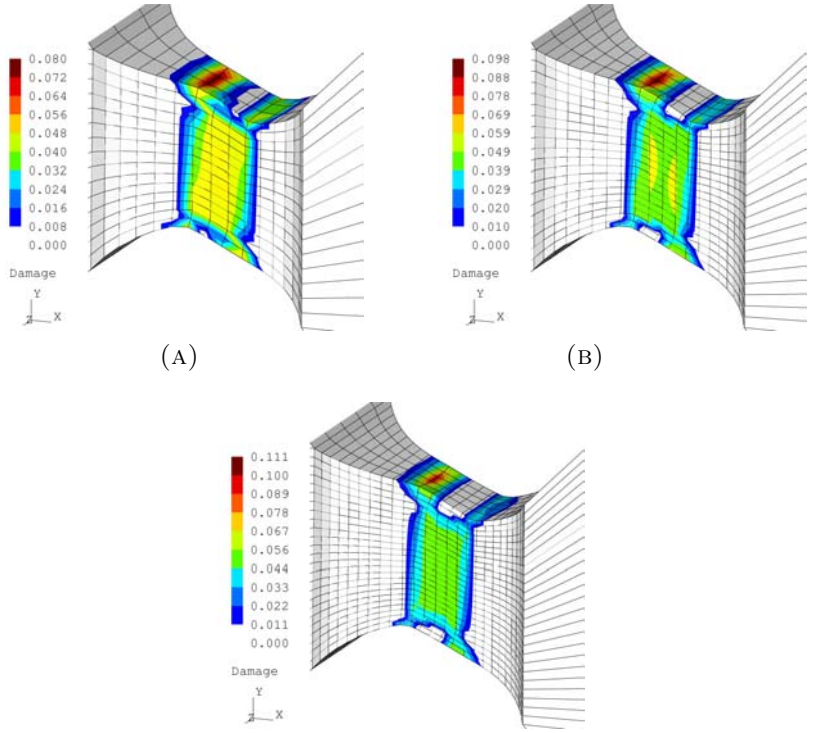

(A) (B)

(C)

FIGURE 4.7: Damage contours at the critical region: local case.

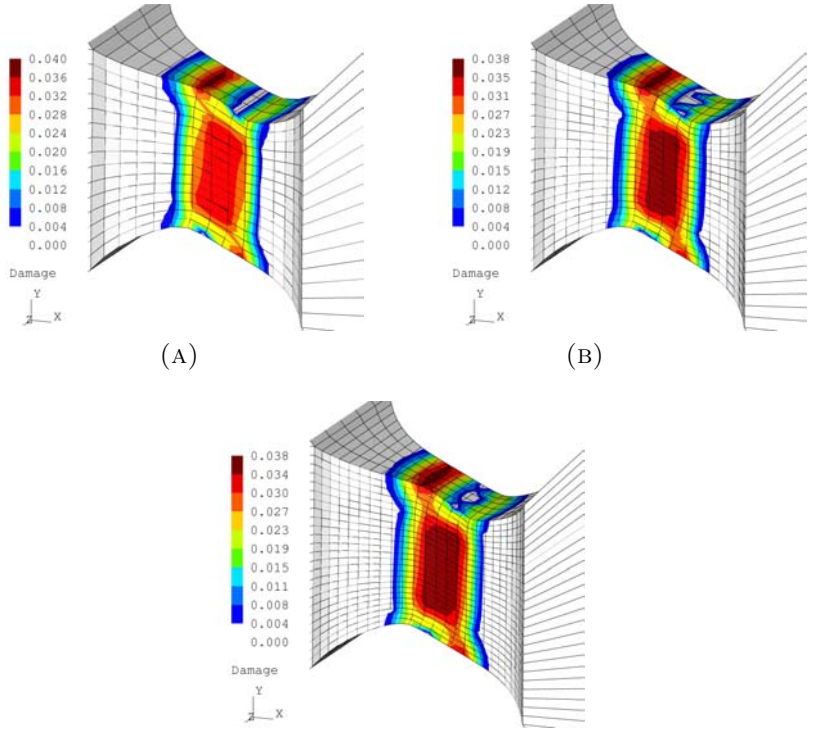

(A) (B)

(C)

FIGURE 4.8: Damage contours at the critical region: non-local case.

solution. Conversely, the modified Newton-Raphson strategy has delivered linear rates of convergence for the same problem. Again, similar to the previous example, the full Newton-Raphson can be computationally more expensive, despite its high convergence rates. This stems from the fact the full scheme requires the solution of a global system of equations meanwhile the modified strategy only updates the constitutive variables on a local level. Therefore, it seems reasonable to adopt a hybrid scheme where the full Newton-Raphson method is only used after a certain residual norm has been reached with the modified scheme.

TABLE 4.3: Typical convergence of the material algorithm: Residual norm.

Iteration	**Full N-R**	**Modified N-R**
1	$3.87 \times 10^{+03}$	$3.87 \times 10^{+03}$
2	$2.76 \times 10^{+00}$	$1.01 \times 10^{+03}$
3	4.12×10^{-02}	$3.31 \times 10^{+02}$
4	3.89×10^{-05}	$6.28 \times 10^{+01}$
5	1.78×10^{-09}	$3.69 \times 10^{+00}$
⋮		⋮
12		7.32×10^{-09}

4.4 Conclusions

In this chapter, a non-local Gurson-based model has been proposed. The main concern was the inclusion of a shear mechanism that accounts for damage evolution under shear-dominated stress states since most Gurson-based constitutive models cannot predict failure in shear. The shear mechanism was based on the proposal of Nahshon and Hutchinson [83], where the mechanism has been slightly changed for better overall numerical performance. A new damage variable has been then defined in the Gurson constitutive theory where the effects of nucleation and coalescence of voids have been based on the damage mechanisms proposed by Tvergaard and Needleman [113].

The damage variable has been chosen to account for non-local effects aiming to avoid any spurious results that may arise from pathological mesh dependency. The non-local framework inevitably leads to a global system of equations whose solution needs to be pursued in a global fashion. Unlike the non-local model of Chapter 3, the present non-local constitutive model has one system of equations, associated with every Gauss point of the finite element mesh, that cannot be

reduced to a single equation. Furthermore, numerical investigation has shown that the modified Newton-Raphson scheme, like the one adopted in Chapter 3, may not deliver remarkably high convergence rates for the present Gurson-based non-local model.

The proposed non-local material model has been assessed by simulating two different specimens. Firstly, an axisymmetric bar has been simulated for which the effects of shear damaging do not take place. The results have clearly shown that the spurious mesh dependency inherent to the local case could be effectively eliminated when the non-local theory was considered. Numerical investigation has shown that the full Newton-Raphson method has a better performance in terms of convergence rates than the modified scheme. However, the full Newton-Raphson demands the solution of a global system of equations, requiring more computational effort, meanwhile the modified scheme is very fast since it can update the solution very quickly.

A shear specimen has been also subject of investigation. The numerical results have shown that the local solution tends to give pathologically mesh dependent results upon mesh refinement. Again, the non-local formulation has been able to avoid such spurious solutions where damage has remained practically constant and distributed over a finite area, regardless of the spatial discretisation. Furthermore, the full Newton-Raphson solution method has presented higher convergence rates than the modified scheme; nevertheless, the computational burden of the full scheme may be impracticable in many circumstances. The modified scheme, on the other hand, requires less memory storage and its update is performed very rapidly.

Based on these results, it seems that the use of a mixed algorithmic strategy, in which the full Newton-Raphson Method is only employed when relatively near the solution, may yield an optimal numerical performance and it is left here as a suggestion for future studies and developments on this topic.

Chapter 5

Consistent Linearisation of Elasto-plastic Non-local Models

In the preceding chapters, elasto-plastic-based non-local ductile damage models of integral-type have been established through suitable formulations aiming to circumvent the inconvenient pathological mesh dependency of strain-softening media. Despite the allegations of some authors, the integral formulation has already proven itself an efficient methodology in computational terms [3, 19, 27, 69, 85, 110]. However, many non-local theories of integral-type lack a consistent tangent operator. A consistent linearisation of the structural problem is highly desired since it guarantees quadratic rates of convergence if the full Newton-Raphson method is employed as it most commonly is in the solution of finite element problems. In other to tackle the problem of consistent linearisation in non-local formulations of integral-type, some approximations have been suggested in the literature. For instance, De Vree et al. [41] and Nguyen and Einav [86] have used the associated local material tangent operator. This option has been also adopted later by Andrade et al. [3] who reported reasonable convergence rates for a considerable number of problems. However, the need for a more robust and efficient convergence is demanded under certain circumstances, especially when damage has achieved high values (in coupled elasto-plastic damage models), the strain-softening regime is active in most elements of the mesh or when ℓ_r is large enough to span a considerable number of elements.

It is important to mention that two main classes of integral non-local models exist. The first one is characterised by the use of non-local variables that are explicitly defined. This is the case of many damage models intended for the description of quasi-brittle materials (e.g. [16, 56, 67]). Generally speaking, the constitutive

behaviour in these models is, in a first step, computed locally. Afterwards, the non-local quantity is explicitly evaluated using a prescribed expression and then the stresses are corrected considering the non-local effect. For these cases, the consistent linearisation has already been provided by Jirásek and Patzák [69].

This chapter, on the other hand, is devoted to the second class of integral non-local models in which the non-local variable is an implicit function of the other constitutive variables. This was the case of the non-local models presented in Chapters 3 and 4, for which regularisation can be only successfully achieved by converting the rate of a given local variable into non-local. This inevitably leads to a constitutive problem that needs to be solved in a global fashion (as discussed in Chapter 3) for which the linearisation strategy presented by Jirásek and Patzák [69] unfortunately cannot be directly used. In the case of implicitly defined non-local models, the constitutive relation, which in the local case is represented by a point-wise relation between stress and strain, turns out to be global as well.

The key idea of the present chapter is to deal with the above mentioned shortcoming by deriving the exact consistent algorithmic tangent operator for the general elasto-plastic case. It is shown that, in the general case, a global compliance matrix needs to be inverted, yielding on a global constitutive relation. Despite the computational burden that such inversion may lead to, a J_2 based non-local model is herein presented for which an elegant closed-form expression for the consistent tangent modulus is established. The closed-form operator avoids the global inversion and therefore a computationally efficient implementation is achieved. The methodology is also employed in the context of the Lemaitre-based non-local model of Chapter 3, for which a closed-form consistent tangent is also herein presented.

This chapter is organised in the following fashion. In Section 5.1, we define a general elasto-plastic non-local model within small strains which will serve as the base for further developments. The absence of a continuum tangent modulus in the non-local case is also highlighted in that section. In Section 5.2, the derivation of the algorithmic consistent tangent operator for a general elasto-plastic non-local model is presented in detail. It is shown that, in the general case, a compliance matrix needs to be inverted. Section 5.3 addresses the application of the developed methodology to the case of a J_2 non-local plasticity model for which a closed-form tangent operator is presented. The developed methodology is also employed in conjunction with the Lemaitre-based non-local model of Chapter 3 whose associated consistent tangent operator is presented in Section 5.4. The chapter is finalised with some numerical examples in Section 5.5 and general conclusive remarks in Section 5.6.

5.1 Non-local modelling in elasto-plasticity

5.1.1 General elasto-plastic non-local model

In order to keep the concepts presented herein as general as possible, we shall adopt a general elasto-plastic model enhanced with non-locality. We shall initially restrict ourselves to the small strain domain for the sake of simplicity[1]. A linear elastic constitutive relation of the kind

$$\boldsymbol{\sigma}(\boldsymbol{x}) = \mathbf{D}^e : \boldsymbol{\varepsilon}^e(\boldsymbol{x}) \tag{5.1}$$

is assumed to exist, where $\boldsymbol{\sigma}(\boldsymbol{x})$ is the stress tensor located at coordinate $\boldsymbol{x}$, $\mathbf{D}^e$ is the standard elasticity modulus and $\boldsymbol{\varepsilon}^e(\boldsymbol{x})$ is the elastic strain tensor. Following Equation (2.21), The stress tensor can be split into two contributions, i.e.,

$$\boldsymbol{\sigma}(\boldsymbol{x}) = \boldsymbol{s}(\boldsymbol{x}) + p(\boldsymbol{x})\boldsymbol{I}, \tag{5.2}$$

where $\boldsymbol{s}(\boldsymbol{x})$ is the deviatoric stress tensor, $p(\boldsymbol{x}) = \frac{1}{3}\mathrm{tr}\left[\boldsymbol{\sigma}(\boldsymbol{x})\right]$ is the hydrostatic stress and $\boldsymbol{I}$ is the second-order identity tensor.

The additive decomposition of the strain is considered, i.e.,

$$\boldsymbol{\varepsilon}(\boldsymbol{x}) = \boldsymbol{\varepsilon}^e(\boldsymbol{x}) + \boldsymbol{\varepsilon}^p(\boldsymbol{x}), \tag{5.3}$$

where $\boldsymbol{\varepsilon}(\boldsymbol{x})$ and $\boldsymbol{\varepsilon}^p(\boldsymbol{x})$ are the total and plastic strain tensors, respectively. At this point, we define two potentials, F_p and F_d, where the former is associated with plastic yielding and the latter with dissipative internal variables. Both potentials may be, in the general case, functions of the stress tensor, $\boldsymbol{\sigma}(\boldsymbol{x})$, and of the set of non-local dissipative internal variables, $\bar{\boldsymbol{\alpha}}$, that is,

$$F_p(\boldsymbol{x}) = F_p\left(\boldsymbol{\sigma}(\boldsymbol{x}), \bar{\boldsymbol{\alpha}}(\boldsymbol{x})\right), \tag{5.4}$$

$$F_d(\boldsymbol{x}) = F_d\left(\boldsymbol{\sigma}(\boldsymbol{x}), \bar{\boldsymbol{\alpha}}(\boldsymbol{x})\right). \tag{5.5}$$

Assuming the normality rule [76], the plastic flow and the evolution of the non-local internal variables are respectively expressed as

$$\dot{\boldsymbol{\varepsilon}}^p(\boldsymbol{x}) = \dot{\gamma}(\boldsymbol{x})\boldsymbol{N}(\boldsymbol{x}), \tag{5.6}$$

$$\dot{\bar{\boldsymbol{\alpha}}}(\boldsymbol{x}) = \int_V \beta(\boldsymbol{x}, \boldsymbol{\xi})\dot{\gamma}(\boldsymbol{\xi})\boldsymbol{H}(\boldsymbol{\xi})\, dV(\boldsymbol{\xi}), \tag{5.7}$$

[1] The extension to the finite strain domain will be addressed in Section 5.2.3.

where $\boldsymbol{N}(\boldsymbol{x})$ is the *flow vector* (at the material point located at $\boldsymbol{x}$) defined as

$$\boldsymbol{N}(\boldsymbol{x}) = \frac{\partial F_p(\boldsymbol{x})}{\partial \boldsymbol{\sigma}(\boldsymbol{x})}, \tag{5.8}$$

and $\boldsymbol{H}(\boldsymbol{\xi})$ is the *generalised hardening modulus* at point $\boldsymbol{\xi}$, expressed by

$$\boldsymbol{H}(\boldsymbol{\xi}) = \frac{\partial F_d(\boldsymbol{\xi})}{\partial \boldsymbol{A}(\boldsymbol{\xi})}. \tag{5.9}$$

In the equation above, $\boldsymbol{A}$ corresponds to the set of conjugate thermodynamical forces associated with $\bar{\boldsymbol{\alpha}}$. The Kuhn-Tucker (or loading/unloading) conditions for the non-local constitutive model read

$$\dot{\gamma}(\boldsymbol{x}) \geq 0; \quad F_p(\boldsymbol{x}) \leq 0; \quad \dot{\gamma}(\boldsymbol{x}) F_p(\boldsymbol{x}) = 0 \quad \forall\, \boldsymbol{x} \in V. \tag{5.10}$$

Note that, due to the implicit non-local character of the internal variables, the above Kuhn-Tucker conditions must hold for all material points *simultaneously* as discussed in more detail in [27].

Remark 5.1. *The normality rule, under which the plastic flow and the internal variables are coupled through a single plastic multiplier, has been here adopted merely for mathematical and numerical convenience. As a matter of fact, all the concepts presented in this chapter can be straightforwardly extended to the general case with several multipliers (e.g., one multiplier for plasticity and another one associated with damage evolution).*

5.1.2 The absence of a point-wise continuum tangent operator

A point-wise stress-strain relation within the non-local continuum framework simply does not exist by definition. Since the Kuhn-Tucker conditions need to hold globally, the non-local constitutive model itself has also a global character, preventing a point-wise continuum material law to be defined.

The absence of a point-wise non-local continuum tangent operator can be easily verified and will be critically demonstrated in the following. To start with, we evaluate the rate of the stress tensor at a generic material point located in $\boldsymbol{x}$, given by

$$\dot{\boldsymbol{\sigma}}(\boldsymbol{x}) = \mathbf{D}^e : \dot{\boldsymbol{\varepsilon}}^e(\boldsymbol{x}). \tag{5.11}$$

Due to the additive decomposition of the strain tensor, we know that

$$\dot{\boldsymbol{\varepsilon}}^e(\boldsymbol{x}) = \dot{\boldsymbol{\varepsilon}}(\boldsymbol{x}) - \dot{\boldsymbol{\varepsilon}}^p(\boldsymbol{x}) = \dot{\boldsymbol{\varepsilon}}(\boldsymbol{x}) - \dot{\gamma}(\boldsymbol{x})\boldsymbol{N}(\boldsymbol{x}). \tag{5.12}$$

Therefore, Equation (5.11) becomes

$$\dot{\boldsymbol{\sigma}}(\boldsymbol{x}) = \mathbf{D}^e : \left(\dot{\boldsymbol{\varepsilon}}(\boldsymbol{x}) - \dot{\gamma}(\boldsymbol{x})\boldsymbol{N}(\boldsymbol{x})\right). \tag{5.13}$$

The rate of the yield function is given by

$$\dot{F}_p(\boldsymbol{x}) = \frac{\partial F_p(\boldsymbol{x})}{\partial \boldsymbol{\sigma}(\boldsymbol{x})} : \dot{\boldsymbol{\sigma}}(\boldsymbol{x}) + \frac{\partial F_p(\boldsymbol{x})}{\partial \bar{\boldsymbol{\alpha}}(\boldsymbol{x})} * \dot{\bar{\boldsymbol{\alpha}}}(\boldsymbol{x}) = 0, \tag{5.14}$$

where $*$ denotes a suitable operation depending on the mathematical nature of the internal variables.

Substituting the expressions for the rate of the stress tensor and non-local internal variables in Equation (5.14), we have

$$\begin{aligned} \dot{F}_p(\boldsymbol{x}) &= \frac{\partial F_p}{\partial \boldsymbol{\sigma}} : \mathbf{D}^e : [\dot{\boldsymbol{\varepsilon}}(\boldsymbol{x}) - \dot{\gamma}(\boldsymbol{x})\boldsymbol{N}(\boldsymbol{x})] \\ &+ \frac{\partial F_p}{\partial \bar{\boldsymbol{\alpha}}} * \int_V \beta(\boldsymbol{x}, \boldsymbol{\xi})\dot{\gamma}(\boldsymbol{\xi})\boldsymbol{H}(\boldsymbol{\xi})\, dV(\boldsymbol{\xi}) = 0. \end{aligned} \tag{5.15}$$

After some straightforward rearrangement, we get the following expression:

$$\dot{\gamma}(\boldsymbol{x}) = \frac{\frac{\partial F_p(\boldsymbol{x})}{\partial \boldsymbol{\sigma}(\boldsymbol{x})} : \mathbf{D}^e : \dot{\boldsymbol{\varepsilon}}(\boldsymbol{x}) + \frac{\partial F_p(\boldsymbol{x})}{\partial \bar{\boldsymbol{\alpha}}(\boldsymbol{x})} * \int_V \beta(\boldsymbol{x}, \boldsymbol{\xi})\dot{\gamma}(\boldsymbol{\xi})\boldsymbol{H}(\boldsymbol{\xi})\, dV(\boldsymbol{\xi})}{\frac{\partial F_p(\boldsymbol{x})}{\partial \boldsymbol{\sigma}(\boldsymbol{x})} : \mathbf{D}^e : \boldsymbol{N}(\boldsymbol{x})}. \tag{5.16}$$

In the standard local case, an explicit function for $\dot{\gamma}(\boldsymbol{x})$ is generally sought so it can be substituted into the stress rate expression (like in Equation 5.13) and, after some algebraic manipulations, a term that relates stress and strain in a point-wise fashion can be established. However, close inspection on Equation (5.16) reveals that, in the non-local case, it is impossible to fully isolate $\dot{\gamma}(\boldsymbol{x})$ due to the integral averaging on the right-hand side of the equation. Thus, this fact clearly demonstrates that it is not possible to determine a point-wise continuum tangent modulus analogous to the local case.

5.2 The non-local consistent algorithmic tangent operator

As in the continuum case, a point-wise tangent modulus, associated with the incremental (discretised) version of the non-local material problem, cannot be obtained. However, the spatial discretisation of the associated finite element problem and the numerical integration of the internal force over the element volume (usually done by means of Gaussian quadratures) allow us to assemble a *finite global constitutive relation.*

To start with, we recall that within a standard finite element framework the equilibrium is sought through the resolution of the following residual equation

$$\mathbf{r}(\mathbf{u}) = \mathbf{f}^{int}(\mathbf{u}) - \mathbf{f}^{ext}, \tag{5.17}$$

where $\mathbf{u}$ are the displacements, $\mathbf{f}^{ext}$ is the external force vector and $\mathbf{f}^{int}$ is the internal force array, given by

$$\mathbf{f}^{int} = \int_V \mathbf{B}^T \boldsymbol{\sigma}\, dV. \tag{5.18}$$

In the equation above, $\mathbf{B}$ is the global matrix that contains the derivatives of the element shape functions as in typical finite element analysis.

Applying the standard Gaussian quadrature, we have

$$\mathbf{f}^{int} = \sum_{i=1}^{n_{ip}} w_i J_i \mathbf{B}_i^T \boldsymbol{\sigma}_{i_{n+1}}, \tag{5.19}$$

where n_{ip} is the total number of material integration points of the finite element mesh. In a given integration point i, the computed algorithmic stress tensor is a function of the kind

$$\boldsymbol{\sigma}_{i_{n+1}} = \boldsymbol{\sigma}_i \left(\boldsymbol{\varepsilon}_1, \boldsymbol{\varepsilon}_2, \cdots, \boldsymbol{\varepsilon}_{n_{ip}}\right). \tag{5.20}$$

One should bear in mind that, in sharp contrast to the local case, the computed algorithmic stress tensor is a function of all other strain tensors of the finite element mesh. This statement is very important for the correct definition of the consistent non-local tangent operator. The conclusion that the stress tensor at a given Gauss point depends on the strain tensors of all other integration points of the finite element mesh can be draw quite easily through the standard linearisation of the non-local stress integration procedure as shown in more detail in Appendix B.

Remark 5.2. *As thoroughly discussed elsewhere (e.g. [40, 106]), consistent algorithmic tangent operators are highly dependent of the specific numerical algorithm employed in the stress integration procedure. In this chapter, we will consider that the stress state has been updated through a global version of the elastic-predictor/return-mapping algorithm like those presented in Chapters 3 and 4.*

The consistent non-local algorithmic tangent operator, $\boldsymbol{K}_T^{nl}$, is obtained from the derivative of the internal force with respect to the displacements, that is,

$$\begin{aligned} \mathbf{K}_T^{nl} = \frac{\partial \mathbf{f}^{int}}{\partial \mathbf{u}} &= \frac{\partial}{\partial \mathbf{u}} \left[\sum_{i=1}^{n_{ip}} w_i J_i \mathbf{B}_i^T \boldsymbol{\sigma}_{i_{n+1}} \right] \\ &= \sum_{i=1}^{n_{ip}} w_i J_i \mathbf{B}_i^T \frac{\partial \boldsymbol{\sigma}_{i_{n+1}}}{\partial \mathbf{u}}. \end{aligned} \tag{5.21}$$

For the sake of clarity, we shall omit the subscript $n+1$ in the following derivations of this section. At this point, it is important to recall that the algorithmic stress, $\boldsymbol{\sigma}_i$, is a function of all the other strains of the mesh. With this in mind, we apply the chain rule to obtain

$$\frac{\partial \boldsymbol{\sigma}_i}{\partial \mathbf{u}} = \frac{\partial \boldsymbol{\sigma}_i}{\partial \boldsymbol{\varepsilon}_1} \frac{\partial \boldsymbol{\varepsilon}_1}{\partial \mathbf{u}} + \frac{\partial \boldsymbol{\sigma}_i}{\partial \boldsymbol{\varepsilon}_2} \frac{\partial \boldsymbol{\varepsilon}_2}{\partial \mathbf{u}} + \cdots + \frac{\partial \boldsymbol{\sigma}_i}{\partial \boldsymbol{\varepsilon}_{n_{ip}}} \frac{\partial \boldsymbol{\varepsilon}_{n_{ip}}}{\partial \mathbf{u}}, \tag{5.22}$$

which can be written in a more compact form:

$$\frac{\partial \boldsymbol{\sigma}_i}{\partial \mathbf{u}} = \sum_{j=1}^{n_{ip}} \frac{\partial \boldsymbol{\sigma}_i}{\partial \boldsymbol{\varepsilon}_j} \frac{\partial \boldsymbol{\varepsilon}_j}{\partial \mathbf{u}}. \tag{5.23}$$

We know that, for a given integration point j,

$$\mathbf{B}_j = \frac{\partial \boldsymbol{\varepsilon}_j}{\partial \mathbf{u}}. \tag{5.24}$$

Thus, the consistent non-local tangent operator is expressed as

$$\mathbf{K}_T^{nl} = \sum_{i=1}^{n_{ip}} w_i J_i \mathbf{B}_i^T \sum_{j=1}^{n_{ip}} \frac{\partial \boldsymbol{\sigma}_i}{\partial \boldsymbol{\varepsilon}_j} \mathbf{B}_j. \tag{5.25}$$

The derivative $\partial \boldsymbol{\sigma}_i / \partial \boldsymbol{\varepsilon}_j$ is a fourth-order tensor that corresponds to the contribution of point j to point i in the constitutive relation. Note that in the local case only the contribution of point i to point i exists. In order to determine the aforementioned derivative, we first make use of the total differentiation of $\boldsymbol{\sigma}_i$, which is

expressed as

$$d\boldsymbol{\sigma}_i = \frac{\partial \boldsymbol{\sigma}_i}{\partial \boldsymbol{\varepsilon}_1} : d\boldsymbol{\varepsilon}_1 + \frac{\partial \boldsymbol{\sigma}_i}{\partial \boldsymbol{\varepsilon}_2} : d\boldsymbol{\varepsilon}_2 + \cdots + \frac{\partial \boldsymbol{\sigma}_i}{\partial \boldsymbol{\varepsilon}_{n_{ip}}} : d\boldsymbol{\varepsilon}_{n_{ip}}, \tag{5.26}$$

or, more shortly,

$$d\boldsymbol{\sigma}_i = \sum_{j=1}^{n_{ip}} \frac{\partial \boldsymbol{\sigma}_i}{\partial \boldsymbol{\varepsilon}_j} : d\boldsymbol{\varepsilon}_j. \tag{5.27}$$

In the general case, the derivative $\partial \boldsymbol{\sigma}_i / \partial \boldsymbol{\varepsilon}_j$ can be, in fact, obtained from a global algorithmic constitutive relation expressed by the following matrix:

$$\begin{bmatrix} d\boldsymbol{\sigma}_1 \\ d\boldsymbol{\sigma}_2 \\ \vdots \\ d\boldsymbol{\sigma}_{n_{ip}} \end{bmatrix} = \begin{bmatrix} \mathbf{D}_{11} & \mathbf{D}_{12} & \cdots & \mathbf{D}_{1n_{ip}} \\ \mathbf{D}_{21} & \mathbf{D}_{22} & \cdots & \mathbf{D}_{2n_{ip}} \\ \vdots & \vdots & \ddots & \vdots \\ \mathbf{D}_{n_{ip}1} & \mathbf{D}_{n_{ip}2} & \cdots & \mathbf{D}_{n_{ip}n_{ip}} \end{bmatrix} \begin{bmatrix} d\boldsymbol{\varepsilon}_1^e \\ d\boldsymbol{\varepsilon}_2^e \\ \vdots \\ d\boldsymbol{\varepsilon}_{n_{ip}}^e \end{bmatrix}. \tag{5.28}$$

The matrix above is obtained through the linearisation of the global non-local system of equations as shown in more detail in Appendix B. Again, the existence of such global constitutive relation appears quite naturally when linearising the non-local constitutive problem and is the cornerstone for the correct definition of the consistent algorithmic tangent operator when the non-local variable is an implicit function of other constitutive variables. As previously mentioned in this section, the computed stress tensor in a given integration point is a function of all other strain tensors of the mesh and the establishment of Equation (5.28) mathematically supports this statement.

Straightforward comparison of Equation (5.27) and Equation (5.28) leads us to the following relation:

$$\mathbf{D}_{ij} = \frac{\partial \boldsymbol{\sigma}_i}{\partial \boldsymbol{\varepsilon}_j}, \tag{5.29}$$

that is, once the global constitutive relation has been found, the derivatives $\partial \boldsymbol{\sigma}_i / \partial \boldsymbol{\varepsilon}_j$, necessary for the tangent stiffness assembly, can be directly extracted from the matrix in (5.28).

We remark that, in the local case, the fourth-order tensor $\mathbf{D}_{ij}$ vanishes if $j \neq i$, yielding on a diagonal matrix in Equation (5.28). In practice, the matrix of

Equation (5.28) is not assembled in the local case. As a matter of fact, the local model can be seen as a particular case of the non-local model.

It is also important to mention that the format of Equation (5.25) *remains exactly the same* for any non-local elasto-plastic constitutive model within small strains. The only difference will be the expression for $\mathbf{D}_{ij}$ which, in turn, is exclusively dependent of the constitutive model adopted.

5.2.1 Derivation of $\mathbf{D}_{ij}$

In local elasto-plastic models, the establishment of analytical expressions for the consistent tangent modulus is extremely dependent of the constitutive model itself. Closed-form expressions are highly desired since they often deliver very efficient numerical implementations. The same is valid for non-local elasto-plastic models where a closed-form expression for Equation (5.29) may also be obtained by employing standard differential calculus.

To demonstrate the use of analytical consistent tangent operators in the context of non-local models of integral-type, we shall, in Section 5.3, enhance the classical J_2 plasticity model by non-locality where it will be shown that straightforward operations lead to an elegant closed-form expression for the non-local tangent operator. Moreover, an analytical expression for the tangent operator associated with the ductile damage model presented in Chapter 3 will be given in Section 5.4. In fact, it seems that, if it is possible to derive a closed-form tangent modulus associated with a given local constitutive model, it is also possible to establish analytical expressions for the terms $\mathbf{D}_{ij}$ in the non-local case. However, such a rule cannot be proved.

As an alternative, $\mathbf{D}_{ij}$ can be obtained through standard numerical differentiation in the case of complex constitutive models. Although the procedure is a direct extension of the one commonly employed in the local case, one should bear in mind that, in the non-local case, *the stress tensor in a given integration point is in fact a function of the strain tensors associated with all the other integration points of the finite element mesh.* This substantially affects the way how the numerical differentiation is performed since all the surrounding strain tensors need to be numerically perturbed in order to obtain $\mathbf{D}_{ij}$. Thus, the direct use of numerical differentiation *exactly like in the local case*, i.e. only computing the $\partial\boldsymbol{\sigma}_i/\partial\boldsymbol{\varepsilon}_i$, *does not render a consistent linearisation of the non-local problem.* Hence, no quadratic rates of convergence are achieved. In other words, even with the use of numerical derivatives, the non-local tangent operator *needs to be assembled accordingly* and

only then are the non-local interactions across the elements consistently taken into account. This fact clearly motivates the analytical derivation of consistent tangent operators for non-local models.

5.2.2 Assembly of the non-local tangent operator

Due to the double sum in Equation (5.25), the non-local tangent operator inevitably needs longer assembly times than the local counterpart. It is important to mention that the sum in j needs not be carried out over all Gauss points of the finite element mesh but rather only over those Gauss points that influence the integration point i. Thus, the computational time needed for the assembly of the tangent operator depends on the quantity of neighbourhood points of non-local influence. As a matter of fact, this quantity is directly linked to the size of the non-local intrinsic length, ℓ_r. Thus, the bigger the intrinsic length, the longer the assembly of the non-local tangent operator. In practice, the additional assembly time required by the non-local tangent is greatly compensated by quadratic convergence rates and mesh-independent solutions.

The assembly of the consistent non-local tangent stiffness can be conveniently carried out from smaller matrices in full analogy to the local case. This has also been stress out by Jirásek and Patzák [69] in their derivation of the non-local consistent tangent. The only difference to the local case lies on the mapping from each contribution to the global stiffness.

Remark 5.3. *In sharp contrast to the tangent operator presented by Jirásek and Patzák [69], the double sum in Equation (5.25) cannot be avoided in the general elasto-plastic case due to the terms* $\mathbf{D}_{ij} = \partial\boldsymbol{\sigma}_i/\partial\boldsymbol{\varepsilon}_j$.

5.2.3 Extension to finite strains

In order to establish the consistent non-local tangent operator at finite strains, we shall consider herein the hyperelastic-based multiplicative framework adopted in Chapter 3. Straightforward extension of the linearisation of the virtual work (Appendix A), applied in conjunction with the concepts presented in this chapter under the assumption of small strains, leads to the following expression for the non-local consistent tangent operator in the finite strain domain for spatial descriptions:

$$\mathbf{K}_T^{nl} = \sum_{i=1}^{n_{ip}} w_i J_i \mathbf{G}_i^T \sum_{j=1}^{n_{ip}} \mathbf{a}_{ij} \mathbf{G}_j, \tag{5.30}$$

where $\mathbf{G}$ is the discrete gradient operator and $\mathbf{a}_{ij}$ is the spatial tangent modulus relating the integration points i and j.

For the case where $j = i$, the consistent spatial modulus is given by

$$\mathbf{a}_{ii} = \frac{1}{2J_i}\mathbf{D}_{ii} : \mathbf{L}_i : \mathbf{B}_i - \mathbf{\Sigma}_i, \tag{5.31}$$

where the fourth order tensor $\mathbf{\Sigma}$ is given by

$$\Sigma_i^{ijkl} = \sigma_i^{il}\delta^{jk}. \tag{5.32}$$

In the equation above, the superscripts i, j, k and l denote tensor components for which the Einstein's sum convention has been adopted. The subscript i corresponds to the i^{th} integration point of the finite element mesh, following the usual notation of this thesis.

If $j \neq i$, the consistent spatial tangent modulus is written

$$\mathbf{a}_{ij} = \frac{1}{2J_i}\mathbf{D}_{ij} : \mathbf{L}_j : \mathbf{B}_j. \tag{5.33}$$

The fourth order tensors $\mathbf{L}_i$ and $\mathbf{B}_i$ are respectively defined as:

$$\mathbf{L}_i = \frac{\partial \ln \left[\boldsymbol{B}_{i\ n+1}^{e\ trial}\right]}{\partial \boldsymbol{B}_{i\ n+1}^{e\ trial}}, \tag{5.34}$$

$$\mathsf{B}_i^{ijkl} = \delta^{ik}\left(\boldsymbol{B}_{i\ n+1}^{e\ trial}\right)^{jl} + \delta^{jk}\left(\boldsymbol{B}_{i\ n+1}^{e\ trial}\right)^{il}. \tag{5.35}$$

Remark 5.4. *As alluded in Chapter 3, Section 3.2.3, both the intrinsic length and the non-local averaging operator are assumed to be completely independent of the history of the deformation. This hypothesis has been taken into account for the establishment of Equations (5.30), (5.31) and (5.33). If the intrinsic length or the non-local averaging operator were assumed to be dependent of the deformation, the establishment of the consistent tangent operator would be considerably more complicated, demanding intricate algebraic operations.*

Remark 5.5. *It should be noted that $\mathbf{D}_{ij}$ is the only term associated with the material model. Therefore, the consistent operator obtained under the hypothesis of small strains can be straightforwardly used at finite strains, for which the necessary operations associated with kinematics are performed in an uncoupled fashion.*

5.3 Application: J_2 non-local plasticity

5.3.1 Non-local J_2 plasticity model

A hybrid local/non-local J_2 plasticity model, similar to the one proposed by Strömberg and Ristinmaa [110], will be adopted in this section. The hybrid formulation is necessary to avoid spurious instabilities as reported in Jirásek and Rolshoven [70]. To start with, we first assume the existence of a local elastic law given by

$$\boldsymbol{\sigma}(\boldsymbol{x}) = \mathbf{D}^e : \boldsymbol{\varepsilon}^e(\boldsymbol{x}) \tag{5.36}$$

where $\mathbf{D}^e$ is the elasticity modulus. Non-locality is introduced by adopting a hybrid local/non-local rate of the isotropic hardening variable, i.e.,

$$\dot{\bar{\kappa}}(\boldsymbol{x}) = m \int_V \beta(\boldsymbol{x}, \boldsymbol{\xi}) \dot{\kappa}(\boldsymbol{\xi})\, dV(\boldsymbol{\xi}) + (1-m)\dot{\kappa}(\boldsymbol{x}), \tag{5.37}$$

where it has been assumed that

$$\dot{\kappa}(\boldsymbol{x}) = \dot{\gamma}(\boldsymbol{x}). \tag{5.38}$$

In the equation above, m is a parameter that adjusts the level of non-locality. For instance, if m is set to the unity, a pure non-local model is achieved. Conversely, if m is set to null, the local theory is recovered. Any other value of m renders mixed contributions of the local and non-local counterparts. Note that the parameter m has no limiting range and its value can therefore be any real number. Nevertheless, after a detailed investigation, Jirásek and Rolshoven [70] have concluded that for a J_2 plasticity model the optimal value for m is around 2. The yield function of the constitutive model is expressed as

$$F_p = q(\boldsymbol{x}) - \sigma_y(\bar{\kappa}(\boldsymbol{x})), \tag{5.39}$$

where $q(\boldsymbol{x})$ is the von Mises equivalent stress, here defined by

$$q(\boldsymbol{x}) = \sqrt{\frac{3}{2}} \left\| \boldsymbol{s}(\boldsymbol{x}) \right\|. \tag{5.40}$$

Associative plasticity is assumed, therefore, the plastic flow is given by

$$\dot{\boldsymbol{\varepsilon}}^p = \dot{\gamma}(\boldsymbol{x}) \frac{\partial F_p(\boldsymbol{x})}{\partial \boldsymbol{\sigma}(\boldsymbol{x})} = \frac{3}{2} \dot{\gamma}(\boldsymbol{x}) \frac{\boldsymbol{s}(\boldsymbol{x})}{q(\boldsymbol{x})}. \tag{5.41}$$

The model is complete with the Kuhn-Tucker conditions:

$$\dot{\gamma}(\boldsymbol{x}) \geq 0; \quad F_p(\boldsymbol{x}) \leq 0; \quad \dot{\gamma}(\boldsymbol{x}) F_p(\boldsymbol{x}) = 0 \quad \forall\, \boldsymbol{x} \in V. \tag{5.42}$$

Since the Kuhn-Tucker conditions need to be fulfilled for every material point simultaneously, the constitutive problem has a global character and demands special care for its numerical implementation [3, 27].

5.3.2 Non-local stress integration

In order to solve the non-local constitutive problem and to compute the updated stress tensor at integration point i, $\boldsymbol{\sigma}_{i_{n+1}}$, the global version of the elastic-predictor/return-mapping algorithm is adopted [3]. In the present case, the elastic trial state is expressed by the following equations:

$$\begin{aligned}
\boldsymbol{\varepsilon}^{e\,trial}_{i_{n+1}} &= \boldsymbol{\varepsilon}^{e}_{i_n} + \Delta\boldsymbol{\varepsilon}_i, && (5.43)\\
p^{trial}_{i_{n+1}} &= K\mathrm{tr}(\boldsymbol{\varepsilon}^{e\,trial}_{i_{n+1}}), && (5.44)\\
\boldsymbol{s}^{trial}_{i_{n+1}} &= 2G\mathbf{I}_d : \boldsymbol{\varepsilon}^{e\,trial}_{i_{n+1}}, && (5.45)\\
q^{trial}_{i_{n+1}} &= \sqrt{\frac{3}{2}}\left\|\boldsymbol{s}^{trial}_{i_{n+1}}\right\|, && (5.46)\\
\bar{\kappa}^{trial}_{i_{n+1}} &= \bar{\kappa}_{i_n}. && (5.47)
\end{aligned}$$

In the equations above, $\mathbf{I}_d$ is the deviatoric projection tensor, defined as

$$\mathbf{I}_d = \mathbf{I} - \frac{1}{3}\boldsymbol{I} \otimes \boldsymbol{I}, \tag{5.48}$$

where $\mathbf{I}$ is the fourth-order identity tensor.

Pseudo-time integration of the constitutive equations using a backward Euler scheme leads, after some algebraic manipulations, to the following non-linear equation:

$$f_i(\Delta\gamma_1, \Delta\gamma_2, \cdots, \Delta\gamma_{n_{ip}}) = q^{trial}_{i_{n+1}} - 3G\Delta\gamma_i - \sigma_y(\bar{\kappa}_{i_{n+1}}), \tag{5.49}$$

which is associated with the i^{th} Gauss point and needs to be solved globally. The algorithm for the global stress integration will be omitted herein and the reader is referred to the references [3, 27, 110]. After finding the solution, the stress tensor at the i^{th} Gauss point is updated as follows:

$$\boldsymbol{\sigma}_{i_{n+1}} = \left(1 - \frac{\Delta\gamma_i 3G}{q^{trial}_{i_{n+1}}}\right)\boldsymbol{s}^{trial}_{i_{n+1}} + p^{trial}_{i_{n+1}}\boldsymbol{I}. \tag{5.50}$$

5.3.3 Closed-form non-local consistent tangent operator

In the last section, a general expression for the non-local tangent elasto-plastic operator has been derived. It remains to derive the terms $\partial\boldsymbol{\sigma}_i/\partial\boldsymbol{\varepsilon}_j$. As a matter of fact, they are dependent of the constitutive model and of the particular algorithm adopted for the stress integration. In the case of the hybrid local/non-local J_2 plasticity model presented above, closed-form expressions for these terms can be straightforwardly obtained. We remark that, in the present case, the inversion of a global matrix associated with the constitutive law is avoided, dramatically reducing the corresponding computational burden and making the use of the exact non-local consistent modulus plausible in computational terms.

The closed-form consistent algorithmic tangent operator for the hybrid local/non-local J_2 plasticity model is summarised as

$$\mathbf{K}_T^{nl} = \sum_{i=1}^{n_{ip}} w_i J_i \mathbf{B}_i^T \sum_{j=1}^{n_{ip}} \mathbf{D}_{ij}\mathbf{B}_j, \tag{5.51}$$

where, for $j = i$,

$$\mathbf{D}_{ii} = \mathbf{D}^e - a\boldsymbol{I}_d + b\bar{\boldsymbol{N}}_{i_{n+1}} \otimes \bar{\boldsymbol{N}}_{i_{n+1}}, \tag{5.52}$$

where

$$a = \frac{\Delta\gamma_i 6G^2}{q_{i_{n+1}}^{trial}}, \tag{5.53}$$

$$b = a - \frac{1}{3G + (1-m)H_i + mw_i J_i \beta_{ii} H_i} \tag{5.54}$$

and $\bar{\boldsymbol{N}}_{i_{n+1}}$ is the unit deviatoric flow vector defined as

$$\bar{\boldsymbol{N}}_{i_{n+1}} = \frac{\boldsymbol{\varepsilon}_{d\,i_{n+1}}^{e\,trial}}{\left\|\boldsymbol{\varepsilon}_{d\,i_{n+1}}^{e\,trial}\right\|}. \tag{5.55}$$

For the case where $j \neq i$:

$$\mathbf{D}_{ij} = c\bar{\boldsymbol{N}}_{i_{n+1}} \otimes \bar{\boldsymbol{N}}_{j_{n+1}} \tag{5.56}$$

where

$$c = a - \frac{1}{3G + (1-m)H_j + mw_i J_i \beta_{ij} H_j}. \tag{5.57}$$

Note that meanwhile the fourth-order tensor of Equation (5.52) is symmetric, the same is not true for Equation (5.56). Although both $\bar{\boldsymbol{N}}_{i_{n+1}}$ and $\bar{\boldsymbol{N}}_{j_{n+1}}$ are symmetric, their product is necessarily symmetric only if they are linearly dependent; however, such condition is not met in the general case. The presence of the non-local factor β_{ij} also contributes to the unsymmetry of the tangent stiffness $\mathbf{K}_T^{nl}$ if the unsymmetric averaging operator in (3.12) is adopted. Nevertheless, even if the symmetric operator of Equation (3.15) is chosen, the global tangent stiffness is still unsymmetric due to the product $\bar{\boldsymbol{N}}_{i_{n+1}} \otimes \bar{\boldsymbol{N}}_{j_{n+1}}$.

5.4 Application: Lemaitre-based ductile damage model

5.4.1 Closed-form non-local consistent tangent operator

In similar manner to the hybrid local/non-local J_2 plasticity model of last section, a closed-form expression for $\mathbf{D}_{ij}$ can also be obtained for the Lemaitre-based non-local ductile damage model of Chapter 3. Note that, in the Lemaitre-based model, no parameter m has been defined. The derivation of the tangent modulus is lengthy but follows standard differentiation procedures and will be omitted here for the sake of readability. Following the expression of the non-local consistent tangent operator at finite strains addressed in Section 5.2.3, the material-related consistent tangent modulus, in the case where $j = i$, is given by

$$\mathbf{D}_{ii} = a_1 \left[\mathsf{I} - \frac{1}{3}\boldsymbol{I} \otimes \boldsymbol{I} \right] + b_1 \bar{\boldsymbol{N}}_{i_{n+1}} \otimes \bar{\boldsymbol{N}}_{i_{n+1}} + c_1 \bar{\boldsymbol{N}}_{i_{n+1}} \otimes \boldsymbol{I} + d_1 \boldsymbol{I} \otimes \bar{\boldsymbol{N}}_{i_{n+1}} + e_1 \boldsymbol{I} \otimes \boldsymbol{I}. \tag{5.58}$$

If $j \neq i$, then $\mathbf{D}_{ij}$ is written:

$$\mathbf{D}_{ij} = b_2 \bar{\boldsymbol{N}}_{i_{n+1}} \otimes \bar{\boldsymbol{N}}_{j_{n+1}} + c_2 \bar{\boldsymbol{N}}_{i_{n+1}} \otimes \boldsymbol{I} + d_2 \boldsymbol{I} \otimes \bar{\boldsymbol{N}}_{j_{n+1}}. \tag{5.59}$$

The scalars a_1, b_1, b_2, c_1, c_2, d_1, d_2 and e_1 are given in Appendix B.

5.5 Numerical results and discussion

5.5.1 Plate in biaxial compression

In this first example, we numerically assess the efficiency and effectiveness of the J_2 non-local model of Section 5.3 by simulating a two-dimensional plate under plane strain conditions (see Figure 5.1). The plate is subjected to a vertical compressive displacement $\|u_y\| = 0.6$ mm. In order to trigger localisation, an imperfection of size 10 mm $\times$ 10 mm has been introduced in the plate. Two mesh refinements have been considered as depicted in Figure 5.1. The elasticity properties adopted in this example are $E = 200.0$ GPa and $\nu = 0.49$. The weakened part has a yield stress of $\sigma_y = 18.0$ MPa meanwhile the rest of the plate yields at $\sigma_y = 20.0$ MPa. In both cases, a negative hardening modulus $H = -245.0$ MPa has been considered. The non-local intrinsic length has been set to $\ell_r = 10.0$ mm.

Firstly, the plate is simulated considering the standard local case (i.e., $\ell_r = 0.0$ mm). As one should expect, the results for the equivalent plastic strain tend to concentrate in a single layer of elements as the mesh is refined (see Figure 5.2) where the size of the shear band gets narrower upon mesh refinement.

The non-local model of Section 5.3 is then employed by adopting three different values for the parameter m, namely $m = 1.0$, 1.5 and 2.0. The results for the coarse and fine meshes are respectively given in Figures 5.3 and 5.4. Close inspection reveals that the non-local formulation was able to prevent the excessive localisation obtained with the local case since the size of the shear band has remained practically constant upon mesh refinement. Despite small differences in

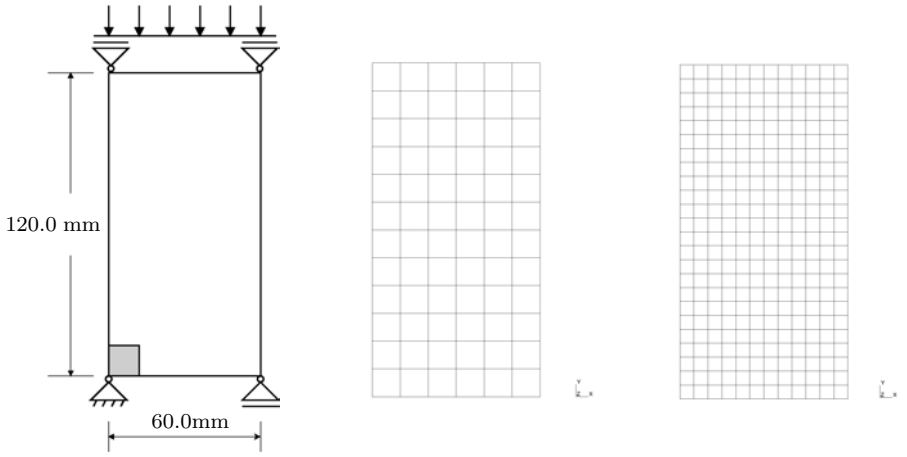

FIGURE 5.1: Plate in biaxial compression: geometry and mesh refinement.

the final contours of equivalent plastic strain, the three different values of m have rendered solutions free of spurious localisation.

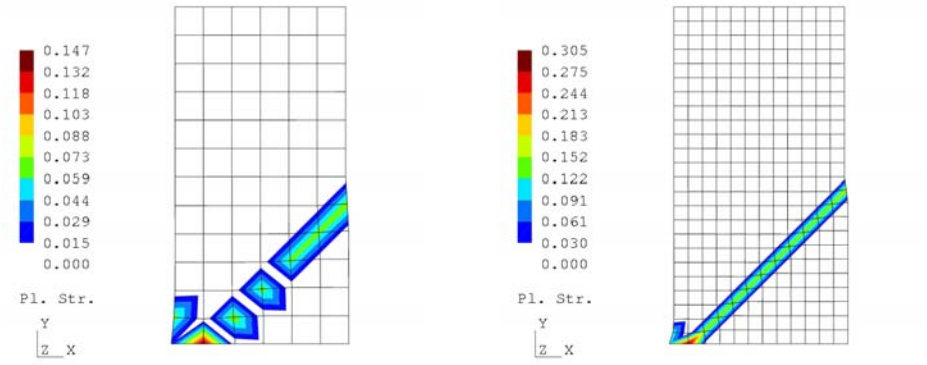

(A) Coarse mesh (B) Fine mesh

FIGURE 5.2: Equivalent plastic strain contours for the local case.

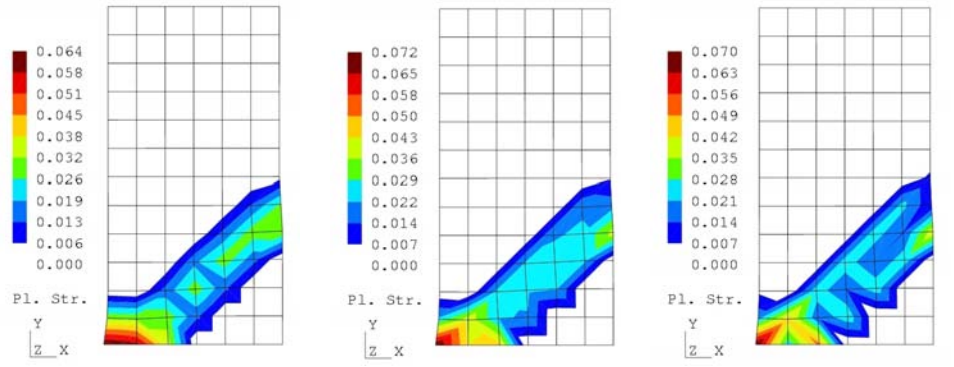

(A) $m = 1.0$ (B) $m = 1.5$ (C) $m = 2.0$

FIGURE 5.3: Equivalent plastic strain contours for different values of m: coarse mesh.

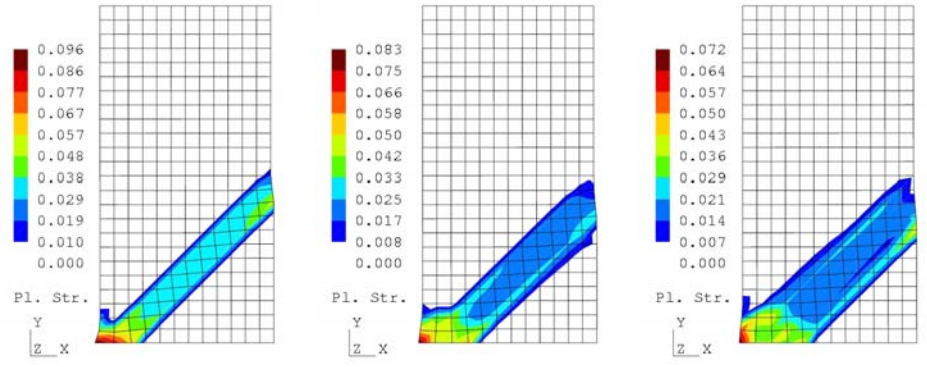

(A) $m = 1.0$ (B) $m = 1.5$ (C) $m = 2.0$

FIGURE 5.4: Equivalent plastic strain contours for different values of m: fine mesh.

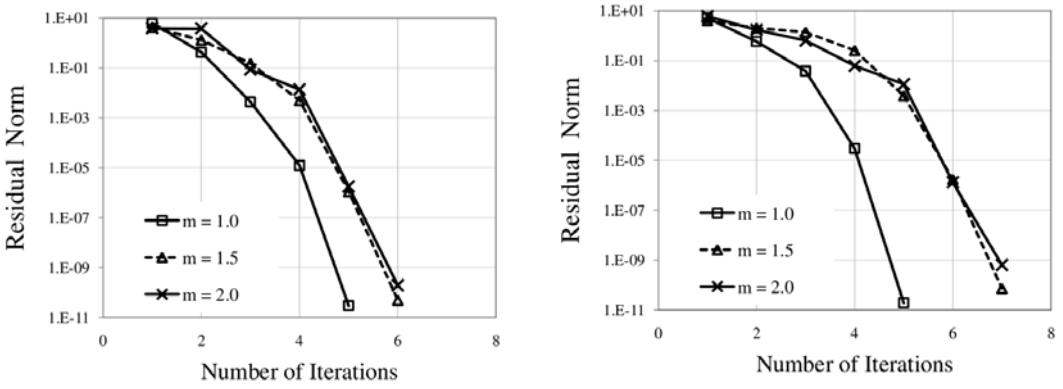

FIGURE 5.5: Convergence pattern for different values of m: coarse mesh (left) and fine mesh (right).

The attention now is focused on the efficiency of the present non-local formulation. Therefore, the convergence of the structural problem, for which the consistent non-local tangent stiffness has been adopted, is carefully analysed. In order to fully assess the consistent linearisation of the non-local model, the convergence patterns obtained with the different values of m are investigated for the two mesh refinements. The logarithmic of the residual function (Equation 5.17) is plotted against the number of iterations as shown in Figure 5.5. Close observation on these plots clearly reveals that the rate of asymptotic convergence remains *quadratic* even for different values of m and for different mesh refinements, hence, proving that the linearisation of the non-local model has been carried out consistently.

5.5.2 Double notched specimen

In order to further illustrate the algorithmic properties of the developed non-local consistent tangent operator, we simulate the double notched shear specimen analysed by Mediavilla [80], for which the Lemaitre-based non-local model of Chapter 3 is here employed. The geometry and boundary conditions of the double notched specimen are depicted in Figure 5.6 where $r_c = 1.0$ mm. A vertical displacement of $u_y = 0.315$ mm is applied (as schematically shown in Figure 5.6), which is divided over 20 equally spaced load increments. The material properties adopted are summarised in Table 5.1. Similar to the example of the last section, two different mesh refinements have been adopted (see Figure 5.7). In the present example, we assess the numerical implementation of the Lemaitre-based non-local model (together with the associated algorithmic consistent tangent operator) for different values of non-local intrinsic length: $\ell_r = 0.5$ mm, $\ell_r = 1.0$ mm and $\ell_r = 1.5$ mm. The different values of ℓ_r are plotted over the two mesh refinements (see Figure

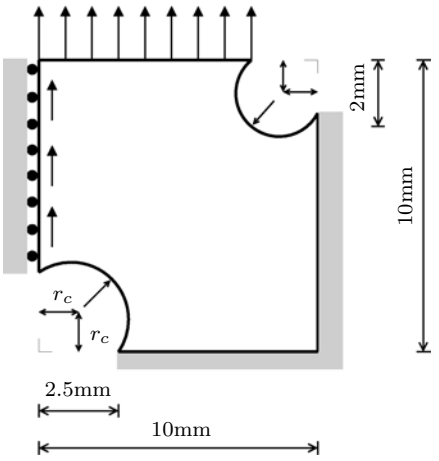

FIGURE 5.6: Double notched specimen: geometry and boundary conditions.

5.7) with the aim of giving a better visual conception of how many elements each of these values of ℓ_r spans. Note that the m parameter has *not* been defined in the case of the Lemaitre-based non-local model.

To start with, we firstly simulate the specimen adopting the local model. In this case, the damage contours tend to very rapidly concentrate into a single layer of elements as the mesh is refined (see Figure 5.8). The spurious localisation is effectively avoided if the non-local model is employed, as it can be concluded after observing Figures 5.9 and 5.10.

The numerical efficiency using the developed consistent linearisation of the non-local model is also assessed with the present example. Firstly, we observe the convergence of the structural problem when $\ell_r = 0.5$ mm at different increments for both mesh refinements (see Figure 5.11). A standard line-search procedure [32, 33] has been adopted in order to optimise the convergence in large incremental steps. A careful inspection of Figure 5.11 clearly reveals that the rate of convergence remains quadratic over the increments. It is worth noting that the steps at increments 15 and 20 were relatively large for which the line-search

TABLE 5.1: Material properties for the double notched specimen.

Property	**Value**
Elastic modulus	$E = 220$ GPa
Poisson's ratio	$\nu = 0.3$
Damage exponent	$s = 1.0$
Damage denominator	$r = 3.0$ MPa
Hardening function	$\tau_y(R) = 700 + 300R^{0.3}$ MPa

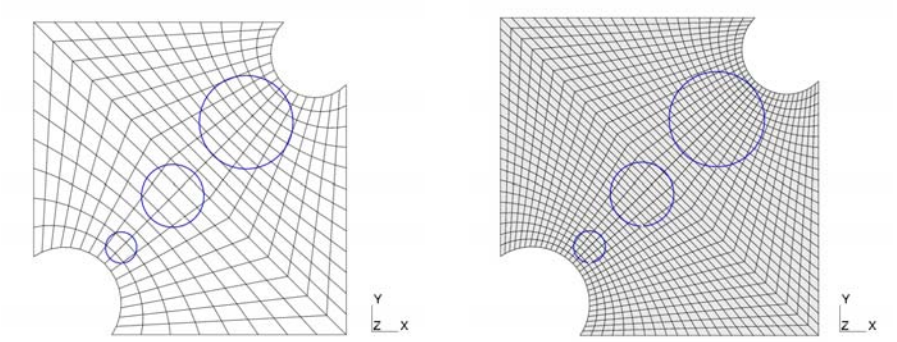

(A) Coarse mesh (B) Fine mesh

FIGURE 5.7: Different values of ℓ_r plotted over the meshes.

scheme has been activated in the first iterations. Nevertheless, as the iterative problem approaches solution, the norm of the residual equation rapidly decreases towards the roots of the residual function, a clear demonstration that the full Newton-Raphson method has been consistently employed.

We now focus on the sensitivity of the consistent linearisation in respect to the non-local intrinsic length, ℓ_r. Therefore, the convergence is observed for the different values of ℓ_r at increment 10 and for both mesh refinements as shown in Figure 5.12. Clearly, the convergence of the structural problem exhibits quadratic rates even for different values of ℓ_r and for different element sizes.

Finally, the sparsity of the non-local stiffness tangent operator, $\boldsymbol{K}_T^{nl}$, at increments 5 and 20 are respectively given in Figures 5.13 and 5.14 for the different values of ℓ_r. As one should expect, the stiffness matrix is much more populated when the non-local intrinsic length is larger and therefore spans more elements. At increment 20, more elements are damaged if compared to increment 5, which has resulted in a larger number of non-zero entries in the stiffness matrix as it can be concluded after inspecting Figures 5.13 and 5.14.

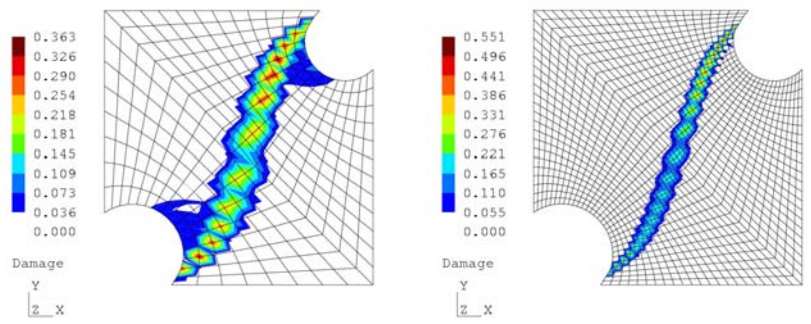

(A) Coarse mesh (B) Fine mesh

FIGURE 5.8: Final damage contours for the double notched specimen: local solution.

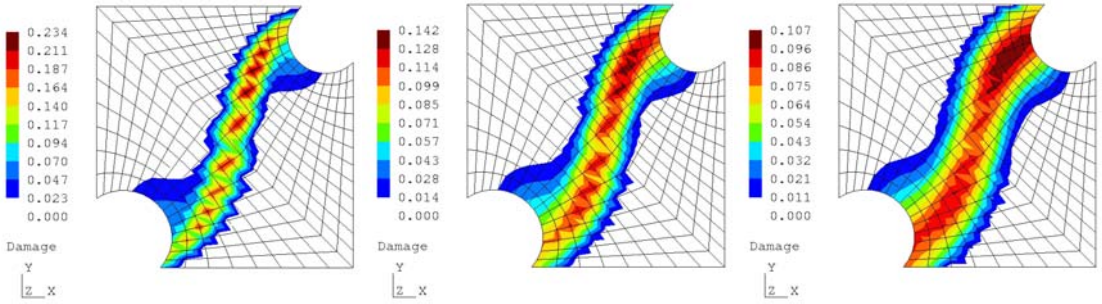

(A) $\ell_r = 0.5$ mm (B) $\ell_r = 1.0$ mm (C) $\ell_r = 1.5$ mm

FIGURE 5.9: Damage contours for the coarse mesh (at increment 20).

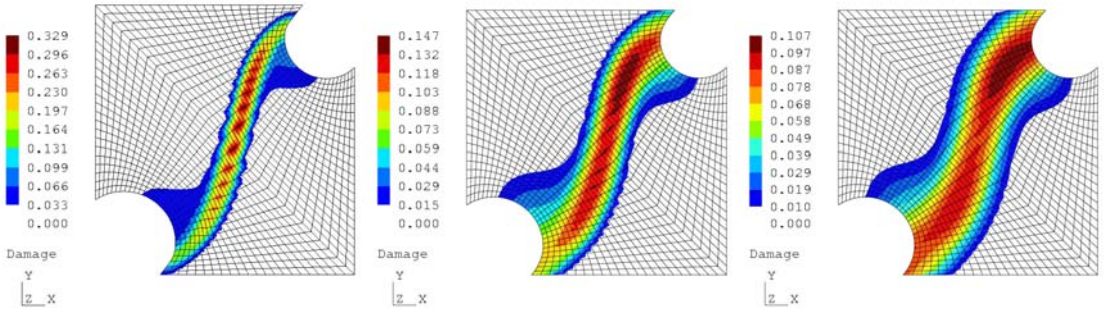

(A) $\ell_r = 0.5$ mm (B) $\ell_r = 1.0$ mm (C) $\ell_r = 1.5$ mm

FIGURE 5.10: Damage contours for the fine mesh (at increment 20).

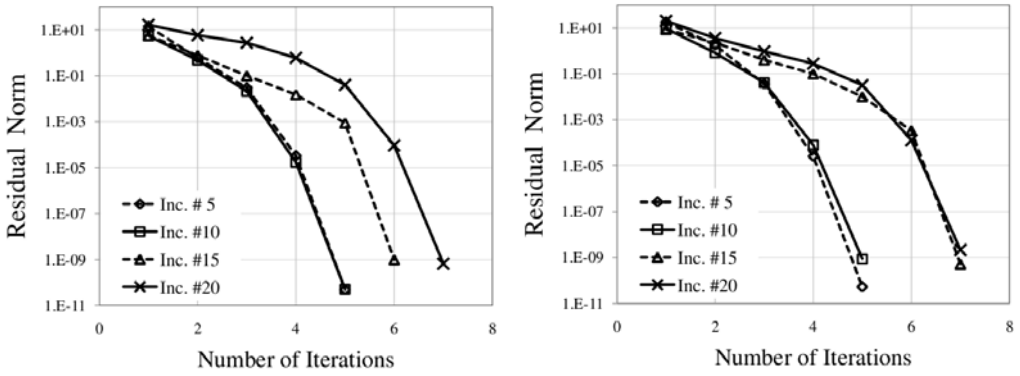

(A) Coarse mesh (B) Fine mesh

FIGURE 5.11: Convergence pattern over the increments: non-local solution with $\ell_r = 0.5$ mm.

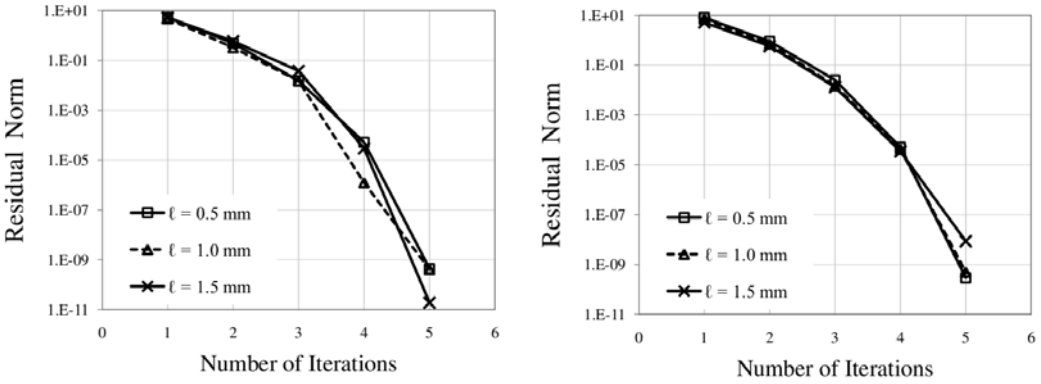

(A) Coarse mesh (B) Fine mesh

FIGURE 5.12: Convergence pattern for different values of ℓ_r.

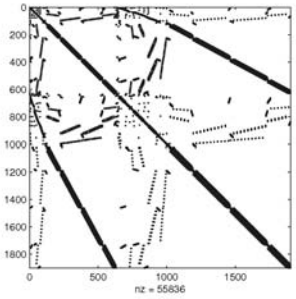

(A) $\ell_r = 0.0$ mm

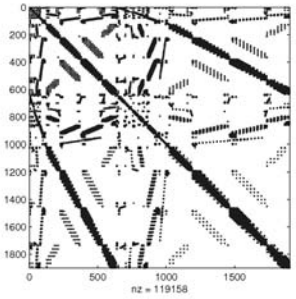

(B) $\ell_r = 0.5$ mm

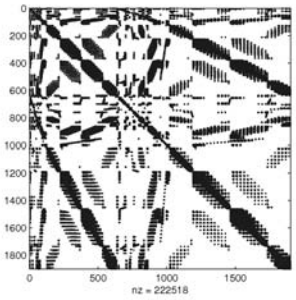

(C) $\ell_r = 1.0$ mm

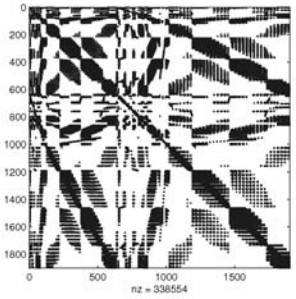

(D) $\ell_r = 1.5$ mm

FIGURE 5.13: Sparsity of the stiffness matrix $\boldsymbol{K}_T^{nl}$ at increment 5 (coarse mesh).

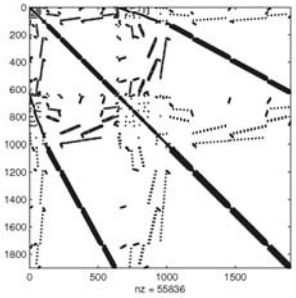

(A) $\ell_r = 0.0$ mm

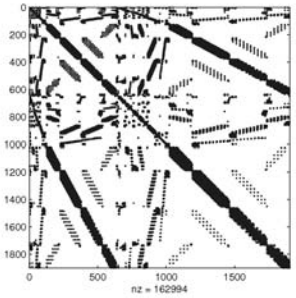

(B) $\ell_r = 0.5$ mm

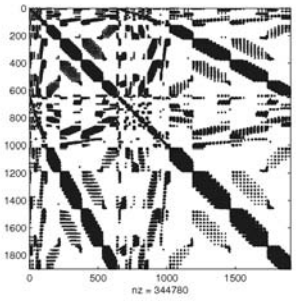

(C) $\ell_r = 1.0$ mm

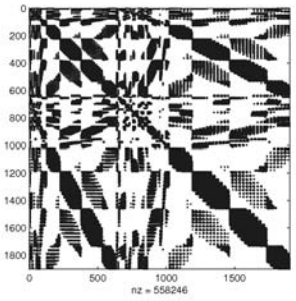

(D) $\ell_r = 1.5$ mm

FIGURE 5.14: Sparsity of the stiffness matrix $\boldsymbol{K}_T^{nl}$ at increment 20 (coarse mesh).

5.6 Conclusions

In this chapter, a general methodology for the consistent linearisation of elasto-plastic non-local models of integral-type has been presented in detail. A consistent linearisation is highly desired since it guarantees the quadratic convergence rates inherent to the full Newton-Raphson method. It has been shown that, when the non-local variable is an implicit function of other constitutive variables, a point-wise continuum tangent modulus does not exist. However, the finite element discretisation permits the establishment of a finite global constitutive relation that, in the general case, is obtained from the inversion of a global compliance matrix.

The computational burden associated with the matrix inversion can be avoided if analytical expressions for the terms $\mathbf{D}_{ij}$ (Equation 5.29) are obtained. It has been shown that, in the case of a J_2 hybrid local/non-local plasticity model and the Lemaitre-based non-local model of Chapter 3, such closed-form analytical expressions can be achieved by employing standard differential calculus, rendering highly efficient numerical implementations.

The results documented in this chapter have clearly demonstrated that the present linearisation is consistent with the associated non-local stress integration procedure. Quadratic rates of convergence have been successfully achieved for both the J_2 hybrid local/non-local plasticity and the Lemaitre-based non-local models, regardless the size of the non-local intrinsic length ℓ_r, the local/non-local parameter m or the mesh refinement adopted.

Finally, it has been also demonstrated that, when compared to the local case, the use of the consistent non-local tangent operator leads to more populated stiffness matrices as shown in Section 5.5.2. This inevitably yields on longer computational times when solving the structural problem. Gradient-enhanced formulations, on the other hand, need additional degrees of freedom per node in order to take the effects of non-locality into account, which also increases the solution time since the system of equations to be solved is larger. Perhaps an interesting and rather important assessment would be the direct comparison of both non-local strategies concerning numerical efficiency, where this idea is left as a suggestion of future work.

Chapter 6

Assessment and Comparison of Non-local Models

Non-local models have been successfully used in the last two decades in the task of circumventing the pathological mesh dependency. Despite the many advances in this topic, many questions still remain unanswered. For instance, up to this date, there is no exact guideline for how should non-locality be introduced in most existing local models. In general, authors have usually chosen a promising candidate variable to be a non-local quantity and have then developed and assessed their models based on this candidate. For example, Pijaudier-Cabot and Bažant [93] have adopted the damage variable as the non-local quantity for an elastic-damage non-local model of integral-type for the description of brittle materials. De Borst and Mühlhaus [35] have discretised the plastic multiplier within a gradient-dependent plasticity framework. The accumulated plastic strain in the classical J_2 plasticity was the choice of Strömberg and Ristinmaa [110], who employed a hybrid local/non-local formulation. Geers et al. [55] have formulated a damage-induced plasticity model where the gradient of the accumulated plastic strain has been accounted for in the global structural problem. Mediavilla et al. [81] have enhanced a damage variable, dependent of both plastic strain and triaxiality, with an implicit gradient formulation. A similar approach was adopted by César de Sá et al. [26] who have regarded damage as non-local within an implicit-gradient framework. More recently, Andrade et al. [3] have adopted the damage variable as a non-local quantity for the modelling ductile damage through a non-local formulation of integral-type. All these works have provided numerical examples where it has been shown that the pathological mesh sensitivity could be effectively eliminated. However, it was unclear if their models could be differently formulated (e.g., with another non-local quantity) and still preserving their regularising characteristics or

if the models would still be able to tackle the mesh sensitivity issue when subjected to different stress states.

Nonetheless, there are a few works which have focused on comparing different non-local models. Perhaps the most valuable contribution to this topic has been given by Jirásek and Rolshoven [70] who have compared various different non-local formulations for elastic-damage and plasticity models. Their assessment has been carried out through the analysis of one-dimensional bars under infinitesimal strains and has focused specifically on verifying the ability of the many non-local models in acting as effective localisation limiters. They have found that some models, previously believed to be mesh-insensitive, could provide only a partial regularisation of the solution and that they fail under some special circumstances.

Many important conclusions have been withdrawn on the comprehensive comparison of Jirásek and Rolshoven [70]; however, their assessment still is not enough to clearly answer the question of how should non-locality be accounted for in the general case. This is mainly due to fact that they have limited their analysis to the one-dimensional case. In fact, real structures are subjected to multi-axial stress states that may dramatically influence their response to external loads. In turn, the material laws that are employed to capture diverse structural responses behave quite differently when subjected to various stress states. This suggests that a given non-local model, which preserves mesh-insensitivity under a given stress state, may also respond differently when subjected to other stress states. Thus, the one-dimensional analysis is not sufficient to completely characterise the effects of non-locality if we are aiming to avoid pathological mesh dependence in real structures.

Particularly in the case of ductile materials, extensive research effort has established that fracture has a strong dependence on the stress state. The works of McClintock [79], Rice and Tracey [102] and Mackenzie et al. [77] have, amongst others, identified, from experimental testing with round smooth and notched bars, a relation between the stress triaxiality ratio and the effective plastic strain at fracture initiation. Later, Hancock and Brown [60] have carried out similar experiments with plane strain specimens and shown that, despite of having a different geometrical fracture pattern due to the occurrence of shear bands at the critical zone, the effective plastic strain at fracture also tends to decrease as triaxiality increases. These works have provided a deeper understanding on the mechanisms that cause material breakage for which many authors have sought to propose constitutive models that could reproduce experimental evidence. Amongst them, Gurson [57] proposed a theory where the material is regarded as a porous medium in which the initially existing micro-voids may grow. The theory has been later

extended by Tvergaard and Needleman [113] who introduced into the material model the mechanisms of nucleation and coalescence of cavities. Following a different strategy by adopting a purely phenomenological approach, Lemaitre [74, 75] has presented a thermodynamically consistent constitutive model where the material progressive degradation has been treated by means of an internal continuous variable. It is important to mention that all these models have particularly sought to capture the effects of high stress triaxiality ratios on material degradation, which, in turn, are closely linked to the phenomenon of nucleation, growth and coalescence of voids.

However, the works of Bao [7], Bao and Wierzbicki [8, 9], Barsoum and Faleskog [10, 11], Bai [6] and Gao et al. [54], amongst others, have more recently shown that the third invariant of the stress tensor, usually regarded by means of the so-called *Lode angle*, also plays an important role on fracture of many metallic alloys. In fact, such works have also introduced the important concept of characterising the stress state not only by the stress triaxiality ratio but also by the normalised Lode angle, a statement also recognised by other authors, e.g. Nahshon and Hutchinson [83].

In view of that, the objective of the present work is to enhance with non-locality the classical models of Lemaitre and GTN, which have been very often adopted to describe ductile deformation. We select different variables to be taken as non-local and assess the established non-local models through numerical simulation under different stress states. The main goal is to identify which options lead to a completely mesh insensitive material description when subjected to different loading conditions.

This chapter is organised in the following fashion. In Section 6.1, general definitions concerning parameters for the characterisation of the stress state are presented. In Section 6.2, we review, very briefly, some general aspects of ductile fracture observed in experimental tests where the main mechanisms of failure are highlighted. This rather brief review will be relevant for the selection of the specimens to be simulated using different non-local formulations. In the following section, both Lemaitre- and Gurson-based models are enhanced by non-locality adopting different non-local variables. Finally, the results and discussion of numerical simulation are presented in Section 6.4, followed by general conclusions in Section 6.5.

6.1 Parameters for stress state characterisation

Firstly, we repeat the definition of the von Mises equivalent stress, q, which is related to the second invariant of the deviatoric stress tensor, to be given by

$$q = \sqrt{3J_2(\boldsymbol{s})} = \sqrt{\frac{3}{2}\boldsymbol{s} : \boldsymbol{s}}, \tag{6.1}$$

and the third invariant-related quantity t, which reads

$$t = \left(\frac{27}{2}\det[\boldsymbol{s}]\right)^{1/3}. \tag{6.2}$$

The *stress triaxiality ratio* [77, 79, 102] is defined as

$$\eta = \frac{p}{q}, \tag{6.3}$$

and is a practical measure of the stress state in a given point.

The third invariant-related quantity, t, can be conveniently normalised:

$$\xi = \left(\frac{t}{q}\right)^3, \tag{6.4}$$

where $-1 < \xi < 1$.

The so-called *Lode angle*, denoted by θ, is a quantity related to the third invariant of the deviatoric stress tensor, given by

$$\theta = \frac{1}{3}\arccos(\xi), \tag{6.5}$$

and has values between $0 < \theta < 0.3$. It can be normalised through the following expression:

$$\bar{\theta} = 1 - \frac{6\theta}{\pi} = 1 - \frac{2}{\pi}\arccos(\xi), \tag{6.6}$$

for which $-1 < \bar{\theta} < 1$.

Remark 6.1. *All the parameters above have been defined using quantities related to the Cauchy stress tensor just for convenience. In fact, they can also be defined using the Kirchhoff stress tensor. Regardless the stress tensor measure adopted, both the triaxiality ratio, η, and the normalised third invariant, ξ, render exactly the same values. This can be easily verified using the relation given in Equation (2.23). However, it is important to mention that this is not true in the case of the equivalent stress, q. Therefore, whenever the symbol q is used in this thesis, it has*

been made clear if the equivalent stress has been defined using the Cauchy or the Kirchhoff stress tensor.

6.2 Some aspects on ductile behaviour and failure

In a general sense, ductile failure is dictated by different mechanisms depending on the stress state under which the material is subjected to. In the literature, it seems consensual among many authors that progressive material degradation plays a major role in the deformability of ductile materials where, in fact, plastic straining and internal deterioration are strongly coupled.

As the result of extensive experimental testing, several authors have found that the stress triaxiality ratio plays a major role upon ductile failure initiation [60, 71, 77, 79, 102]. These (and other) authors have then established a relation between triaxiality and the effective strain at fracture, ε_f^p, where the latter decreases as the former increases. This behaviour is typically observed in many metallic alloys commonly employed in industrial applications. More recently, it has been reported that some other metals may have a different behaviour for triaxialities below $\eta = 1/3$, (e.g., [6, 7], among others). Both these behaviours are schematically depicted in Figure 6.1, where the two-dimensional fracture curve defines the boundary of fracture and no-fracture zone on the space of ε_f^p versus η. In fact, relatively recent research effort has additionally shown that not only triaxiality but also the third invariant of the deviatoric stress tensor (very often regarded through the Lode angle) can substantially affect the material behaviour. These developments have lead to a more appropriate curve to depict fracture loci, where instead of using two-dimensional plots (like in Figure 6.1), a third axis, denoting the third invariant [120], has been included (see Figure 6.2)[1]. Indeed, the identification of the role of the third invariant upon ductile failure was a major breakthrough in material sciences.

In order to capture the curves like the ones depicted in Figures 6.1 and 6.2, various specimens have been designed aiming to test materials at several triaxialities and different values of the third invariant. For instance, smooth and notched round bars are employed to capture values of $\eta \geq 1/3$ meanwhile ξ remains constant and around 1.0. Similar values of triaxiality can be obtained with plane strain

[1]It is important to remark that the two-dimensional fracture curves of Figure 6.1 are in fact a projection of the three-dimensional fracture surface of the material.

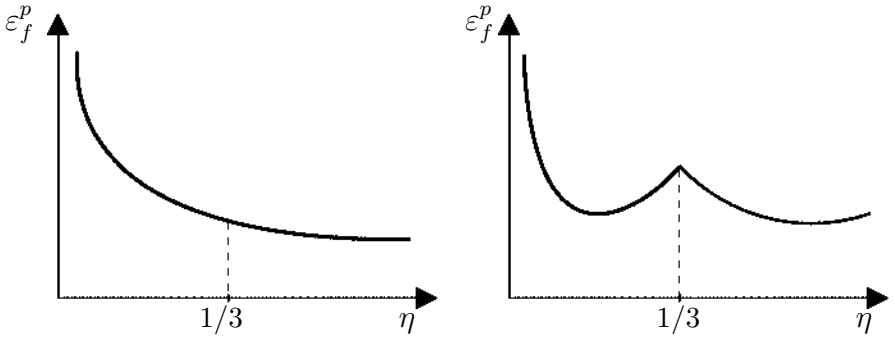

FIGURE 6.1: Stress triaxiality ratio (η) versus equivalent strain at fracture (ε_f^p): behaviour typically observed in different ductile metals.

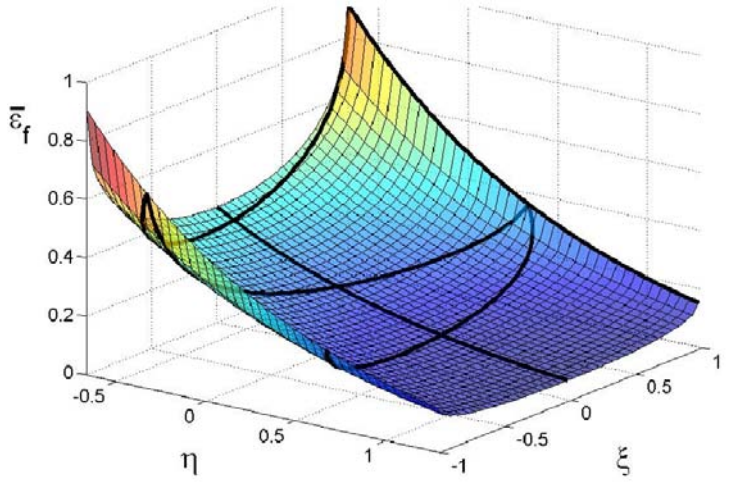

FIGURE 6.2: A (symmetric) three-dimensional fracture locus as proposed by Wierzbicki and co-authors [120] (adapted from Bai [6]).

specimens; however, the normalised third invariant parameter is completely different and has in this case the value of $\xi = 0.0$. In practice, the different value of ξ characterises a different stress state than the one in the case of cylindrical specimens. In the assessment carried out in this chapter, a notched bar and a plane strain specimen have been selected for investigation

Since it has been identified that, for many metallic alloys, the pattern of the fracture locus changes around the triaxiality of $\eta = 1/3$, some researchers have concentrated their efforts in investigating plastic straining and fracture at this turning point. For this purpose, Bao [7] has conducted a series of experiments using a perforated plate specimen. This specimen has been simulated in the context of the Lemaitre-based non-local damage model of Chapter 3 and will be again adopted in the present chapter.

To achieve pure shear stress states, i.e., when the triaxiality is zero, many specimens have been considered as reported in many contributions (for instance, see [6]). Within the scope of this chapter, we shall limit ourselves to adopt the shear specimen used by Brünig et al. [23]. Note that the same specimen has also been used in Chapter 4 to assess the non-local Gurson-based model proposed in that chapter under shear-dominated stress states. It is worth recalling that, in the pure shear condition, the normalised third invariant is zero.

For reference, some of these different specimens have been schematically arranged in a diagram (see Figure 6.3) as function of the triaxiality and the normalised third invariant, closely following the diagram presented by Bai [6]. In Figure 6.4, a schematic representation of the geometry of the aforementioned specimens is depicted in three-dimensions. These are the specimens that have been selected for the present assessment

The general concepts of ductile failure briefly reviewed in this section are of extreme importance for a consistent assessment of non-local models. It has been widely recognised that ductile materials behave quite differently under different stress states; therefore, this statement highly suggests that the issues of pathological mesh dependency may also behave quite differently under different loading conditions. Thus, aiming to unfold the question of which variable should be regularised in a given ductile damage model, a comprehensive comparison of different non-local formulations, when applied in the simulation of different stress states, will be carried out in this chapter.

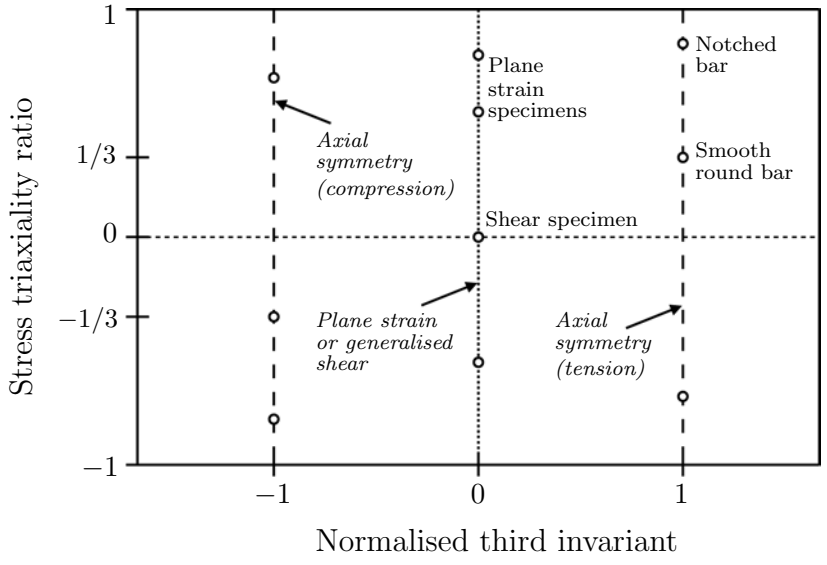

FIGURE 6.3: Stress triaxiality ratio versus normalised third invariant.

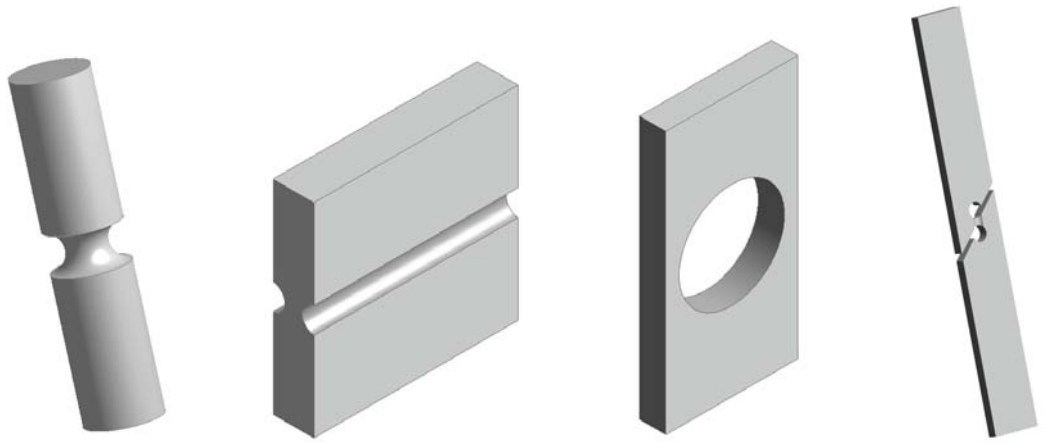

(A) Notched Bar (B) Plane Strain Specimen (C) Perforated Plate (D) Shear Specimen

FIGURE 6.4: Schematic three-dimensional representation of the specimens.

6.3 Non-local models

The first step for the non-local enhancement of a previously existing local material model is to choose where the integral operator (like in Equation 3.10) should be incorporated in the constitutive equations. This step can be interpreted, to some extent, as 'the choice of the non-local variable'. For the sake of readability, this terminology will be frequently used throughout this chapter.

Since every single variable of a given constitutive model can be enhanced by non-locality, a large number of possibilities seems to exist. Of course, some options are at first glance more promising than others; however, a simple guess does not guarantee a constitutive model free of spurious mesh dependence. Among the limited number of contributions who worked in this direction, Bažant and Chang [13] have concluded that the internal variables are the best candidates for non-local quantities when compared to other quantities such as the stress and the total strain tensors. However, which internal variable should be selected among the many possibilities is, to a larger extent, uncertain for most models. Other important contributions on the issue of the choice of the non-local variable are due to Jirásek [67] and Jirásek and Rolshoven [70], who assessed many different non-local formulations in order to verify their regularising properties, as mentioned in the beginning of this chapter.

However, none of these efforts has focused on ductile damage models. Besides, the aforementioned works have concentrated in one-dimensional analysis exclusively. As stressed out in the beginning of this chapter, real structures are subject to multi-axial stress states and extensive experimental investigation has already shown that

the materials that compose these structures behave quite differently when under different loading conditions.

During this investigation, several options have been considered and thoroughly tested for both Lemaitre- and Gurson-based damage models. Inevitably, this has lead to a huge amount of results whose comprehensive scrutiny would exhaust the objectives of this chapter. Since many of the several considered options have lead to very similar conclusions, we have limited ourselves herein to present the results of four choices associated with each of the two constitutive local models. Consistency has also been a concern in the present contribution, thus, some effort has been made aiming to only regularise constitutive variables that are, to a some extent, equivalent in both the Lemaitre- and Gurson-based models.

For the case of Lemaitre-based models, the following four options have been considered:

- regularisation of damage, $\bar{D}$;
- regularisation of the isotropic hardening variable, $\bar{R}$;
- regularisation of elastic energy release rate, $-\bar{Y}$;
- simultaneous regularisation of damage, $\bar{D}$, and the isotropic hardening variable, $\bar{R}$.

The choices listed above modify the Lemaitre local model in such manner that for each case one (or more) evolution equation of the local model needs to be modified. The necessary modifications in the constitutive model are directly summarised in Table 6.1. For the sake of simplicity, we have attributed a reference label for each non-local model. This will be particularly helpful when reporting the numerical results in Section 6.4. We remark that all models listed in Table 6.1 belong to the class of *classical non-local models* [27], which are simply ad-hoc formulated based on a previously existing local constitutive model. In Chapter 3, it has been shown that the classical non-local model formulated with $\bar{D}$ does not violate thermodynamical principles, i.e., the model does not predict negative dissipations. In fact, the same conclusion can be straightforwardly withdrawn with the other non-local models listed above by following similar procedures as the ones employed to demonstrate thermodynamical admissibility in the case of `L-D`.

Remark 6.2. *In the present assessment, the thermodynamically consistent model proposed in Chapter 3 will not be considered. Our intention with that is to keep*

consistency by only comparing non-models that have been established without resorting to thermodynamics. It it nonetheless worth mentioning that, during this study, numerical analysis has shown that the results obtained with the thermodynamically consistent model of Chapter 3 were qualitatively very similar to the case of `L-D`*, where the former has presented a slightly higher diffusive effect than the latter, exactly as elucidated in the conclusions of Chapter 3. This statement has persisted regardless the stress state investigated in the present study. In practice, the main difference between* `L-D` *and the thermodynamically consistent model is that each model will lead to slightly different values of ℓ_r when the model is calibrated to match experimental results, since the thermodynamic model produces a higher diffusive effect.*

Table 6.1: Lemaitre-based non-local models.

Associated Variable	**Symbol**	**Associated Evolution Eq.**	**Ref.**
Damage	$\bar{D}$	$\dot{\bar{D}} = \mathcal{R}\left(\dot{D}\right)$	`L-D`
Isotropic Hardening	$\bar{R}$	$\dot{\bar{R}} = \mathcal{R}\left(\dot{R}\right)$	`L-R`
Energy Release Rate	$-\bar{Y}$	$\dot{D} = \frac{\dot{\gamma}}{(1-D)}\left[\frac{\mathcal{R}\left(-Y\right)}{r}\right]^s$	`L-Y`
Damage, Isotropic Hardening	$\bar{D}, \bar{R}$	$\dot{\bar{D}} = \mathcal{R}\left\{\frac{\dot{\gamma}}{(1-D)}\left[\frac{-Y}{r}\right]^s\right\}$, $\dot{\bar{R}} = \mathcal{R}\left(\dot{R}\right)$	`L-DR`

Similarly to the case of Lemaitre model, four candidate variables have been chosen for the Gurson-based damage model:

- regularisation of damage, $\bar{f}$;
- regularisation of the isotropic hardening variable, $\bar{R}$;
- regularisation of the equivalent plastic strain, $\bar{\varepsilon}^p_{eq}$;
- simultaneous regularisation of damage, $\bar{f}$, and the isotropic hardening variable, $\bar{R}$.

Again, each choice requires modifications in one or more evolutions equations that are associated with the chosen constitutive variable, where the necessary modifications are summarised in Table 6.2 for convenience. We remark that the present Gurson-based models very closely follows the model proposed in Chapter 4 where the only difference is the non-local variable associated with each of the choices listed above.

TABLE 6.2: Gurson-based non-local models.

Associated Variable	**Symbol**	**Associated Evolution Eq.**	**Ref.**
Damage	$\bar{f}$	$\dot{\bar{f}} = \mathcal{R}\left[\mathcal{A}\dot{\varepsilon}^p_{eq} + (1-f)\dot{\varepsilon}^p_v + \dot{f}^S\right]$	G-F
Isotropic Hardening	$\bar{R}$	$\dot{\bar{R}} = \mathcal{R}\left(\dot{R}\right)$	G-R
Equivalent Plastic Strain	$\bar{\varepsilon}^p_{eq}$	$\dot{f} = \mathcal{A}\mathcal{R}\left(\dot{\varepsilon}^p_{acc}\right) + (1-f)\dot{\varepsilon}^p_v + \dot{f}^S$	G-EP
Damage, Isotropic Hardening	$\bar{f}, \bar{R}$	$\dot{\bar{f}} = \mathcal{R}\left[\mathcal{A}\dot{\varepsilon}^p_{eq} + (1-f)\dot{\varepsilon}^p_v + \dot{f}^S\right]$, $\dot{\bar{R}} = \mathcal{R}\left(\dot{R}\right)$	G-FR

Remark 6.3. *In Chapters 3 and 4, the decision of taking damage as the non-local variable has been simply justified 'as a natural choice' since damage is the variable that triggers the softening regime in both Lemaitre and Gurson models. Interestingly, this has also been the motivation of Pijaudier-Cabot and Bažant [93] when they have, following the very same idea, chosen damage to be non-local in a constitutive model intended to describe deformation and failure of quasi-brittle materials. Later, Jirásek [67] and Jirásek and Rolshoven [70] have shown that the choice of damage, in that particular situation, leads to locking results and that the regularisation of other variables, such as the equivalent strain or the energy release rate, $-Y$, would be preferred in order to achieve completely mesh-independent solutions. We remark that this conclusion has, so far and to the author's knowledge, been verified for explicit damage models only, i.e., when the damage variable is explicitly calculated from other quantities, such as the plastic strain. This is not the case of the ductile damage models addressed in this thesis, which take material degradation into account in an implicit fashion. As it will be made clear in the following section, the conclusions obtained for explicit damage models regarding the choice of the non-local variable* do not apply *for implicit*

damage models. In fact, the conclusions are completely different. This implies that one has to be very careful when selecting the non-local quantity associated with a given constitutive model.

6.4 Numerical analysis

In this section, we numerically assess the different non-local models formulated in Section 6.3 when subjected to different combinations of stress triaxiality ratios, η, and normalised third invariant, ξ. As pointed out in Section 6.2, ductile materials may have very different behaviour upon fracture, with less or more dependency on the parameters η and ξ. It is also true that certain materials exhibit more strain-driven softening than others, so the need of non-local modelling is, in quantitative terms, highly dependent of the specific material which one aims to simulate. Our intention in this chapter is to numerically investigate the performance of the different non-local models of Section 6.3 rather than reproducing experimental evidence with accuracy. Therefore, for the present assessment, we will simply adopt henceforth generic material properties that very much resemble those typically observed and calibrated from experimental testing of high strength steel alloys (see Tables 6.3, 6.4 and 6.5). The same material properties will be used in all simulations for consistency.

Three different mesh refinements will be used in each case, for which the following line pattern has been adopted in the XY-plots: the coarse, medium and fine meshes are respectively represented by a full $(-)$, a dashed $(--)$ and a dotted $(\cdots)$ line.

Again, the main objective of the present assessment is to verify, exclusively through numerical simulation, how each non-local model behaves under several different stress states and to check whether the desired regularising effects are consistently achieved. The conclusions withdrawn on the results obtained in the present investigation are fundamental for the correct use of the non-local method when matching the results of new constitutive models with experimental evidence. Only so it is possible to be certain that the numerical framework, to be adopted in the parameter identification procedure, prevents spurious mesh dependency under several stress states, providing a reliable calibration of the material properties.

TABLE 6.3: Basic material properties employed in all simulations.

Property	**Value**
Elastic modulus	$E = 220$ GPa
Poisson's ratio	$\nu = 0.3$
Hardening function	$\tau_y(R) = 700 + 300R^{0.3}$ MPa

TABLE 6.4: Lemaitre-related material properties.

Property	**Value**
Lemaitre damage exponent	$s = 1.0$
Lemaitre damage denominator	$r = 3.0$ MPa

TABLE 6.5: Gurson-related material properties.

Property	**Value**
Micro-void volumetric fraction for nucleation	$f_N = 0.04$
Mean strain for void nucleation	$\varepsilon_N = 0.2$
Standard deviatoric strain for nucleation	$s_N = 0.1$
Critical damage	$f_c = 0.06$
Damage at fracture	$f_f = 0.22$
Shear-damage factor	$k = 3.0$

6.4.1 Analysis at high stress triaxiality ($\eta > 1/3$)

We start the assessment of the several non-local models by first observing how they behave when subjected to triaxialities above the value of 1/3. It is consensual in the literature that, for ductile materials at such high triaxialities, the predominant internal degradation mechanism is governed by the phenomena of nucleation, growth and coalescence of micro-voids.

To a major extent, the ductile damage models in this thesis (i.e., based on the models of Lemaitre and Gurson) have been particularly conceived to capture the aforementioned phenomena. Indeed, this fact was the main motivation for the inclusion of the additional damage mechanism in Gurson's model in Chapter 4, since without the adopted modification no damage evolution would take place in shear-dominated stress states with that model. In the case of Lemaitre, damage does evolve when subjected to both high and low stress triaxialities.

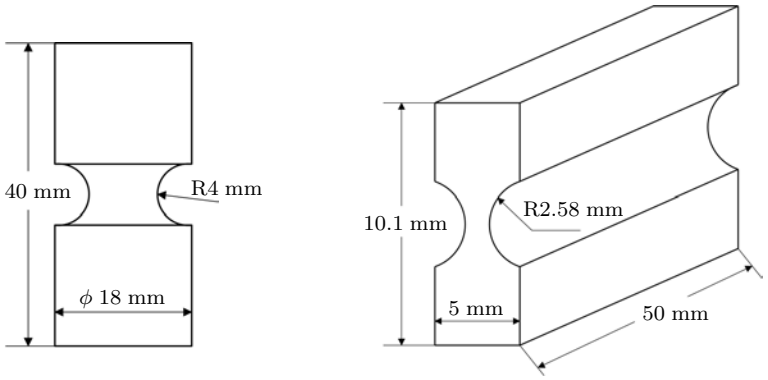

FIGURE 6.5: Geometry for the axisymmetric (left) and plane strain (right) specimens.

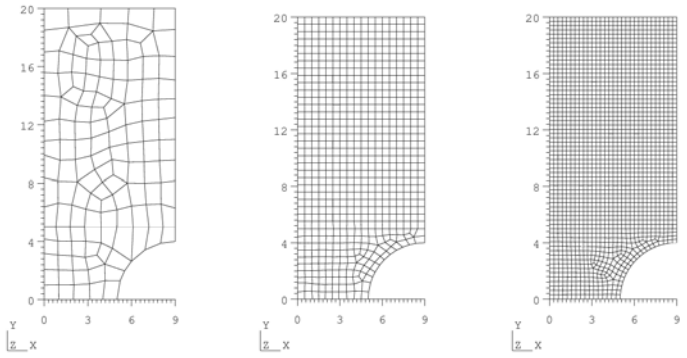

FIGURE 6.6: Mesh refinements for the notched axisymmetric specimen.

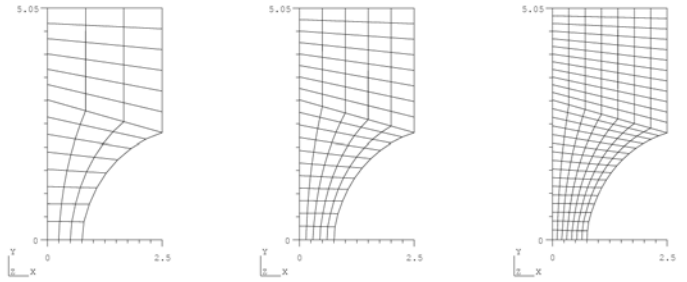

FIGURE 6.7: Mesh refinement for the plane strain specimen.

For the analysis at high triaxialities, two specimens will be considered in the present assessment: an axisymmetric notched bar and a grooved plate under plane strain condition (see Figure 6.5). In order to facilitate readability, the labels `NOTCHED` and `PLANE` will be henceforth adopted to make reference to these specimens. The mean values of triaxiality are very similar in both cases ($\eta_{avg} \cong 0.8$ for `NOTCHED` and $\eta_{avg} \cong 0.7$ for `PLANE`). Conversely, the mean values of the normalised third invariant are quite different ($\xi_{avg} \cong 1.0$ in the `NOTCHED` case and $\xi_{avg} = 0.0$ in the case of `PLANE`), characterising different stress states. As it will become quite clear after careful scrutiny of the results in this chapter, the stress state plays a

major role on the issue of pathological mesh dependency.

Both specimens have been discretised with quadrilateral quadratic elements where reduced integration has been adopted to avoid spurious element locking (see Figures 6.6 and 6.7). Three mesh refinements have been considered in order to capture the effects of mesh dependency where only one quarter of the geometry has been simulated in both cases. Different non-local intrinsic lengths have been assigned to the specimens, namely $\ell_r = 0.6$ mm for the `NOTCHED` case and $\ell_r = 0.35$ mm for the `PLANE` specimen. These values correspond to intrinsic lengths that span a minimum necessary of elements (and their associated integration points) in order to activate the effects of the non-local formulation.

Remark 6.4. *We recall that, within the context of this work, the intrinsic non-local length ℓ_r has been exclusively treated as a numerical parameter, for which comparison with experimental evidence is necessary for the validation of many results presented in this thesis. However, in the present assessment, an accurately calibrated ℓ_r is of minor importance since the main goal of this investigation is to determine how each non-local model behaves when subjected to different triaxialities. Again, the yet qualitatively nature of the results obtained in the present analysis is fundamental for a correct calibration of the constitutive parameters of a given material model, ensuring that the appropriate non-local variable is selected for the numerical parameter identification procedure.*

Firstly, we observe how both the Lemaitre- and Gurson-based models behave in the local case (i.e., $\ell_r = 0.0$ mm) when subjected to triaxiality ratios greater than 1/3. Figure 6.8 shows the reaction curves for both models when simulated for the `NOTCHED` and `PLANE` cases. A close inspection on these curves reveals that both Lemaitre- and Gurson-based models have the tendency of being much more susceptible to mesh dependency in the `PLANE` case (when the normalised third invariant is equal to $\xi = 0.0$) than in the `NOTCHED` case. Note that, despite the fact that the underlying assumptions for the establishment of both ductile damage models are very different, a very similar behaviour regarding spurious mesh dependency has taken place in both cases. The more pronounced mesh dependency in the `PLANE` case is again observed when the damage evolution is plotted against the applied displacement (see Figure 6.9). Although the curves in Figures 6.8 and 6.9 have shown almost no mesh dependency for the `NOTCHED` case, the damage contours clearly reveal that spurious dependency has taken place as it can be concluded by inspecting Figures 6.10 and 6.11. As one should expect, the effects of pathological mesh dependency are more evident when observing the damage contours in the `PLANE` case (see Figures 6.12 and 6.13).

Remark 6.5. *In all simulations of the present assessment, the damage values used in the plots were always the maximum value of damage obtained in the specimen at each time step. In most cases, the point of occurrence of the maximum value of damage, which can be easily identified by observing the associated contours plots provided throughout this chapter, has not changed during the simulation.*

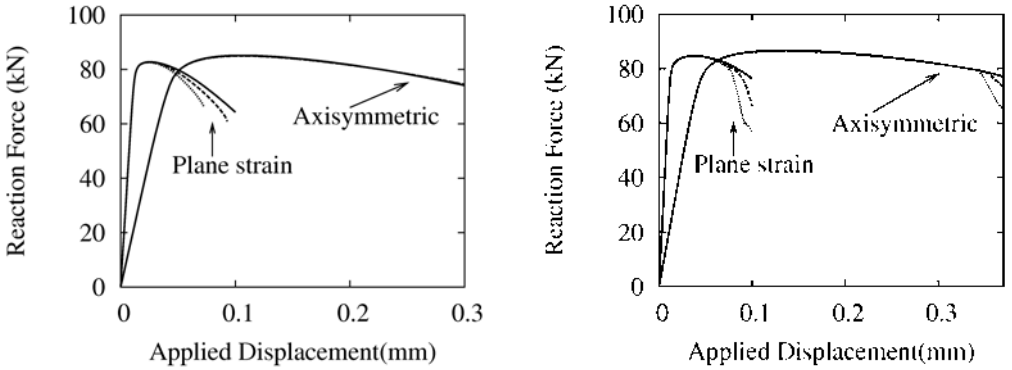

FIGURE 6.8: Reactions in the local case. Results for the Lemaitre- (A) and Gurson- (B) based models.

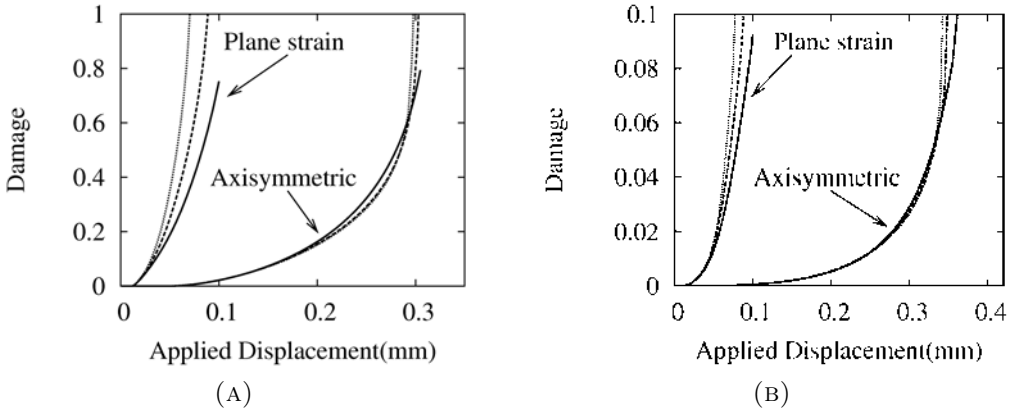

FIGURE 6.9: Evolution of damage in the local case. Results for the Lemaitre- (A) and Gurson- (B) based models.

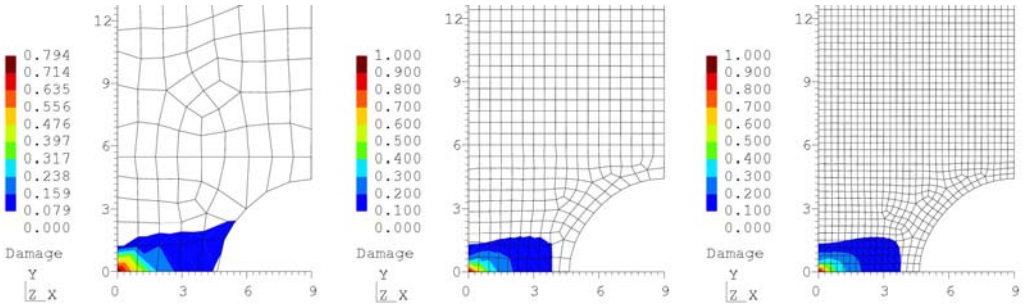

FIGURE 6.10: Damage contours for the Lemaitre-based model in the local case.

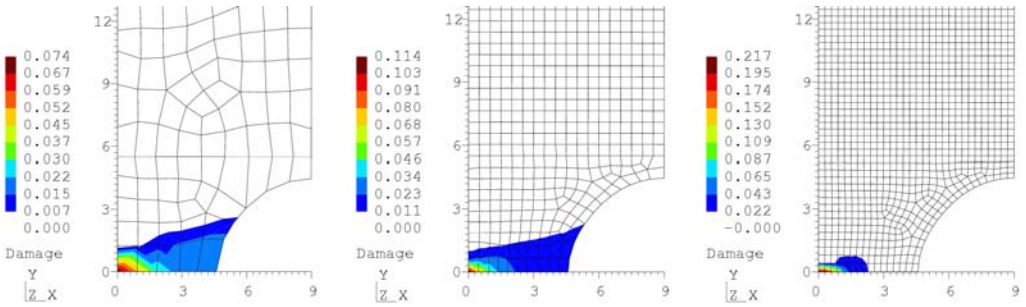

FIGURE 6.11: Damage contours for the Gurson-based model in the local case.

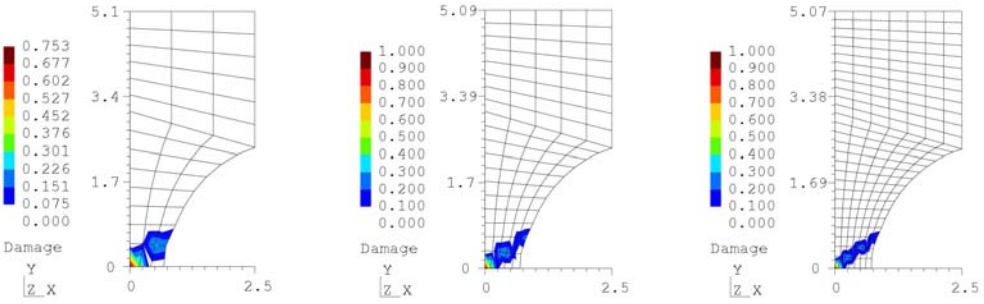

FIGURE 6.12: Damage contours for the Lemaitre-based model in the local case.

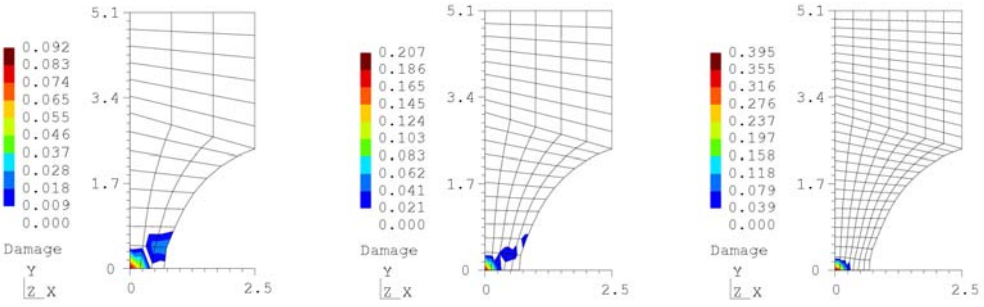

FIGURE 6.13: Damage contours for the Gurson-based model in the local case.

We observe now how the different non-local models respond when subject to the same circumstances of the local case. The reaction diagrams for the several non-local formulations are given in Figures 6.14 and 6.15 meanwhile the evolution of damage is depicted in Figures 6.16 and 6.17. A first inspection on these curves demonstrates that, as expected, there are no differences in the reactions of the local and non-local cases when the Lemaitre-based model is adopted for the NOTCHED case. This prevents us to draw any conclusions concerning the question if any of the adopted non-local formulations was able to alleviate the spurious dependency clearly present when looking at the local damage contours in Figure 6.10. This limitation is overcome if we observe the damage evolution for the different non-local formulations in Figure 6.16 from which it is straightforward to deduce that, for the `NOTCHED` case, the formulations `L-D`, `L-Y` and `L-DR` have provided mesh independent solutions. Further observation of Figures 6.14 and 6.16 reveals that only `L-D` and `L-DR` have eliminated the pathological mesh dependency in the `PLANE`. Note that this statement automatically excludes the formulations `L-Y` and `L-R` from being adequate variables for the non-local enhancement of Lemaitre-based models since they cannot eliminate the loss of ellipticity for different stress states.

Remark 6.6. *The conclusion that `L-Y` is not a good candidate for non-local variable in an implicit damage model is particularly important. In the assessment of non-local explicit damage models of Jirásek and Rolshoven [70], it has been established that the regularisation of the energy release rate, $-Y$, delivers mesh independent results. Conversely, in their investigation, the regularisation of damage has rendered locking results and therefore it was not a recommended non-local variable. Those conclusions dramatically differ from the ones drawn on the investigation carried out in this chapter. In fact, as already alluded in this text, the choice of the non-local variable substantially depends if either an implicit or an explicit damage model is used as the underlying local constitutive model.*

Remark 6.7. *It is worth mentioning that `L-Y` has provided slightly different results when compared to the local case for the plane strain specimen. In fact, a certain tendency to alleviate the pathological mesh dependency was to observe. However, such tendency was substantially small, not enough to eliminate the issues of spurious mesh dependency. Further numerical experimentation has demonstrated that higher values of ℓ_r have tended to mesh-independent solutions; however, such solutions have required very large values of ℓ_r, triggering unwanted numerical instabilities and over-stiff responses.*

We focus attention now in the results obtained with the non-local models based on Gurson model (see Figures 6.15 and 6.17). Similarly to the case of the non-local

Lemaitre-based non-local models, the regularisation of damage (`G-F`) has eliminated pathological mesh dependency for both the `NOTCHED` and `PLANE` cases. In similar manner, the simultaneous regularisation of both damage and the hardening variable (`G-FR`) has clearly provided mesh-independent results in the `PLANE` case; however, inspection of Figure 6.17(d) reveals that a slightly spurious behaviour has appeared for the Mesh 3 after a certain displacement was applied in the `NOTCHED` case. Unexpectedly, `G-R` has effectively diminished the effects of the loss of ellipticity in the `NOTCHED` case. Nonetheless, this option has revealed itself inadequate since if fails to avoid mesh dependency in the `PLANE` case. Finally, the formulation denoted by `G-EP` could substantially alleviate the effects of spurious mesh dependency for both `NOTCHED` and `PLANE`, where in the latter case the regularisation effects seem not to have been enough. Since the choice of damage (`G-F`) as non-local variable has presented superior results, and recalling that the evolution of equivalent plastic strain is embedded in the evolution of damage itself, these results suggest that the evolution of volumetric plastic strain, ϵ_v^p, also plays a significant role in the issue of pathological mesh dependency. Therefore, the regularisation of both evolutions through the regularisation of damage seems to be the optimal choice.

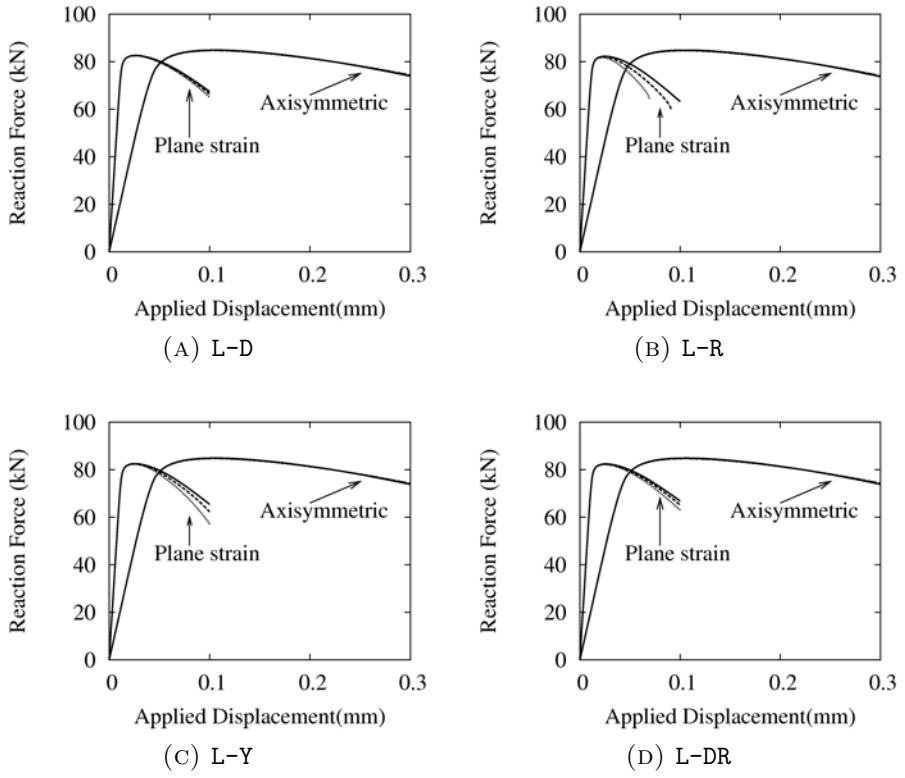

(A) `L-D` (B) `L-R`

(C) `L-Y` (D) `L-DR`

FIGURE 6.14: Reactions for the Lemaitre-based non-local models.

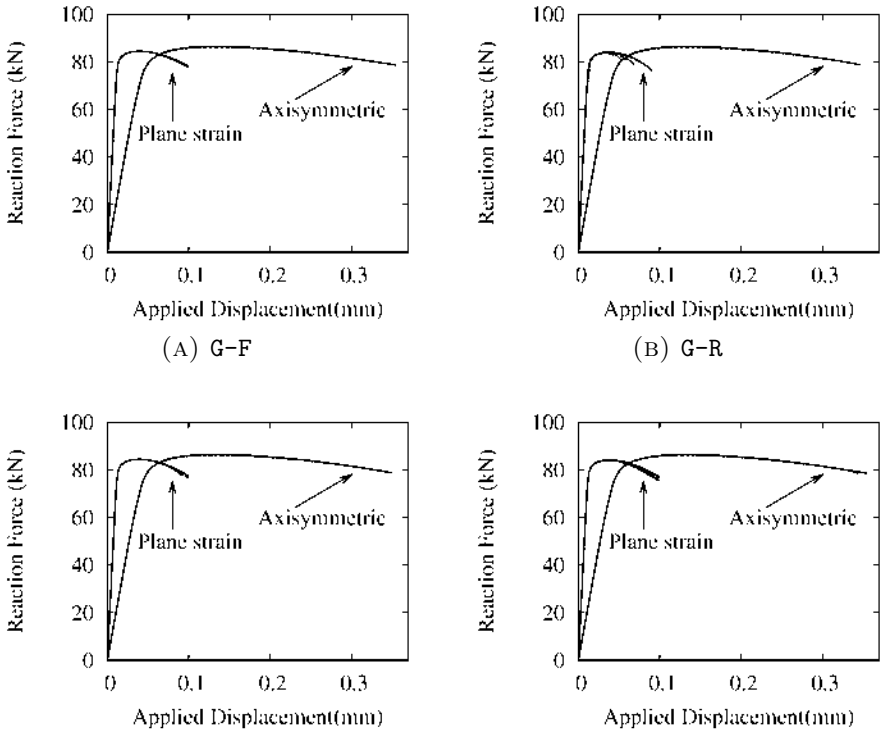

FIGURE 6.15: Reactions for the Gurson-based non-local models.

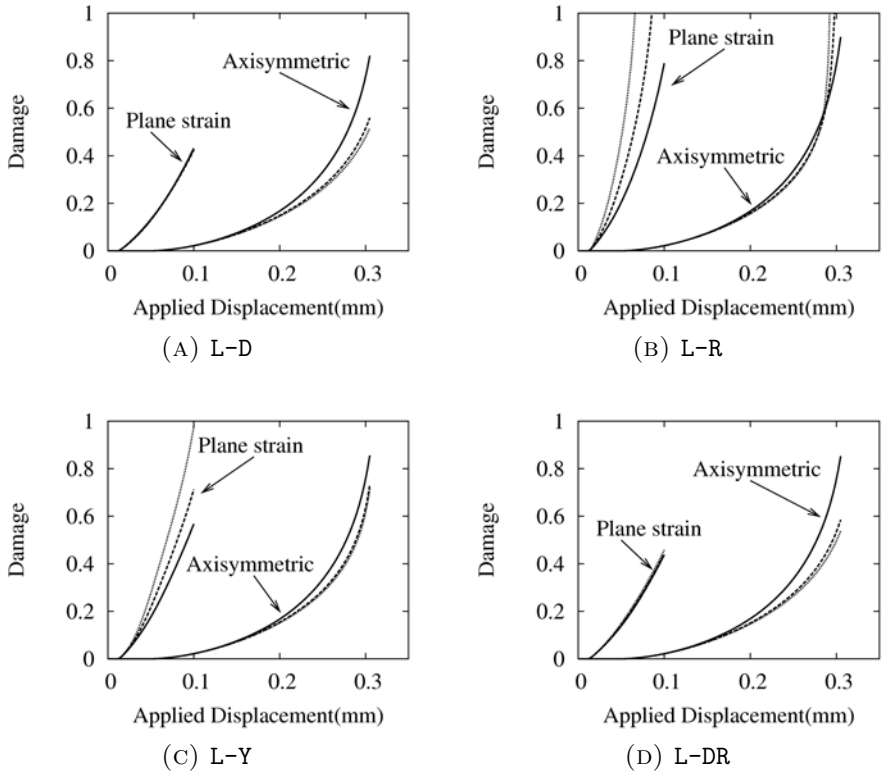

FIGURE 6.16: Damage evolution for the Lemaitre-based non-local models.

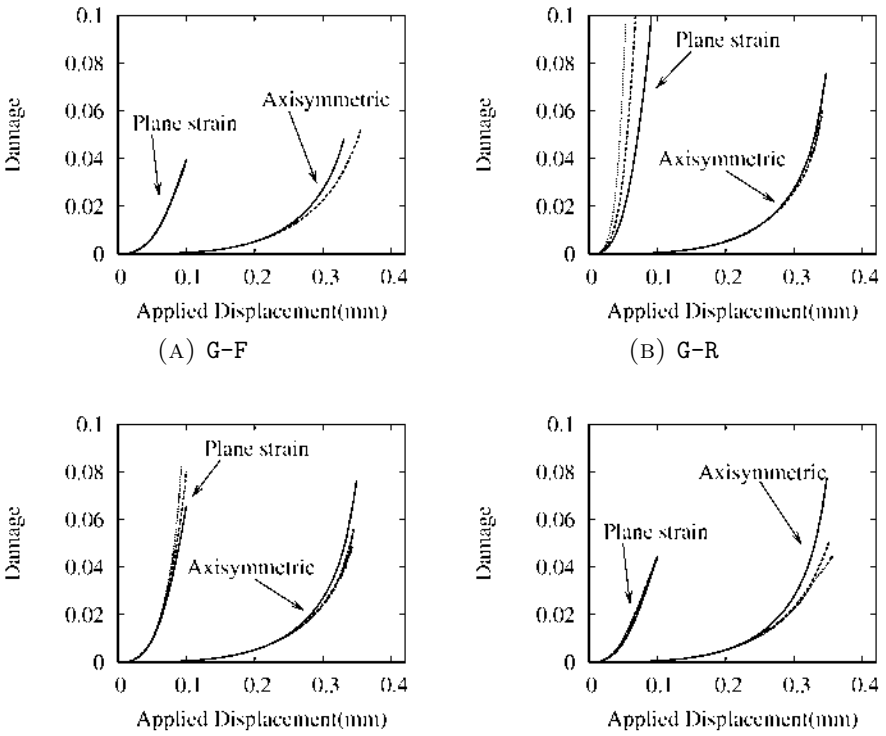

(A) G-F (B) G-R

(C) G-EP (D) G-FR

FIGURE 6.17: Damage evolution for the Gurson-based non-local models.

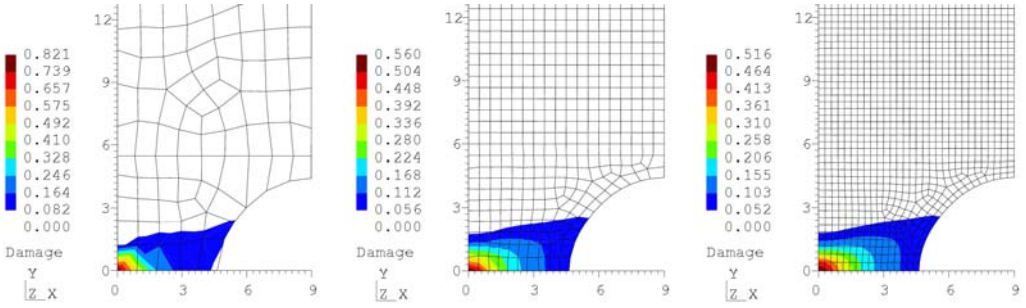

FIGURE 6.18: Damage contours for the Lemaitre-based model non-local case (L-D).

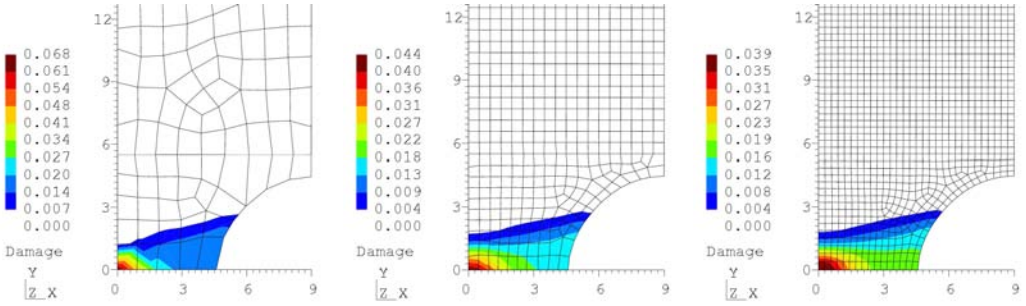

FIGURE 6.19: Damage contours for the Gurson-based model non-local case (G-F).

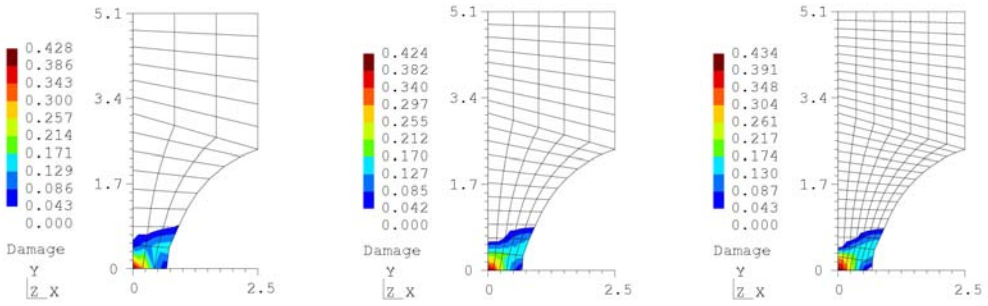

FIGURE 6.20: Damage contours for the Lemaitre-based model non-local case (`L-D`).

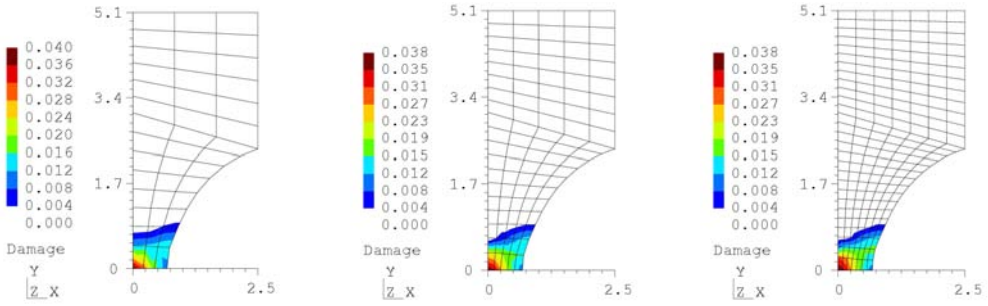

FIGURE 6.21: Damage contours for the Gurson-based model non-local case (`G-F`).

6.4.2 Analysis at moderate stress triaxiality ($\eta = 1/3$)

In order to assess the different non-local models defined in this chapter under the triaxiality of $\eta = 1/3$, we simulate a perforated plate specimen (see Figure 6.22). We recall that this same specimen has already been the focus of analysis in Chapter 3 where it has been shown that the thermodynamically admissible non-local model proposed in that chapter could effectively eliminate the effects of pathological mesh dependency. Three mesh refinements are considered (see Figure 6.22) where 8-noded hexahedra finite elements have been used to discretise the geometry. Like in Chapter 3, the F-bar element formulation is again adopted in order to avoid spurious element locking. As discussed in that chapter, the use of the F-bar formulation is straightforward within the present non-local framework since the non-local enhancement is strictly kept on the material level.

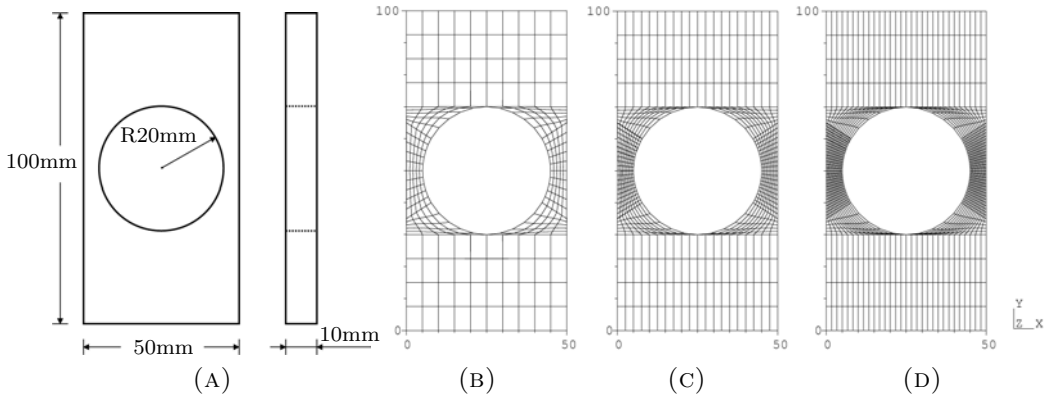

FIGURE 6.22: Geometry and different mesh refinements for the perforated plate.

Firstly the plate is simulated considering the local case. Figures 6.23 and 6.24 respectively depict the reaction diagram and the evolution of damage against the applied displacement for both Lemaitre- and Gurson-based models. The contours of damage are also plotted on the specimen in Figures 6.25 and 6.26. Clearly, pathological mesh dependency has taken place in both cases. In particular, a very peculiar behaviour is observed in the case of Gurson. Looking at Figures 6.23b and 6.24b, it is possible to notice that Mesh 2 has actually given a more critical response than Mesh 3. In Figure 6.26, we observe that a much higher value of damage has been achieved with Mesh 2 than with Mesh 3, contrary to what has been mostly seen in the results throughout this thesis. Such result is, to some extent, unexpected and could perhaps mislead to the conclusion that some sort of error has been made in the simulation set up. In fact, although unlikely, such behaviour is not impossible to emerge within the present context. Pathological mesh dependency within local constitutive frameworks occurs whenever material

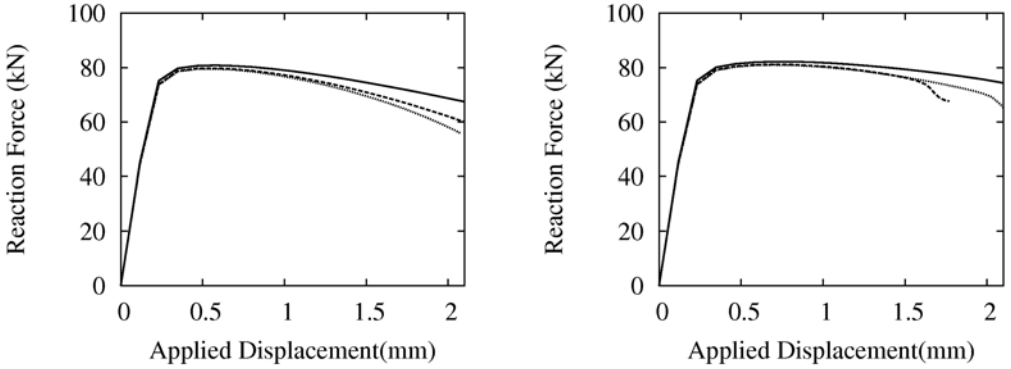

(A) (B)

FIGURE 6.23: Reactions in the local case. Results for the Lemaitre- (A) and Gurson- (B) based models.

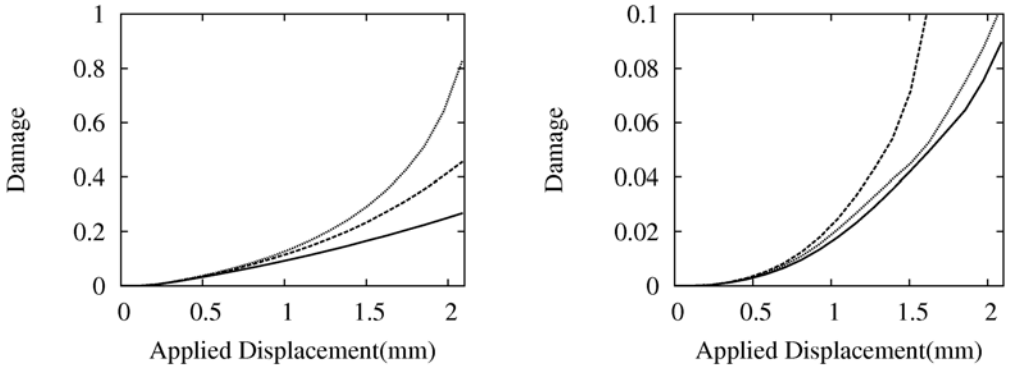

(A) (B)

FIGURE 6.24: Damage evolution in the local case. Results for the Lemaitre- (A) and Gurson- (B) based models.

softening is active (like in the present case) and can virtually lead to any result, since there is no uniqueness of solution. Even very small round-off errors in the definition of a structured mesh can lead to very unexpected results by triggering the spurious effects of loss of ellipticity. This is most probably the source of the rather odd behaviour observed in the present case.

In Figures 6.27 and 6.28, the evolution of damage for the non-local case is presented. Observing the results for the Lemaitre-based non-local models, we conclude that the best results where achieved with formulations `L-D` and `L-DR` with almost no differences between them. As expected, `L-R` was not able to regularise the problem, still giving solutions that are very sensitive to spatial discretisation. In the case of `L-Y`, some improvement in the solution when compared to the local case can be observed (see Figures 6.24(a) and 6.27(c)), although not sufficient. Similar to the case of `PLANE`, numerical experimentation with higher values of ℓ_r

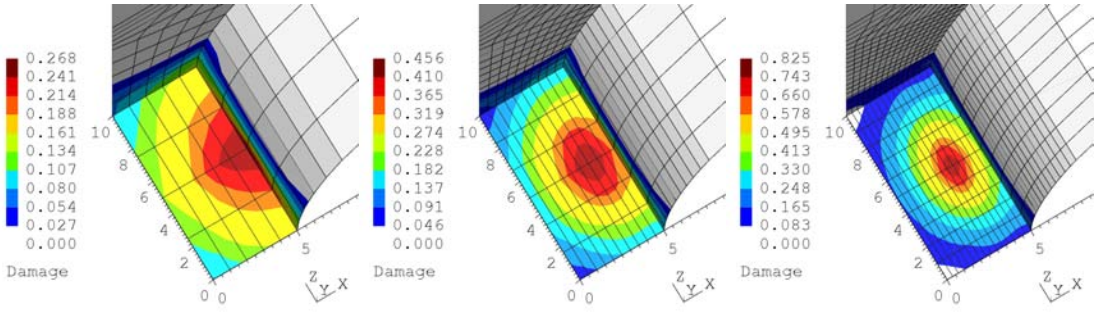

(A) (B) (C)

FIGURE 6.25: Damage contours for the local case at the critical region: Lemaitre-based model.

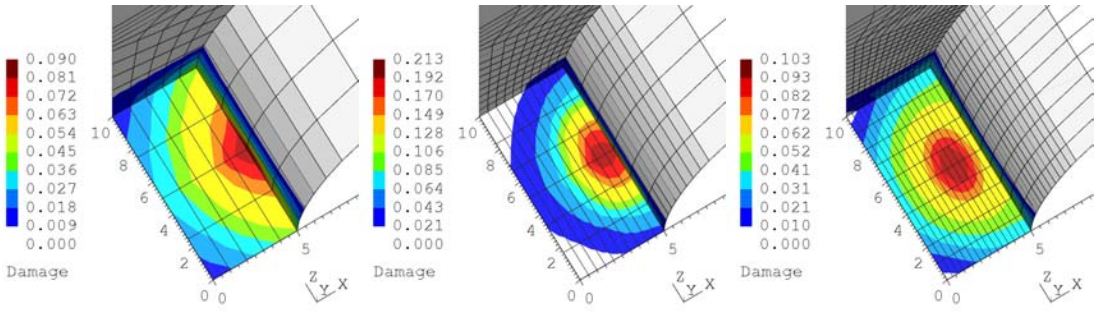

(A) (B) (C)

FIGURE 6.26: Damage contours for the local case at the critical region: Gurson-based model.

have provided more regularising effects; however, such higher values of ℓ_r were too large and, like in the `PLANE`, some numerical instabilities have been experienced.

In the case of the Gurson-based models, all the four non-local formulations, `G-F`, `G-R`, `G-EP` and `G-FR` have eliminated the effects of spurious mesh dependency. Note that the peculiar behaviour observed in the local case has been completely eliminated when the non-local theory was activated (see Figures 6.29 and 6.30). This again supports the assumption that the odd results in Figure 6.26 are a direct consequence of the loss of ellipticity of the equilibrium equation when under softening. Due to its robustness, the non-local formulation was able to avoid that spurious behaviour. This stems from the fact that, in contrast to other regularising techniques, the non-local formulation effectively eliminates the source of pathological mesh dependency by incorporating an intrinsic length into the constitutive framework.

Finally, the initial and final contours of the norm of normalised third invariant of

the deviatoric stress, $\|\xi\|$, are plotted in Figures 6.31 and 6.32[2]. Noticeably, these values vary substantially for the Lemaitre- and Gurson-based non-local models where a much lower value of ξ at the critical region has been achieved in the Lemaitre case. Comparing with the results obtained at high stress triaxiality (where two different values of ξ were examined), the present results seem to suggest that the third invariant has a more pronounced effect on the issue of pathological mesh dependency than the triaxiality. For instance, the `L-Y` formulation was able to eliminate spurious dependency when $\eta = 0.8$ and $\xi = 1.0$ (`NOTCHED` case); however, `L-Y` was not effective when $\xi = 0.0$ and $\eta = 0.7$ (`PLANE` case, see Figure 6.16(c)). In the perforated plate, a third invariant close to zero has predominated the critical region with Lemaitre-based models; in this situation, `L-Y` was again insufficient to resolve mesh dependency, which is in agreement with the conclusion drawn in the high triaxility analysis: `L-Y` does not result under low values of ξ.

A similar thought seems to apply for the Gurson-based models in the present case. In the perforated plate, the associated third invariant value in the critical region was much higher than in Lemaitre case, now tending to the unity. Remarkably, all the Gurson-based non-local formulations were able to eliminate the spurious mesh dependency, following the same tendency observed in the analysis of the notched round specimen (`NOTCHED`). Noticeably, the value of the third invariant in the notched specimen is precisely equal to 1.0.

[2]The norm of ξ has been chosen to facilitate visualisation. Note that, in the particular case of the present assessment, distinction between positive and negative values of ξ is not important.

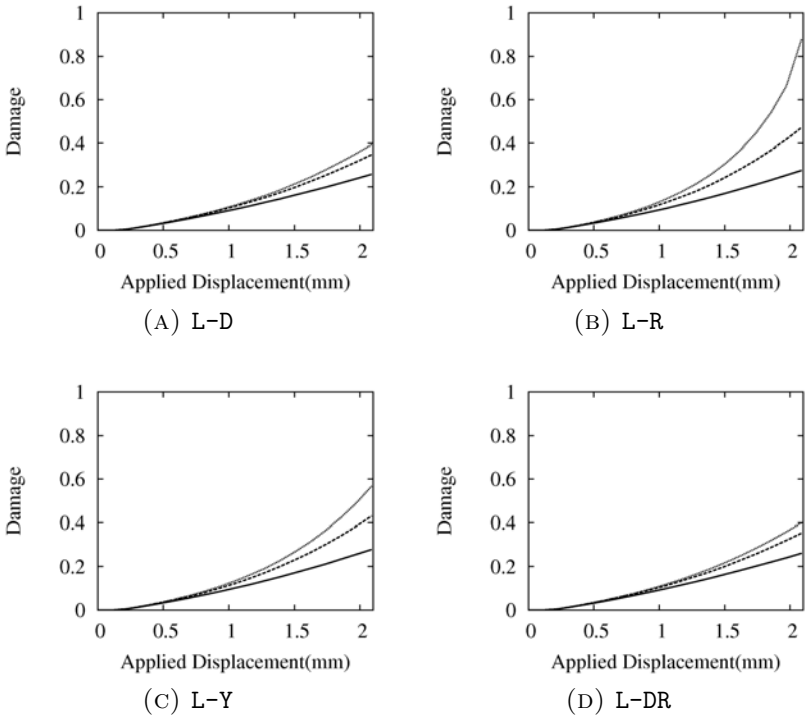

(A) L-D (B) L-R

(C) L-Y (D) L-DR

FIGURE 6.27: Damage evolution for the Lemaitre-based non-local models.

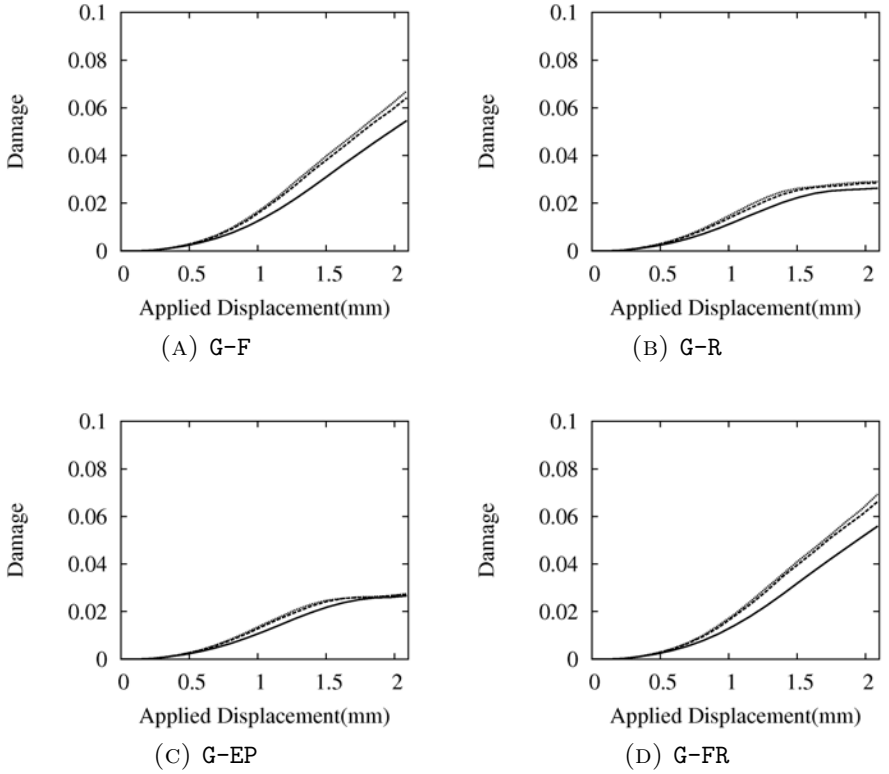

(A) G-F (B) G-R

(C) G-EP (D) G-FR

FIGURE 6.28: Damage evolution for the Lemaitre-based non-local models.

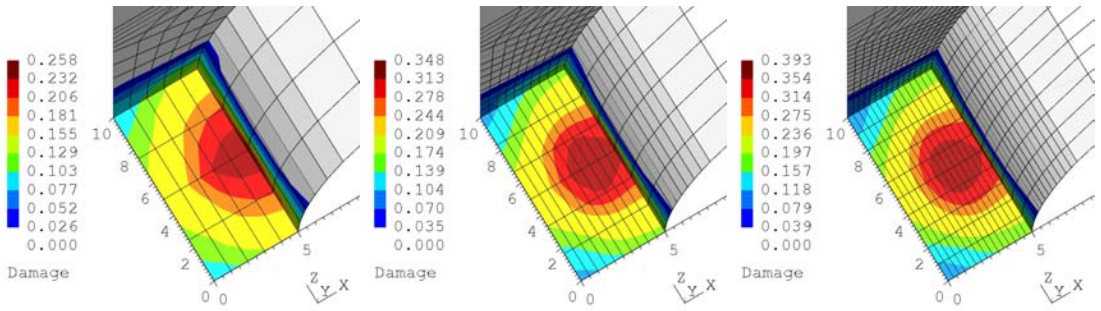

(A) (B) (C)

FIGURE 6.29: Damage contours for the non-local case at the critical region: Lemaitre-based model (`L-D`).

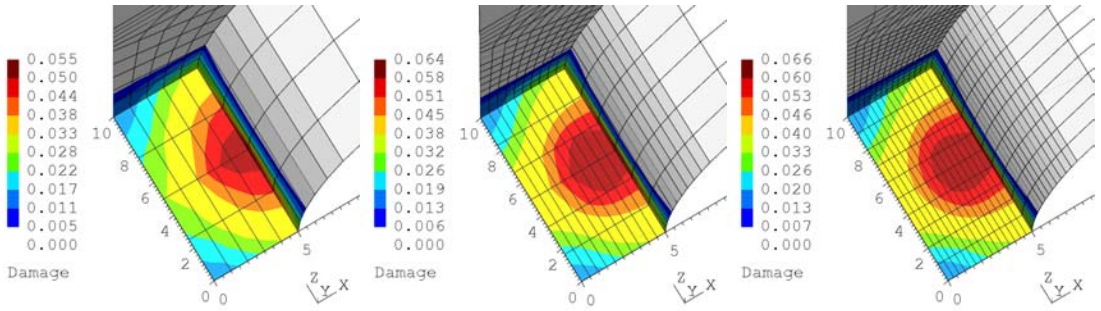

(A) (B) (C)

FIGURE 6.30: Damage contours for the non-local case at the critical region: Gurson-based model (`G-F`).

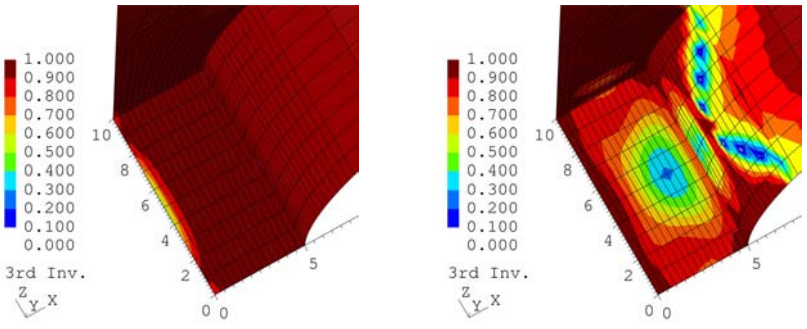

(A) Initial (B) Final

FIGURE 6.31: Contours of the norm of the third invariant of the deviatoric stress tensor, $\|\xi\|$, for the Lemaitre-based non-local model (`L-D`).

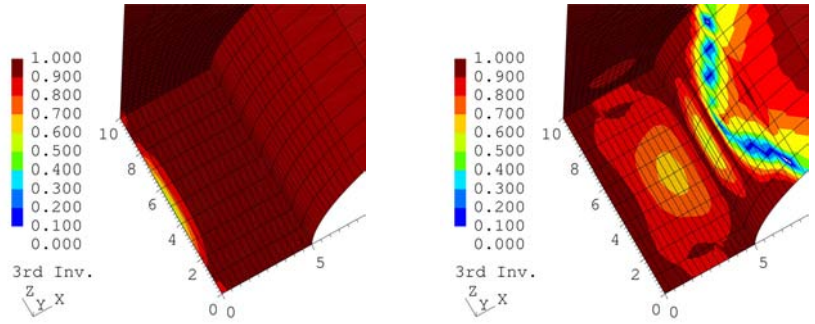

(A) Initial (B) Final

FIGURE 6.32: Contours of the norm of the third invariant of the deviatoric stress tensor, $\|\xi\|$, for the Gurson-based non-local model (`G-F`).

6.4.3 Analysis at low stress triaxiality ($0 < \eta < 1/3$)

Finally, we assess the non-local models listed in Tables 6.1 and 6.2 when subject to low stress triaxiality. In the present study, we shall limit ourselves to observe the behaviour of these models under pure shear stress states (i.e., $\eta = 0$) and no analysis under compressive loadings will be carried out. The shear specimen used by Brünig et al. [23] will be adopted for the present assessment where the geometry of the specimen is depicted in Figure 6.33. Like in the previous sections, three different mesh refinements have been considered in the analysis (see Figure 6.34). In the present case, 20-noded quadratic hexahedra have been used in the spatial discretisation of the specimen where reduced integration has been adopted.

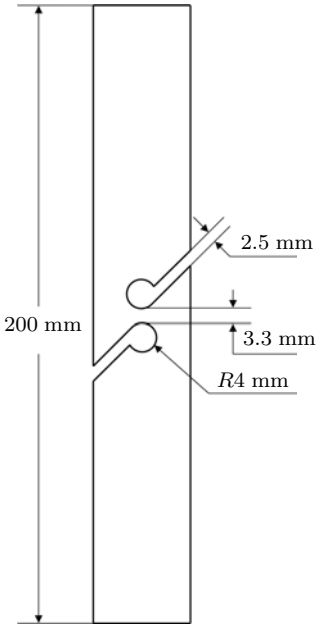

FIGURE 6.33: Geometry of the shear specimen.

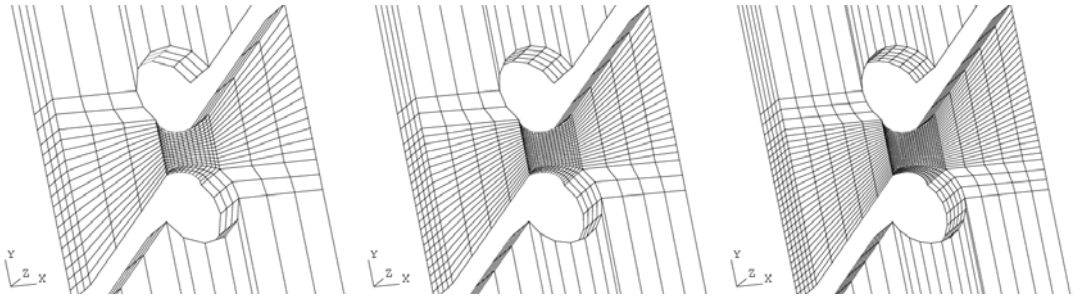

FIGURE 6.34: Shear specimen: different mesh refinements at the critical region.

We start our assessment by looking at the reaction diagrams for both models (Lemaitre- and Gurson-based) when the local case is considered (see Figure 6.35). At a first glance, it seems that the Lemaitre-based model presents a moderate spurious mesh dependency meanwhile the Gurson-based model shows no mesh dependency at all. In Figure 6.36, the evolution of damage in the local case is given. A close observation of these plots reveals a more pronounced mesh dependency with the Lemaitre-based model than with the Gurson-based one. This statement is supported when we look at the damage contours for both cases in Figures 6.37 and 6.38. In particular, mesh dependent solutions are not so evident in the Gurson case, although some sensitivity to spatial discretisation is noticeable, specially because damage tends to concentrate in a single element upon mesh refinement. We recall that such behaviour has been noticed in Chapter 4, where in the analysis of the same shear specimen little mesh dependency was observable. Again, as discussed in that chapter, it seems that this less pronounced mesh sensitivity is associated with the added shear mechanism into the constitutive equations, which allows for a more realistic modelling of the material behaviour when under shear stress states. In turn, experiments tend to show that, under pure shear, localisation is not as evident as in tension, corroborating the idea that mesh dependency should be less present when subjected to shear stress states. Notice that, contrary to the present Gurson-based model, Lemaitre's model has not been established focusing on capturing the effects of material behaviour in shear.

Figure 6.39 shows the reactions for the Lemaitre-based non-local models. As expected, the `L-R` solution is very mesh dependent, just like in all other cases analysed in this chapter. The solutions with `L-D` and `L-DR` have, on the other hand, been able to effectively eliminate the pathological mesh sensitivity, meanwhile `L-Y` has presented an enhanced solution (if compared to the local case) but not completely free of spurious dependency on the spatial discretisation. These conclusions are greatly corroborated when we observe the evolution of damage for all cases in Figure 6.40. Similar to the cases in Sections 6.4.1 and 6.4.2, `L-Y` can progressively improve the solution when the non-local intrinsic length is increased.

In the case of Gurson-based non-local solutions, the reaction diagrams have remained exactly like the one of Figure 6.35. Therefore, we shall omit these plots for the sake of readability. However, if one carefully observes the evolution of damage in Figure 6.41, it becomes quite clear that only `G-F` and `G-FR` could achieve mesh-insensitive solutions upon mesh refinement.

The contours of damage are given for the Lemaitre- (`L-D`) and Gurson-based(`G-F`) non-local models in Figures 6.42 and 6.43, respectively. Clearly, the effects of pathological mesh dependency have been consistently eliminated since the damage contours practically remain constant and distributed over a finite area as the mesh is refined. Again, this undoubtedly demonstrates the effectiveness of these two non-local models (`L-D` and `G-F`) where it is worth mentioning that they have been able to tackle the issues of spurious mesh sensitivity in all cases analysed in this chapter, regardless of the stress state.

Finally, the contours of the normalised third invariant are plotted in Figures 6.44 and 6.45. Clearly, it remains zero for the Lemaitre-based model and around $\xi = 0.1$ for the Gurson case. Comparing these values with those obtained in Sections 6.4.1 and 6.4.2, it is possible to note a certain tendency in the results. For instance, in the case of `PLANE` (where $\xi = 0.0$), `L-D` resulted in mesh independent results meanwhile `L-DR` has lead to satisfactory results. Such conclusions are in agreement with the shear case of the present section, whose associated value for the normalised third invariant is also around zero. The same idea seems to apply for the Gurson-based non-local models, whose results under pure shear stress states agree, to a larger extent, with the results observed in the `PLANE` case. In other words, the results of the present assessment demonstrate a certain tendency that the third invariant may have more influence in the issues of pathological mesh dependency than the triaxiality.

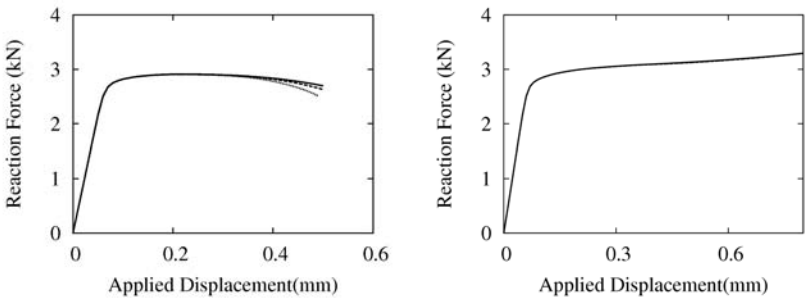

(A) (B)

FIGURE 6.35: Reactions in the local case. Results for the Lemaitre- (A) and Gurson- (B) based models.

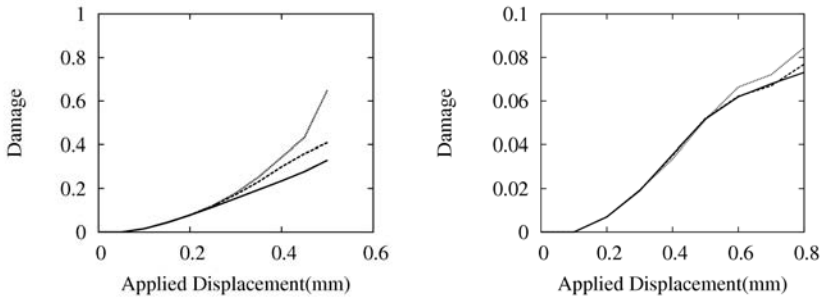

(A) (B)

FIGURE 6.36: Damage evolution in the local case. Results for the Lemaitre- (A) and Gurson- (B) based models.

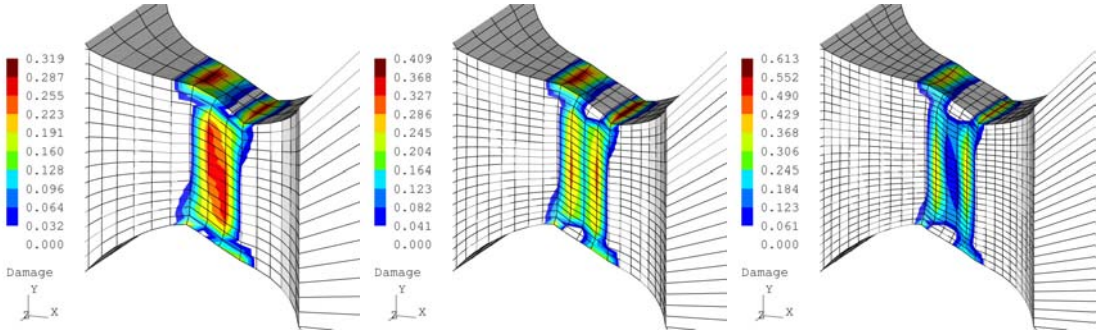

(A) (B) (C)

FIGURE 6.37: Damage contours for the local case at the critical region: Lemaitre-based model.

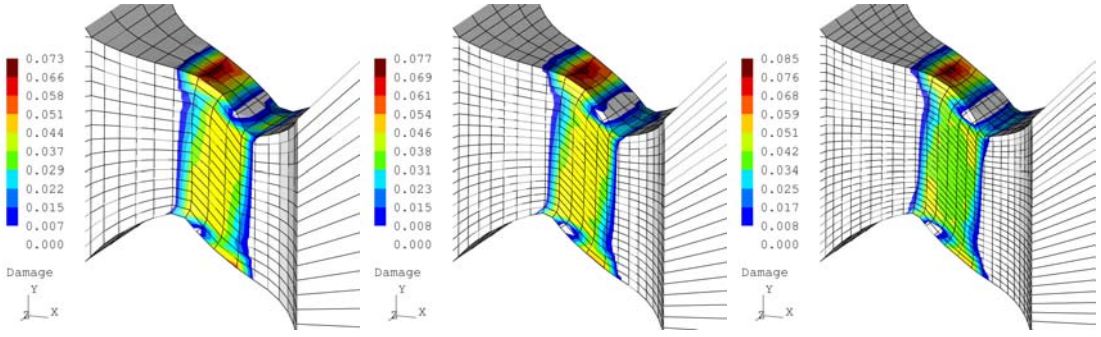

(A) (B) (C)

FIGURE 6.38: Damage contours for the local case at the critical region: Gurson-based model.

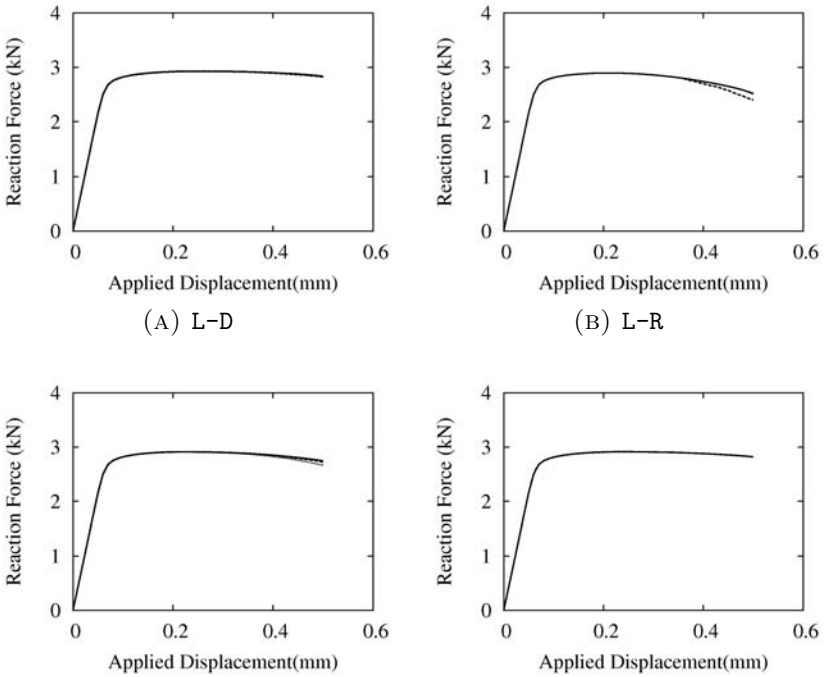

(A) `L-D` (B) `L-R`

(C) `L-Y` (D) `L-DR`

FIGURE 6.39: Reactions for the Lemaitre-based non-local models.

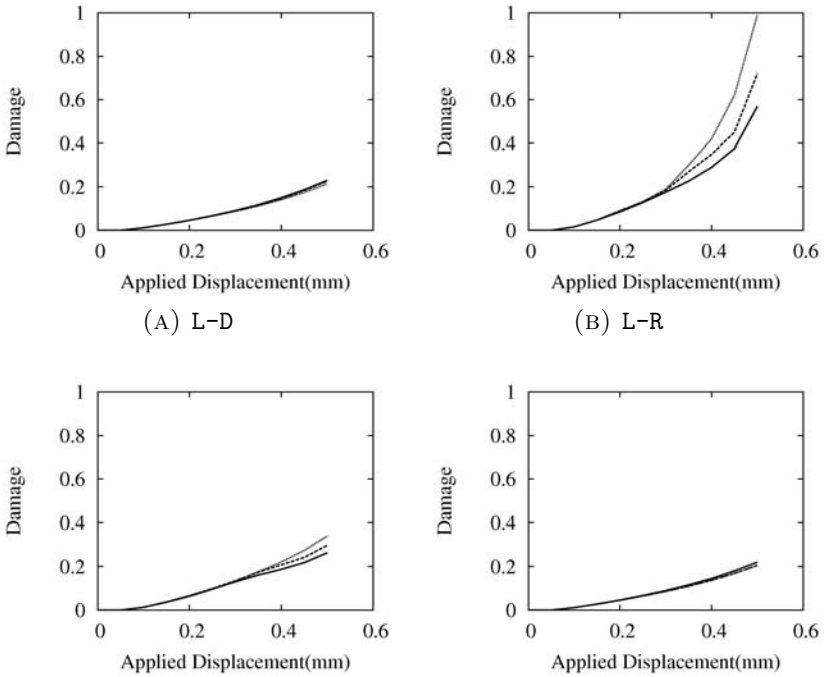

(A) `L-D` (B) `L-R`

(C) `L-Y` (D) `L-DR`

FIGURE 6.40: Damage evolution for the Lemaitre-based non-local models.

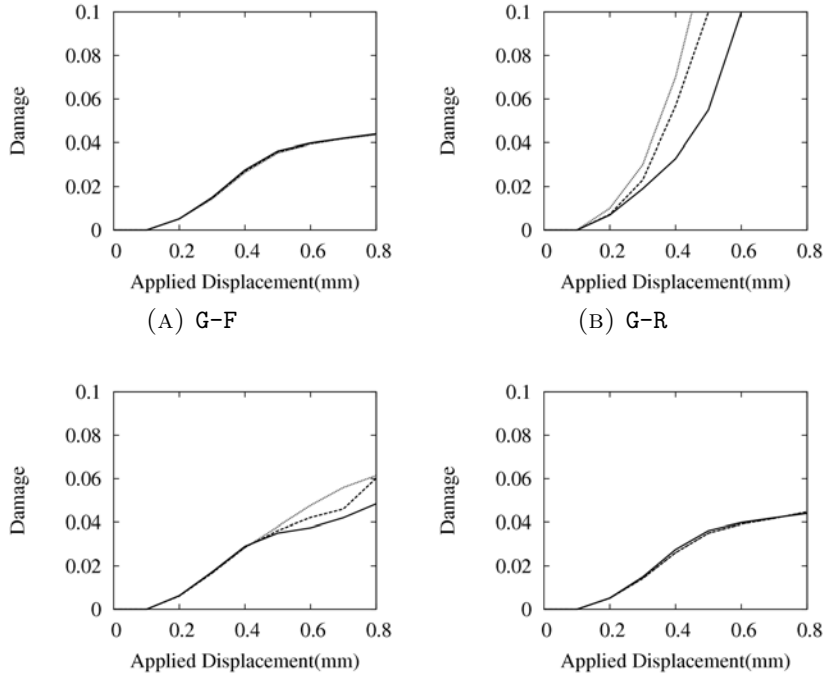

(A) G-F (B) G-R

(C) G-EP (D) G-FR

FIGURE 6.41: Damage evolution for the Gurson-based non-local models.

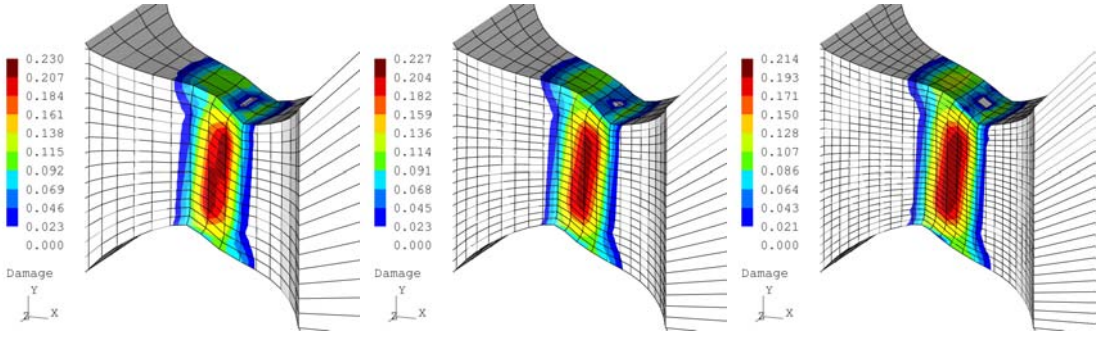

(A) (B) (C)

FIGURE 6.42: Damage contours for the non-local case at the critical region: Lemaitre-based model (L-D).

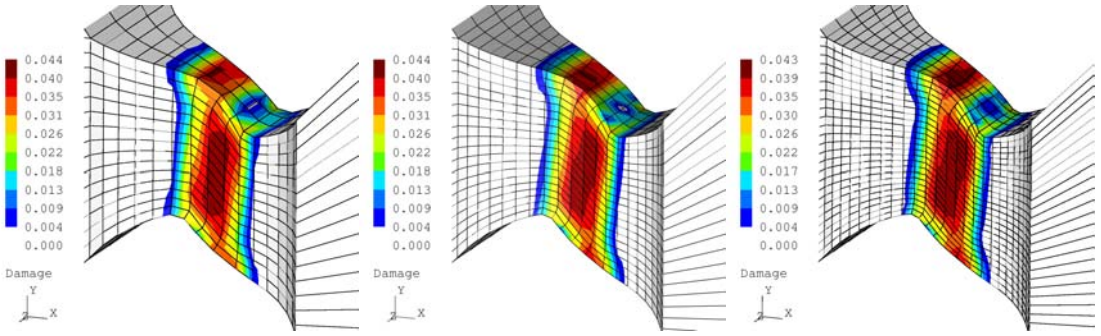

(A) (B) (C)

FIGURE 6.43: Damage contours for the non-local case at the critical region: Gurson-based model (`G-F`).

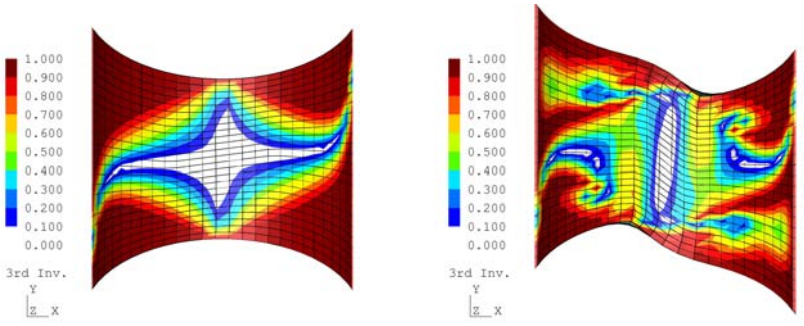

(A) Initial (B) Final

FIGURE 6.44: Contours of the norm of the third invariant of the deviatoric stress tensor, $\|\xi\|$, for the Lemaitre-based non-local model (`L-D`).

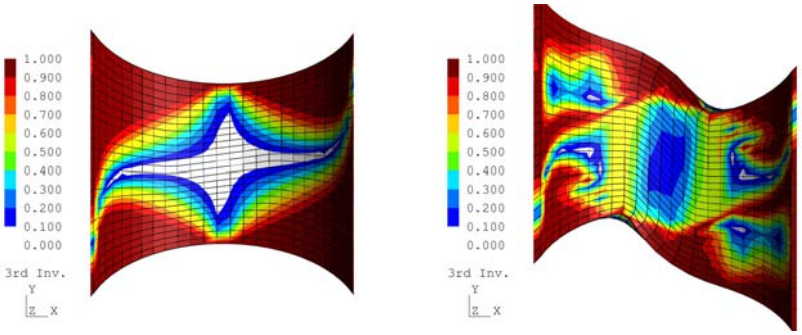

(A) Initial (B) Final

FIGURE 6.45: Contours of the norm of the third invariant of the deviatoric stress tensor, $\|\xi\|$, for the Gurson-based non-local model (`G-F`).

6.4.4 Summary of results

The large number of analysis that the present assessment has required makes the scrutiny of the results difficult if one aims to have a general overview. Thus, in order to facilitate comprehension, we have schematically summarised all the results obtained in this chapter in Table 6.6. Reference values for the initial triaxiality and the average normalised third invariant have been given for convenience. The results suggest, to some extent, that the third invariant may have more influence in the issue of pathological mesh dependency than the triaxiality.

Furthermore, the solutions in which damage has been regularised have been effective in all cases. Although `L-D`, `L-DR`, `G-F` and `G-FR` have in most cases resulted, from a numerical point of view, it seems more advantageous the regularisation of damage only than regularising both damage and the isotropic hardening variable simultaneously. In the latter case, a dual integral averaging has to be carried out, being more computationally costly.

We remark again that the conclusion that damage is the preferred variable to be regularised in the case of Lemaitre- and Gurson-based models is significantly important. It seems that this is an inherent characteristic of implicit damage models. In the case of explicit damage models, often used to model quasi-brittle materials, the conclusion is completely different. As reported by Jirásek and Rolshoven [70], the damage variable is a bad candidate for non-local variable for such explicit damage models and should be avoided. Again, this utterly implies that one has to be very careful when choosing the non-local variable for a given constitutive model; in particular, it should analysed if the damage formulation of such material model is done in an implicit or explicit fashion.

TABLE 6.6: Summary of results.

Analysis	η_0	ξ_{avg}	L-D	L-R	L-Y	L-DR	G-F	G-R	G-EP	G-FR
NOTCHED	0.8	1.0	++	−−	++	++	++	++	++	++
PLANE	0.7	0.0	++	−−	−	+	++	−−	+	++
PLATE	1/3		++	−−	−	++	++	++	++	++
SHEAR	0.0	0.0	++	−−	+	++	++	−−	+	++

++ full regularisation
\+ partial but acceptable regularisation
− poor/little regularisation
−− no regularisation

6.5 Conclusions

The main goal of this chapter was to unfold the question of which variable should be regularised in order to obtain mesh-insensitive results under strain-softening regimes. Therefore, several non-local models based on the constitutive theories of Lemaitre and Gurson have been established. A brief overview on the aspects of ductile behaviour and failure has been done where it has been emphasized the importance of the stress state in the description of ductile materials. Since the stress state plays a major role in material behaviour, several specimens, which yield on different values of triaxiality and third invariant, have been considered for the assessment of the distinct non-local models.

The results of the present assessment suggest that the third invariant of the deviatoric stress, rather than the triaxiality, may play a more important role in the issue of pathological mesh dependency. Scrutiny of the results have revealed that in both cases (Lemaitre- and Gurson-based models) the damage variable seems to be the optimal candidate for non-local variable.

Chapter 7

An Explicit Finite Element Formulation of Non-local Models

As thoroughly discussed and demonstrated throughout this thesis, the issue of pathological mesh dependency can be conveniently overcome by the introduction of a non-local enhancement, for which efficient algorithms for the numerical implementation of the non-local formulation have been presented in detail in Chapters 3 and 4. These algorithms integrate the constitutive equations in a global fashion, requiring access to all integration points of the mesh. Unfortunately, this requirement is often not met in most commercial FE-packages used by the industry, which brings some difficulties when implementing the non-local enhancement in such codes.

In the present chapter, we overcome this adversity by adopting an approximation of the non-local theory that is suitable to be used with existing local models, requiring only little modification. The technique is restricted to explicit finite element implementations and it is designed to be easily incorporated as a general user-defined feature in LS-DYNA. The shortcoming of accessing the neighbour integration points at once is overcome by adopting an implementation strategy that saves and uses information of the previous time step. In a general sense, the disadvantage of such approximated non-local formulation is the requirement of small time steps for enough accuracy. However, this does not represents a problem in the present case since the explicit integration scheme of LS-DYNA naturally demands very small time steps in order to guarantee stable solutions. As a consequence, the results obtained with the present technique are sufficiently accurate to attenuate the mesh dependency issue.

In order to assess its validity, the proposed non-local technique is used with three different material models. The first one is based on Lemaitre's material model, similar to the one proposed in Chapter 3. The second constitutive theory is the J_2 based elasto-plastic damage model of Engelen et al. [47] intended for the simulation of ductile materials. The third one is a recently proposed transversely-isotropic constitutive model suitable for the description of fibre-reinforced materials presetend by Vogler et al. [116]. Numerical simulation shows that the non-local technique is also able to avoid the spurious mesh dependency for these two different material models, proving that the proposed strategy is suitable for a wider spectrum of applications.

This chapter is organised in the following fashion. Section 7.1 reviews very briefly some aspects concerning explicit finite element frameworks. In particular, the assumptions and conventions taken in the commercial software LS-DYNA are addressed, since the non-local enhancement of this chapter has been implemented in that software. In Section 7.2, we review the three local models that will be enhanced with the present non-local strategy. The non-local technique suitable for the explicit integration scheme is presented in Section 7.3, where the necessary modifications in the local models are demonstrated. Section 7.4 addresses the numerical implementation in LS-DYNA, where the main necessary steps are described in detail. Finally, selected numerical examples demonstrate the effectiveness of the proposed non-local strategy, followed by some concluding final remarks.

7.1 General aspects of the explicit finite element framework

In this section, we briefly review some important aspects commonly associated with explicit finite element formulations, in particular those adopted in the present chapter. The present review has not the intention to be exhaustive since the main objective of this chapter is to demonstrate how the non-local formulation can be simplified to be very easily incorporated in explicit FE codes and therefore motivating its direct use in industrial applications. We remark that comprehensive accounts about the general aspects addressed here can be found elsewhere (e.g. [17]). Moreover, since the non-local strategy, yet to be presented in this chapter, has been implemented in LS-DYNA, we shall restrict ourselves to the concepts that have been considered in this particular FE code.

7.1.1 Objective stress rates

In the preceding chapters, hyperelastic-based plasticity models have been exclusively considered.

The need for objective stress rates can be easily understood as follows. To start with, let us superimpose a rigid body motion, denoted by $\boldsymbol{Q}$, over the Cauchy stress tensor:

$$\boldsymbol{\sigma} = \boldsymbol{Q}\boldsymbol{\sigma}\boldsymbol{Q}^T. \tag{7.1}$$

Clearly, the true stress tensor, $\boldsymbol{\sigma}$, remains unaltered after the rigid body motion and therefore we can conclude that $\boldsymbol{\sigma}$ remains the same regardless the observer. Such property is called as *objectivity* and is necessary for a concise, physically sound constitutive theory.

Differentiating Equation (7.1) in respect to time, we get

$$\dot{\boldsymbol{\sigma}} = \boldsymbol{Q}\dot{\boldsymbol{\sigma}}\boldsymbol{Q}^T + \dot{\boldsymbol{Q}}\boldsymbol{\sigma}\boldsymbol{Q}^T + \boldsymbol{Q}\boldsymbol{\sigma}\dot{\boldsymbol{Q}}^T. \tag{7.2}$$

Note that, since $\dot{\boldsymbol{\sigma}} \neq \boldsymbol{Q}\dot{\boldsymbol{\sigma}}\boldsymbol{Q}^T$, the rate of the Cauchy stress tensor is *not* objective. In order to keep objectivity, many different expressions for the stress rate have been proposed in the literature. In following, we review the three most usually adopted.

The Jaumann stress rate

The *Jaumann* stress rate, $\boldsymbol{\sigma}^{\triangledown}$, is defined as

$$\boldsymbol{\sigma}^{\triangledown} \equiv \dot{\boldsymbol{\sigma}} + \boldsymbol{\sigma}\boldsymbol{W} - \boldsymbol{W}\boldsymbol{\sigma}, \tag{7.3}$$

where $\boldsymbol{W}$ is the spin tensor, given by

$$\boldsymbol{W} = \text{skew}[\boldsymbol{L}], \tag{7.4}$$

where $\boldsymbol{L}$ is the velocity gradient, defined as

$$\boldsymbol{L} \equiv \dot{\boldsymbol{F}}\boldsymbol{F}^{-1}.$$

In LS-DYNA, the Jaumann stress rate is the default option and it will be used in all the developments of this chapter.

The Green-Naghdi stress rate

Another commonly used stress rate is the *Green-Naghdi* rate of the Cauchy stress tensor. It is defined as:

$$\boldsymbol{\sigma}^{\diamondsuit} \equiv \dot{\boldsymbol{\sigma}} + \boldsymbol{\sigma}\boldsymbol{\Omega} - \boldsymbol{\Omega}\boldsymbol{\sigma}, \tag{7.6}$$

where

$$\boldsymbol{\Omega} \equiv \dot{\boldsymbol{R}}\boldsymbol{R}^T. \tag{7.7}$$

The Truesdell stress rate

The *Truesdell* stress rate is defined as

$$\boldsymbol{\sigma}^{\circ} \equiv \dot{\boldsymbol{\sigma}} - \boldsymbol{L}\boldsymbol{\sigma} - \boldsymbol{\sigma}\boldsymbol{L}^T + (\mathrm{tr}[\boldsymbol{L}])\boldsymbol{\sigma}. \tag{7.8}$$

7.1.2 Hypoelastic-based elastoplastic model

In LS-DYNA, hypoelastic-based plasticity is the formulation considered for most material models. Note that up to this point in this thesis only hyperelastic-based plasticity has been considered. One of the main advantages of hyperelastic models is that, in sharp contrast to hypoelastic models, they are more physically consistent since they do not generate dissipation in the elastic range. This can be crucial in a large number of applications and therefore it is preferred than hypoelastic-based formulations. However, hypoelastic frameworks are still dominant among FE commercial codes, which are in turn extensively used by the industry. Therefore, if one aims to apply a certain modelling strategy on industrial problems, it turns out to be quite difficult to avoid using hypoelasticity.

Considering a general hypoelastic-plastic model, an additive decomposition of the rate of deformation, $\boldsymbol{D}$, into an elastic and a plastic part is usually assumed, that is:

$$\boldsymbol{D} = \boldsymbol{D}^e + \boldsymbol{D}^p. \tag{7.9}$$

The elastic response is established by considering the following hypoelastic law:

$$\boldsymbol{\sigma}^{\triangledown} = \mathbf{D}^e : \boldsymbol{D}^e = \mathbf{D}^e : (\boldsymbol{D} - \boldsymbol{D}^p), \tag{7.10}$$

where $\mathbf{D}^e$ is the elasticity tensor, here considered to be constant and isotropic.

The yield function is defined in similar manner to hyperelastic-based plastic models, that is, a certain function of the form

$$F_p = F_p(\boldsymbol{\sigma}, \boldsymbol{\alpha}), \tag{7.11}$$

is assumed to exist where $\boldsymbol{\alpha}$ is the set of internal variables. Finally, we define the plastic flow:

$$\boldsymbol{D}^p = \dot{\gamma} \frac{\partial G_p(\boldsymbol{\sigma}, \boldsymbol{\alpha})}{\partial \boldsymbol{\sigma}}, \tag{7.12}$$

where G_p is the plastic potential.

In LS-DYNA, the rate of deformation is used as the strain rate measure, i.e.,

$$\dot{\varepsilon}^{ij} = \frac{1}{2}\left(\frac{\partial v^i}{\partial x^j} + \frac{\partial v^j}{\partial x^i}\right). \tag{7.13}$$

where $\boldsymbol{v}$ and $\boldsymbol{x}$ are, respectively, the current velocity and position vectors of a given point. The aforementioned assumption considerably facilitates the establishment of the material integration algorithm since small strains can be directly considered within an incremental framework.

7.1.3 Integration of the constitutive law

Within an infinitesimal time interval, the stress tensor is given by

$$\sigma^{ij}(t + dt) = \sigma^{ij}(t) + \dot{\sigma}^{ij} dt. \tag{7.14}$$

As pointed out before, the Jaumann rate is the stress rate considered in the present case. Within the incremental framework, we have

$$\dot{\sigma}^{ij} = \sigma^{\nabla\, ij} + \sigma^{ik} W^{kj} + \sigma^{jk} W^{ki}, \tag{7.15}$$

where the spin tensor is given, in index notation, by

$$W^{ij} = \text{skew}\,(\boldsymbol{L})^{ij} = \frac{1}{2}\left(\frac{\partial v^i}{\partial x^j} - \frac{\partial v^j}{\partial x^i},\right), \tag{7.16}$$

and $\boldsymbol{\sigma}^{\nabla} = \boldsymbol{\sigma}^{\nabla}(\dot{\boldsymbol{\varepsilon}}, \boldsymbol{\alpha})$ is the increment of the stress tensor, computed in the small strain constitutive integration algorithm.

The stress update procedure in LS-DYNA follows an incremental strategy, that is, the stresses are updated from instant t_n to t_{n+1} in the following fashion:

$$\sigma^{ij}_{n+1} = \sigma^{ij}_n + r^{ij}_n + \sigma^{\nabla\, ij}_{n+\frac{1}{2}} \Delta t_{n+\frac{1}{2}}, \tag{7.17}$$

where the expression $\sigma^{\nabla\, ij}_{n+\frac{1}{2}} \Delta t_{n+\frac{1}{2}}$ is the time discretised version of $\boldsymbol{\sigma}^{\nabla}$ and is retrieved in the small strain material integration routine. The term r^{ij}_n gives the rotation of the stress from t_n to t_{n+1} through

$$r^{ij}_n = \left(\sigma^{ip}_n W^{pj}_{n+\frac{1}{2}} + \sigma^{jp}_n W^{pi}_{n+\frac{1}{2}} \right) \Delta t_{n+\frac{1}{2}}. \tag{7.18}$$

7.1.4 Discretised explicit finite element framework

In Chapter 2, the theory for the description of continua under motion has been restricted for the quasi-static case. In that case, the components associated with accelerations can be disregarded, since inertial forces are negligible. However, in the explicit case, the consistent consideration of these forces is fundamental. Therefore, we firstly recall the equilibrium equation in its strong form:

$$\mathrm{div}_x \boldsymbol{\sigma} + \boldsymbol{b} = \rho \ddot{\boldsymbol{u}}. \tag{7.19}$$

Adopting the same procedures as in Chapter 2, Section 2.3, Equation 7.19 can be rewritten, in its weak form, as

$$\int_{\varphi(\Omega)} \left[\boldsymbol{\sigma} : \nabla_x \boldsymbol{\eta} - \boldsymbol{b} - \rho \ddot{\boldsymbol{u}} \right] \, dV - \int_{\varphi(\partial\Omega)} \boldsymbol{t} \cdot \boldsymbol{\eta} \, dA = 0. \tag{7.20}$$

Similar to the framework provided in Chapter 2, the above equation has analytical solutions only for a limited number of special cases and practical engineering applications require solutions using some sort of numerical strategy. As alluded in Chapter 2, the numerical method chosen in this thesis is the Finite Element Method, which requires Equation (7.20) to be discretised in space. A suitable time discretisation of the Equation (7.20) is also generally required for which the Finite Difference Method is herein adopted.

Discretisation in space

In the present case, the space discretisation follows exactly the same steps as in Chapter 2, where geometry and displacements have been interpolated through

shape functions. The use of these shape functions eventually leads to a set of semi-discrete equilibrium equations:

$$\mathbf{Ma} + \mathbf{Cv} + \mathbf{f}^{int}(\mathbf{u}) = \mathbf{f}^{ext}, \tag{7.21}$$

where $\mathbf{M}$ and $\mathbf{C}$ are the mass and damping matrices, $\mathbf{a} = \ddot{\mathbf{u}}$ and $\mathbf{v} = \dot{\mathbf{u}}$ are the acceleration and velocity vectors and $\mathbf{u}$ is the displacement vector

Remark 7.1. *For efficient numerical implementations, it is highly desirable that the mass and damping matrices,* $\mathbf{M}$ *and* $\mathbf{C}$*, be diagonal lumped. In this case, the system of equations, defined in Equation (7.21), becomes uncoupled and each equation can be solved separately, yielding on computationally efficient finite element programs. Diagonal mass and damping matrices are the standard option in LS-DYNA.*

Discretisation in time

In order to set up an incremental finite element framework, where at every incremental step we advance in time from t_n to t_{n+1}, the set of equations (7.21) needs to be integrated over time. In LS-DYNA, the central difference scheme is adopted for the time integration of the equilibrium equation. After some straightforward manipulations, one gets

$$\mathbf{v}_{n+\frac{1}{2}} = \mathbf{v}_{n-\frac{1}{2}} + \Delta t_n \mathbf{a}_n, \tag{7.22}$$

$$\mathbf{u}_{n+1} = \mathbf{u}_n + \mathbf{v}_{n+\frac{1}{2}} \Delta t_{n+\frac{1}{2}}, \tag{7.23}$$

where

$$\mathbf{a}_n = \mathbf{M}^{-1} \left(\mathbf{f}_n^{ext} - \mathbf{f}_n^{int} - \mathbf{C}\mathbf{v}_n \right), \tag{7.24}$$

and

$$\Delta t_{n+\frac{1}{2}} = \frac{\Delta t_{n+1} + \Delta t_n}{2}. \tag{7.25}$$

For convenience, the general algorithm for the explicit time integration is given in Box 5 where the main steps are schematically depicted.

Critical time step

Unlike implicit integration schemes, explicit finite element frameworks are *conditionally stable*, i.e., they require suitable time steps in order to keep overall stability. In the one-dimensional case, the critical time step is given through a

Box 5: General algorithm for the explicit time integration.

(i) Initialise stresses, displacements, velocities and accelerations for $t = t_0$

(ii) Update global velocity and displacement vectors

$$\begin{aligned} \mathbf{v}_{n+\frac{1}{2}} &= \mathbf{v}_{n-\frac{1}{2}} + \Delta t_n \mathbf{a}_n \\ \mathbf{u}_{n+1} &= \mathbf{u}_n + \mathbf{v}_{n+\frac{1}{2}} \Delta t_{n+\frac{1}{2}} \end{aligned}$$

(iii) Update stress state, $\boldsymbol{\sigma}_{n+1}$

(iv) Calculate the element internal force vector and assemble its contribution to the global vector

$$\mathbf{f}_{(e)}^{int} = \int_V \mathbf{B}^T \boldsymbol{\sigma}_{n+1} \, dV,$$

$$\mathbf{f}_{n+1}^{int} = \text{ASSEMBLE}_{e=1}^{nelem} \left[\mathbf{f}_{(e)}^{int} \right]$$

(v) Compute the global external force vector, $\mathbf{f}^{ext_{n+1}}$

(vi) Calculate the associated accelerations

$$\mathbf{a}_{n+1} = \mathbf{M}^{-1} \left(\mathbf{f}_{n+1}^{ext} - \mathbf{f}_{n+1}^{int} - \mathbf{C}\mathbf{v}_{n+\frac{1}{2}} \right)$$

(vii) If final time has not been reached, GOTO (ii).

relation of the following type:

$$\Delta t_{crit} = \frac{L_e}{c}, \tag{7.26}$$

where L_e is the characteristic element length and c is the *wave speed*, which reads, in the general case,

$$c = \sqrt{\frac{E}{\rho}}, \tag{7.27}$$

where E is the Young's modulus and ρ is the density. If $\Delta t > \Delta t_{crit}$, numerical oscillations may arise, dramatically reducing the quality of the solution. In LS-DYNA, a standard time step of the form $\Delta t < 0.9 \Delta t_{crit}$ is adopted in order to prevent any numerical instability to take place.

Within the scope of this chapter, two- and three-dimensional elements have been considered in the numerical analysis. In the case of two-dimensional elements, the quantities L_e and c read

$$L_e^{2D} = \frac{A_e}{\max(L_1, L_2, L_3, L_4)}, \tag{7.28}$$

$$c^{2D} = \sqrt{\frac{E}{\rho\,(1-\nu^2)}}, \tag{7.29}$$

where A_e is the area of the element and L_1, L_2, L_3 and L_4 are the lengths of the four sides of the elements.

Finally, in the three-dimensional case, we have

$$L_e^{3D} = \frac{V_e}{A_e^{max}}, \tag{7.30}$$

$$c^{3D} = \sqrt{\frac{E(1-\nu)}{(1+\nu)(1-2\nu)\rho}}, \tag{7.31}$$

where V_e is the element volume and A_e^{max} is the area of the largest size.

7.2 Local modelling of damage

In this section, we define the constitutive equations of three material models in the local case. These models will serve as examples for application of the non-local scheme yet to be presented in this chapter. For the sake of completeness, we also provide the equations for the numerical implementation of these models but only in a brief manner. Since local implementations of these models are already well described elsewhere, we shall make reference to those contributions.

It is important to recall that the present hypoelastic-based plasticity formulation allows the definition of the material integration algorithm under the hypothesis of small strains where all the necessary kinematic operations are performed outside of the material routine. Therefore, we shall restrict ourselves henceforth to present the constitutive equations considering small strains.

7.2.1 Lemaitre's ductile damage model

The constitutive model proposed by Lemaitre [see 74, 75, 76] was based on a thermodynamic framework with internal variables. Recalling the first principle of thermodynamics, Lemaitre stated that for isothermal processes there exists a Helmholtz free energy potential such that

$$\psi = \psi\left(\boldsymbol{\varepsilon}, \boldsymbol{\varepsilon}^e, \boldsymbol{\varepsilon}^p, R, D\right), \tag{7.32}$$

where $\boldsymbol{\varepsilon}$ is the total strain tensor, $\boldsymbol{\varepsilon}^e$ is the elastic strain tensor, ε^p is the plastic strain tensor, R is the isotropic hardening variable and D is the isotropic damage variable. For the sake of simplicity, the effects of kinematic hardening have been neglected here, differently of Lemaitre's original formulation. Within the assumption of small strains, the additive split of the strain tensor is valid, i.e.,

$$\boldsymbol{\varepsilon} = \boldsymbol{\varepsilon}^e + \boldsymbol{\varepsilon}^p. \tag{7.33}$$

The free energy function is re-phrased as being composed by the sum of two distinct parts, i.e.,

$$\psi = \psi^e\left(\boldsymbol{\varepsilon}^e, D\right) + \psi^p\left(R\right), \tag{7.34}$$

where $\psi^e\left(\boldsymbol{\varepsilon}^e, D\right)$ and $\psi^p\left(R\right)$ are the amount of free energy due to elastic-damage and due to plasticity, respectively.

The second principle of the thermodynamics of irreversible processes states that the dissipated energy must be equal or greater than zero. Making use of the Clausis-Duhem inequality, we write the dissipation φ as

$$\varphi = \sigma : \dot{\boldsymbol{\varepsilon}} - \rho\dot{\psi} \geq 0, \tag{7.35}$$

where ρ is the density of the material. The rate of the free energy function, $\dot{\psi}$, is given by

$$\dot{\psi} = \frac{\partial \psi}{\partial \boldsymbol{\varepsilon}^e} : \dot{\boldsymbol{\varepsilon}}^e + \frac{\partial \psi}{\partial R}\dot{R} + \frac{\partial \psi}{\partial D}\dot{D}. \tag{7.36}$$

The partial derivatives in Equation (7.36) are thermodynamic forces given by

$$\boldsymbol{\sigma} = \rho\frac{\partial \psi}{\partial \boldsymbol{\varepsilon}^e}, \qquad \chi = \rho\frac{\partial \psi}{\partial R}, \qquad Y = \rho\frac{\partial \psi}{\partial D}, \tag{7.37}$$

where $\boldsymbol{\sigma}$ is the Cauchy stress tensor, χ is the thermodynamic force conjugated with the isotropic hardening variable and Y is the damage energy release rate. Substituting these relations in Equation (7.35), yields on

$$\varphi = \boldsymbol{\sigma} : \dot{\boldsymbol{\varepsilon}}^p - \chi\dot{R} - Y\dot{D} \geq 0. \tag{7.38}$$

In order to obtain the evolution of the internal variables ε^p, R and D, a dissipation potential F can be defined as

$$F = F\left(\boldsymbol{\sigma}, \chi, -Y\right) = F_p\left(\boldsymbol{\sigma}, \chi\right) + F_d\left(-Y\right), \tag{7.39}$$

where F_p is the plastic dissipation potential and F_d is the dissipation potential due to damage. Assuming the so-called *normality rule*, the rate equations for the

plastic strain tensor, the isotropic hardening variable and the damage variable are respectively given by

$$\dot{\boldsymbol{\varepsilon}}^p = \dot{\gamma}\frac{\partial F}{\partial \boldsymbol{\sigma}}, \tag{7.40}$$

$$\dot{R} = -\dot{\gamma}\frac{\partial F}{\partial \chi}, \tag{7.41}$$

$$\dot{D} = \dot{\gamma}\frac{\partial F}{\partial\left(-Y\right)}, \tag{7.42}$$

where $\dot{\gamma}$ is the plastic multiplier. In order to obtain the final equations for the constitutive model, expressions for the dissipation potentials F_p and F_d in Equation (7.39) must be defined. For the dissipation potential due to plasticity, the von Mises yield function will be adopted:

$$F_p = \frac{q}{1-D} - \sigma_y\left(\chi(R)\right), \tag{7.43}$$

where q is the von Mises equivalent stress and σ_y is the yield stress. Furthermore, we adopt the damage dissipation potential proposed by Lemaitre [76]:

$$F_d = \frac{r}{(s+1)(1-D)}\left(\frac{-Y}{r}\right)^{s+1}, \tag{7.44}$$

where r and s are material parameters and $-Y$ is the damage energy release rate given by

$$-Y = \frac{q^2}{2E\left(1-D\right)^2}\left[\frac{2}{3}\left(1+\nu\right) + 3\left(1-2\nu\right)\left(\frac{p}{q}\right)^2\right], \tag{7.45}$$

where p is the hydrostatic stress, ν is the Poisson's ratio and E is Young's modulus. Alternatively, it can also be expressed as

$$-Y = \frac{q^2}{6G(1-D)^2} + \frac{p^2}{2K(1-D)^2}, \tag{7.46}$$

where G and K are respectively the shear and the bulk moduli. Considering the above expressions for F_p and F_d in the dissipation potential $F = F_p + F_d$, the evolution of each internal variable is given by

$$\dot{\boldsymbol{\varepsilon}}^p = \frac{3}{2}\frac{\dot{\gamma}}{\left(1-D\right)}\frac{\boldsymbol{s}}{q}, \tag{7.47}$$

$$\dot{R} = \dot{\gamma}, \tag{7.48}$$

$$\dot{D} = \frac{\dot{\gamma}}{\left(1-D\right)}\left(\frac{-Y}{r}\right)^s, \tag{7.49}$$

where $\boldsymbol{s}$ is the deviatoric stress tensor given by

$$\boldsymbol{s} = \boldsymbol{\sigma} - p\boldsymbol{I}, \tag{7.50}$$

where $\boldsymbol{I}$ is the second order identity tensor. Finally, the constitutive model is complete with the loading/unloading conditions,

$$F_p \leq 0, \quad \dot{\gamma} \geq 0, \quad \dot{\gamma} F_p = 0, \tag{7.51}$$

which must hold for any deformation process.

Numerical implementation

A detailed account of the numerical implementation of Lemaitre's ductile damage model without kinematic hardening can be found in [27, 36]. Therefore, we shall only review some of the main steps. The algorithm for the numerical integration of the local constitutive model follows a typical elastic predictor/return-mapping strategy and therefore starts with the definition of the elastic trial state. Notice that the constitutive behaviour is meant to be locally computed at every material point within a generic time interval $[t_n, t_{n+1}]$, where the constitutive variables $\boldsymbol{\varepsilon}^p_n$, $\boldsymbol{\sigma}_n$, R_n and D_n are known 'a priori'. The goal of the algorithm is to find the updated values of $\boldsymbol{\varepsilon}^p_{n+1}$, $\boldsymbol{\sigma}_{n+1}$, R_{n+1} and D_{n+1}. The elastic trial tensor is given by

$$\boldsymbol{\sigma}^{trial}_{n+1} = \boldsymbol{\sigma}_n + (1 - D_n)\, \mathbf{D}^e : \Delta\boldsymbol{\varepsilon} \tag{7.52}$$

where $\Delta\boldsymbol{\varepsilon}$ is the incremental strain tensor. Plastic admissibility is checked using the yield function of Equation (7.43). If it is not satisfied, i.e. $F_p > 0$, the following residual equation is solved:

$$\mathrm{r}(\Delta\gamma) := 3G\Delta\gamma - (1 - D_n)(q^{trial}_{n+1} - \sigma_y(\Delta\gamma)) + \frac{(q^{trial}_{n+1} - \sigma_y)^2}{3G}\left(\frac{-Y(\Delta\gamma)}{r}\right). \tag{7.53}$$

After convergence has been achieved, the stress state is updated as follows:

$$\begin{aligned}
R_{n+1} &= R_n + \Delta\gamma, && (7.54)\\
D_{n+1} &= 1 - \left(\frac{3G\Delta\gamma}{q^{trial}_{n+1} - \sigma_y}\right), && (7.55)\\
\boldsymbol{\varepsilon}^e_{n+1} &= \boldsymbol{\varepsilon}^{e\,trial}_{n+1} - \sqrt{\frac{3}{2}}\frac{\Delta\gamma}{(1 - D_{n+1})}\frac{\mathrm{dev}\left(\boldsymbol{\varepsilon}^{e\,trial}_{n+1}\right)}{\left\|\mathrm{dev}\left(\boldsymbol{\varepsilon}^{e\,trial}_{n+1}\right)\right\|}, && (7.56)\\
\boldsymbol{\sigma}_{n+1} &= (1 - D_{n+1})\mathbf{D}^e : \boldsymbol{\varepsilon}^e_{n+1}. && (7.57)
\end{aligned}$$

7.2.2 Engelen and co-workers' ductile damage model

We will adopt herein a constitutive framework similar to the one proposed by Engelen et al. [47]. The model of Engelen and co-authors was formulated in such manner that non-locality was introduced through an implicit gradient approach. Their results have shown that the gradient methodology is able to successfully eliminate pathological mesh dependency. Our intention by adopting a similar constitutive model is to show that our non-local technique, yet to be presented in this chapter, has the same regularising characteristics of Engelen and co-authors' formulation.

We firstly introduce the constitutive equations using the local theory. The yield function of the present ductile damage model is given by

$$F_p = q - (1 - D(\kappa))\sigma_y(\kappa), \tag{7.58}$$

where $q = \sqrt{J_2(\boldsymbol{s})}$ is the equivalent von Mises stress, $\boldsymbol{s} = \boldsymbol{\sigma} - p\boldsymbol{I}$ is the stress deviator, $\boldsymbol{\sigma}$ is the stress tensor, $p = \frac{1}{3}\text{tr}\boldsymbol{\sigma}$ is the pressure, σ_y is the yield stress and κ is the accumulated plastic strain. The scalar $D(\kappa)$ is the local damage, which here is considered to be

$$D(\kappa) = \frac{\kappa}{\kappa_c}, \tag{7.59}$$

where κ_c is the critical value of accumulated plastic strain at which full material failure occurs.

Associative plasticity is assumed, therefore, plastic flow reads

$$\dot{\boldsymbol{\varepsilon}}^p = \dot{\gamma}\frac{\partial F_p}{\partial \boldsymbol{\sigma}} = \dot{\gamma}\sqrt{\frac{3}{2}}\frac{\boldsymbol{s}}{\|\boldsymbol{s}\|}. \tag{7.60}$$

Within the present constitutive framework, plasticity and damage are assumed to take place respecting the loading/unloading conditions:

$$\dot{\gamma} \geq 0; \quad F_p \leq 0; \quad \dot{\gamma}F_p = 0. \tag{7.61}$$

Numerical implementation

The present ductile damage model has been implemented in LS-DYNA via user-defined subroutines (`umat41`) where the classical elastic-predictor/return-mapping scheme has been adopted in the numerical implementation. In the algorithm, the

following trial state

$$\boldsymbol{\sigma}_{n+1}^{trial} = \boldsymbol{\sigma}_n + \mathbf{D}^e : \Delta\boldsymbol{\varepsilon}, \tag{7.62}$$

is initially assumed and plastic admissibility is checked using the yield function in Eq. (7.58). If $F_p > 0$, then the following residual equation is solved for $\Delta\gamma$ through the Newton-Raphson method:

$$\mathrm{r}(\Delta\gamma) := q_{n+1}^{trial} - 3G\Delta\gamma - [1 - D_{n+1}(\kappa_{n+1})]\,\sigma_y(\kappa_{n+1}), \tag{7.63}$$

where $\kappa_{n+1} = \kappa_n + \Delta\gamma$. When a certain prescribed tolerance is reached, the stress tensor is updated as

$$\boldsymbol{\sigma}_{n+1} = \left(1 - \frac{3G\Delta\gamma}{q_{n+1}^{trial}}\right) \boldsymbol{s}_{n+1}^{trial} + p_{n+1}^{trial}\boldsymbol{I}. \tag{7.64}$$

7.2.3 Vogler and co-workers' material model for short fibre-reinforced polymers

The transversely-isotropic constitutive framework proposed by Vogler and co-workers [116, 117] has been conceived to describe the observed material non-linear behaviour of fibre-reinforced materials by means of an elastoplastic law. Unlike conventional anisotropic theories, the present approach relies on the use of structural tensors, so that the constitutive equations are independent of the coordinate system. Thus, the constitutive equations are established in a straightforward manner meanwhile the material parameters can be determined more easily.

In contrast to metals, thermoplastic materials in general exhibit a strong pressure-dependent material behaviour, which results in different yielding in uniaxial tension and compression, under shear and under biaxial loadings. Furthermore, the assumption of volume constancy during plastification does not hold for thermoplastic polymers. Especially in the tensile range (uniaxial and biaxial tensile stress states) this effect cannot be neglected. Due to reorientation of molecule chains and due to fibre reinforcements, most thermoplastics also exhibit anisotropic material behaviour. This direction-dependent behaviour does not only affect the plastic yielding, but also the strain rate sensitivity. A material and failure model, aiming to predict these effects, is therefore summarised in the following. A more detailed description is given in references [116] and [117].

The yield surface, a function of the transversely-isotropic invariants, is formulated as

$$F_p = \alpha_1 I_1 + \alpha_2 I_2 + \alpha_3 I_3 + \alpha_{32} I_3^2 + \alpha_4 I_4 + \alpha_{42} I_4^2 - 1, \tag{7.65}$$

with the yield surface parameters α_1, α_2, α_3, α_{32}, α_4 and α_{42}. The detailed definition of the invariants is given by Vogler et al. [116]. Each of these parameters represents a loading state. The parameter α_1 stands for transverse shear, α_2 for in-plane shear, α_3 and α_{32} represent uniaxial compression and tensile loading transverse to the preferred direction and the parameters α_4 and α_{42} control yielding in fibre direction both in compression and tension. The yield surface parameters are directly related to the current yield stress, given by the respective hardening curve for each stress state. Thus, different yielding and hardening in uniaxial compression and tension transverse to the fibre direction and in fibre direction as well as different yielding under in-plane and transverse shear can be described using the present constitutive theory.

In order to enable a realistic representation of plastic Poisson's coefficients observed in experiments, a non-associated flow rule is adopted. The plastic flow potential, which gives the direction of the projection onto the yield surface, is formulated as

$$G_p = \beta_1 I_1 + \beta_2 I_2 + \beta_3 I_3 + \beta_{32} I_3^2 + \beta_4 I_4^2 - 1. \tag{7.66}$$

The failure surface follows the same equation as the yield surface formulation, see Equation (7.65). Therefore, the experimentally identified ultimate strengths in each loading state are required for calculating the six failure surface parameters in Equation (7.65). In particular, these are the fibre parallel strengths in tension and compression, $R_{\parallel}^t$ and $R_{\parallel}^c$, the uniaxial tensile and compressive strength perpendicular to the fibre direction, $R_{\perp}^t$ and $R_{\perp}^c$, and the material strength of transverse shear $R_{\perp\perp}$ and in-plane shear $R_{\parallel\perp}$. If the failure criterion is active, a degradation of the stresses is performed using a damage approach, where damage is added into the model in an explicit fashion through the linear expression

$$D_{n+1} = \alpha(\varepsilon_{n+1}^p - \varepsilon_{fail}), \tag{7.67}$$

where α is a damage-related parameter and ε_{n+1}^p is the norm of the plastic strain tensor. In the equation above, ε_{fail} denotes a strain value, associated with failure, obtained by applying the failure criterion. The stress tensor is then substituted by

$$\boldsymbol{\sigma}_{n+1}^{dam} = (1 - D_{n+1})\boldsymbol{\sigma}_{n+1}. \tag{7.68}$$

Numerical implementation[1]

The numerical implementation follows a standard elastic-predictor/plastic-corrector scheme assuming an additive decomposition of the strain increment. The stresses at the end of each time step $t = t_{n+1}$ are

$$\boldsymbol{\sigma}_{n+1} = \boldsymbol{\sigma}_{n+1}^{trial} - \Delta\gamma_{n+1}\mathbb{C}^e : \boldsymbol{N}_{n+1}, \tag{7.69}$$

where $\boldsymbol{\sigma}_{n+1}^{trial}$ are the elastic trial stresses, $\mathbb{C}^e$ is the transversely-isotropic elasticity tensor, $\Delta\gamma_{n+1}$ is the sought plastic multiplier and $\boldsymbol{N}_{n+1}$ is the direction of the plastic flow, given by the plastic potential

$$\boldsymbol{N}_{n+1} = \frac{\partial G_p(\boldsymbol{\sigma}_{n+1})}{\partial \boldsymbol{\sigma}_{n+1}}. \tag{7.70}$$

Inserting the stresses $\boldsymbol{\sigma}_{n+1}$ into the yield surface formulation and enforcing the yield surface to be zero at the end of the time step (consistency condition $F_{p_{n+1}} = 0$) leads to a non-linear equation in $\Delta\gamma_{n+1}$ whose solution is pursued by employing the Newton-Raphson method. When solution is reached, the plastic strains are updated at the end of each time step by

$$\boldsymbol{\varepsilon}_{n+1} = \boldsymbol{\varepsilon}_n + \Delta\gamma_{n+1}\boldsymbol{N}_{n+1}. \tag{7.71}$$

7.3 Non-local formulation

As discussed in Chapter 1, a constitutive model formulated within the non-local framework has the major advantage of being effectively free of spurious mesh dependency, for which the size of the localizing zone (dictated by the internal length) can be easily controlled. However, the non-local method is very often avoided due to its non-standard implementation requirements.

In this chapter our intention is to present an alternative numerical implementation that aims to considerably simplify the process of turning a local model into non-local within the LS-DYNA environment. The technique has been designed in such manner that the non-local enhancement has to be implemented in LS-DYNA (via

[1]The implementation of the local material routine of the present transversely isotropic material model in LS-DYNA has been carried out by Dipl. Ing. Matthias Vogler, who is here greatly acknowledged. The implementation was part of a cooperative work whose developments and results have been published in [4, 117]. Again, the objective of this chapter is to demonstrate the great applicability of the present non-local strategy with many different constitutive models rather than exhaustively review material formulations that are already well established.

user-defined subroutines) just once. After this initial implementation, any user-defined local material model implemented in LS-DYNA can be transformed into non-local in a few minutes.

The cornerstone of the technique is based on the approximation of the non-local formulation proposed by Tvergaard and Needleman [114]. To start with, let us consider that a generic variable z is the desired local quantity to be converted to non-local. Using the approximated non-local strategy, the updated value of the local variable, z_{n+1}, is re-phrased as

$$z^*_{n+1} = K^{nl} z_{n+1}, \tag{7.72}$$

where K^{nl} is a non-local penalty factor defined as

$$K^{nl} = \frac{\bar{z}_n}{z_n}. \tag{7.73}$$

In the equation above, z_n and $\bar{z}_n$ are respectively the local and non-local values at the last converged incremental step. Therefore, the stress integration is performed locally where the chosen variable z is penalized with the coefficient K^{nl}. Note that, in order to obtain stable results with the present strategy, it is imperative to keep the size of the time step small enough[2]. As a matter of fact, an explicit finite element framework naturally demands very small time steps dictated by a given stability criterion. Therefore, the technique is perfectly suitable if the explicit scheme is adopted.

The non-local average at a given spatial point $\boldsymbol{x}$ is defined as

$$\bar{z}_n(\boldsymbol{x}) = \int_V \beta(\boldsymbol{x}, \boldsymbol{\xi}) z_n(\boldsymbol{\xi})\, dV(\boldsymbol{\xi}), \tag{7.74}$$

where $\beta(\boldsymbol{x}, \boldsymbol{\xi})$ is the non-local operator expressed by

$$\beta(\boldsymbol{x}, \boldsymbol{\xi}) = \frac{\alpha(\boldsymbol{x}, \boldsymbol{\xi})}{\int_V \alpha(\boldsymbol{x}, \boldsymbol{\zeta})\, dV(\boldsymbol{\zeta})}, \tag{7.75}$$

and $\alpha(\boldsymbol{x}, \boldsymbol{\xi})$ is the weighting function, here considered to be the bell-shaped function, i.e.,

$$\alpha(\boldsymbol{x}, \boldsymbol{\xi}) = \left\langle 1 - \frac{\|\boldsymbol{x} - \boldsymbol{\xi}\|^2}{\ell_r^2} \right\rangle^2. \tag{7.76}$$

[2]Since the present methodology is actually an approximation of the full non-local formulation, increases in the time step inevitably correspond to increases in the error of such approximation.

7.3.1 Lemaitre's ductile damage model

We start by modifying Lemaitre's ductile damage model, described in Section 7.2.1. We recall that in Chapter 6 it has been concluded that, for implicit damage models, damage is the most suitable choice for non-local quantity. Therefore, the increment of damage is changed in Lemaitre's case to be given by

$$\Delta D^*_{t_{n+1}} = K^{nl} \Delta D_{t_{n+1}}, \tag{7.77}$$

where

$$K^{nl} = \frac{\Delta \bar{D}_{t_n}}{\Delta D_{t_n}}. \tag{7.78}$$

7.3.2 Engelen and co-workers' based non-local ductile damage model

In the case of the ductile damage model of Section 7.2.2, the updated damage assumes the form

$$D_{n+1}(\kappa^*_{n+1}) = \frac{\kappa^*_{n+1}}{\kappa_c}, \tag{7.79}$$

for which

$$\kappa^*_{n+1} = K^{nl} \kappa_{n+1}, \tag{7.80}$$

where K^{nl} is the non-local penalty factor given by

$$K^{nl} = \frac{\bar{\kappa}_n}{\kappa_n}. \tag{7.81}$$

Remark 7.2. *As pointed out in Chapter 6, in the case of explicit damage models, the choice of damage as the non-local quantity leads to locking results as reported by Jirásek and Rolshoven [70]. In this case, the regularisation of the variable that drives damage is preferred. In the present model, this variable corresponds to the accumulated plastic strain given by the quantity κ. For this reason, κ has been chosen to be affected by the non-local penalty fractor, K^{nl}.*

7.3.3 Vogler and co-workers' non-local transversely-isotropic model

In a similar manner to the ductile damage model, the transversely-isotropic model of Section 7.2.3 has incorporated damage in an explicit fashion. To avoid spurious

results, we will replace Equation (7.67) by

$$D_{n+1} = \alpha(\varepsilon^{p\,*}_{n+1} - \varepsilon^{p}_{fail}), \tag{7.82}$$

where

$$\varepsilon^{p\,*}_{n+1} = K^{nl}\varepsilon^{p}_{n+1}, \tag{7.83}$$

and

$$K^{nl} = \frac{\bar{\varepsilon}^{p}_{n}}{\varepsilon^{p}_{n}}. \tag{7.84}$$

Remark 7.3. *Similarly to the case of Engelen and co-workers' model, the variable that drives damage, which is in the present model related to the norm of the plastic strain tensor, has been here chosen to be non-local. This stems from the fact that the damage law in the transversely-isotropic model of Vogler and co-workers has been established in an explicit fashion.*

7.4 Numerical Implementation in LS-DYNA

It is worth mentioning that LS-DYNA has the option of using non-local formulations through the keyword MAT_NONLOCAL since Version 960 [1]. However, this option is restricted to some elastoplastic models and is not accessible for user-defined constitutive models.

Concerning the implementation of the proposed non-local technique, the first step is the spatial discretisation of the integral of Equation (7.74). Following the same procedures of Chapters 3 and 4, we adopt the Gaussian quadrature, i.e.,

$$\bar{z}_i = \sum_{j=1}^{npg_i} w_j J_j \beta_{ij} z_j \tag{7.85}$$

where $\beta_{ij} \equiv \beta(\boldsymbol{x}, \boldsymbol{\xi})$ is the averaging factor that relates the Gauss points i and j respectively located at global coordinates $\boldsymbol{x}$ and $\boldsymbol{\xi}$. The quantities $\bar{z}_i$ and z_j are the constitutive variables associated to the Gauss points i and j, respectively. The quantity w_j is the Gaussian weight and J_j is the Jacobian, both evaluated at the Gauss point j. Finally, npg_i is the number of Gauss points that lie inside the non-local volume of interaction measured from point i. In the numerical implementation, z is substituted by the associated constitutive variable according to the model that is enhanced with non-locality.

In order to facilitate comprehension, a schematic flowchart for the implementation of the non-local technique in LS-DYNA is depicted in Figure 7.1. In Appendix C,

we have listed a FORTRAN code excerpt with the main steps of the implementation in file `dyn21.f`. Two main steps are need for the implementation of the non-local stratey. The first one concerns the computation of the factors w_j, J_j and β_{ij} of Equation (7.85). These factors are merely geometrical[3], i.e., they depend on the finite element mesh itself and not on the material model. Therefore, once this step has been implemented, it can be re-used whenever the non-local formulation is activated.

Remark 7.4. *In the case of large strain analysis, different strategies for the non-local averaging can be considered as discussed in Chapter 3, Section 3.2.2. In the case of explicit integration schemes, where the time steps are much smaller than the ones employed in implicit analysis, the computational burden associated with the non-local averaging of Eulearian-type makes it a very unattractive option, since the β_{ij} factors need to computed at every time step with that strategy. On the other hand, a modified version of the updated Lagrangian-type of non-local averaging, described in Chapter 3, Section 3.2.2, could be adopted, in which the β_{ij} factors should be updated every n time steps. However, it does not seem to exist any evidence supporting the fact that such strategy should be preferred over the total Lagrangian-type, for instance. Hence, the total Lagrangian-type of non-local averaging seems to be the most appropriate strategy in explicit integration schemes, especially due its high computational efficiency (the β_{ij} factors just need to be computed once), and therefore it has been adopted in all the simulations carried out in this chapter.*

The second step concerns the computation of the non-local penalty factor, K^{nl}. Since it uses the local values of the previous time step, the local variable can be stored in the array `var_loc` after calling the user material routine `umat41`. Note that in the code excerpt of Appendix C the arrays `var_loc` and `var_nonloc` contain the local and non-local values of every element of the mesh. The statement `SAVE var_loc` guarantees that the information stored in the array `var_loc` will be available in the next time step. It is important to remark that the calculations performed for the computation of the non-local values (through the discretised integral of Equation 7.85) and of the non-local penalty factor are the same for any material model. The only difference is in the variable which is used in these calculations. For instance, in the case of the ductile damage model of Section 7.2.2, one needs to store the updated accumulated plastic strain, κ_{n+1}, in `var_loc`. In the case of the transversely-isotropic model of Section 7.2.3, the updated values of the plastic strain norm are saved in the array `var_loc` at every time step.

[3]In order to compute the non-local factors, one needs to have the element connectivities and the nodal coordinates.

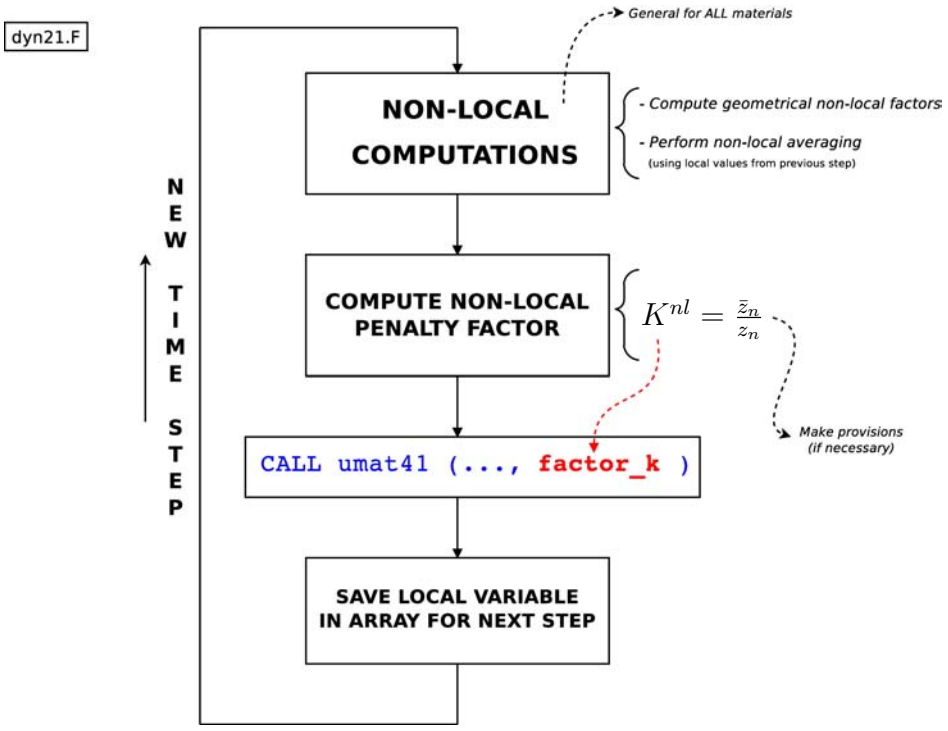

FIGURE 7.1: Schematic flowchart of the implementation of the non-local strategy.

One important aspect for the non-local technique to be successful is the use of numerical provisions after the calculation of the penalty factor, K^{nl}, where such provisions are, to some extent, model-dependent and, therefore, they need to be adjusted to different constitutive models accordingly. This step has been represented in the sample code of Appendix C in the line `CALL analyse_k`. Numerical instabilities and round-off errors may arise whenever one of the variables used for the penalty factor calculation reaches extreme values (for instance, very small values in the denominator of Equation 7.73), which may cause unwanted oscillations in the results. During this study, a much greater sensitivity to numerical instabilities in the implicit damage model has been experienced than in the explicit ones. This is mainly due to the fact that, in the case of implicit damage models, the magnitudes of the rate of the chosen non-local variable are in general very small at each time-step. Thus, the implementation of the non-local technique with implicit damage models requires special attention. Nonetheless, adjusting the numerical provisions is not a time-consuming task, especially when compared with the implementation of a full non-local model from scratch.

It is also worthwhile emphasizing that, since the non-local effects are incorporated using values of previous time steps, the present non-local technique can be employed either in scalar or in vectorized LS-DYNA implementations. Thus, the

advantages of parallel processing are not lost within the present non-local framework.

7.5 Examples

7.5.1 Lemaitre's ductile damage model

In this first example, the analysis of an axisymmetric specimen (see Figure 7.2) is carried out in order to assess the regularising effects of the proposed numerical implementation. We recall that a similar specimen has been investigated by the authors in Chapter 3 using an implicit finite element formulation. Three mesh refinements using linear quadrilateral elements with reduced integration (see Figure 7.2) have been considered in order to capture the pathological mesh dependency. The material properties adopted are given in Table 7.1.

It is worth mentioning that the regularising effects of the non-local theory can only be achieved if the characteristic length is large enough to span at least some elements. Therefore, in the present case, the value of ℓ_r has been chosen aiming to fulfil this condition rather than based on experimental measurements. Nonetheless, this consideration is reasonable enough to assess the non-local algorithm.

The specimen is loaded at its ending edge with a low velocity that grows linearly with time, therefore, minimising the effects of inertia. Figure 7.3 shows the damage contours for the local case. We notice that damage tends to concentrate at the critical element meanwhile its numerical value also tends to increase. Conversely,

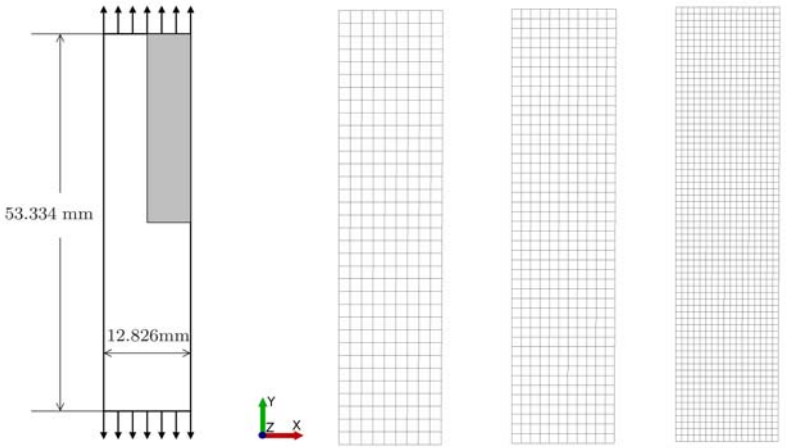

FIGURE 7.2: Geometry and meshes for the axisymmetric specimen.

TABLE 7.1: Material properties for the axisymmetric specimen.

Property	**Value**
Elastic modulus	$E = 210$ GPa
Poisson's ratio	$\nu = 0.3$
Damage exponent	$s = 1.0$
Damage denominator	$r = 2.5$ MPa
Initial yield stress	$\sigma_{y0} = 80.559$ MPa
Hardening function	$\sigma_y(R) = \sigma_{y0} + \left[589\,(10^{-4} + R)^{0.216} - \sigma_{y0}\right]$ MPa
Non-local intrinsic length	$\ell_r = 1.0$ mm

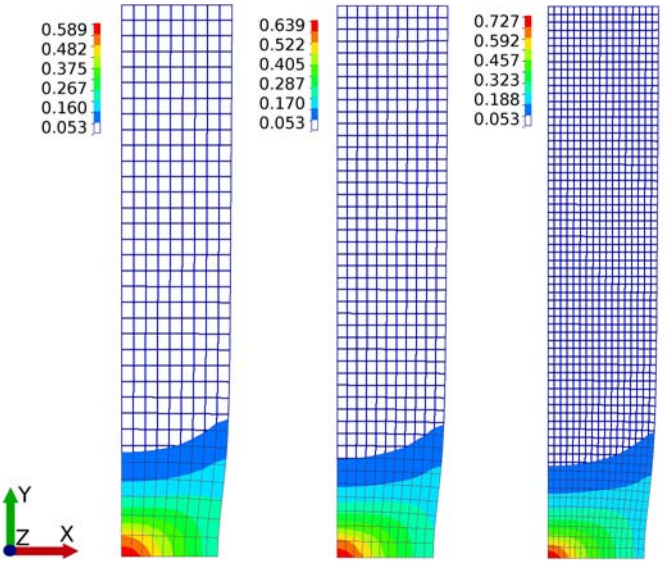

FIGURE 7.3: Damage contours in the local case.

the non-local solution provides a different behaviour. Observing Figure 7.4, it is possible to notice that both the damaging area and the damage values are kept nearly constant upon mesh refinement.

In Figure 7.5, the evolution of the damage variable and of the non-local penalty factor, K^{nl} , are plotted at the critical point of the finest mesh. At the initial stages, when damage is still low, the penalty factor is kept constant and equal to unity. However, when damage begins to evolve rapidly, the penalty factor decreases accordingly, which slows down the rate of damage evolution. As a consequence, spurious localisation is avoided. Note that some oscillations in the penalty factor are observed (see Figure 7.5). This stems from the fact that the rates used in the computation of the penalty factor are very small due to the small time steps of

the explicit analysis. The use of numerical provisions, as pointed out in Section 7.4, tends to minimise such oscillations.

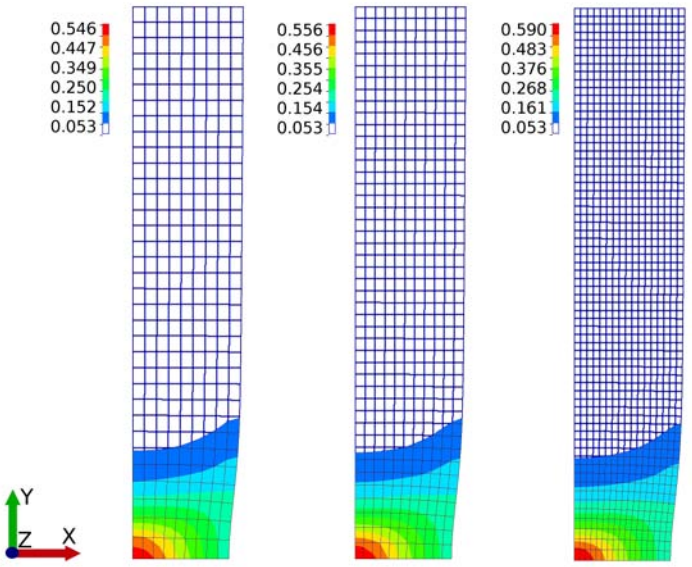

FIGURE 7.4: Damage contours in the non-local case.

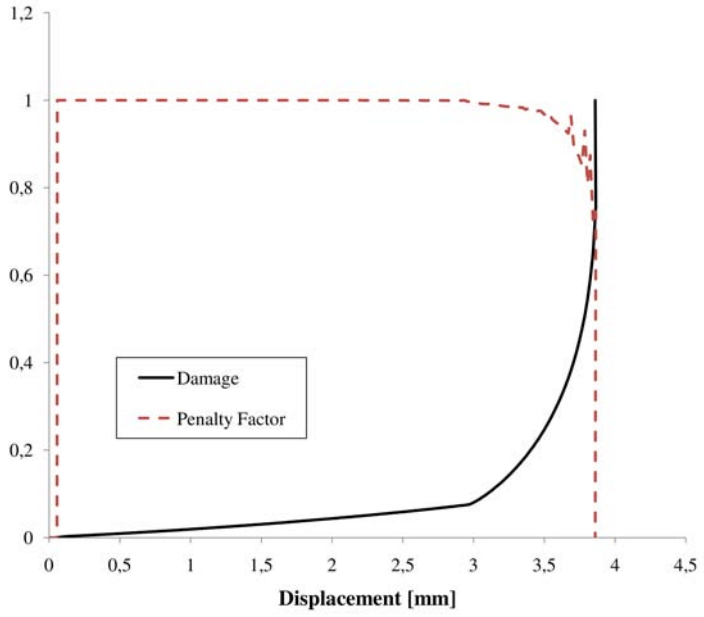

FIGURE 7.5: Evolution of damage and the non-local penalisation factor, K^{nl}.

7.5.2 Engelen and co-workers' ductile damage model

We continue to assess the non-local strategy with the ductile damage model of Section 7.2.2. Therefore, we simulate two specimens commonly used in the experimental determination of the properties of metals (see Figure 7.6). The first specimen can be simulated using an axisymmetric formulation meanwhile the second one can be analysed considering a plane strain state. It is worth mentioning that both specimens deliver similar triaxiality ratios at the critical region ($0.7 \lesssim \eta \lesssim 0.8$); however, the value of the normalised third invariant, ξ, is different (i.e., around 1.0 in the axisymmetric specimen and about 0.0 in the plane strain one). As discussed in Chapter 6, not only the triaxiality but also the third invariant of the deviatoric stress tensor plays an important role in the characterisation of the stress state and also in the failure onset. The specimens have been considered to be made of steel ($E = 200$ GPa, $\nu = 0.3$) with a yield stress function given by $\sigma_y(\kappa) = 700 + 300\kappa^{0.3}$ MPa.

The damage contours resulting from the simulation of axisymmetric and plane strain specimens are respectively given in Figures 7.7 and 7.8. The force displacement diagrams are also plotted for both specimens. Close inspection on these figures reveals that spurious mesh dependency is much stronger in the plane strain specimen than in the axisymmetric one. This fact has also been alluded in Chapter 6 where local and non-local models based on the constitutive theories of Lemaitre and Gurson have been comprehensively compared. Note that those models are quite different from the one employed in the present analysis. Finally, it is evident from the results that the proposed non-local technique has effectively alleviated the spurious mesh dependency associated with the strain-softening.

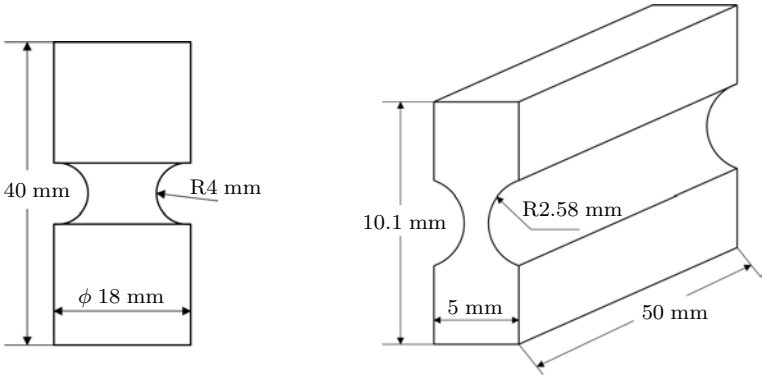

FIGURE 7.6: Geometry of the specimens for the ductile damage analysis using Engelen and co-workers' based model.

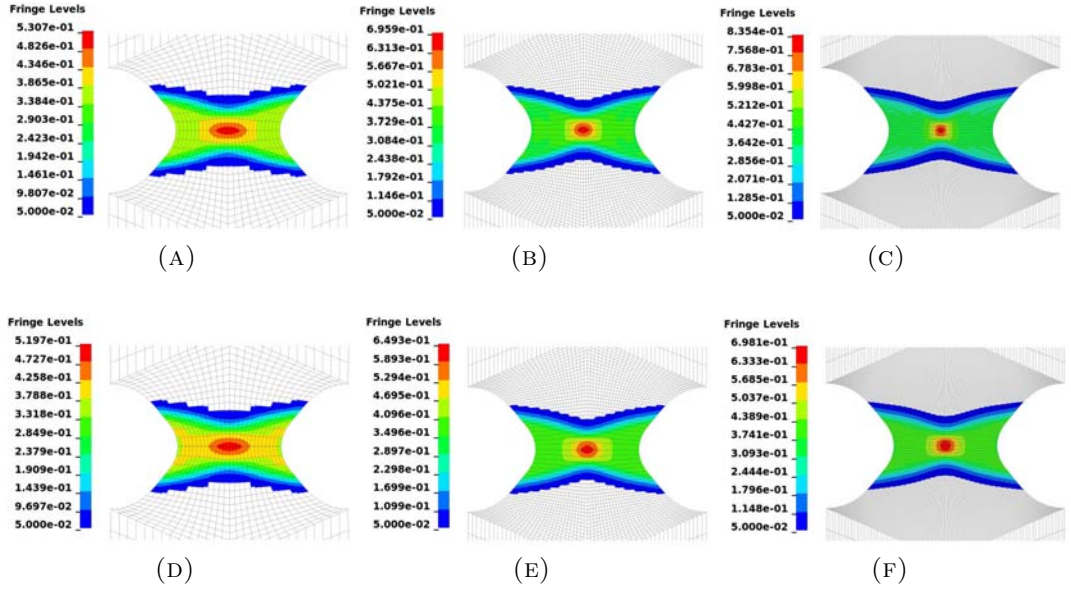

FIGURE 7.7: Damage contours for the axisymmetric specimen: (a–c) local; (d–f) non-local.

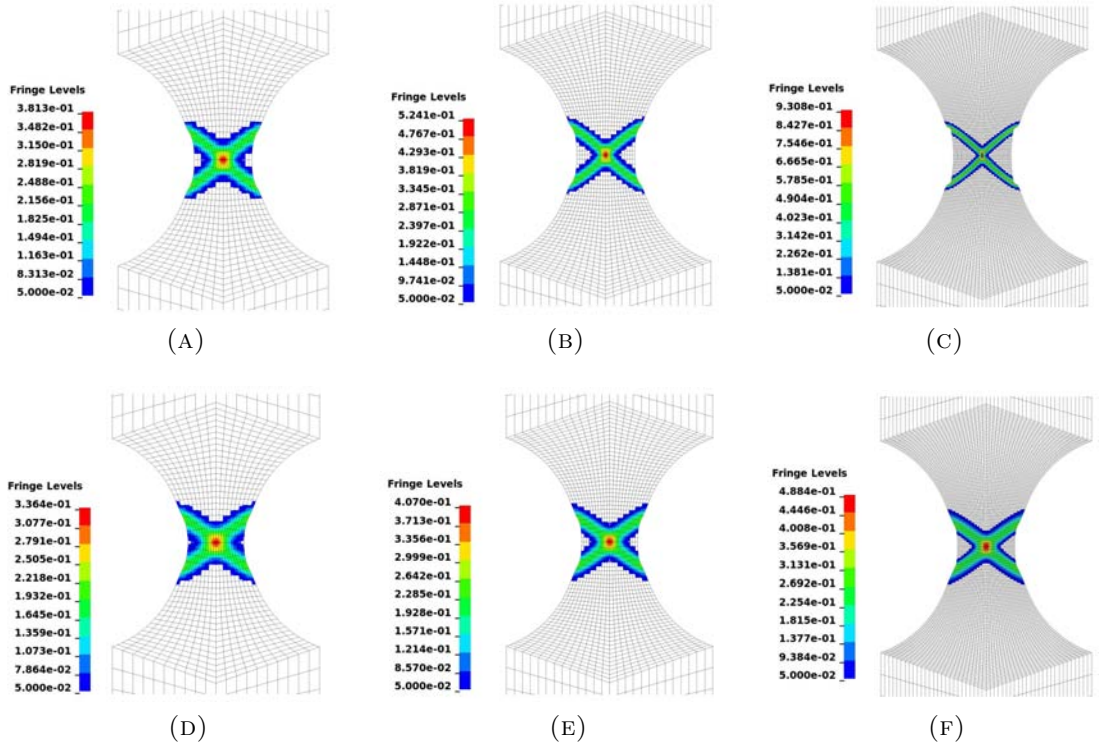

FIGURE 7.8: Damage contours for the plane strain specimen: (a–c) local; (d–f) non-local.

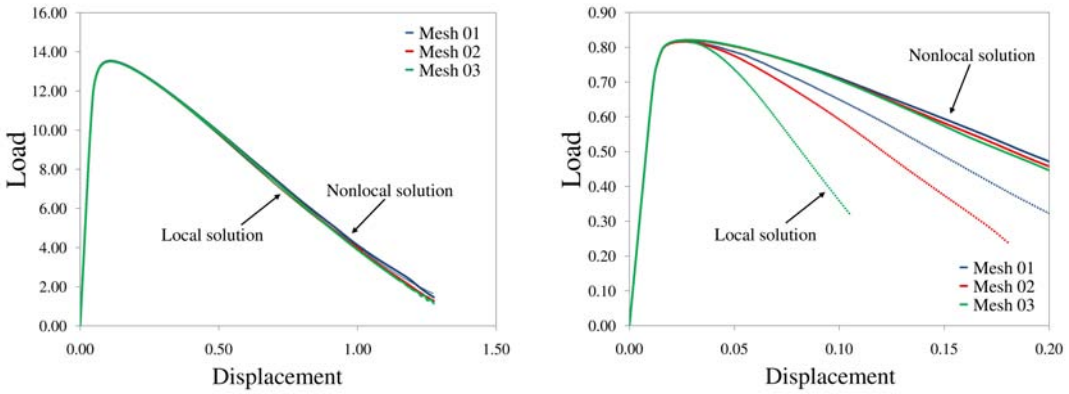

(A) (B)

FIGURE 7.9: Force-displacement diagrams: (a) axisymmetric specimen; (b) plane strain specimen.

7.5.3 Fibre-reinforced materials

In order to further assess the proposed non-local technique, we simulate three specimens commonly used in the experimental determination of the properties of fibre-reinforced materials (see Figure 7.10). The transversely-isotropic material model of Section 7.2.3 is then adopted for the numerical analysis. The selected specimens comprise three different stress states, namely tension, compression and shear. Each specimen has been discretised with three different mesh refinements in order to verify if the non-local formulation is able to prevent spurious results.

In Figure 7.11, the results for the tension specimen are illustrated. Clearly, if the local theory is assumed, the numerical solutions become highly mesh dependent when the softening regime takes place. The non-local solution, on the other hand,

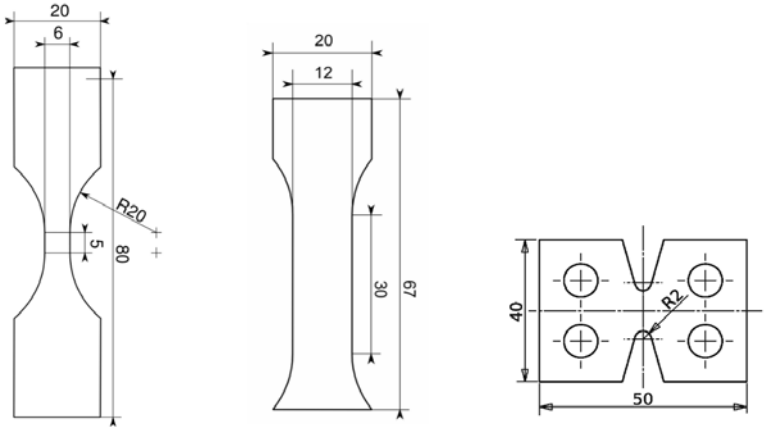

(A) (B) (C)

FIGURE 7.10: Specimens for (a) tension, (b) compression and (c) shear test.

is able to provide mesh-insensitive results since damage spreads over the elements at the central region. The results for the shear specimen are provided in Figure 7.12. We observe a very accentuated mesh sensitivity of the local solution, where damage tends to concentrate into a single layer of elements. When the non-local strategy is activated, the spurious mesh dependency is prevented, rendering more physically sound results. Finally, Figure 7.13 depicts the results obtained in the compression test. Again, pathological mesh dependency is evident within the standard local theory, which has been significantly alleviated with the use of the non-local formulation.

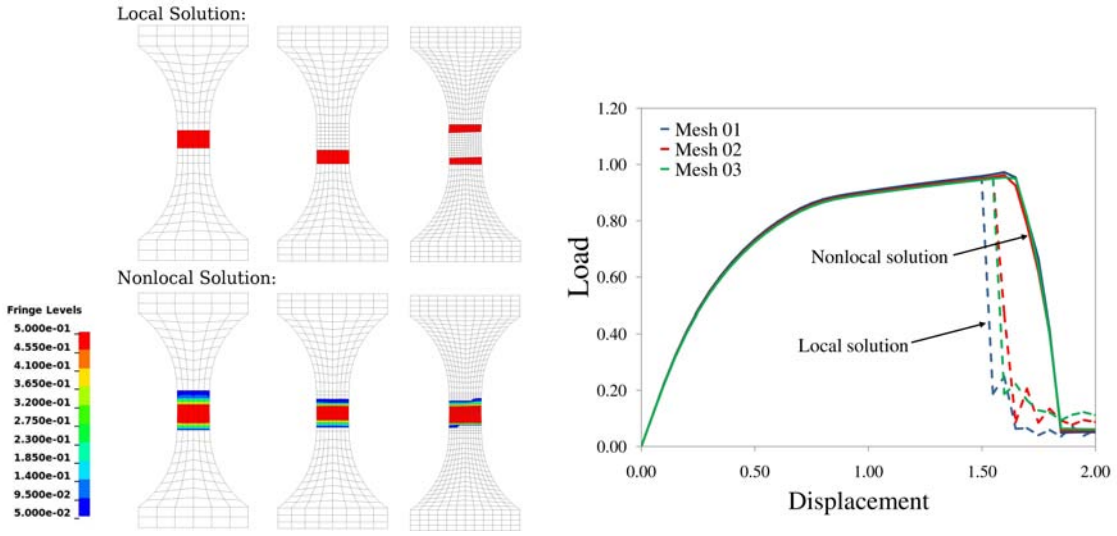

(A) (B)

FIGURE 7.11: Results for the tension specimen: (a) damage contours; (b) force-displacement diagram.

7.6 Conclusions

In this chapter, a strategy for the implementation of non-local models in LS-DYNA has been presented. The technique has been designed to be generically applicable to several user-defined material models, requiring only little modification in the original local routines. Three different constitutive models, two of them suitable for the description of ductile metals and the other one intended for the simulation of fibre-reinforced materials, have been coupled with the present non-local technique. The numerical analysis has demonstrated that the non-local strategy has been able to prevent unlimited localisation and physically sound results have been obtained. It is important to mention that, once the general routines of the non-local scheme have been implemented, the non-local extension of the aforementioned material models was straightforward. Thus, the obtained mesh-insensitive

results and the generality of implementation make the present non-local technique a strong candidate against other competitive regularisation methods and also plausible for industrial applications.

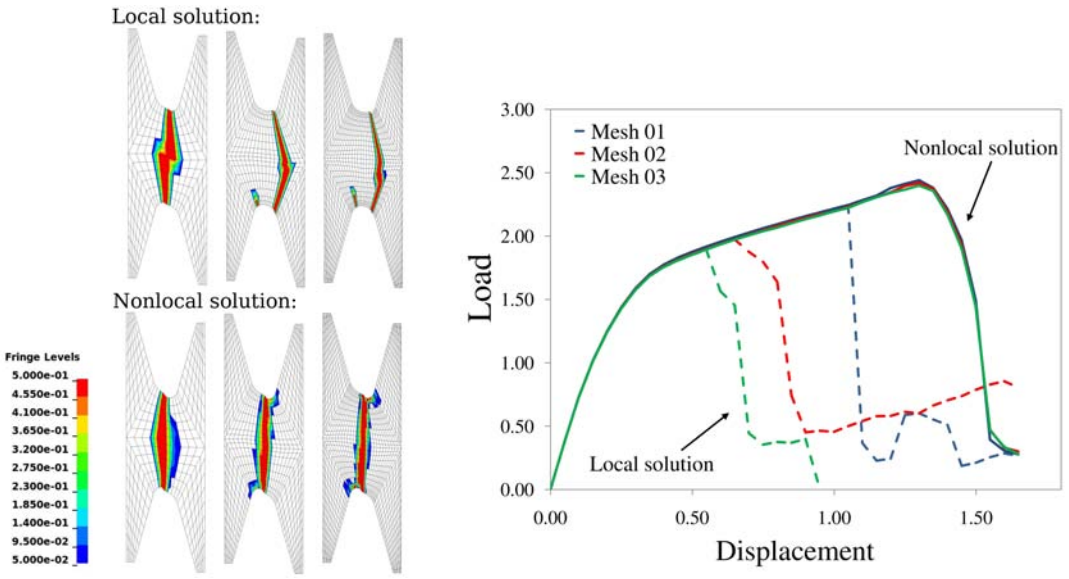

(A) (B)

FIGURE 7.12: Results for the shear specimen: (a) damage contours; (b) force-displacement diagram.

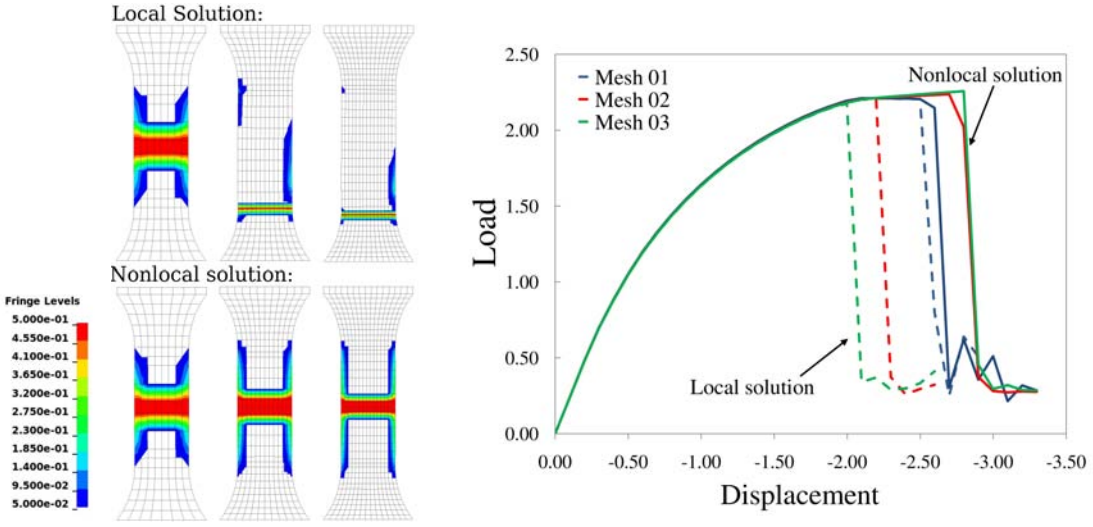

(A) (B)

FIGURE 7.13: Results for the compression specimen: (a) damage contours; (b) force-displacement diagram.

Chapter 8

Final Remarks

Indeed, in a progressively more competitive industrial scenario, the need for more reliable predictions of ductile deformation and material failure is fundamental. Only so it is possible to substantially reduce the use of unnecessary material and thus achieving robust designs. A precise modelling of the ductile behaviour inevitably involves the description of observed phenomena like plastic straining and strain-driven softening, often requiring highly non-linear constitutive models. In particular, the use of strain softening laws inevitably leads to pathological mesh dependency if the standard local continuum theory is considered.

The main goal of this thesis was to resolve the issues of spurious mesh sensitivity through a non-local approach of integral-type, especially because many questions were open and and some are still matter of dispute in the specialised literature. In particular, the integral-type formulation of the non-local theory seems to have been ignored by most researchers. The main claim was that non-local formulations of integral-type are prohibitive, rendering in inefficient numerical implementations. Throughout this thesis, it has been shown that such argument is not true, where efficient algorithms have been presented in detail. In particular, it is worth mentioning that a general framework for the establishment of consistent tangent stiffness for non-local models of integral-type has been developed, making the integral approach competitive with gradient-enhanced models.

In the following, the main advances accomplished in this thesis have been summarised by chapter, where the principal achievements are again reviewed.

Chapter 3

In Chapter 3, some important theoretical aspects concerning non-local theories of integral-type have been addressed. In particular, we have shed some light on the underlying hypothesis that either the non-local averaging operator or the non-local intrinsic length are independent of the deformation history. This clarification is fundamental for the correct establishment of the non-local models addressed in this thesis. It is due to this assumption that the extension of the non-local theory to the finite strain domain can be done straightforwardly. Some finite strain gradient-dependent theories available in the literature have directly assumed that kinematics are local. As a matter of fact, local kinematics are a direct consequence of the independence of the non-local averaging operator (or the non-local gradient kernel, in gradient-dependent theories) on the history of deformation. This tacitly implies that the intrinsic length is kept constant with regard to deformation.

The advances of thermodynamically consistent non-local models, first exclusively adopted in the literature to model quasi-brittle materials, have been extended to describe deformation of ductile materials at finite strains. Nonetheless, it has been shown that the simple ad-hoc extension of the local model to the non-local case do not infringe thermodynamic principles since no negative dissipations are generated.

A general numerical framework for the numerical integration of the constitutive equations considering the non-local case has been developed and presented in detail. An algorithm that integrates all the Gauss points of the structure simultaneously has been proposed. It has been shown that, in the case of the Lemaitre-based ductile damage model, a modified Newton-Raphson approach that substantially saves computational time and storage space provides high convergence rates.

Chapter 4

Since most Gurson-based damage models available in the literature are not able to describe material degradation when subject to shear stress states, an additional shear mechanism, based on the work of Nahshon and Hutchinson [83], has been incorporated in the constitutive model of Chapter 4. In order to avoid spurious mesh dependency, the damage variable has been rewritten to be non-local. The establishment of the associated constitutive equations as well as the numerical framework for the update procedure have been present in detail. It has been shown that in the case of the non-local Gurson-based damage model, a global system of equations that contains smaller system of equations (each one associated

with a given Gauss point of the mesh) has to be solved. A full and a modified Newton-Raphson strategies have then been established for the solution of the constitutive problem. Numerical investigation has shown that the additional shear mechanism together with the regularised damage approach have lead to mesh-insensitive results when subjected to different stress states.

Chapter 5

Many authors have advocated that non-local models of integral-type are prohibitive especially because it is (allegedly) not possible to define consistent tangent operators and therefore the convergence rates obtained with those models are rather poor. In Chapter 5, it has been shown that this is not true and, indeed, it is possible to have consistent tangent operators, associated with the non-local integral scheme, that are plausible in computational terms. The absence of a continuum tangent modulus has been clarified in this chapter, where it has been demonstrated that the discrete finite element problem allows us to define a global constitutive relation. A general procedure for the establishment of non-local consistent tangent operators has been then developed and demonstrated in detail. Later, the presented framework has been particularised for the cases of J_2 plasticity and the Lemaitre-based ductile damage model of Chapter 3. Numerical examples have clearly shown that the quadratic rates of convergence inherent to the Newton-Raphson method have been achieved.

Chapter 6

The main goal of Chapter 6 was to unfold the question of which constitutive variable should be regularised to avoid spurious mesh dependency. In order to properly answer this question, a comprehensive assessment of several non-local models has been carried out where these models have been subjected to different values of stress triaxiality and third invariant of the deviatoric stress tensor. Since the stress state plays a fundamental role in the behaviour and fracture of ductile materials, it was the main concern to observe how the different non-local models respond under distinct external load conditions. It has been found that some options that are able to tackle spurious mesh sensitivity in a certain stress state fail completely when subject to another stress triaxiality or third invariant. Furthermore, the conclusions reported by other authors in the context of explicit damage models are completely different from those drawn in the assessment of Chapter 6, where implicit damage models have been considered. This utterly implies that one

has to be very careful when choosing the non-local variable of a given constitutive model. After a very careful scrutiny, the assessment has shown that, in the case of implicit damage models, the damage variable seems to be the optimal choice.

Chapter 7

In Chapter 7, a numerical strategy concerning non-local models of integral-type suitable for explicit finite element frameworks has been presented. The main advantage of the strategy is that it avoids the solution of a global system of equations, making it particularly useful for the implementation in commercial codes. This is accomplished by taking advantage of the explicit scheme itself. Since the critical time step requirements necessary to keep stability in the explicit scheme are very small, an approximation of the non-local integral operator can be done where it is evaluated using the constitutive quantities of the previous time step. Therefore, the integration of the constitutive equations is kept local, where a penalisation factor based on a non-local average is applied. Another advantage of the technique is that it is very flexible, which permits its use with different material models. In Chapter 7, the strategy has been applied to two ductile damage models and to a recently proposed transversely isotropic constitutive model intended to describe deformation and failure of fibre-reinforced materials. The proposed non-local approach has been implemented in the FE commercial code LS-DYNA and the numerical results have shown that it was able to effectively eliminate spurious mesh dependency for different materials under different stress states.

8.1 Suggestions for future work

Identification of the non-local intrinsic length

Throughout this thesis, the non-local intrinsic length, ℓ_r, has been regarded as a numerical parameter. The main intention of that was to concentrate in specific theoretical and numerical aspects that, from the author's point of view, still needed developments as of the writing of thesis. However, a comprehensive comparison with experimental results should be performed. Up to this date, there is no procedure for the measurement of the non-local intrinsic length, especially in the case of ductile materials. In fact, a direct measurement seems impracticable, so that some sort of parameter identification procedure should be adopted in order to quantify ℓ_r. Recent advances accomplished in the non-local field have achieved a

very mature stage that allow the combination of the available numerical tools with optimisation strategies in order to identify the non-local intrinsic length properly.

Comparison between the integral and gradient non-local approaches

As pointed out in Chapter 3, gradient and integral non-local theories seem to have been employed to model distinct materials; the former mostly used to describe ductile materials like steel and aluminium, the latter for quasi-brittle materials like concrete. Some comparisons between the two competitive approaches have been done in the literature (e.g., see [89]). However, most of them have solely concentrated in demonstrating that the implicit gradient and the integral schemes are equivalent. One of the main arguments against the non-local formulation of integral-type was the lack of consistent linearisation. However, the work of Jirásek and Patzák [69] and the developments carried out in Chapter 5 of this thesis have shown that consistent tangents are also practicable in the integral non-local case. An important future study is therefore to compare both implicit gradient and integral approaches in terms of numerical efficiency, so that future regularised constitutive models may adopt, already from its conception, the most efficient regularisation method.

Application of the non-local theory with complex constitutive models

The majority of the non-local developments of this thesis have been combined with classical constitutive models. However, in the last few years, many new material models, able to describe complicated strain path more accurately, have been proposed in the literature. An important step for the precise prediction of plastic straining, material degradation and failure in practical applications would combine these novel advanced models with an appropriate non-local formulation, so that softening regimes can be simulated without spurious mesh dependency, for which complicated strain paths can be described properly.

Development of theories containing an evolving non-local intrinsic length

A main assumption made in the developments of this thesis was that the history of deformation has no influence on the non-local averaging operator. This means that, in the underlying formulation, the non-local intrinsic length remains constant as the body undergoes deformation. Thus, the size of the fracturing area is inherently assumed to be related to a constant dictated by ℓ_r. However, there

is no experimental evidence neither supporting nor contradicting this hypothesis. Apparently, a more realistic modelling would consider an evolving non-local intrinsic length, for which ℓ_r would be a function of other variables that are known to significantly influence the dissipative fracturing process (e.g. the plastic strain, the stress state, the damage or the history of deformation itself). However, the consideration of a non-local theory with a non-constant intrinsic length as well as an averaging operator which is dependent on the history of deformation (or some other constitutive quantity) is still very challenging, both from the theoretical and the computational point of view. Nevertheless, the development of such enhanced theories would help to better understand material failure and also would widen the application of the non-local theory to a larger number of materials.

Appendix A

Linearisation of the Weak Equilibrium Equation

The linearisation of the equilibrium equation in its weak form (also often called *virtual work equation*) is a very well-established procedure in the literature (e.g., see [40]) and will be briefly reviewed here. The intention is not to be exhaustive but rather to provide a reference for the developments addressed in this thesis. The correct linearisation of the equilibrium equation is crucial for the consistent derivation of tangent moduli, either in the local or in the non-local case.

To start with, we define a functional, G, associated with the material version of the equilibrium equation, by writing

$$G(\boldsymbol{u}, \boldsymbol{\eta}) = \int_{\Omega} \boldsymbol{P} : \nabla_p \boldsymbol{\eta} \, dV - \int_{\partial\Omega} \bar{\boldsymbol{t}} \cdot \boldsymbol{\eta} \, dA. \tag{A.1}$$

Applying the concept of *directional derivative* [62], we have

$$\mathrm{D}G(\boldsymbol{u}^*, \boldsymbol{\eta})[\boldsymbol{d}] = \frac{\mathrm{d}}{\mathrm{d}\epsilon}\bigg|_{\epsilon=0} \int_{\Omega} \boldsymbol{P}(\boldsymbol{F}(\epsilon)) : \nabla_p \boldsymbol{\eta} \, dV - \int_{\partial\Omega} \bar{\boldsymbol{t}} \cdot \boldsymbol{\eta} \, dA. \tag{A.2}$$

Assuming that the surface traction field, $\bar{\boldsymbol{t}}$, is configuration-independent, Equation (A.2) reduces to

$$\mathrm{D}G(\boldsymbol{u}*, \boldsymbol{\eta})[\boldsymbol{d}] = \frac{\mathrm{d}}{\mathrm{d}\epsilon}\bigg|_{\epsilon=0} \int_{\Omega} \boldsymbol{P}(\boldsymbol{F}(\epsilon)) : \nabla_p \boldsymbol{\eta} \, dV \tag{A.3}$$

where the first Piola-Kirchhoff stress tensor is a function of the perturbed gradient deformation, $\boldsymbol{F}(\epsilon)$, defined by

$$\begin{aligned} \boldsymbol{F}(\epsilon) &= \boldsymbol{I} + \nabla_p(\boldsymbol{u}^* + \epsilon\boldsymbol{d}) && \text{(A.4)} \\ &= \boldsymbol{F}^* + \epsilon\nabla_p\boldsymbol{d} && \text{(A.5)} \end{aligned}$$

where $\boldsymbol{F}^*$ denotes the deformation gradient for the displacement field $\boldsymbol{u}^*$, which reads

$$\boldsymbol{F}^* = \boldsymbol{I} + \nabla_p\boldsymbol{u}^*. \tag{A.6}$$

Straightforward multi-variable calculus leads to

$$\mathrm{D}G(\boldsymbol{u}*, \boldsymbol{\eta})[\boldsymbol{d}] = \int_\Omega \mathbf{A} : \nabla_p\boldsymbol{d} : \nabla_p\boldsymbol{\eta}\, dV \tag{A.7}$$

where $\mathbf{A}$ is the *material tangent modulus*, defined by

$$\mathbf{A} \equiv \left.\frac{\partial \boldsymbol{P}}{\partial \boldsymbol{F}}\right|_{\boldsymbol{F}^*}. \tag{A.8}$$

Considering the standard identities [58]

$$\begin{aligned} \nabla_x\boldsymbol{a} &= \nabla_p\boldsymbol{a}\boldsymbol{F}^{-1}, && \text{(A.9)} \\ \int_{\varphi(\Omega)} a(\boldsymbol{x})\, dV &= \int_\Omega J(\boldsymbol{p})a(\varphi(\boldsymbol{p}))\, dV, && \text{(A.10)} \end{aligned}$$

which are valid for any scalar field a and vector field $\boldsymbol{a}$, straightforward substitutions and re-arrangements allows us to express the directional derivative for the spatial description as

$$\mathrm{D}G(\boldsymbol{u}*, \boldsymbol{\eta})[\boldsymbol{d}] = \int_{\varphi(\Omega)} \mathbf{a} : \nabla_x\boldsymbol{d} : \nabla_x\boldsymbol{\eta}\, dV \tag{A.11}$$

where $\mathbf{a}$ is the *spatial tangent modulus*, which in index notation is defined as

$$\mathsf{a}^{ijkl} = \frac{1}{J}\mathrm{A}^{imkn}F^{jm}F^{ln} \tag{A.12}$$

where $\mathbf{A}$ is the material tangent modulus, defined by

$$\mathsf{A}^{imkn} = \frac{\partial P^{im}}{\partial F^{kn}}. \tag{A.13}$$

The first Piola-Kirchhoff stress tensor $\boldsymbol{P}$ can be related to the Cauchy and Kirchhoff stress tensors by the expressions $\boldsymbol{P} = J\boldsymbol{\sigma}\boldsymbol{F}^{-T}$ and $\boldsymbol{P} = \boldsymbol{\tau}\boldsymbol{F}^{-T}$, respectively. These identifies allows us to straightforwardly re-phrase Equation (A.13) to be given by

$$\mathsf{A}^{imkn} = \frac{\partial}{\partial F^{kn}} \left[\tau^{ip} \left(F^{mp} \right)^{-1} \right]. \tag{A.14}$$

By making use of the chain rule, we have

$$\mathsf{A}^{imkn} = \frac{\partial \tau^{ip}}{\partial F^{kn}} \left(F^{mp} \right)^{-1} + \tau^{ip} \frac{\partial \left(F^{mp} \right)^{-1}}{\partial F^{kn}} \tag{A.15}$$

where derivative of the last term of the right hand side of Equation (A.15) is given by

$$\frac{\partial \left(F^{mp} \right)^{-1}}{\partial F^{kn}} = - \left(F^{mk} \right)^{-1} \left(F^{np} \right)^{-1}. \tag{A.16}$$

In the derivation above, Equation (A.16) has been obtained using relations for the derivative of the inverse of a tensor given in the literature [40, 66, 73]. Substituting (A.16) into (A.15) gives

$$\mathsf{A}^{imkn} = \frac{\partial \tau^{ip}}{\partial F^{kn}} \left(F^{mp} \right)^{-1} - \tau^{ip} \left(F^{mk} \right)^{-1} \left(F^{np} \right)^{-1}. \tag{A.17}$$

Finally, the substitution of (A.17) into (A.12) eventually leads, after some straightforward algebraic manipulations, to the following expression for the spatial tangent modulus:

$$\mathsf{a}^{ijkl} = \frac{1}{J} \frac{\partial \tau^{ij}}{\partial F^{km}} F^{lm} - \sigma^{il} \delta^{jk}. \tag{A.18}$$

Appendix B

Linearisation of the Non-local Stress Integration

B.1 Linearisation in the general case

Let us firstly consider a local constitutive model which has been discretised with the typical fully implicit backward Euler scheme:

$$\left\{ \begin{array}{l} A_\sigma = \boldsymbol{\sigma}_{n+1} - \mathbf{D}^e : \left[\boldsymbol{\varepsilon}_{n+1}^{e\,trial} - \Delta\gamma \boldsymbol{N}_{n+1} \right] \\ \\ A_\alpha = \boldsymbol{\alpha}_{n+1} - \boldsymbol{\alpha}_n - \Delta\gamma \boldsymbol{H_{n+1}} \\ \\ A_F = F_{p_{n+1}} \end{array} \right\} = \left\{ \begin{array}{c} \mathbf{0} \\ \\ \mathbf{0} \\ \\ 0 \end{array} \right\}. \tag{B.1}$$

In the equations above, $\boldsymbol{N}$ is the flow vector and $\boldsymbol{H}$ is the generalised hardening modulus. In the general case, the non-local constitutive problem is a global system of constitutive equations for which the solution must be found simultaneously, i.e.,

$$\left\{ \begin{array}{c} S_1 \\ S_2 \\ \vdots \\ S_{n_{ip}} \end{array} \right\} = \left\{ \begin{array}{c} O_1 \\ O_2 \\ \vdots \\ O_{n_{ip}} \end{array} \right\} \tag{B.2}$$

where

$$S_i = \begin{cases} A_{\sigma_i} &= \boldsymbol{\sigma}_{i_{n+1}} - \mathbf{D}^e : \left[\boldsymbol{\varepsilon}^{e\,trial}_{i_{n+1}} - \Delta\gamma_i \boldsymbol{N}_{i_{n+1}}\right] \\ A_{\alpha_i} &= \bar{\boldsymbol{\alpha}}_{i_{n+1}} - \bar{\boldsymbol{\alpha}}_{i_n} - \sum_{j=1}^{n_{ip}} w_j J_j \beta_{ij} \Delta\gamma_j \boldsymbol{H}_{\boldsymbol{j_{n+1}}} \\ A_{F_i} &= F_{p\,i_{n+1}} \end{cases} \tag{B.3}$$

and

$$O_i = \begin{cases} \mathbf{0} \\ \mathbf{0} \\ 0 \end{cases} \tag{B.4}$$

In order to keep the notation clear, we shall omit the subscript $n+1$ in the following derivations. The global system of equations in (B.2) in its linearised form is expressed by

$$\begin{Bmatrix} L_1 \\ L_2 \\ \vdots \\ L_{n_{ip}} \end{Bmatrix} = \begin{Bmatrix} B_1 \\ B_2 \\ \vdots \\ B_{n_{ip}} \end{Bmatrix} \tag{B.5}$$

where

$$L_i = \begin{cases} \displaystyle\sum_{j=1}^{n_{ip}} \frac{\partial A_{\sigma_i}}{\partial \boldsymbol{\sigma}_j} : d\boldsymbol{\sigma}_j + \sum_{j=1}^{n_{ip}} \frac{\partial A_{\sigma_i}}{\partial \bar{\boldsymbol{\alpha}}_j} * d\bar{\boldsymbol{\alpha}}_j + \sum_{j=1}^{n_{ip}} \frac{\partial A_{\sigma_i}}{\partial \Delta\gamma_j} d\Delta\gamma_j \\ \displaystyle\sum_{j=1}^{n_{ip}} \frac{\partial A_{\alpha_i}}{\partial \boldsymbol{\sigma}_j} : d\boldsymbol{\sigma}_j + \sum_{j=1}^{n_{ip}} \frac{\partial A_{\alpha_i}}{\partial \bar{\boldsymbol{\alpha}}_j} * d\bar{\boldsymbol{\alpha}}_j + \sum_{j=1}^{n_{ip}} \frac{\partial A_{\alpha_i}}{\partial \Delta\gamma_j} d\Delta\gamma_j \\ \displaystyle\sum_{j=1}^{n_{ip}} \frac{\partial A_{F_i}}{\partial \boldsymbol{\sigma}_j} : d\boldsymbol{\sigma}_j + \sum_{j=1}^{n_{ip}} \frac{\partial A_{F_i}}{\partial \bar{\boldsymbol{\alpha}}_j} * d\bar{\boldsymbol{\alpha}}_j + \sum_{j=1}^{n_{ip}} \frac{\partial A_{F_i}}{\partial \Delta\gamma_j} d\Delta\gamma_j \end{cases} \tag{B.6}$$

and

$$B_i = \begin{cases} d\boldsymbol{\varepsilon}^{e\,trial}_j \\ \mathbf{0} \\ 0 \end{cases} \tag{B.7}$$

The linearised system can be conveniently organised in a symbolic matrix format, i.e.,

$$\begin{bmatrix} [\mathrm{C}]_{11} & [\mathrm{C}]_{12} & \cdots & [\mathrm{C}]_{1n_{ip}} \\ [\mathrm{C}]_{21} & [\mathrm{C}]_{22} & \cdots & [\mathrm{C}]_{2n_{ip}} \\ \vdots & \vdots & \ddots & \vdots \\ [\mathrm{C}]_{n_{ip}1} & [\mathrm{C}]_{n_{ip}2} & \cdots & [\mathrm{C}]_{n_{ip}n_{ip}} \end{bmatrix} \begin{bmatrix} [\mathrm{X}]_1 \\ [\mathrm{X}]_2 \\ \vdots \\ [\mathrm{X}]_{n_{ip}} \end{bmatrix} = \begin{bmatrix} [\mathrm{B}]_1 \\ [\mathrm{B}]_2 \\ \vdots \\ [\mathrm{B}]_{n_{ip}} \end{bmatrix} \tag{B.8}$$

where

$$[\mathrm{C}]_{ij} = \begin{bmatrix} \dfrac{\partial A_{\sigma_i}}{\partial \boldsymbol{\sigma}_j} & \dfrac{\partial A_{\sigma_i}}{\partial \bar{\boldsymbol{\alpha}}_j} & \dfrac{\partial A_{\sigma_i}}{\partial \Delta\gamma_j} \\ \dfrac{\partial A_{\alpha_i}}{\partial \boldsymbol{\sigma}_j} & \dfrac{\partial A_{\alpha_i}}{\partial \bar{\boldsymbol{\alpha}}_j} & \dfrac{\partial A_{\alpha_i}}{\partial \Delta\gamma_j} \\ \dfrac{\partial A_{F_i}}{\partial \boldsymbol{\sigma}_j} & \dfrac{\partial A_{F_i}}{\partial \bar{\boldsymbol{\alpha}}_j} & \dfrac{\partial A_{F_i}}{\partial \Delta\gamma_j} \end{bmatrix} \tag{B.9}$$

and

$$[\mathrm{X}]_i = \begin{bmatrix} d\boldsymbol{\sigma}_i \\ d\bar{\boldsymbol{\alpha}}_i \\ d\Delta\gamma_i \end{bmatrix}. \tag{B.10}$$

In practical terms, we have two vectors of order $n_{cv} \times n_{ip}$ and one square matrix of order $(n_{cv} \times n_{ip}) \times (n_{cv} \times n_{ip})$ where n_{cv} is the number of constitutive variables per integration point. The exact global constitutive relation between stresses and strains is established by inverting the global compliance matrix, [C], which yields on

$$\begin{bmatrix} [\mathrm{X}]_1 \\ [\mathrm{X}]_2 \\ \vdots \\ [\mathrm{X}]_{n_{ip}} \end{bmatrix} = \begin{bmatrix} [\mathrm{E}]_{11} & [\mathrm{E}]_{12} & \cdots & [\mathrm{E}]_{1n_{ip}} \\ [\mathrm{E}]_{21} & [\mathrm{E}]_{22} & \cdots & [\mathrm{E}]_{2n_{ip}} \\ \vdots & \vdots & \ddots & \vdots \\ [\mathrm{E}]_{n_{ip}1} & [\mathrm{E}]_{n_{ip}2} & \cdots & [\mathrm{E}]_{n_{ip}n_{ip}} \end{bmatrix} \begin{bmatrix} [\mathrm{B}]_1 \\ [\mathrm{B}]_2 \\ \vdots \\ [\mathrm{B}]_{n_{ip}} \end{bmatrix} \tag{B.11}$$

where [E] = [C]$^{-1}$. The lines and rows associated with the other constitutive variables can be disregarded of the final matrix and only the terms associated with the stress and strain are needed. Therefore, the global constitutive relation, written in symbolic matrix notation, assumes the following form

$$\begin{bmatrix} d\boldsymbol{\sigma}_1 \\ d\boldsymbol{\sigma}_2 \\ \vdots \\ d\boldsymbol{\sigma}_{n_{ip}} \end{bmatrix} = \begin{bmatrix} \mathbf{D}_{11} & \mathbf{D}_{12} & \cdots & \mathbf{D}_{1n_{ip}} \\ \mathbf{D}_{21} & \mathbf{D}_{22} & \cdots & \mathbf{D}_{2n_{ip}} \\ \vdots & \vdots & \ddots & \vdots \\ \mathbf{D}_{n_{ip}1} & \mathbf{D}_{n_{ip}2} & \cdots & \mathbf{D}_{n_{ip}n_{ip}} \end{bmatrix} \begin{bmatrix} d\boldsymbol{\varepsilon}_1^{e\,trial} \\ d\boldsymbol{\varepsilon}_2^{e\,trial} \\ \vdots \\ d\boldsymbol{\varepsilon}_{n_{ip}}^{e\,trial} \end{bmatrix}. \tag{B.12}$$

Thus, the constitutive relation of a given integration point is always dependent of the surrounding points. The global relationship of matrix in Equation (B.12) has to be afterwards used in the assemblage of the global stiffness matrix.

B.2 Non-local tangent operator: Lemaitre-based non-local model

We repeat here again the non-local consistent tangent operator associated with the Lemaitre-based non-local ductile damage model of Chapter 3. For the case when $j = i$, it is given by

$$\mathbf{D}_{ii} = a_1 \left[\mathsf{I} - \frac{1}{3} \boldsymbol{I} \otimes \boldsymbol{I} \right] + b_1 \bar{\boldsymbol{N}}_{i_{n+1}} \otimes \bar{\boldsymbol{N}}_{i_{n+1}} + c_1 \bar{\boldsymbol{N}}_{i_{n+1}} \otimes \boldsymbol{I} + d_1 \boldsymbol{I} \otimes \bar{\boldsymbol{N}}_{i_{n+1}} + e_1 \boldsymbol{I} \otimes \boldsymbol{I}. \tag{B.13}$$

If $j \neq i$, then $\mathbf{D}_{ij}$ is written:

$$\mathbf{D}_{ij} = b_2 \bar{\boldsymbol{N}}_{i_{n+1}} \otimes \bar{\boldsymbol{N}}_{j_{n+1}} + c_2 \bar{\boldsymbol{N}}_{i_{n+1}} \otimes \boldsymbol{I} + d_2 \boldsymbol{I} \otimes \bar{\boldsymbol{N}}_{j_{n+1}}. \tag{B.14}$$

The scalars used above are given by

$$a_1 = s_{12}, \tag{B.15}$$
$$b_1 = s_{11} - \frac{s_{13}}{F'_{11}} F_{11}, \tag{B.16}$$
$$b_2 = s_{21} - \frac{s_{23}}{F'_{21}} F_{21}, \tag{B.17}$$
$$c_1 = -\frac{s_{13}}{F'_{11}} F_{12}, \tag{B.18}$$
$$c_2 = -\frac{s_{23}}{F'_{21}} F_{22}, \tag{B.19}$$
$$d_1 = p_{12} - \frac{p_{13}}{F'_{11}} F_{11}, \tag{B.20}$$
$$d_2 = p_{22} - \frac{p_{23}}{F'_{21}} F_{21}, \tag{B.21}$$
$$e_e = p_{11} - \frac{p_{13}}{F'_{11}} F_{12}, \tag{B.22}$$

where

$$F_{11} = \sqrt{\frac{2}{3}} \left(\frac{-Y_{n+1}}{r} \right)^s - 2G \sqrt{\frac{3}{2}} \frac{(1 - D_{n+1})}{\left(\tilde{q}^{trial}_{n+1} - \tau_y \right)}, \tag{B.23}$$

$$F_{12} = \frac{s}{r} \frac{\left(\tilde{q}^{trial}_{n+1} - \tau_y \right) K}{3G} \left(\frac{-Y_{n+1}}{r} \right)^{s-1} \frac{1}{3} \mathrm{tr} \left(\boldsymbol{\varepsilon}^{e\ trial}_{i_{n+1}} \right), \tag{B.24}$$

$$p_{11} = (1 - D_{n+1}) K, \tag{B.25}$$

$$p_{12} = -2GK \sqrt{\frac{3}{2}} \frac{(1 - D_{n+1})}{\left(\tilde{q}^{trial}_{n+1} - \tau_y \right)} \frac{1}{3} \mathrm{tr} \left(\boldsymbol{\varepsilon}^{e\ trial}_{i_{n+1}} \right), \tag{B.26}$$

$$p_{13} = \left[3G + (1 - D_{n+1}) H \right] \frac{K}{\left(\tilde{q}^{trial}_{n+1} - \tau_y \right)} \frac{1}{3} \mathrm{tr} \left(\boldsymbol{\varepsilon}^{e\ trial}_{i_{n+1}} \right), \tag{B.27}$$

$$s_{11} = -2G\left(1-D_{n+1}\right)\frac{\left(2\tilde{q}_{n+1}^{trial}-\tau_y\right)\tau_y}{\left(\tilde{q}_{n+1}^{trial}-\tau_y\right)\tilde{q}_{n+1}^{trial}}, \tag{B.28}$$

$$s_{12} = 2G\left(1-D_{n+1}\right)\frac{\tau_y}{\tilde{q}_{n+1}^{trial}}, \tag{B.29}$$

$$s_{13} = \sqrt{\frac{2}{3}}\left[\frac{3G\tau_y}{\left(\tilde{q}_{n+1}^{trial}-\tau_y\right)}+\frac{\left(1-D_{n+1}\right)\tau_y H}{\left(\tilde{q}_{n+1}^{trial}-\tau_y\right)}+\left(1-D_{n+1}\right)H\right], \tag{B.30}$$

$$\begin{aligned} F'_{11} &= 3G+\left(1-D_n\right)H \\ &- \frac{2}{3G}\left(\tilde{q}_{n+1}^{trial}-\tau_y\right)H\left(\frac{-Y_{n+1}}{r}\right)^s \\ &+ \frac{s}{r}\frac{\left(\tilde{q}_{n+1}^{trial}-\tau_y\right)^2\tau_y H}{9G^2}\left(\frac{-Y_{n+1}}{r}\right)^{s-1}. \end{aligned} \tag{B.31}$$

$$F_{11} = \sqrt{\frac{2}{3}}\left(\frac{-Y_{n+1}}{r}\right)^s - 2G\sqrt{\frac{3}{2}}\frac{\left(1-D_{n+1}\right)}{\left(\tilde{q}_{n+1}^{trial}-\tau_y\right)}, \tag{B.32}$$

$$F_{12} = \frac{s}{r}\frac{\left(\tilde{q}_{n+1}^{trial}-\tau_y\right)K}{3G}\left(\frac{-Y_{n+1}}{r}\right)^{s-1}\frac{1}{3}\mathrm{tr}\left(\boldsymbol{\varepsilon}_{i_{n+1}}^{e\,trial}\right), \tag{B.33}$$

$$p_{11} = \left(1-D_{n+1}\right)K, \tag{B.34}$$

$$p_{12} = -2GK\sqrt{\frac{3}{2}}\frac{\left(1-D_{n+1}\right)}{\left(\tilde{q}_{n+1}^{trial}-\tau_y\right)}\frac{1}{3}\mathrm{tr}\left(\boldsymbol{\varepsilon}_{i_{n+1}}^{e\,trial}\right), \tag{B.35}$$

$$p_{13} = \left[3G+\left(1-D_{n+1}\right)H\right]\frac{K}{\left(\tilde{q}_{n+1}^{trial}-\tau_y\right)}\frac{1}{3}\mathrm{tr}\left(\boldsymbol{\varepsilon}_{i_{n+1}}^{e\,trial}\right), \tag{B.36}$$

$$s_{11} = -2G\left(1-D_{n+1}\right)\frac{\left(2\tilde{q}_{n+1}^{trial}-\tau_y\right)\tau_y}{\left(\tilde{q}_{n+1}^{trial}-\tau_y\right)\tilde{q}_{n+1}^{trial}}, \tag{B.37}$$

$$s_{12} = 2G\left(1-D_{n+1}\right)\frac{\tau_y}{\tilde{q}_{n+1}^{trial}}, \tag{B.38}$$

$$s_{13} = \sqrt{\frac{2}{3}}\left[\frac{3G\tau_y}{\left(\tilde{q}_{n+1}^{trial}-\tau_y\right)}+\frac{\left(1-D_{n+1}\right)\tau_y H}{\left(\tilde{q}_{n+1}^{trial}-\tau_y\right)}+\left(1-D_{n+1}\right)H\right], \tag{B.39}$$

$$\begin{aligned} F'_{11} &= 3G+\left(1-D_n\right)H \\ &- \frac{2}{3G}\left(\tilde{q}_{n+1}^{trial}-\tau_y\right)H\left(\frac{-Y_{n+1}}{r}\right)^s \\ &+ \frac{s}{r}\frac{\left(\tilde{q}_{n+1}^{trial}-\tau_y\right)^2\tau_y H}{9G^2}\left(\frac{-Y_{n+1}}{r}\right)^{s-1}. \end{aligned} \tag{B.40}$$

Appendix C

LS-DYNA Implementation Code Excerpt

We provide herein an excerpt of the FORTRAN code necessary for the implementation of the non-local strategy in LS-DYNA as a user-defined option (see Chapter 7). Only the main steps have been listed here and the sample code is intended to serve as a general guide only. The implementation has to be incorporated in file `dyn21.f`.

```
SUBROUTINE urmathn (...)
....
COMMON/bk06/idmmy,iaddp,ifil,maxsiz,ncycle,time(2,30)
....
! Declare dimensions for nonl-ocal formulation
DIMENSION betaij(...), var_loc(mxelem), var_nonloc(mxelem)
DIMENSION connect(mxelem,8), coord(mxnode,3)
! Save data for the next step
SAVE betaij, var_loc, connect, coord
....
! Get connectivities and nodal coordinates (only at cycle #1)
IF(ncycle.EQ.1)THEN
  CALL get_connectivities (..., connect )
  CALL get_coordinates (..., coord , r_mem(dm_x) )
ENDIF
! Compute non-local factors beta_ij (only at cycle #2)
IF(ncycle.EQ.2)THEN
  CALL compute_nonlocal_factors  (..., betaij , connect , coord )
```

```
ENDIF
! Compute non-local variable (at every cicle)
IF(ncycle.GE.2)THEN
  CALL compute_nonlocal_variable (..., betaij , var_loc , var_nonloc )
ENDIF
....
DO 90 i=lft,llt
  ! Get external element ID (solids)
  ielem=lqfinv(nnm1+i,2)
  ! Compute penalty factor K
  factor_k=var_nonloc(ielem)/var_loc(ielem)
  CALL analyse_k (...)
  ....
  ! Local user material routine
41 CALL umat41 (..., factor_k)
  ....
  ! Store local variable to be used in the next step
  var_loc(ielem)= hsv(...)
....
90 CONTINUE
....
END SUBROUTINE urmathn
```

Bibliography

[1] *LS-DYNA Keyword User's Manual - Version 971*, 2007.

[2] R.K. Abu Al-Rub and G.Z. Voyiadjis. A direct finite element implementation of the gradient-dependent theory. *International Journal for Numerical Methods in Engineering*, 63:603–629, 2005.

[3] F.X.C. Andrade, J.M.A. César de Sá, and F.M. Andrade Pires. A ductile damage nonlocal model of integral-type at finite strains: formulation and numerical issues. *International Journal of Damage Mechanics*, 20:515–557, 2011.

[4] F.X.C. Andrade, M. Vogler, J.M.A. César de Sá, and F.M. Andrade Pires. User-defined nonlocal models in LS-DYNA. In *Proceedings of the 8th European LS-DYNA Users Conference, Strasbourg*, 2011.

[5] F.M. Andrade Pires, E.A. De Souza Neto, and D.R.J. Owen. On the finite element prediction of damage growth and fracture initiation in finitely deforming ductile materials. *Computer Methods in Applied Mechanics and Engineering*, 193:5223–5256, 2004.

[6] Y. Bai. *Effect of Loading History on Necking and Fracture*. PhD thesis, Department of Ocean Engineering, Massachusetts Institute Technology, 2008.

[7] Yingbin Bao. *Prediction of Ductile Crack Formation in Uncracked Bodies*. PhD thesis, Department of Ocean Engineering, Massachusetts Institute Technology, 2003.

[8] Yingbin Bao and T. Wierzbicki. On fracture locus in the equivalent strain and stress triaxiality space. *International Journal of Mechanical Sciences*, 46:81–98, 2004.

[9] Yingbin Bao and T. Wierzbicki. A comparative study on various ductile crack formation criteria. *Journal of Engineering Materials and Technology*, 126:314–24, 2004.

[10] I. Barsoum and J. Faleskog. Rupture mechanisms in combined tension and shear – experiments. *International Journal of Solids and Structures*, 44: 1768–1786, 2007.

[11] I. Barsoum and J. Faleskog. Rupture mechanisms in combined tension and shear – micromechanics. *International Journal of Solids and Structures*, 44: 5481–5498, 2007.

[12] K.-J. Bathe. *Finite Element Procedures*. Prentice-Hall, Englewood Cliffs, New Jersey, 1996.

[13] Z.P. Bažant and T.-P. Chang. Instability of nonlocal continuum and strain averaging. *Journal of Engineering Mechanics*, ASCE 110:1441–1450, 1984.

[14] Z.P. Bažant and M. Jirásek. Nonlocal integral formulations of plasticity and damage: Survey of progress. *Journal of Engineering Mechanics*, 128(11): 1119–1149, 2002.

[15] Z.P. Bažant and F.-B. Lin. Nonlocal yield-limit degradation. *International Journal for Numerical Methods in Engineering*, 26:1805–1823, 1988.

[16] Z.P. Bažant and G. Pijaudier-Cabot. Nonlocal continuum damage, localization instability and convergence. *Journal of Applied Mechanics*, 55:287–290, 1988.

[17] T. Belytschko, W.K. Liu, and I. Doghri. *Nonlinear finite elements for continua and structures*. Wiley, New York, 2000.

[18] E. Benvenuti and G. Borino. A thermodynamically consistent nonlocal formulation for damaging materials. *European Journal of Mechanics A/Solids*, 21:535–553, 2002.

[19] E. Benvenuti and A. Tralli. Iterative LCP solver for non-local loading-unloading conditions. *International Journal for Numerical Methods in Engineering*, 58:2343–2370, 2003.

[20] J. Bonet and R.D. Wood. *Nonlinear continuum mechanics for finite element analysis*. Cambridge University Press, Cambridge, 2nd edition, 2008.

[21] G. Borino, P. Fuschi, and C. Polizzotto. A thermodynamic approach to nonlocal plasticity and related variational principles. *Journal of Applied Mechanics*, 66:952–963, 1999.

[22] G. Borino, B. Failla, and C. Polizzotto. A symmetric nonlocal damage theory. *International Journal of Solids and Structures*, 40:3621–3645, 2003.

[23] M. Brünig, O. Chyra, D. Albrecht, L. Driemeier, and M. Alves. A ductile damage criterion at various stress triaxialities. *International Journal of Plasticity*, 24:1731–1755, 2008.

[24] M. Cervera and M. Chiumenti. Size effect and localization in J2 plasticity. *International Journal of Solids and Structures*, 46:3301–3312, 2009.

[25] M. Cervera, M. Chiumenti, and C. Agelet de Saracibar. Softening, localization and stabilization: capture of discontinuous solutions in J2 plasticity. *International Journal for Numerical and Analytrical Methods in Geomechanics*, 28:373–393, 2004.

[26] J.M.A. César de Sá, P.M.A. Areias, and C. Zheng. Damage modelling in metal forming problems using an implicit non-local gradient model. *Computer Methods in Applied Mechanics and Engineering*, 195:6646–6660, 2006.

[27] J.M.A. César de Sá, F.M. Andrade Pires, and F.X.C. Andrade. Local and nonlocal modeling of ductile damage. In M. Vaz Jr., E.A. De Souza Neto, and P.A. Muñoz-Rojas, editors, *Advanced Computational Materials Modelling: From Classical to Multi-Scale Techniques*, chapter 2, pages 23–72. Wiley-VCH, Weinheim, 2010.

[28] J.L. Chaboche. Continuum damage mechanics - a tool to describe phenomena before crack initiation. *Nuclear Engineering Design*, 64:233–247, 1981.

[29] J.L. Chaboche. Anisotropic creep damage in the framework of continuum damage mechanics. *Nuclear Engineering Design*, 79:309–319, 1984.

[30] C. Comi. A non-local model with tension and compression damage mechanisms. *European Journal of Mechanics A/Solids*, (20):1–22, 2001.

[31] R.D. Cook, D.S. Malkus, and M.E. Plesha. *Concepts and Applications of Finite Element Analysis*. John Wiley & Sons Ltd, New York, 3rd edition, 1989.

[32] M.A. Crisfield. An arc-length method including line searches and accelerations. *International Journal for Numerical Methods in Engineering*, 19: 1269–1289, 1983.

[33] M.A. Crisfield. *Non-linear Finite Element Analysis of Solids and Structures. Volume 1: Essentials*. John Wiley & Sons Ltd, Chichester, England, 1991.

[34] M.A. Crisfield. *Non-linear Finite Element Analysis of Solids and Structures. Volume 2: Advanced Topics*. John Wiley & Sons Ltd, Chichester, 1997.

[35] R. De Borst and H. Mühlhaus. Gradient-dependent plasticity: formulation and algorithmic aspects. *International Journal for Numerical Methods in Engineering*, 35:521–539, 1992.

[36] E.A. De Souza Neto. A fast, one-equation integration algorithm for the Lemaitre ductile damage model. *Communications in Numerical Methods in Engineering*, 18:541–554, 2002.

[37] E.A. De Souza Neto. On general isotropic tensor functions of one tensor. *International Journal for Numerical Methods in Engineering*, 61:880–895, 2004.

[38] E.A. De Souza Neto, D. Perić, and D.R.J. Owen. A model for elastoplastic damage at finite strains: algorithm issues and applications. *Engineering Computations*, 11:257–281, 1994.

[39] E.A. De Souza Neto, D. Perić, D. Dutko, and D.R.J. Owen. Design of simple low order finite elements for large strain analysis of nearly incompressible solids. *International Journal of Solids and Structures*, 33:3277–3296, 1996.

[40] E.A. De Souza Neto, D. Perić, and D.R.J. Owen. *Computational Methods for Plasticity: Theory and Applications*. Wiley, 2008.

[41] J.H.P. De Vree, W.A.M. Brekelmans, and M.A.J. Van Gils. Comparison of nonlocal approaches in continuum damage mechanics. *Computers & Structures*, 55(4):581–588, 1995.

[42] G. Duvaut and J. Lions. *Inequalities in Mechanics and Physics*. Springer-Verlag, Berlin, 1976.

[43] D.G.B. Edelen and N. Laws. On the thermodynamics of systems with nonlocality. *Archive for Rational Mechanics and Analysis*, 43:24–35, 1971.

[44] D.G.B. Edelen, A.E. Green, and N. Laws. Nonlocal continuum mechanics. *Archive for Rational Mechanics and Analysis*, 43:36–44, 1971.

[45] K. Enakousta, J.B. Leblond, and G. Perrin. Numerical implementation and assessment of a phenomenological nonlocal model of ductile rupture. *Computer Methods in Applied Mechanics and Engineering*, 196:1946–1957, 2007.

[46] R.A.B. Engelen. *Plasticity-induced Damage in Metals: nonlocal modelling at finite strain*. PhD thesis, Technische Universiteit Eindhoven, Eindhoven, The Netherlands, 2005.

[47] R.A.B. Engelen, M.G.D. Geers, and R.L.J.M. Ubachs. Nonlocal implicit gradient-enhanced elasto-plasticity for the modelling of softening behaviour. *International Journal of Plasticity*, 19(4):403–433, 2003.

[48] A.C. Eringen. A unified theory of thermomechanical materials. *International Journal of Engineering Science*, (4):179–202, 1966.

[49] A.C. Eringen. On nonlocal plasticity. *International Journal of Engineering Science*, (19):1461–1474, 1981.

[50] A.C. Eringen. Theories of nonlocal plasticity. *International Journal of Engineering Science*, (21):741–751, 1983.

[51] M. Feucht. *Ein gradientenabhängiges Gursonmodell zur Beschreibung duktiler Schädigung mit Entfestigung*. PhD thesis, Technische Universität Darmstadt, 1999.

[52] M. Feucht and W. Faßnacht. Simulation der duktilen Rissbildung in Crashberechnungen mit Hilfe des Gurson-Modells. *17th CADFEM User's Meeting*, III-4.3, 1999.

[53] M. Feucht, D.-Z. Sun, T. Erhart, and T. Frank. Recent development and applications of the Gurson model. In *5th German LS-DYNA Forum*, 2006.

[54] X. Gao, G. Zhang, and C. Roe. A study on the effect of the stress state on ductile fracture. *International Journal of Damage Mechanics*, 19, 2010.

[55] M.G.D. Geers, R.L.J.M. Ubachs, and R.A.B. Engelen. Strongly non-local gradient-enhanced finite strain elastoplasticity. *International Journal for Numerical Methods in Engineering*, 56:2039–2068, 2003.

[56] P. Grassl and M. Jirásek. Plastic model with non-local damage applied to concrete. *International Journal for Numerical and Analytrical Methods in Geomechanics*, (30):71–90, 2006.

[57] A.L. Gurson. Continuum theory of ductile rupture by void nucleation and growth - part I: Yield criteria and flow rule for porous media. *Journal of Engineering Materials and Technology*, 99:2–15, 1977.

[58] M.E. Gurtin. *An Introduction to Continuum Mechanics*. Academic Press, 1981.

[59] P. Hakansson, M. Wallin, and M. Ristinmaa. Thermomechanical response of non-local porous material. *International Journal of Plasticity*, 22:2066–2090, 2006.

[60] J.W. Hancock and D.K. Brown. On the role of strain and stress state in ductile failure. *Journal of the Mechanics and Physics of Solids*, 31(1):1–24, 1983.

[61] H. Hencky. Zur Theorie der plastischer Deformationen und der dafür im Material hervorgerufenen Nachspannungen. *Zeitschrift für Angewandte Mathematik und Mechanik*, 4:323–334, 1924.

[62] G.A. Holzapfel. *Nonlinear Solid Mechanics: A Continuum Approach for Engineering*. John Wiley & Sons Ltd, Chichester, 2000.

[63] M.T. Huber. Specific work of strain as a measure of material effort. *Archives of Mechanics*, 56(3):173–190, 2004. Translation from the original paper in Polish published in 1904.

[64] T.J.R. Hughes. Generalization of selective integration procedures to anisotropic and nonlinear media. *International Journal for Numerical Methods in Engineering*, 15:1413–1418, 1980.

[65] T.J.R. Hughes. *The Finite Element Method: Linear Static and Dynamic Finite Element Analysis*. Dover Publications Inc., New York, 2000.

[66] M. Itskov. On the theory of fourth-order tensors and their applications in computational mechanics. *Computer Methods in Applied Mechanics and Engineering*, 189:419–438, 2000.

[67] M. Jirásek. Nonlocal models for damage and fracture: comparison of approaches. *International Journal of Solids and Structures*, 35:4133–4145, 1998.

[68] M. Jirásek. Nonlocal damage mechanics. *Revue Européene de Génie Civil*, 11:993–1021, 2007.

[69] M. Jirásek and B. Patzák. Consistent tangent stiffness for nonlocal damage models. *Computers & Structures*, (80):1279–1293, 2002.

[70] M. Jirásek and S. Rolshoven. Comparison of integral-type nonlocal plasticity models for strain-softening materials. *International Journal of Engineering Science*, 41:1553–1602, 2003.

[71] G.R. Johnson and W.H. Cook. Fracture characteristics of three metals subjected to various strains, strain rates, temperatures and pressures. *Engineering Fracture Mechanics*, 21(1):31–48, 1985.

[72] L.M. Kachanov. Time of the rupture process under creep condition. *Izv. Akad. Nauk. SSSR, Otd. Tekhn. Nauk.*, 8:26–31, 1958.

[73] O. Kintzel and Y. Başar. Fourth-order tensors – tensor differentiation with applications to continuum mechanics. Part I: Classical tensor analysis. *Journal of Applied Mathematics and Mechanics*, 86(4):291–311, 2006.

[74] J. Lemaitre. A continuous damage mechanics model for ductile fracture. *Journal of Engineering Materials and Technology*, 107:83–89, 1985.

[75] J. Lemaitre. Coupled elasto-plasticity and damage constitutive equations. *Computer Methods in Applied Mechanics and Engineering*, 51:31–49, 1985.

[76] J. Lemaitre. *A course on damage mechanics*. Springer, New York, 1996.

[77] A.C. Mackenzie, J.W. Hancock, and D.K. Brown. On the influence of state of stress on ductile failure initiation in high strength steels. *Engineering Fracture Mechanics*, 9:167–188, 1977.

[78] L.E. Malvern. *Introduction to the Mechanics of Continuous Medium*. Prentice-Hall, Englewood Cliffs, New Jersey, 1969.

[79] F.A. McClintock. A criterion for ductile fracture by the growth of holes. *Journal of Applied Mechanics*, 35:363–371, 1968.

[80] J. Mediavilla. *Continuous and discontinuous modelling of ductile fracture*. PhD thesis, Technische Universiteit Eindhoven, 2005.

[81] J. Mediavilla, R.H.J. Peerlings, and M.G.D. Geers. A nonlocal triaxiality-dependent ductile damage model for finite strain plasticity. *Computer Methods in Applied Mechanics and Engineering*, 195:4617–4634, 2006.

[82] C. Miehe and M. Lambrecht. Algorithms for computation of stresses and elasticity moduli in terms of Seth-Hill's family of generalized strain tensors. *Communications in Numerical Methods in Engineering*, 17(5):337–353, 2001.

[83] K. Nahshon and J.W. Hutchinson. Modification of the Gurson model for shear failure. *European Journal of Mechanics A/Solids*, 27:1–17, 2008.

[84] A. Needleman. Material rate dependence and mesh sensitivity in localization problems. *Computer Methods in Applied Mechanics and Engineering*, 67:69–85, 1988.

[85] G.D. Nguyen. A thermodynamic approach to non-local damage modelling of concrete. *International Journal of Solids and Structures*, (45):1918–1934, 2008.

[86] G.D. Nguyen and I. Einav. A stress-return algorithm for nonlocal constitutive models of softening materials. *International Journal for Numerical Methods in Engineering*, 2009. doi: 10.1002/nme.2790. DOI: 10.1002/nme.2790.

[87] G.D. Nguyen and G.T. Houlsby. A coupled damage-plasticity model for concrete based on thermodynamic principles: Part II: non-local regularization and numerical implementation. *International Journal for Numerical and Analytrical Methods in Geomechanics*, (32):391–413, 2008.

[88] R.H.J. Peerlings, R. De Borst, W.A.M. Brekelmans, and J.H.P. De Vree. Gradient-enhanced damage for quasi-brittle materials. *International Journal for Numerical Methods in Engineering*, 39:1512–1533, 1996.

[89] R.H.J. Peerlings, M.G.D. Geers, R. De Borst, and W.A.M. Brekelmans. A critical comparison of nonlocal and gradient-enhanced softening continua. *International Journal of Solids and Structures*, 38(44–45):7723–7746, 2001.

[90] D. Perić. On a class of constitutive equations in viscoplasticity: Formulation and computational issues. *International Journal for Numerical Methods in Engineering*, 36:1365–1393, 1993.

[91] D. Perić, D.R.J. Owen, and M.E. Honnor. A model for finite strain elasto-plasticity based on logarithmic strain: computational issues. *Computer Methods in Applied Mechanics and Engineering*, 94:35–61, 1992.

[92] P. Perzyna. Application of the thermodynamical theory of elasto–viscoplasticity in modern manufacturing processes. In G.Z. Voyiadjis, editor, *Damage Mechanics and Micromechanics of Localized Fracture Phenomena in Inelastic Solids*. Springer, 2011.

[93] G. Pijaudier-Cabot and Z.P. Bažant. Nonlocal damage theory. *Journal of Engineering Mechanics*, 113(10):1512–1533, 1987.

[94] G. Pijaudier-Cabot, Z.P. Bažant, and M. Tabbara. Comparison of various models for strain softening. *Engineering Computations*, 5:141–150, 1988.

[95] C. Polizzotto. A nonlocal strain gradient plasticity theory for finite deformations. *International Journal of Plasticity*, 25(7):1280–1300, 2009.

[96] C. Polizzotto, G. Borino, and P. Fuschi. A thermodynamically consistent formulation of nonlocal and gradient plasticity. *Mechanics Research Communications*, 25(1):75–82, 1998.

[97] Y.N. Rabotnov. On the equations of state for creep. In *Progress in Applied Mechanics, Prager Aniversary VOLUME*, page 307. MacMillan, 1963.

[98] F.J.P. Reis, L. Malcher, F.M. Andrade Pires, and J.M.A. César de Sá. A comparison of shear mechanisms for the prediction of ductile failure under low stress triaxiality. *International Journal of Structural Integrity*, 2010. (in press).

[99] F. Reusch, B. Svendsen, and D. Klingbeil. A non-local extension of Gurson-based ductile damage modeling. *Computational Materials Science*, 26:219–229, 2003.

[100] F. Reusch, B. Svendsen, and D. Klingbeil. Local and non-local Gurson-based ductile damage and failure modelling at large deformation. *European Journal of Mechanics A/Solids*, 22:779–792, 2003.

[101] S. Ricci and M. Brünig. Numerical analysis of nonlocal anisotropic continuum damage. *International Journal of Damage Mechanics*, 16:283–299, 2007.

[102] J.R. Rice and D.M. Tracey. On the ductile enlargement of voids in triaxial stress fields. *Journal of the Mechanics and Physics of Solids*, 17:201–217, 1969.

[103] D. Rogula. Influence of spatial acoustic dispersion on dynamical properties of dislocations. *Bulletin de l Academie Polonaise des Sciences-Serie des Sciences Techniques*, 13:337–343, 1965.

[104] S. Rolshoven. *Nonlocal plasticity models for localized failure*. PhD thesis, École Polytechnique Fédérale de Lausanne, Switzerland, 2003.

[105] M.K. Samal, M. Seidenfuss, E. Roos, B.K. Dutta, and H.S. Kushwaha. Finite element formulation of a new nonlocal damage model. *Finite Elements in Analysis and Design*, 44:358 – 371, 2008.

[106] J.C. Simo and T.J.R. Hughes. *Computational Inelasticity*. Springer, New York, 1998.

[107] J.C. Simo and M. Ortiz. Unified approach to finite deformation plasticity based on the use of hyperelastic constitutive equations. *Computer Methods in Applied Mechanics and Engineering*, 49:221–245, 1985.

[108] P. Steinmann. Formulation and computation of geometrically non-linear gradient damage. *International Journal for Numerical Methods in Engineering*, 46:757–779, 1999.

[109] L. Strömberg. A special case of equivalence between nonlocal plasticity and gradient plasticity in a one-dimensional formulation. *International Journal of Engineering Science*, 46(8):835–841, 2008.

[110] L. Strömberg and M. Ristinmaa. FE-formulation of a nonlocal plasticity theory. *Computer Methods in Applied Mechanics and Engineering*, 136:127–144, 1996.

[111] M.H. Tresca. Mémoire sur l'écoulement des corps solides soumis à de fortes pressions. *Comptes Rendus Hebdomadaires des Séances de l'Académie des Sciences*, 59:754–758, 1864.

[112] C. Truesdell. *A First Course in Rational Continuum Mechanics*, volume 1. Academic Press, New York, 1977.

[113] V. Tvergaard and A. Needleman. Analysis of cup-cone fracture in a round tensile bar. *Acta Metallurgica*, 32:157–169, 1984.

[114] V. Tvergaard and A. Needleman. Effects of nonlocal damage in porous plastic solids. *International Journal of Solids and Structures*, 32(8/9):1063–1077, 1995.

[115] M. Vaz Jr. and D.R.J. Owen. Aspects of ductile fracture and adaptive mesh refinement in damaged elasto-plastic materials. *International Journal for Numerical Methods in Engineering*, 50:29–54, 2001.

[116] M. Vogler, G. Ernst, and R. Rolfes. Invariant based transversely-isotropic material and failure model for fiber-reinforced polymers. *Computers, Materials & Continua*, 16(1):25–50, 2010.

[117] M. Vogler, F.X.C. Andrade, J. Schöpfer, S. Kolling, and R. Rolfes. A novel transversely-isotropic of 3d elastic-viscoplastic constitutive law for modeling fiber matrix composites. In *Proceedings of the 8th European LS-DYNA Users Conference, Strasbourg*, 2011.

[118] R. von Mises. Mechanik der festen Körper im plastisch-deformablen Zustand. *Nachrichten von der Gesellschaft der Wissenschaften zu Göttingen, mathematisch-physikalische Klasse*, 1:582–592, 1913.

[119] G. Weber and L. Anand. Finite deformation constitutive equations and a time integration procedure for isotropic, hyperelastic-viscoplastic solids. *Computer Methods in Applied Mechanics and Engineering*, 79:173–202, 1990.

[120] T. Wierzbicki, Y. Bao, Y.-W. Lee, and Y. Bai. Calibration and evaluation of seven fracture models. *International Journal of Mechanical Sciences*, 47 (4-5):719– 743, 2005.

[121] L. Xue. Constitutive modeling of void shearing effect in ductile fracture of porous materials. *Engineering Fracture Mechanics*, 75:3343–3366, 2008.

[122] O.C. Zienkiewicz and R.L. Taylor. *The Finite Element Method. Volume II: Solid Mechanics*. Butterworth-Heinemann, 5th edition, 2000.

[123] T. Zümendorf. *Ein gradientenabhängiges Modell für Schädigung bei viskoplastischem Materialverhalten*. PhD thesis, Technische Universität Braunschweig, 2005.